Towards dimetallic biologically inspired aerobic oxidation catalysts

PhD Thesis

Sam P. Ring

Sam.ring@sheffield.ac.uk

Supervisor: Dr. Nathan J. Patmore

01/10/2014

Acknowledgements

Firstly I would like to thank Nathan Patmore for his supervision, guidance, patience and unwavering optimism throughout this project and the challenging chemistry it has entailed. Next, thanks to my colleagues past and present including, Dr. Raquel Gracia, Luke Wilkinson, and the groups of Prof. Richard Jackson & Prof. Ian Coldham for making it a such a great place to work.

I would also like to thank the technical staff of the University of Sheffield Chemistry Department whose collaboration helped make this work possible. Particular thanks go out to: Simon Thorpe of the Mass Spectrometry service for trusting me to use his MALDI-TOF-MS spectrometer on which this work relies heavily; Harry Adams for his help with X-Ray crystallography, Sue Bradshaw for her help with extended Evens NMR studies; Dan Jackson the department glass blower who fixed and fabricated countless essential items of equiptment; Nick Smith & Pete Farran the chemistry stores technicians for their good humour and their great help in keeping the lab stocked with essential supplies.

The University of Sheffield & E-Futures DTC are thanked for a Postgraduate research studentship; E-Futures DTC & Energy Research Councils Uk (ERCUK) are additionally thanked for funding.

Finally the author would like to add his heartfelt thanks to all his long-suffering friends and family whose unconditional love and support has carried me through. My parents, Steve and Lesley for their un-ending support and for providing me a roof under which to write my thesis. Sarah for having been a part of my life for many years, but having always provided me with the space I needed to focus on my work. For my flatmates in providing a lovely place to live and some much needed comic relief. This is all for you guys as much as for me. Thank you.

Abstract

We report herein the synthesis and properties of a range of group 8 dimetallic paddlewheel complexes incorporating a range of formamidinate and amidate ligands. The potential of some of these complexes as aerobic oxidation catalysts is explored and the electronic structures probed via the aid of DFT calculations under B3LYP and PBE0 on the model complex $Ru_2(dmf)_4$ (where dmf = N,N'-diphenylformamidinate).

Attempts to extend a previous synthetic precedent for the synthesis of $Fe_2^{II,II}(DPhF)_4$ (where DPhF = N,N'-Diphenylformamidine) to other diiron tetra-formamidinates are reported, and the structure of the first novel symmetrically basic beryllium acetate structured tetra-iron cluster species ***$Fe_4^{II}(O)(DMOPhFm)_6$ (IX)*** (where DMOPhFm = N,N'-bis(3,5-dimethoxyphenyl)formamidine) published.

An alternative assignment for the redox process observed in the cyclic voltammogram of $Ru_2^{II,II}$(formamidinate) complexes is reported as evidenced by UV-Vis spectroelectrochemical analysis. Additionally, the nature of an unknown reversible interaction of the species ***$Ru_2^{II,II}(DMOPhFm)_4$ (X)*** (and ***$Ru_2^{II,II}(4FPhFm)_4$ (XI)*** (where 4FPhFm = N,N'-bis(4-flourophenyl)formamidine) on exposure to dioxygen is explored by a wide range of analytical techniques. A provisional computational model of this interaction is proposed and compared to the available data but requires some further refinement in order to better model the phenomenon observed experimentally.

List of publications

Structural, Spectroscopic and Theoretical Studies of a Diruthenium(II,II) Tetraformamidinate that Reversibly Binds Dioxygen

Ring, S.; Meijer, A. J. H. M.; Patmore, N. J., *Polyhedron* **2016**, *103,* 87-93.

DOI: 10.1016/j.poly.2015.09.051

Abstract: The reaction of $Ru_2(O_2CMe)_4$ with N,N'-bis(3,5-dimethoxyphenyl)formamidine (Hdmof) in refluxing toluene solutions yields $Ru_2(dmof)_4$ as a diamagnetic red solid that is extremely air-sensitive. The crystal structure reveals the expected paddlewheel arrangement of ligands around the Ru_2^{4+} core, with a relatively long Ru-Ru bond (2.4999(8) Å) that is consistent with a $\sigma^2\ \pi^4\ \delta^2\ \pi^{*4}$ electronic configuration. This is supported DFT calculations that show this electronic structure results from destabilization of the δ^* orbital due to antibonding interactions with the formamidinate ligands. The cyclic voltammogram of $Ru_2(dmof)_4$ in a 0.1 M $^nBu_4NPF_6$ / CH_2Cl_2 solution shows two redox processes, assigned as successive oxidations corresponding to the $Ru_2^{4+}/^{5+}$ and $Ru_2^{5+/6+}$ redox couples. Changes in the electronic absorption spectra associated with these oxidation processes were probed using a UV/vis spectroelectrochemical study. $Ru_2(dmof)_4$ reacts with dioxygen in solution to generate a purple compound that decomposes within an hour at room temperature. Bubbling N_2 gas through the purple solution regenerates $Ru_2(dmof)_4$, as evidenced by UV/vis spectrometry and cyclic voltammetry, suggesting that the dioxygen reversibly binds to the diruthenium core.

Tuning the electronic structure of Mo–Mo quadruple bonds by N for O for S substitution

Hicks, J.; Ring, S. P.; Patmore, N. J., *Dalton. Trans.* **2012**, *41* (22), 6641–6650.

DOI: 10.1039/C2DT30234A

Abstract: A series of quadruply bonded dimolybdenum compounds of form $Mo_2(EE'CC{\equiv}CPh)_4$ (EE' = {NPh}$_2$, $Mo_2$2NN; {NPh}O, $Mo_2$2NO;{NPh}S, $Mo_2$2NS; OO, $Mo_2$2OO) have been synthesised by ligand exchange reactions of $Mo_2(O_2CCH_3)_4$ with the acid or alkali metal salt of $\{PhC{\equiv}CCEE'\}^-$. The compounds $Mo_2$2NO, $Mo_2$2NS and $Mo_2$2OO were structurally characterised by single crystal X-ray crystallography. The structures show that $Mo_2$2NO adopts a cis-2,2 arrangement of the ligands about the Mo_2^{4+} core, whereas $Mo_2$2NS adopts the trans-2,2 arrangement. The influence of heteroatom substitution on the electronic structure of the compounds was investigated using cyclic voltammetry and UV-Vis spectroscopy. Simple N for O for S substitution in the bridging ligands significantly alters the electronic structure, lowering the energy of the Mo_2-δ HOMO and reducing the $Mo_2^{4+/5+}$ oxidation potential by up to 0.9 V. A different trend is found in the optoelectronic properties, with the energy of the Mo_2-δ-to-ligand-π* transition following the order $Mo_2$2OO > $Mo_2$2NO > $Mo_2$2NN > $Mo_2$2NS. Electronic structure calculations employing density functional theory were used to rationalise these observations.

List of compounds

H[DMOPhFm] – N,N'-bis(3,5-dimethoxyphenyl)formamidine

H[4FPhFm] – N,N'-bis(4-fluorophenyl)formamidine

H[TMOPhFm] – N,N'-bis(3,4,5-trimethoxyphenyl)formamidine

H[(3,5-CF_3)$_2$PhFm] – N,N'-bis(3,4,5-trimethoxyphenyl)formamidine

(I) $Fe^{II}Cl_2(H[DMOPhFm])_2$

(II) $Fe^{II}Cl_2(H[4FPhFm])_2$

(III) $Fe^{II}Cl_2(H[TMOPhFm])_2$ – Not isolated

(IV) $Fe^{II}Cl_2(H[(3,5\text{-}CF3)PhFm])_2$ – Not isolated

(V) $Fe_2^{II,II}(DMOFPhFm)_4$ – Not isolated

(VI) $Fe_2^{II,II}(4FPhFm)_2$ – Not isolated

(VII) $Fe_3^{II,II,I}(O)(DMOPhFm)_3$ – Not isolated

(VIII) $Fe_3^{II}(O)(DMOPhFm)_4$ – Not isolated

(IX) $Fe_4^{II}(O)(DMOPhFm)_6$

(X) $Ru_2^{II,II}(DMOFPhFm)_4$

(XI) $Ru_2^{II,II}(4FPhFm)_4$

(XII) $Ru_2^{II,II}((3,5\text{-}CF3)FPhFm)_4$

(XIII) $Ru_2^{II,II}((3,5\text{-}CF3)FPhFm)_3(OAc)$

(XIV) $Ru_2^{II,II}(TMOPhFm)_4$

(XV) $Ru_2^{II,II}(OAc)_4(H[DMOPhFm])_2$

(XVI) $Ru_2^{II,II}(Ben)_4$

(XVII) $Ru_2^{II,II}(pTPhAm)_4$

(XVIII) $Ru_2^{II,III}(Ben)_4Cl$

(XIX) $Ru_2^{II,III}(pTPhAm)_4Cl$

(XX) $Ru_2^{II,III}(TiPBAm)_4Cl$

List of abbreviations

DMFC – Direct methanol fuel cell

PEMFC – Proton exchange membrane fuel cell

SMR – Steam methane reformation

Bpym – 2,2'-Bipyrimidine

M. Caps. – Methylococcus capsulatus

M. Trich. – Methylosinus trichosporium OB3b

BMM – Bacterial multi-component monooxygenase

MMO – Methane monooxygenase

sMMO – Soluble form of MMO

pMMO – Particulate form of MMO

NADH – Nicotinamide adenine dinucleotide

MMOH – Hydroxylase protein subunit of MMO

MMOR – NADH Reductase subunit of MMO

MMOB – Regulatory protein subunit of MMO

FD – Ferredoxin

FAD – Flavin adenine dinucleotide

RNR – Ribonucleotide reductase

Δ^9 D – Δ^9 stearoyl-acyl carrier protein; Δ^9 desaturase

MLCT – Metal-ligand charge transfer

DFT / TD-DFT –Density functional theory / Time-dependant -DFT

DEB – 1,2-diethynylbenzene

D. Gigas – Desulfovibrio gigas

HS / LS – High / low spin

TPA – tris(2-pyridymethyl)amine.

TBAHF – tetrabutyl ammonium hexaflourophosphate

MALDI-TOF-MS – Matrix assisted laser desorption ionisation time of flight mass spectrometry.

Table of Contents

1 Introduction

1.1 Group 8 catalysts for the generation of alternative fuels

When considering catalysts, few areas of the periodic table hold quite as much proven potential as the transition metals of group 8. To the synthetic chemist the later transition metals in particular provide a versatile tool-kit for catalytic functionalization,[1,2] whilst early transition metals such as iron are utilised extensively as catalysts both industrially[3,4] and in nature to great effect.

Industrially, group 8 catalysts are already integral to a wide range of processes, including the Haber-Bosch synthesis of ammonia[5] which is perhaps the single most pivotal example of industrial catalysis in history. In the course of the development of the process, Haber[6,7] and latterly Bosch[8] considered all of the naturally occurring group 8 metals, noting a readily observable correlation between their activity and stability descending the group. Later transition metals showed a greater degree of activity but significantly lower stability than their early transition metal alternatives.

In nature, iron catalysis is ubiquitous. Iron provides the active, functional core of a vast number of biologically critical enzymes which may be broadly divided into those that adopt a haem structure and those that do not (non-haem). Examples of the former include the highly diverse and metabolically critical cytochrome P450 family, whilst the latter includes examples of dimetallic chemistry such as in the enzyme methane monooxygenase (MMO).

These families of enzymes conduct a rich and varied array of oxidative chemistry which in the case of cytochrome P450 has been the focus of significant research for many years. Such efforts have focused on both understanding their mechanistic operation,[9–14] and in the development of functional synthetic models[15] to replicate their function. In contrast, some other non-haem systems such as that of MMOs have seen far less development. MMOs are of particular interest for their ability to perform partial oxidation of saturated organic substrates. This has potentially critical applications in current industrial processes and in strategies to leverage these products (e.g. Methanol) as potential alternative fuels.

1.2 Methanol as a viable alternative fuel

The prospect of providing for a burgeoning global populace and increasing energy demand with declining fossil fuel reserves presents a significant scientific, engineering and societal challenge. This challenge is then further complicated by the simultaneously need to mitigate the impact of global warming of current energy usage. Due to the multifaceted nature of this challenge it is highly unlikely that a single technological solution will be found.[16–18] In addition to developing new technologies therefore there is also a significant need to improve upon the efficiency of current major industrial processes, and to diversify the range of usable fuels at our disposal.[3,17]

Methanol in particular presents and attractive option as one such alternative fuel as it is highly adaptable and able to be readily used with both existing internal combustion engines[19,20] and emerging technologies such as direct methanol fuel cells (DMFCs).[17,21] As a liquid fuel, it presents none of the additional safety considerations that have hampered the uptake of gaseous alternative fuels such as hydrogen[3,16,17,22] and additionally could utilise the existing petroleum industry infrastructure without significant modification.[17,23]

Improvements to the highly energy intensive process currently used to synthesise methanol would provide both a more viable alternative transport fuel to current crude oil derived petroleum and improve energy security.[17,19,20,24] Like many catalysed industrial processes however, despite iterative improvement in catalyst design and process optimisation compared to biological systems, current practice remains highly inefficient.[25,26]

The potential to improve the efficiency of partially oxidised fuel synthesis would also have a profound impact on related Fischer-Tropsch chemistry, which is conducted on an increasing scale globally especially in Qatar, South Africa and Malaysia.[24,27]

1.3 Industrial methanol synthesis

As a common bulk chemical, methanol is already synthesised in significant volume, primarily for the synthesis of secondary bulk chemicals (e.g. formaldehyde), various polymer precursors and as a common solvent. Current industrial practice sees it synthesised from synthesis gas (syngas), which itself is most commonly derived from otherwise unusable sources of natural gas. Any hydrocarbon source, such as coal or biomass could however in principle be used.[28,29] Despite the extensive industrial use of this process for over half a century some elements of the mechanism by which this reaction occurs are still not fully understood and remain controversial.[30,31]

1.3.1 Syngas production

Synthesis gas generation may be conducted via several methods including catalytic steam methane reforming (SMR), partial oxidation (POX) and auto-thermal reforming (ATR). The most significant difference between these methods is the ratio of syngas components (H_2 : CO) produced, however economic and scale considerations render SMR the predominantly method used in practice.[3,32]

The SMR methodology uses the markedly endothermic reformation of methane with steam over a $Ni/MgAl_2O_4$ spinel catalyst[33] (1.1) coupled with the somewhat exothermic water gas shift (WGS) reaction (1.2) to minimise the required energy input, resulting in the overall reaction shown (1.3).

$$CH_4 + H_2O \leftrightarrows CO + 3H_2 \qquad \Delta H°_{298} = +205 \text{ KJ mol}^{-1} \qquad (1.1)$$

$$CO + H_2O \leftrightarrows CO_2 + H_2 \qquad \Delta H°_{298} = -41 \text{ KJ mol}^{-1} \qquad (1.2)$$

$$CH_4 + 2H_2O \leftrightarrows CO_2 + 4H_2 \qquad \Delta H°_{298} = +156 \text{ KJ mol}^{-1} \qquad (1.3)$$

This process still requires quite extreme conditions, typically operating at 800°C and pressures of 30-40 bar to ensure efficient operation; i.e. mandating significant energy input and tight regulatory control. Given the volume expansion expected from the reaction stoichiometry the chosen conditions may appear counter-initiative; but these conditions are required for efficient catalyst operation. This is due to the ability of the nickel catalyst used to catalyse the reverse reaction regenerating CH_4 under uncontrolled, non-ideal

conditions.[34] In order to maximise conversion, both the temperature and pressure are modulated between the two stages of the reactor, with an initial stage at conditions noted above, followed by a cooler second stage at 400 °C and 25 bar. Current operating conditions are the product of studies that balance favourable reaction kinetics with the need to ensure catalyst longevity and overall efficiency. Other, typically noble metal catalysts, derived from Pd, Pt, Rh and in particular Ru have been shown to act as more efficient and robust catalysts for syngas generation,[33,35,36] however these are not widely used industrially due to their prohibitive cost.

1.3.2 Methanol synthesis

Once the reformation of methane to synthesis gas is complete the generation of methanol is achieved via the passing of syngas over a $CuO/ZnO/Al_2O_3$ catalyst[30] at 200-300 °C and 50-100 bar.[34,37] The pressure used ostensibly serves to drive the reaction equilibrium in favour of the desired products. This reaction may then be described as follows:[38]

$CO + H_2O \leftrightarrows CO_2 + H_2$	$\Delta H°_{298} = -41$ KJ mol^{-1}	(1.2)
$CO_2 + 3H_2 \leftrightarrows CH_3OH + H_2O$	$\Delta H°_{298} = -50$ KJ mol^{-1}	(1.4)
$CO + 2H_2 \leftrightarrows CH_3OH + H_2O$	$\Delta H°_{298} = -91$ KJ mol^{-1}	(1.5)

It is necessary to include the WGS reaction as part of this description as methanogenesis may occur via CO_2 (1.4) or CO (1.5). The best yields for this process are however obtained from $CO/CO_2/H_2$ syngas mixture; generation via either CO/H_2 or CO_2/H_2 in isolation proceeds at lower yield.[32,39]

1.4 Other synthetic routes to methanol

In addition to the industrially performed synthesis of methanol via the generation of syngas a number of other, more direct means of methane oxidation have been extensively reported in the literature. The main issue common to all these alternative methods is one of selectivity; due simply to the inherent difficulty in achieving alkane partial cf. complete oxidation. Alkanes are by nature comparatively stable, whereas the intended products, e.g. MeOH are actually marginally more reactive. The C-H bond strength in MeOH is, for example, 23 kJ mol^{-1} less than observed in CH_4.[40] This then renders the products more likely to undergo further unwanted oxidation proliferating the generation of unwanted by-products.

1.4.1 Transition metals and their oxides

A very wide range of transition metals and their oxides (both free and supported) have been investigated for use as direct 1 step partial oxidation catalysts. These may be loosely divided into those intended for high (10+ bar) and low (~1 bar) operation and which both typically require temperatures between 600-800°C. Of those studied $FePO_4$ showed the best reported selectivity for methanol, >50 % at <660 K but only achieved a methane conversion of 1.2%.[41–44] Despite decades of active research it has been shown that such catalysts will never likely be viable. This is because gas phase and radical reactions exhibit greater influence on product distribution than the metal catalyst surface used under the conditions required for catalytic activity.[45–47] Further explanation may be found in a number of excellent and very comprehensive reviews on the topic.[48–54]

1.4.2 Targeting stable analogues

A number of the reported strategies for facile conversion of methane to methanol actually proceed via the intentional formation of closely related methanol analogues, such as esters or acids[55] which then require further workup to obtain the intended product.

The best example of this is perhaps provided by Periana *et al.*[56,57] who demonstrated the conversion of methane to methyl bisulphate through use of the bipyrimidyl Pt (II) complex, $(bpym)PtCl_2$ (where bpym = 2,2'-Bipyrimidine) at *ca.* 220°C in H_2SO_4. (Figure 1.4.1) Despite

having been one of the most favourable methane to methanol conversion efficiencies of any strategy at 73% this methodology is still ultimately too flawed to see practical usage. As a catalytic system its turnover is several orders of magnitude too low, recovery of the intended product is both protracted and prohibitively expensive, and the re-oxidation of SO_2 to H_2SO_4 is neither scalable nor practical.[3] Other analogous catalysts based on Pt(II)[42] and similar metals Pd(II)[55,58,59] and Rh(III)[60] have also been reported whilst other work by Periana *et al.* has also seen the use of a similar scheme for Hg(II)[61] and Ag(III).[62]

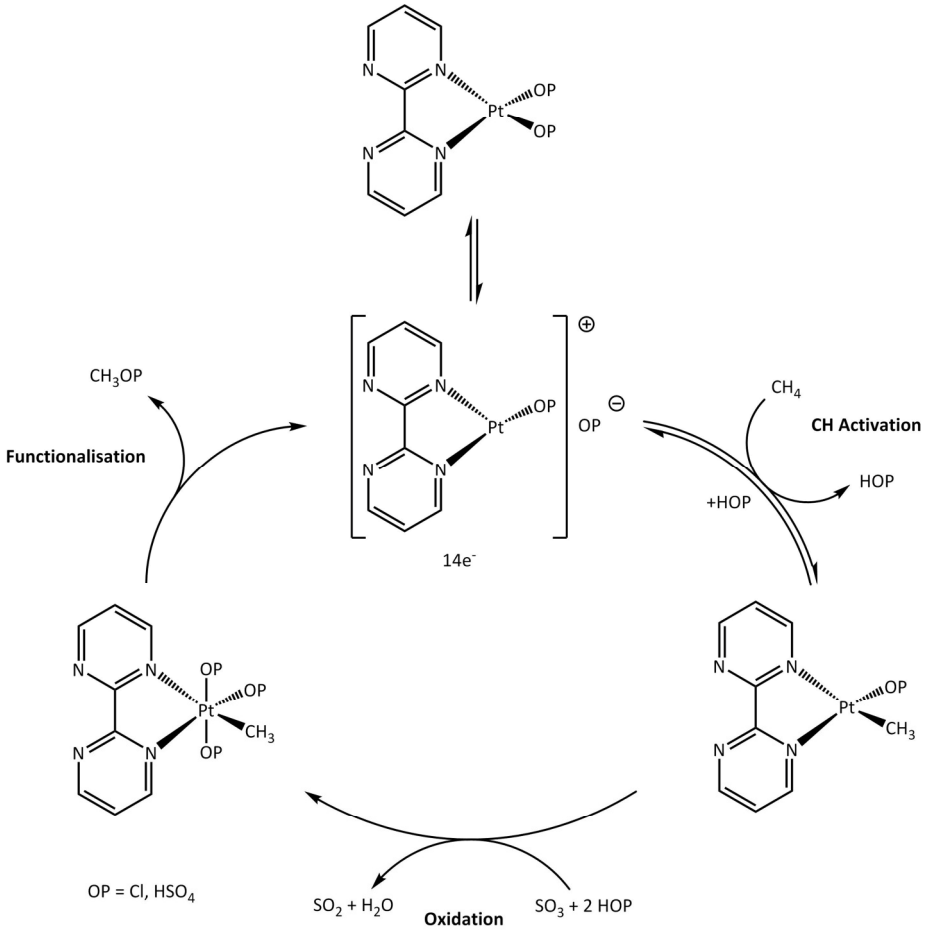

Figure 1.4.1 - Scheme of the proposed mechanism for the oxidation of methane using (bpym)$PtCl_2$

Mechanistically this catalytic but short lived process is somewhat analogous to aqueous chloroplatinum (IV) catalytic systems as developed by Shilov,[40,63] one of the earliest examples of C-H activation. This approach has since been further developed more recently by Muehlhofer *et al.*[64,65] whose Pd (II) carbene in trifluroacetic acid (TFA) shows greatly extended catalyst lifetime, provides facile product recovery via distillation and operates in milder conditions (90°C / 30 bar).

1.5 Applications of (mono) ruthenium compounds in synthetic chemistry

1.5.1 General properties

Ruthenium is a remarkably versatile element which finds wide and varied uses across the traditional synthetic disciplines. This is in part due to the wide range of oxidation states it can adopt, ranging from Ru^{-2} in unorthodox lanthanide ruthenides[66–68] such as $CeRu_2$, to highly aggressive oxidants such as RuO_4 wherein Ru is formally Ru^{VIII}.[69,70] Examples of all intermediate oxidation states are known with the singular exception of Ru^{-1}, affording it the widest usable oxidation state range of any 2nd row transition metal.[70–72]

Along with other d^8 metals, some lower oxidation state complexes such as those of Ru (III) (d^5) and Ru (IV) (d^4) possess the potential for both paramagnetism and/or differing spin states. Whilst the vast majority of reported ruthenium complexes are low spin (LS), in recent years a number of non-low spin examples have been reported.[73–75] Of these examples it is notable that recent reports have indicated that an intermediate spin did not have the same effect on substitutional lability as is observed between iron complexes of differing spin states.[73]

1.5.2 (Mono) ruthenium (II) – A versatile metallocentre

The strong optical absorptions of many ruthenium (II) containing species such as $[Ru(bpy)_3]Cl_2$ (where bpy = 2,2'-bipyridine) has led to the extensive investigation of related complexes in recent decades. These have found use as photosensitizers,[76–79] imaging agents,[80,81] and as components of larger systems e.g. synthetic mimics of photosystem II.[82,83] The rich photochemistry of such species has similarly led to their investigation and utilisation in molecular electronics[84] as both inorganic sensors[85,86] and molecular switches.[87,88] They also find to their usage as photoredox catalysts in their own right.[89–92] Development of photoredox catalysts has been of renewed interest in recent years was the subject of a series of recent reviews.[93–95] The prior art in the field of ruthenium chemistry as a whole ably demonstrates that precise control of the optical, electronic and magnetic properties of a ruthenium centre may be readily effected by judicious control of its

coordination environment and the steric demands and constraints this may impose on the metal centre.[96–98] In so doing it is then possible to tune the properties and chemistry of a ruthenium centre for a wide range of applications.

Considering the extensive development of mono ruthenium complexes however, especially those of Ru^{2+}, it is surprising how comparatively little is known of the chemistry of related dimetallic Ru_2^{4+} complexes. It follows logically that a dimetallic centre should offer a greater scope for electronic tunability and that this consequently might give rise to similarly useful reactive activity. This is evident from the numerous enzymatic examples of dimetallic metallocentres in Nature and can be readily observed through interrogation of their probable electronic structure via computational modelling using density functional theory (DFT).

1.5.3 Ruthenium as a catalytic synthetic tool

As synthetic tools ruthenium complexes provide catalysts for range of synthetically important processes,[1] perhaps the most well-known of which are the Grubbs[99,100] and their related Hoveyda-Grubbs[101,102] olefin metathesis catalysts (Figure 1.5.1). Grubbs was jointly (with Chauvin and Schrock) awarded the Nobel Prize in Chemistry in 2005 for his work in the development two generations of olefin metathesis catalysts. The Hoveyda-Grubbs catalyst is a modification of the original 1st and 2nd generation Grubbs catalysts wherein the phosphine ligand is supplanted by a chelating pendant *ortho*-isopropoxy group on the existing benzylidene ligand. This has the effect of affording greater stability of the active catalyst but at a reduction to the overall rate of reaction as noted in an excellent recent review of the area.[2]

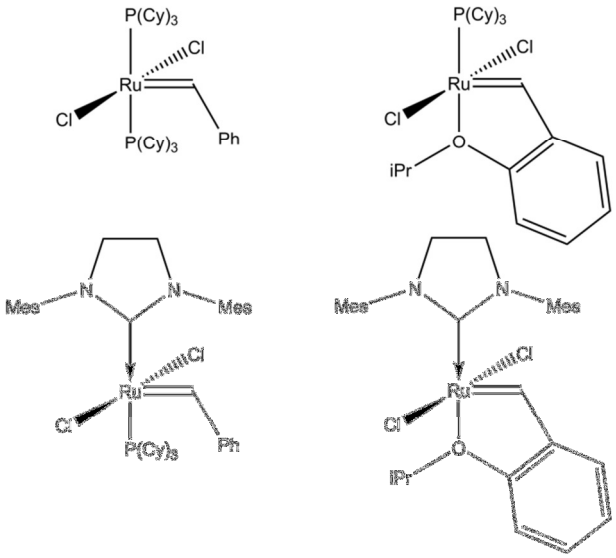

Figure 1.5.1 - (Left) Grubbs 1st & 2nd Generation catalysts with their Hoveyda analogues (right)

Beyond olefin metathesis, ruthenium systems have found diverse applications in the selective activation and functionalization of C-H bonds which was the subject of a recent review of the area by Dixneuf.[1] These predominantly Ru (II) dichloride dimer species such as those illustrated below (Figure 1.5.2) provide a means to achieve a means to achieve a wide range of transformations. These include: arene and alkene arylation or hydroarylation; arene alkylation; electrophilic substitution of arene C-H bond by acylation, sulfonation, aminocarbonylation and alkoxycarbonylation; and arene oxidative dehydrogenative cross-coupling.[1]

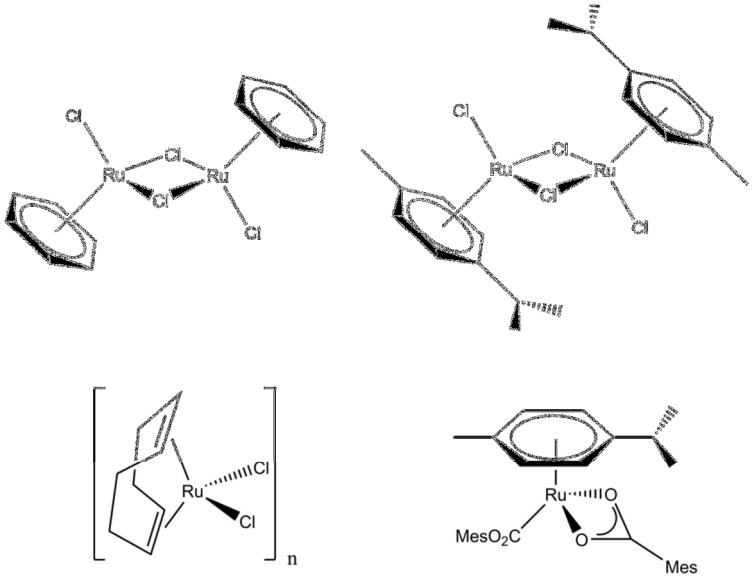

Figure 1.5.2 - Mono Ru catalysts - clockwise from top left: $[RuCl_2(C_6H_6)]_2$, $[RuCl_2(p\text{-cymene})]_2$, $[RuCl_2(cod)]_n$ and $Ru(O_2CMes)_2(p\text{-cymene})$

1.6 Dimetallic Complexes

1.6.1 Recognition of M-M multiple bonding

The field of M-M multiple bonding is, by contrast to traditional inorganic chemistry relatively young. The development of this field started in the 1960s in response to a number of compounds whose properties it was determined could not be accurately rationalised under traditional Wernerian coordination chemistry.

Wernerian coordination chemistry did not account for, nor did it consider, the potential for metal-metal interactions even amongst recognised polynuclear complexes. Instead the structure of such complexes was rationalised as being of multiple monomeric complexes joined via shared ligands, which whilst correct for the complexes he reported, is insufficient for rationalising some more complex systems. [103]

The most widely noted of the early examples which provided inconsistent with his theories is that of Blomstrand *et al.*[104–106] and their observations on a compound they believed to be of the form Mo_3X_6. Whilst these reports predate Werners birth they were the subject of several editions of his published series *Neuere Anschauungen auf dem gebiete der Anorganischen Chemie* wherein he proposed the structure below (Figure 1.6.1).[103]

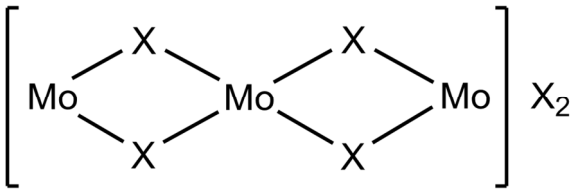

Figure 1.6.1 - Proposed structure of polynuclear Mo_3X_6 by Werner wherein X denotes a halide

It was not until the advent of X-ray crystallography and the early experiments by Brosset[107,108] and latterly by Pauling[109] that the first concrete indications of close M-M contracts was established. Brosset then even postulated this as potentially constituting a bonding interaction[110,111] yet in the wake of both his and Pauling's observations this idea was developed further.

In 1957, focus on the topic was renewed with the presentation of unequivocal evidence presented by Dahl *et al.*[112] indicating the necessity of a metal-metal bond in $Mn_2(CO)_{10}$. This discovery caught the attention of the laboratories of Bertrand and Robinson who in 1963 then independently reported[113–115] $[Re_3Cl_{12}]^{3-}$ which, by virtue of molecular orbital (MO) analysis, was determined to contain the first instance of a multiply bonded M-M interaction.[116]

In the years that followed the chemistry of rhenium halides was rapidly expanded, providing the first reported instance of a quadruple M-M bond in Re_2Cl_8 in 1964 (Figure 1.6.2a).[117] This remained the highest degree bond order reported in an isolated complex until 2005 when Power reported the first instance of a quintuply bonded complex (Figure 1.6.2b).[118]

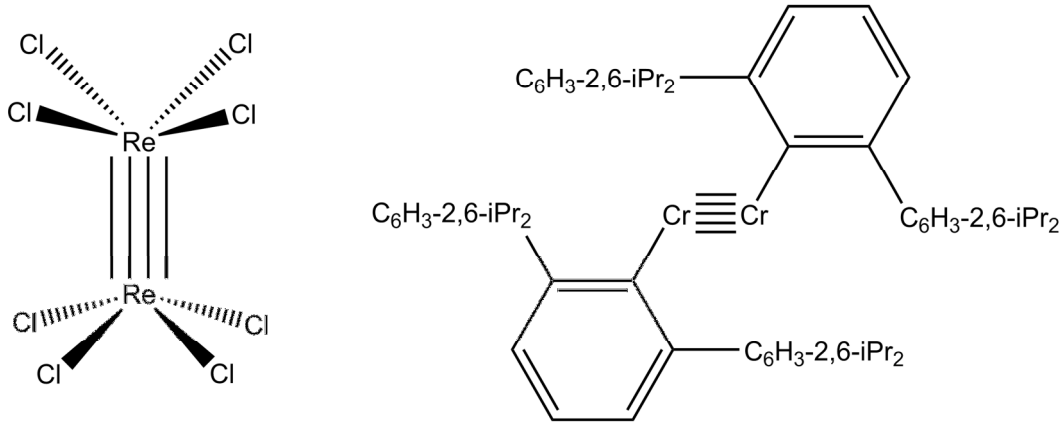

Figure 1.6.2 - a) Cotton's Re_2Cl_8 Quadruple bond; b) Power's dichromium quintuple bond

1.6.2 Multiple bonding

Since the initial description of a formal quadruple bond by Cotton *et al.* in 1964[117] an enormous body of work has been done on a significant proportion of the d block, and beyond resulting in the addition of thousands of novel compounds to the literature. Symmetry dictates that when two transition metals are placed adjacent to one another that you will only observe 5 non-zero overlaps of the d orbitals which collectively allow the formation of up to a quintuple bond. These positive orbital overlaps occur between pairs of equivalent of orbitals on the two atoms, such that where z is defined as the M-M axis is possible to observe: a σ-type overlap between a the pair of overlapping d_z^2 orbitals; 2 π

combinations between equivalent $d_{xz,}$ and d_{yz} orbitals and two δ combinations arising from overlap of d_{xy} and $d_{x^2-y^2}$ combinations. This is shown graphically below (Figure 1.6.3). Overall under Hückel MO theory this would give a nominal $\sigma^2\pi_2^4\delta_2^4$ configuration for a formal bond order of 5. It is only in low coordinate environments such as that observed in Power's dichromium example that this second δ overlap is practically observed.

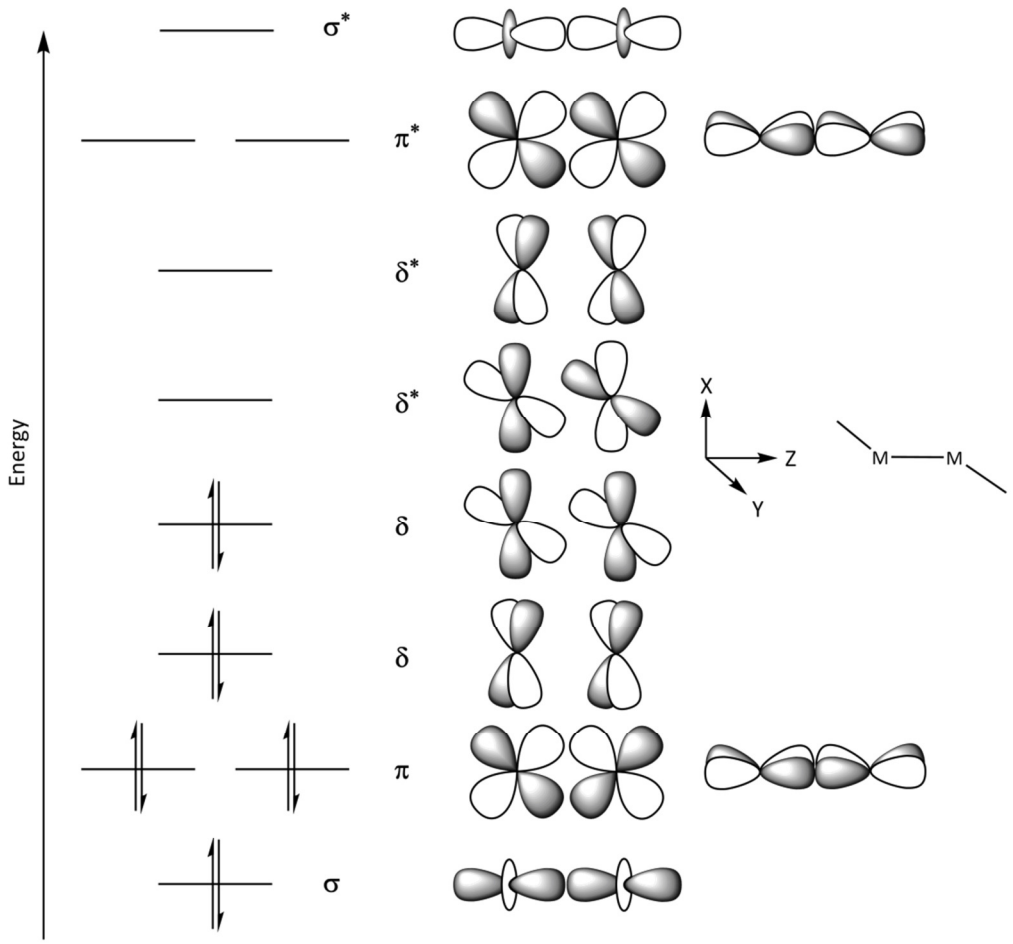

Figure 1.6.3 - Qualitative M_2 2-coordinate MO diagram, of the type reported by Power,

Despite plausible initial expectations of the two δ orbitals to exhibit degeneracy this is not observed in the DFT calculations conducted by Power, who highlighted a 0.41eV energy difference which was attributed to the steric constraints imposed by the ligand backbone.[118]

It should be noted however that the $d_{x^2-y^2}$ combination is simply too high in energy to contribute to M-M bonding at all in many instances and may be omitted from description of the frontier orbitals as is the case for 4 coordinate environments as is observed for Re_2Cl_8 and all paddlewheel type compounds we will report. In this instance the MO description shown above (Figure 1.6.3) is no longer valid and instead MO diagrams of are of the form shown in Figure 1.6.4 below.

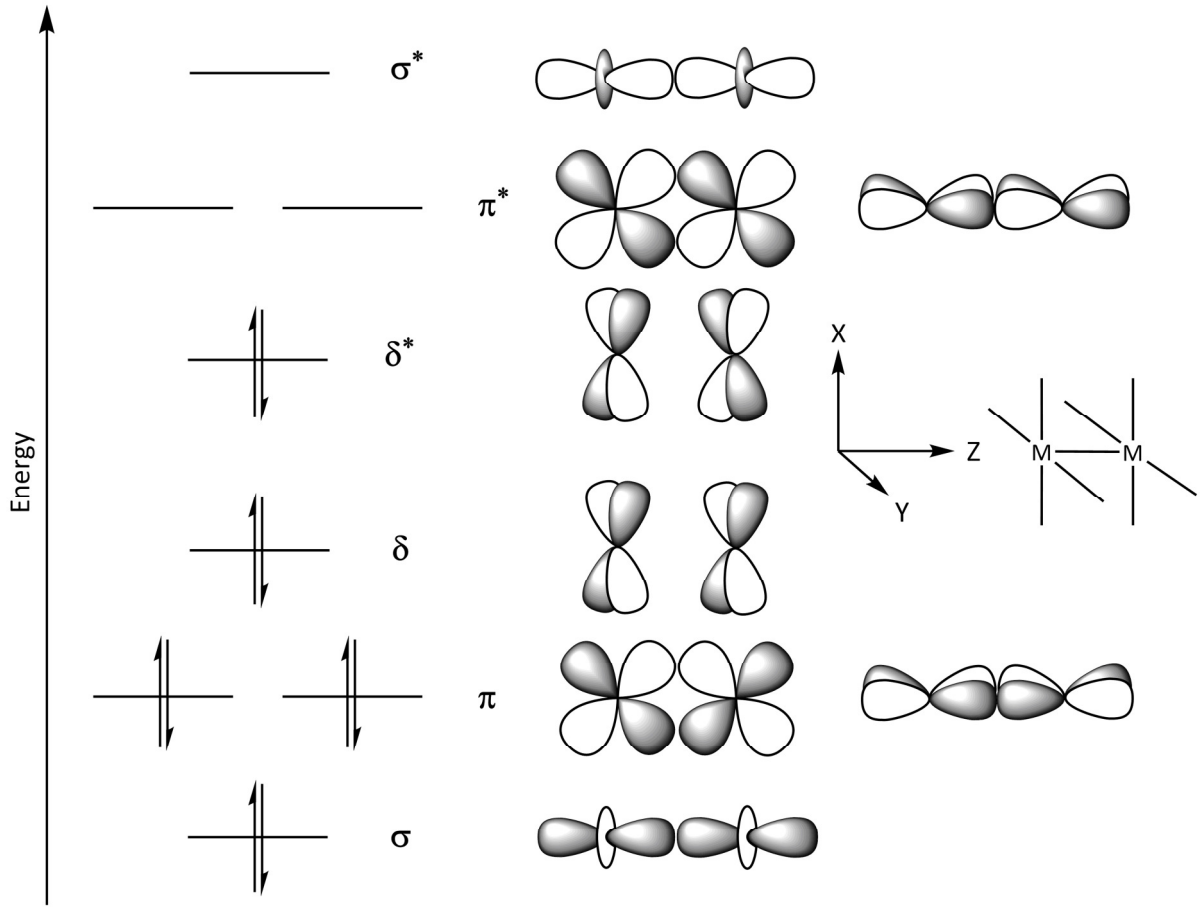

Figure 1.3.4 - A qualitative MO for a typical 4-coordinate paddlewheel type dimetallic complex

Note that in addition to the increased separation observed between the two δ bonding orbital overlaps of pairs of d_{xy} and $d_{x^2-y^2}$, (of which $d_{x^2-y^2}$ is now omitted in Figure 1.3.4), the HOMO is now the anti-bonding combination of the lower energy d_{xz} overlap.

1.7 Diruthenium complexes – Chemistry of the MM bond

As with many dimetal complexes most diruthenium species adopt a paddlewheel configuration (Figure 1.7.1) and whilst many bridged and higher order clusters species are known, ruthenium generally has a more tightly defined range of coordination environments than other 2nd and 3rd row TMs.

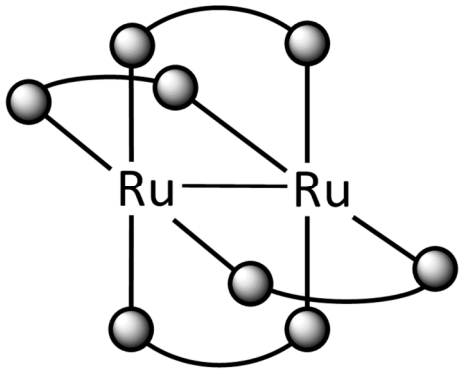

Figure 1.7.1 - Schematic of 'paddlewheel' coordination environment

The structure of these paddlewheel complexes is generally achieved via templation with O-O bridging ligands, typically carboxylates to form a species of the form $Ru_2(O_2CR)_4$ and subsequent ligand metathesis.

1.7.1 Ru_2^{5+} Complexes

The bulk of the prior art with regards to diruthenium chemistry concerns the mixed valence $Ru_2^{II/III}$ state, this is both readily accessible via air stable starting materials via the synthesis of $Ru_2^{II/III}(OAc)_4$ as developed by Wilkinson[119–121] and also represents the most thermodynamically favoured of the available oxidation states.[103,122,123] This stabilisation is derived from the half-filled HOMOs and the near degeneracy of the π* and δ* orbitals which in many instances facilitates a paramagnetic ($\sigma^2\pi^4\pi^{*2}\delta^{*1}$) configuration.

1.7.1.1 O-O bridged complexes – the common starting materials

The first reported example of a $Ru_2^{II/III}$ complex is that provided by Wilkinson[119] for $Ru_2^{II/III}(OAc)_4Cl$. Along with the majority of the early reported examples this consisted of a simple tetra carboxylate paddlewheel complex with a comparatively short Ru-Ru distance of ~2.28 Å.[103,121] A revised synthesis for this complex was provided by Wilkinson in 1973 and may be summarised as below.[120]

$$RuCl_3 \cdot xH_2O \xrightarrow[MeOH,\ reflux,\ 18\ hrs]{LiCl,\ HOAc,\ Ac_2O,\ O_2} Ru_2^{II,III}(OAc)_4Cl$$

As was noted in the initial report by Wilkinson[119] and later confirmed by Cotton[121] these Ru_2 (II/III) complexes formed infinite polymeric, zig-zagging chains in the solid state, forming Ru – Ru – Cl –Ru – Ru bridging interactions between neighbouring dimetal centres (Figure 1.7.2). This arrangement is not notable perturbed by changing the counter ion, however it remains possible to isolate non-polymeric diadduct such as $[Ru_2(O_2CR)_4L_2]X$ where X is a suitably charged counter ion.[124] This is often achieved via reaction with $AgBF_4$ or similar salt to remove the halide, where after other ligands are free to coordinate in the vacant axial positions resulting in the inclusion of axial functionalistaion. Whilst alternative synthetic methods utilising microwave heating have in some instances yielded linear chains, there is a noted thermodynamic drive towards the zig-zag packing arrangement.

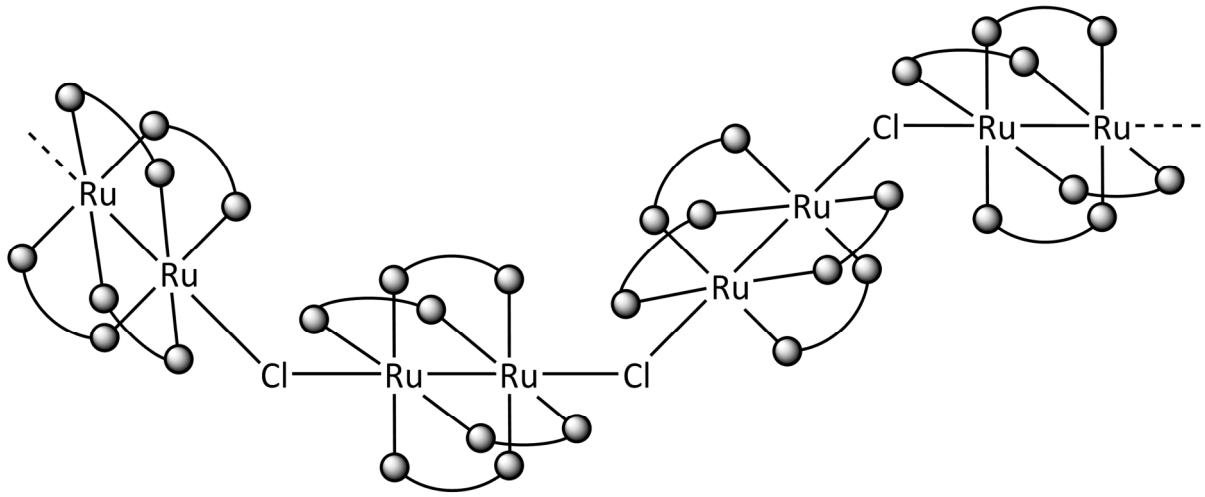

Figure 1.7.2 - Zig-zag packing arrangement observed for $Ru_2^{II,III}(OAc)4Cl$ in solid state

1.7.1.2 N-O Bridged complexes

The synthesis of amidate and hydroxypyridinate (HN(O=C)R) bridge complexes is typically conducted via one of three methods, all originating from the corresponding tetra tetraacetate:

Substitution – As with most dimetal complexes, it is often possible to achieve at least partial substitution of the dimetal coordination environment by ligand exchange facilitated via elevated temperatures. However in the case of weakly binding ligands such as amides this strategy is often ineffectual when conducted in the presence of solvent, especially methanol, which tends to result in disproportionation and decomposition.[103]

Melt reactions – Limited success has been reported when utilising melt reactions with sufficiently unhindered amides such as $Ru_2(HNOCPh)_4Cl$, however this remains ineffective for volatile or bulky ligands.[125–128]

Soxhlet scrubbed substitution – A recent report by the Ren group[129] indicated they had success in thermodynamically driving substitutions to completion via combination of high temperatures and the utilisation of a Soxhlet extraction setup. Such a setup is equipped with a thimble containing K_2CO_3 which act as a scrubbing agent by removing the liberated acetic acid. On cycling the reaction mixture is continually scrubbed of free acetic acid driving the formation of the more weakly bound tetra-amidate.

As with any complexes with asymmetric donor atoms, N-O bridged complexes can adopt up to 4 different structural isomers, however in most instances the preference observed is largely dictated by the steric bulk of the ligand. Substituted hydroxypyridines of the form $Ru_2(Xhp)_4Cl$ (e.g. where Xhp = 2-hydroxypyridine) display a clear preference for the (4,0) isomer (Figure 1.7.3)[128], but where the X substituent is sufficiently bulky the *cis*-(2,2) is readily adopted.[128,130] By contrast amidate complexes such as $Ru_2(HNOCPh)_4Cl$ are almost exclusively trans-(2,2),[126] but those complexes reported lack the bulk to consider the impact of sterics on such a preference.

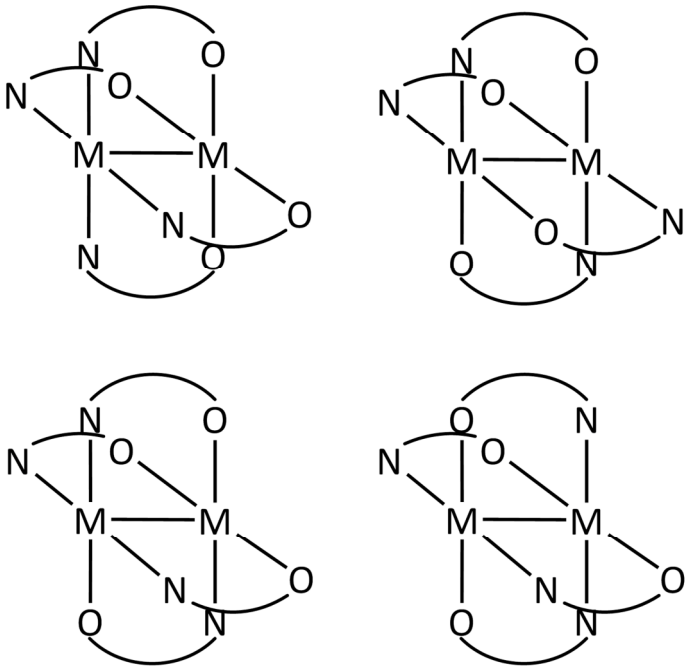

Figure 1.7.3 - Structural isomers, Clockwise from top left: (4,0); Cis-(2,2); (3,1); Trans-(2,2). This notation provides a means by which to indate the directionality of the bound ligand in a given isomer.

1.7.1.3 N-N Bridged complexes

By contrast to N-O bridging ligands, substitution of N-N ligands is easier, and is generally conducted in THF or as melt reactions. Such reactions typically proceed without the need to utilise a Soxhlet extraction setup or other methodology to drive the reaction to completion besides simply heating. The typical $Ru_2^{II/III}(OAc)_4Cl$ starting material used to obtain these complexes affords the required tetra-substituted N-N complex in most instances simply by elevation of reaction temperature to 160 °C for several days. Intermediate levels of ligand substitution can be achieved via moderation of the reaction conditions and reaction stoichiometry.

Non-symmetrical ligands such as amino pyridinates in complexes of the form $Ru_2(Xap)_4Cl$ (e.g. where Xap = 2-(2-methylanilino)pyridinate) which one might expect to exhibit a distribution of structural isomers again show a clear preference (4,0). As steric constraints increase these can be forced to adopt (3,1) readily in spite of this resulting in unfavourable rotation about the M-M axis.[131] Modification of the electron donor/acceptor ability of the ligand has been shown to lead to a distribution of all four isomers as noted for some

perfluorinated derivatives of $Ru_2(F_5ap)_4Cl$ (where F_5ap = 2-(2,3,4,5,6-pentafluoroanilino)pyridinate.[131,132]

1.7.2 Ru_2^{4+} Complexes

By marked comparison to the extensive body of research on mono ruthenium (II) complexes and even those of the related diruthenium $Ru_2^{II/III}$ oxidation state, the chemistry of diruthenium $Ru_2^{II/II}$ complexes is poorly represented in the literature. The highly sensitive nature of diruthenium $Ru_2^{II/II}$ complexes compounds has often been noted as providing a significant barrier to their study.[103,133–135]

Only a comparatively small number of $Ru_2^{II/II}$ compounds are known and many of these were synthesised indirectly from related diruthenium $Ru_2^{II/III}$ complexes. Common methods to achieve this include the use of bulk electrolysis[136,137] or via disproportionation reactions in a poor solvent.[138] Due to the use of indirect, *in-situ* generation however the clean isolation of many reported species was precluded, as was their full characterisation.

Relative to the more robust complexes of $Ru_2^{II/III}$, complexes of $Ru_2^{II/II}$ show significantly greater thermal instability, and in many instances extreme sensitive towards air and moisture.[103,139] Consequently, the synthesis of these reactive complexes presents a number of additional synthetic challenges. The inherent sensitivity and reactively of these species often precludes some traditional post-synthetic purification techniques including column chromatography, largely for practical reasons. The propensity for some samples to interact deleteriously with some commonly used solvents equally frustrates their clean isolation and analysis in some instances.[103,139]

The syntheses of complexes of this form are consequently conducted with very significant emphasis on extensive pre-purification of starting materials and solvents to minimise the potential for side reactions. Additionally the variety of competing interactions present during the formation of dimetallic complexes often necessitates the preformation of the dimetallic unit via the use of substitionally labile templating ligands such as carboyxlates.[134,135] Consequently most synthetic pathways to $Ru_2^{II/II}(L)_x$ complexes are conducted via the preformation of $Ru_2^{II/II}$ tetracarboxylates such as those reported by Wilkinson.[140,141]

Typically whilst quoted as $Ru_2^{II/II}(X)_4$, such complexes may exist as solvates, having great affinity for Lewis bases which readily occupy the axial positions. Ligands or solvents with strong π-acceptor character however have the potential to result in M-M bond cleavage and the generation of unwanted monometallic side products, as often occurs in the presence of PPh_3.[103,133,142,143]

1.7.2.1 O-O bridged complexes – the common starting materials

Despite their common use as starting materials for the synthesis of $Ru_2^{II/II}$ complexes the initial literature precedent for these complexes was the subject of some confusion. Initial publication of the synthesis of $Ru_2^{II/II}(OAc)_4$ by Wilkinson[133] was subsequently shown to be a oxo-decomposition product of the form $Ru_3O(L)_6$ by X-Ray diffraction studies conducted by Cotton & Norman.[142,143] It wasn't until 1984 that the first confirmed example of a $Ru_2^{II/II}$ complex, again that of $Ru_2^{II/II}(OAc)_4$ was reported.[144] Wilkinson's initial synthesis via the $Ru_2^{II/III}$ analogue and 1 electron reduction via a Grignard reagent was then surpassed by a simpler procedure the following year. This method utilised alkali metal salts of the intended carboxylate in conjunction with ruthenium blue.[140] The wide range of potential competing side products[135] and the enigmatic nature of the '$RuCl_2$' 'Ruthenium blue' cluster species from which the target compounds were derived[133,134] was the source of several key publications in earlier years building toward the above synthetic precedent. Attempts however to resolve the structure of 'Ruthenium blue', have to date failed to elucidated significant further information but it is generally accepted to be a cluster anion source of $RuCl_2$.[103,134]

$$RuCl_3{\cdot}xH_2O \xrightarrow[MeOH,\ rt.,\ 3\ hrs]{H_2\ /\ Pt\ Black} \text{'Ruthenium blue'} \xrightarrow[MeOH,\ reflux,\ 18\ hrs]{xs\ NaOAc} Ru_2^{II,II}(OAc)_4$$

Several alternative means of obtaining $Ru_2^{II/II}$ complexes from their $Ru_2^{II/III}$ analogues have also since been published using other reductants such as Zn/Hg amalgams, or in some instances other mild acids. The latter of these has no proven mechanism but, in conjunction with similar reports, is generally presumed to occur via a disproportionation pathway.[103,145,146]

Determining the ground state electronic structure of such complexes was found to be a complex and non-trivial problem. The ground state determined by theoretical calculations utilising differing levels of theory was the subject of several conflicting reports. Attempts to provide supporting evidence in favour of the differing reported ground states via inference from other supporting techniques such as EPR and PES which were similarly inconclusive.[147,148]

Initial calculations under a self-consistent field X-alpha scattered wave (SCF-Xα-SW)[149,150] method contended a general electronic configuration of $\sigma^2\pi^4\delta^2\pi^{*3}\delta^{*1}$,[151] whilst other more contemporary Hartree-Fock (HF) *Ab initio* simulations[147] tended to favour a $\sigma^2\pi^4\delta^2\delta^{*2}\pi^{*2}$ ground state. The later of these more closely correlates with the observed Ru–Ru bond lengths in X-ray crystallographic studies.[152] The source of this discrepancy is perhaps the marked closeness in energy of the δ and π orbitals in these complexes and the differing biases of the methods employed. Further to this the relative energetic stability of these two orbitals is also known to be strongly impacted by ligand field effects.[103]

Attempts to validate either of the above configurations via leveraging alternative techniques are frustrated by inconclusive results. EPR[153] and PES spectra[148] show nothing definitive which may indicate something in of itself however both results could equally be attributed to the large zero-field splitting associated with these species.[140] Variable temperature magnetic susceptibility determination, whilst of proven utility in larger analogues, (such as long chain carboxylates[154]), has to date proven equally non-infomative.[140]

Recent outputs from our group have highlighted the effects of added steric bulk on the ligand backbone and the L-M-M-L bond torsion this can impose. Increased torsion angle was observed to decrease the M-M atomic orbital overlap and results in a shorter than expected M-M bond length. In some instances this was even shorter than that of the corresponding $Ru_2^{II/III}$ analogue.[155–157]

1.7.2.2 N-O Bridged complexes

Synthesis of $Ru_2^{II/II}(NO)_4$ presents the same challenges as with their $Ru_2^{II/III}$ analogues with the additional thermal restrictions inherent to the less thermally robust tetracarboxylate starting material. As $Ru_2^{II/II}(OAc)_4$ more readily decomposes on prolonged heating than its

$Ru_2^{II/III}$ analogue some additional modifications to the synthetic procedure are often needed. A single literature precedent for an NO bridge $Ru_2^{II/II}$ species however that predates even the $Ru_2^{II/II}$ O-O bridged complexes, that of $Ru_2^{II/II}(mhp)_4$, (where mhp = methylhydroxypyridinate). This is however synthesised from $Ru_2^{II/III}(OAc)_4Cl$.[158] Modern synthetic approaches rely on melt reactions utilising an excess of ligand or the use of stoichiometric quantities of alkali metal ligand salts.

Structural isomerism amongst hydroxypyridinate bridged NO complexes is largely dictated but the incumbent steric bulk of the ligand, choosing primarily to favour trans-(2,2) where substituent in the 6- position is large, or polar configurations (4,0) or (3,1) when the substituent is small. In the case of (3,1) configurations the unfavourable interaction between two ligands is mitigated by the axial coordination of solvent in all reported instances.

Very few examples of $Ru_2^{II/II}(NO)_4$ complexes utilising other ligand types are known, and at the time of writing no known amidate complexes have been reported. However, due to the increasing interest in $Ru_2^{II/III}(NO)_4$ amidate complexes in the group of Ren in the application of such complexes to aerobic catalysis, this may soon change.

1.7.2.3 N-N Bridged complexes

The synthesis of $Ru_2^{II/II}(NN)_4$ complexes proceeds via ligand metathesis utilising NN ligands such as amidinates, triazenates and naphthyridines (Figure 1.7.4), and is typically facile at elevated temperatures. The degree of substitution can also be controlled via stoichiometry and moderation of temperature to generate a range of substituted products. Control over the degree of substitution allows further post synthetic modification and inclusion of the dimetal unit in larger arrays or molecular wires. The synthesis of these complexes may be conducted using the alkali metal ligand salt, or in many instances simply via excess ligand which in many instance offers cleaner results. Several of the reported $Ru_2^{II/II}(NN)_4$ complexes in the literature were also generated via bulk electrolysis from the corresponding, markedly more stable $Ru_2^{II/III}(NN)_4$ analogue.

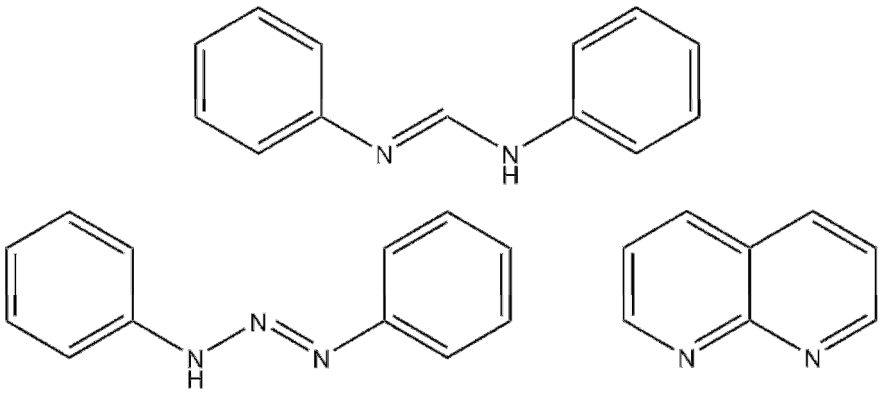

Figure 1.7.4 - Common NN Ligand archetypes, clockwise from top: diaryl formamidinate, diaryl triazenate, naphthyridine

$Ru_2^{II/II}(NN)_4$ formamidinate complexes are diamagnetic having an electronic configuration $\sigma^2\pi^4\delta^2\pi^{*4}$ and exhibit the longest Ru-Ru bond lengths observed for $Ru_2^{II/II}$ paddlewheel complexes, typically ~2.474 Å. In contrast to carboxylate bridged complexes exposure to strong π-acid ligand such as THF and CO does not lead to M-M cleavage and decomposition. Instead these ligands bind strongly in an axial position forming a mono adduct. Ruthenium amidinates have also been shown to display exceptionally air sensitive. The current literature characterisation provided for the only directly synthesised complex of this type, $Ru_2^{II/II}(DFM)_4$, where DFM = (ptol)NCHN(p-tol),$^-$ by Cotton was not able adequately explain this sensitivity.[103,139]

$Ru_2^{II/II}(NN)_4$ naphthyridine complexes have garnered significant attention from the groups of Kadish and Bear who have investigated the structural property relationship between isomers of a range of $Ru_2^{II/II}(NN)_4$ and $Ru_2^{II/III}(NN)_4$ complexes.[159] The $Ru_2^{II/II}(NN)_4$ analogues are generated via melt reactions or prolonged reflux in MeOH so as to cause disproportionation of the (II/III) starting material to corresponding (II/II).[160]

Though only nominally a single atom different, in contrast to the widely reported sensitivity of $Ru_2^{II/II}(NN)_4$ formamidinates, a number of the reported triazenates complexes synthesised have been air stable.[141] Despite their stability in air however such complexes will readily form strong bis-adducts with Lewis bases that exhibit strong π-acceptor character such as NO and CO whilst they remain unreactive towards pyridine and PPh_3.[103]

1.8 Synthetic model systems of complex biologically active metallocenters

Biological systems are typically highly complex in form and operation, as such it is often beneficial to be able to model them with simpler synthetic inorganic complexes. This allows us to better understand their mechanistic operation, and ideally, to replicate their function.[161,162]

Simple, small molecule model systems serve a range of functions and are often far easier to probe spectroscopically and study than their natural parent systems. Small molecule analysis being inherently less complex than that of the study of an entire enzyme or its wider protein supported structure which may be several hundred times the size. Small model system allows greater flexibility in both their design and synthesis allowing the rapid evaluation of steric, electronic and ligand environment effects on the modelled metal core. As a result of the wide range of potential applications for such models, they are generally divided into one of three types, depending on their intended purpose.[163]

1. 'Speculative models' allow the inference and deduction of structural or compositional data of a given biological system by comparison of available spectroscopic data with that obtained for the model complex.[164,165] This approach is of particular importance where a crystal structure for a given protein or enzyme is unavailable or the identity of the active species is otherwise unknown.
2. Similarly, once the structure of a biological system's active site is known, 'corroborative models' allow for the further examination and elucidation of structure-activity relationships within the site.[165–167] This often allows further investigation of coordination, orientation and solvation effects on activity and active species stability.
3. The third class of synthetic model system is the 'functional mimic'; such models are often the culmination of extensive modelling work, combining mechanistic and structural information to design a model that replicates the functionality of a biological system. These models will often be markedly different and more complex than speculative or corroborative models, as to achieve functionality it is often necessary to consider the influence of the wider protein or enzyme environment. To

that end influence outside of the first/second coordination sphere need be considered and the model adapted accordingly.

1.8.1 Ruthenium as a functional mimic of biological Iron

When designing functional mimics, it is often preferable to include some degree of metallocenter isolation however, the use of suitable sterically demanding ligands can itself result in a marked decrease in catalytic activity due to poor substrate diffusion into the active site.[168–170] One alternative to this approach is to reduce the steric demand of the ligand system and substitute the metal cofactors for chemically related but less reactive alternatives. This then affords the potential for greater catalytic activity by better allowing substrate access. Given the periodicity of elements the selection of appropriate substitutes is trivial, with 2nd row transition metals generally being the substitute of choice. Second row transition metals often represent a suitable mid-point between catalytic activity and stability, showing a greater degree of kinetic inertness than periodically related first row metals. This enables complexes of 2nd row transition metals to often display a degree of catalytic activity but under less rigorously shielded conditions than required for their first row equivalent. These models then allow the elucidation of the structure-property and electronic structural information that may in turn be used to infer the probable behaviour of periodically related species. Such an approach is of particular utility where the first row transition metal species and its related intermediates are either insufficiently stable for *in-situ* analysis or which are spectroscopically silent.

1.8.2 Catalytic RuNi mimic of FeNi system – Informing mechanistic and structural design

A particularly good example of metal cofactor substitution in a functional mimic can be found in recent work by Ogo.[171] He and his collaborators reported a [RuNi] hetero dimetallic functional mimic of the [FeNi] hydrogenase active site as found in *Desulfovibrio gigas (D. gigas),* a subspecies of the gram negative sulphate reducing genus *Desulfovibrio*.[172] Species such as this have been of interest for their ability to couple the reversible oxidation of molecular hydrogen to other process via various Ferredoxin cofactors. It is hoped such hydrogenases may represent a potential future means of more efficient hydrogen

production.[163,172] Since the solution of the X-ray crystal structure of the hydrogenase from *D. gigas,*[173] a significant number biomimetic complexes have been synthesised. The particular significance of the work reported by Ogo *et al.* is that, whilst direct FeNi functional mimics initially proved elusive, by adaption of the model mimic to include Ru his showed catalytic activity.[171] This became the impetus for a renewed effort towards understanding the mechanistic underpinning of the means by which this functional mimic operated. Several subsequent DFT studies probing its structure provided significant insight into the how the electronic structure of this mimic enables its functionality.[174–176] Not only did the initial model provide the base for iterative improvement of Ogo's mimic[174,177] but the subsequent studies eventually led shortly thereafter to a number of iron based FeNi mimics that showed partial functionality themselves.[178,179]

1.9 Methane monooxygenase

As with many useful chemical processes, the partial oxidation of methane to methanol is a well-established process in nature. This particular process is known to occur in a range of methanotrophic bacteria that are commonly found in largely anaerobic sediments in stagnant water. These bacteria utilise methane evolved from biomass decomposition as their primary means of energy uptake.[25] *Methylococcus capsulatus* (*M. Caps.*) is a prominent and well-studied example of such a bacterium which utilises methane in this way, providing its sole source of nutritional carbon. The internal conversion of methane to methanol provides both a source of energy by its further oxidation to CO_2, and also as a means of internal energy storage.[180]

Methanotrophs such as *M. capsulatus* achieve the initial conversion of methane to methanol by use of an enzyme called methane monooxygenase (MMO), which facilitates this reaction under ambient conditions. MMOs are part of a larger class of enzyme termed bacterial multi-component monooxygenases (BMMs) which have been of particular scientific interest for their potential use in a range of biocatalytic and biodegradation applications.

1.9.1 Enzyme structure

Methane monooxygenase itself is known to exist in two discrete and differing forms; the particulate membrane bound form pMMO, and the soluble form sMMO. The X-ray crystal structures of both forms have been solved, revealing a hydroxyl bridged non-heme diiron(III) active site in sMMO[26] (Figure 1.9.3) and what is thought to be a dicopper core[181] in pMMO.[182] Due to the inherent difficulty of isolating pMMO and the limiting resolution (2.8 Å) obtained in the better of the two reported crystal structures, the exact identity of the active site in pMMO remains unknown and highly contested. Many differing metal cofactor configurations have been proposed including mono-,[183,184] di-,[185] and tri-nuclear[186,187] copper in addition to a number of Fe/Cu mixed clusters.[188,189] More recent developments in the field have tended to give credence to the proposed dicopper core model as being the most accurate of the models proposed,[190,191] however this research is still very much on-

going. As we are primarily concerned with sMMO however this shall not be covered further in this review.

1.9.1.1 sMMO structure and operation

Structurally sMMO, as with other BMMs, consists of a number of distinct protein subunits each with a distinct function: a hydroxylase (MMOH), a nicotinamide adenine dinucleotide (NADH) reductase (MMOR), and a regulatory protein (MMOB).[192] The structure of sMMO is dominated by MMOH, itself consisting of a dimer of three distinct polypeptide chains. The chains dubbed αβγ form a hemispherical, handed motif with the larger αβ chains pointing outward from the coiled γ chain. Two sets of these motifs are then joined α-α and β-β forming an overall pseudo spherical motif with both of the diiron containing α sections the located on the same face with the regulatory protein MMOB (B) and reductase MMOR (R) able to bind as indicated below (Figure 1.9.1).[193]

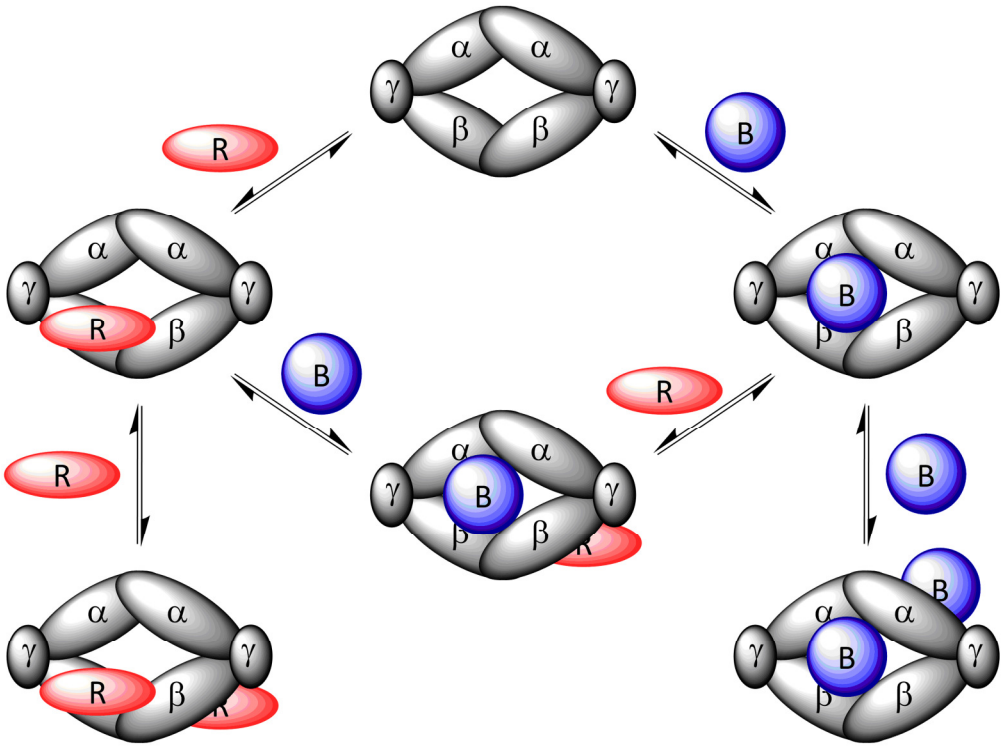

Figure 1.9.1 - Half sites mechanism and structure of sMMO; Hydroxylase MMOH (grey), NADH reductase MMOR (red) and regulatory protein MMOB (blue).

In order to facilitate the intended partial oxidation it is necessary for the various component subunits to bind, process and shuttle all four of the required substrates: hydrocarbons, dioxygen, electrons and protons. This control is achieved and facilitated by the complex interplay between the enzyme subunits' relative binding affinities and cooperative effects.

The structure of MMOH for example is such that redox processes in the α polypeptide unit, such as the reductive activation of the diiron core from Fe(III) to Fe(II), strain the protein framework in such a way that other remote areas of other bound protein subunits may undergo partial re-arrangement. This re-arrangement then serves to selectively gate the entry of the larger substrates toward the active diiron core.[194] Equally subtle changes can affect inter-subunit binding affinity such that protective temporary binding between subunits may occur to establish and stabilise intermediate charge separated states. This, for example, allows the temporary storage of the substrate electrons in MMOR. Electrons are initially obtained from NADH oxidation at a [2Fe-2S]-ferredoxin (FD) cofactor, itself bound in a flavin adenine dinucleotide (FAD) cofactor. The consumption of these electrons is coupled to hydrocarbon oxidation by the requirement of MMOB to be bound to MMOH. This facilitates the structural changes in MMOH required for the shuttling of electrons from MMOR-FAD to the active site in MMOH.[195,196] There are two main proposed schematic explanations for the inter-subunit binding behaviour required to achieve this: the half sites model (Figure 1.9.1) and the non-interacting sites model (not shown).[197]

Once the various required substrates have been obtained and suitably delivered to the diiron active site in the α-chain of MMOH, the catalytic partial oxidation may proceed. The proposed catalytic cycle for this overall process is shown overleaf (Figure 1.9.2).

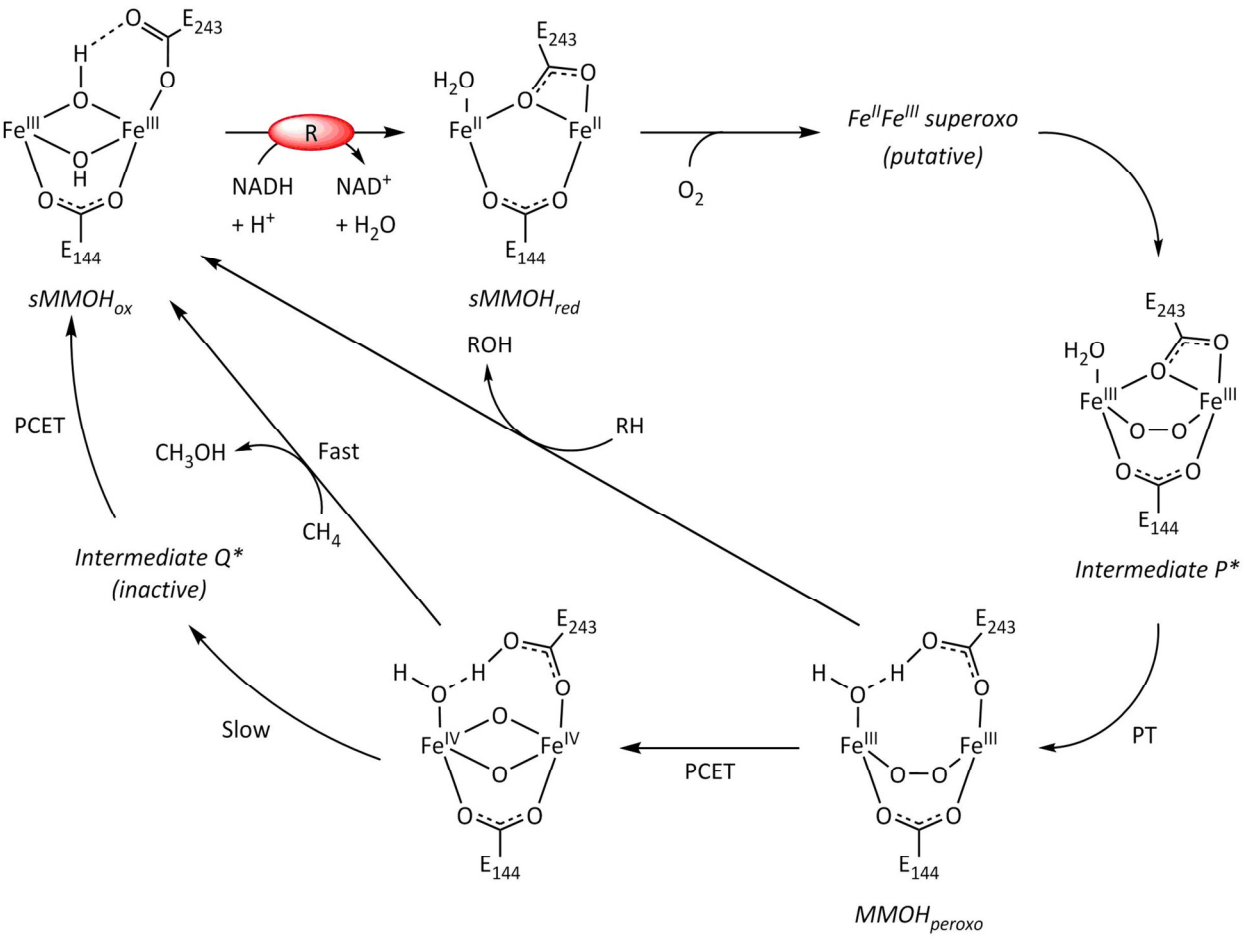

Figure 1.9.2 - Proposed mechanism for sMMO catalytic cycle. R indicates involvement of MMOR and at each step the regulatory protein MMOB is either bound or required to be (re)bound to MMOH in order for the cycle to progress. PCET – proton coupled electron transfer

In its resting, oxidised state ($MMOH_{ox}$) the diiron core, is (μ^2-OH)$_2$ bridged; upon reductive activation and the binding of MMOR the active species $MMOH_{red}$ is formed and it is only this activated form which exhibits reactivity towards dioxygen. The two labelled intermediates Q and H_{peroxo} (also known as intermediate P) meanwhile perform the actual oxidation of the alkyl substrate. These two intermediates have been of particular interest to researchers as they both display very differing chemistry. Intermediate Q is known to be the active species with respect to methane,[198–200] whilst other hydrocarbon substrates (e.g. Et_2O) are known to interact only with P.[201] Despite many years of research however, many elements of the mechanism by which this cycle proceeds, including the means by which the O-O bond in dioxygen is cleaved, are not yet fully resolved.[202] Recent modelling studies on this particular point do suggest however, that such a cleavage is most likely homolytic.[203,204]

1.9.2 Active site coordination environment

Beyond the functional operation of the enzyme, of particular interest to many chemists is the geometry and arrangement of the diiron core coordination environment. It is hoped that through understanding and suitably mimicking this environment it may then be possible to replicate a degree of catalytic activity using small, non-protein bound catalysts under ambient conditions. This is a major goal in this field of research, as such developments could potentially revolutionise industrial methanogenesis, negating the need for the highly energy intensive processes currently employed such as SMR (Section 1.3).

Both sMMO,. and other related BMMs such as ribonucleotide reductase (RNR) and the Δ^9 stearoyl-acyl carrier protein Δ^9 desaturase (Δ^9 D), have very similar active site coordination environments: all containing a diiron core ligated by two histidine imidazole rings and four carboxylates. Despite this however the coordination environments of these BMMs are clearly distinct with the metals exhibiting differing coordination numbers and often ligated by a varying number of water and hydroxide ligands; carboxylate binding modes may also change from bridging to chelating in differing conditions.[205] In the case of MMOH, the hydroxylase component of sMMO this environment is as shown below (Figure 1.9.2).

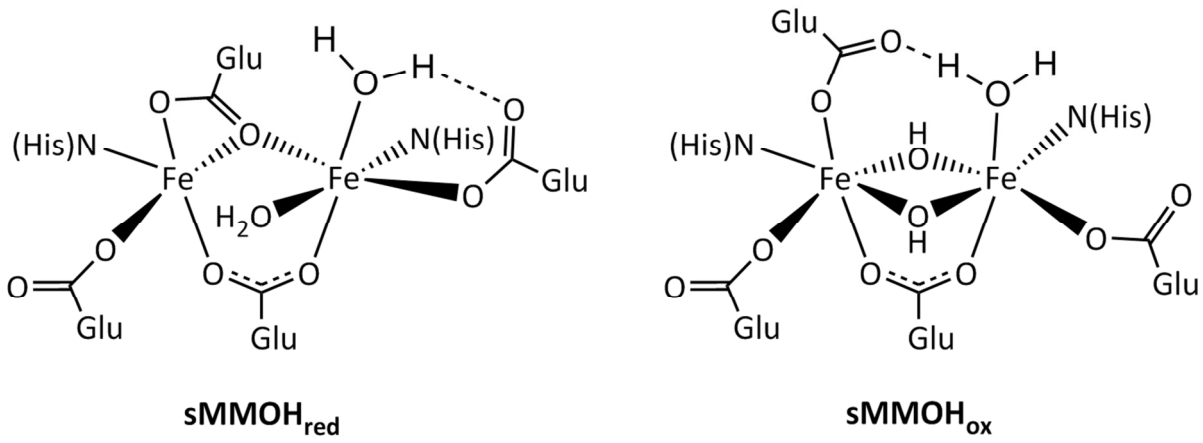

Figure 1.9.3 - Active site coordination environment of MMOH (M. Caps) in the active reduced form (a) shown left, and inactive oxidised form (b) shown right.

Crystal structures of two forms of sMMO are known that, that observed in *M. Caps.* and in the closely related methanotrope *Methylosinus trichosporium OB3b (M. Trich.).* The determination of the coordination environments of their active sites has enabled the synthesis of a range of model diiron complexes with a view to better understanding their functional operation.

1.10 Iron complexes designed as MMOH mimics

1.10.1 Diiron carboxylates

One of the most numerous classes of early MMOH mimics is based on iron carboxylate complexes. These were synthesised under mild conditions by combination of an appropriate source of Fe^{2+}, typically as a metal salt, with an alkyl metal salt of the intended carboxylate under strictly anaerobic conditions. Given the labile nature of carboxylate ligands and the rapid kinetics of ligand exchange observed however, it was quickly discovered that poor ligand selection lead to a range of unwanted monomeric and polymeric products. In order to successfully synthesise diiron (II) systems, the associated steric bulk of the ligand requires tight control.

Very bulky ligands *m*-terphenyl ligands e.g. 2,6-bis(4-tert-butylphenyl)benzoate, (Figure 1.10.1 – Bottom left), may only generate monomeric species as their bulk precludes the formation of larger species. In contrast sterically undemanding ligands such as benzoate, (Figure 1.10.1 – Bottom right), tend to form polymeric chains. Without any significant steric constraints there is no means to control nuclearity.

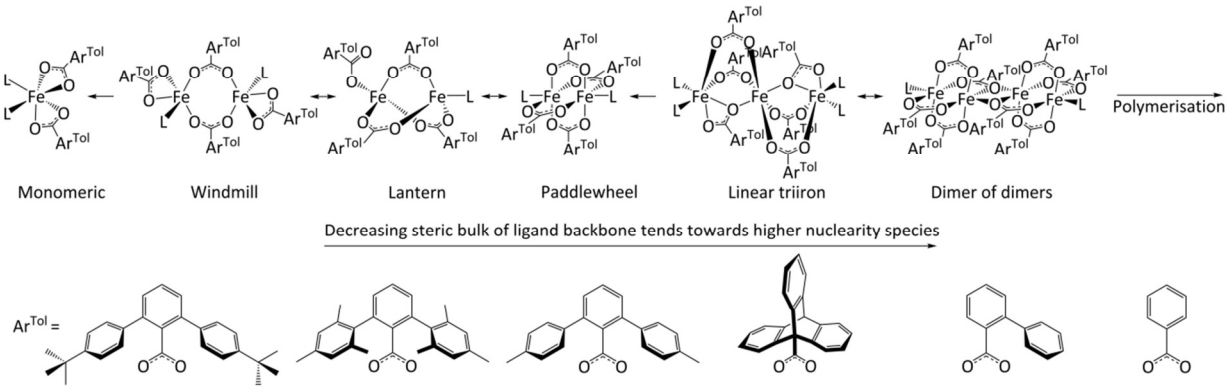

Figure 1.10.1 - Effect of carboxylate steric bulk on nuclearity of Iron carboxylate complexes.

The more interesting species however are formed by ligands of intermediate bulk, often forming a mixture of structures with differing connectivity. Of those structures formed, the paddlewheel complexes formed using less-hindered *m*-terphenyl ligands was noted to provide the most promising model. The coordination environment of such complexes resembles the first coordination sphere of the MMOH core (Figure 1.9.3), whilst the bulk of the ligands provides significant degree of encapsulation to the dimetal centre. In so doing

such complexes partially replicate the hydrophobic pocket observed in nature around the diiron core in the protein interior.[206] Attempts to synthesise these complexes generally resulted in a mixture of the windmill, triply bridged and paddlewheel structures and it was found that these may interconvert in solution via carboxylate shifts showing both dependence on the axial donor ligands (L) and temperature, with the paddlewheel being preferred at lower temperatures (Figure 1.10.2).

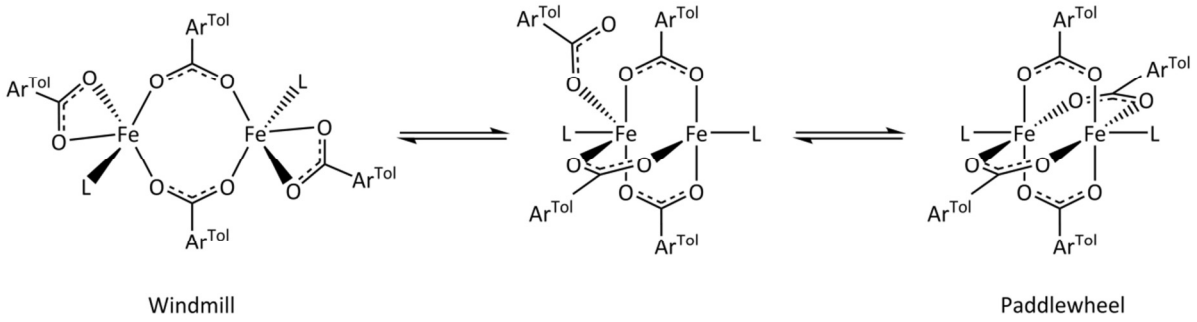

Figure 1.10.2 - Inter-conversion of $Fe_2(O_2CAr^{Tol})_4L_2$ (where e.g. $[O_2CAr^{Tol}]^-$ =2,6-diphenylbenzoate) between three differing structures via carboxylate shifts. Note that the centre configuration differs from the discrete trigonal lantern conformer shown previously in Figure 1.10.1 which represents a more fundamental reconfiguration.

The ability to perform carboxylate shifts is critical to the rearrangement of MMOH to accommodate dioxygen (Figure 1.9.2) which in addition to formation of high valent Fe (IV) species on reaction with oxygen both serve to further validate the use of $Fe_2(O_2CAr^{Tol})_4L_2$ systems as a model of MMOH.[205]

1.10.2 Specialised diiron carboxylate MMOH mimics

One of the complications in both understanding and modelling systems like MMOH is the variability inherent to the structures in question. The core of MMOH, buried deep in the protein, exists in a highly ordered environment which is extremely difficult to accurately replicate in a naked complex. Often there are only subtle changes that differentiate active sites in otherwise functionally disparate BMMs. Such changes within the primary coordination sphere may include: hydration, overall hydrophobicity, carboxylate binding mode, relative geometry, spacing, coordination number and protonation site occupancy. In the primary coordination sphere of naked model complexes it remains possible to exert some degree of control over such factors, albeit to a far lesser extent that is possible within a structured protein. This may be achieved either through ligand pre-organisation or

modification of synthetic procedures. Structural and electronic contributions from the wider protein environment however are much harder to model or control without over-complicating ligand design. The following sections explore a number of examples where one of more of these considerations been addressed.

1.10.2.1 Effects of complex hydration

The addition of water to a model system of the form $Fe_2(O_2CR)_4$ (where R = Ar^{Tol}, or $Ar^{FPh)}$ has been shown to act to quantitatively shift the equilibrium between the three available isomeric forms of such complexes (Figure 1.10.2) strongly toward the windmill configuration. This inter-conversion is thought to be facilitated via carboxylate shifts induced by H_2O coordination.[207–209]

The action of H_2O in enabling rapid ligand exchange and coordinative reconfiguration additionally has a profound effect on the reaction kinetics observed with target substrates e.g. O_2.[210] Complexes of the form $Fe_2(O_2CR)_4L_2$, (where R = as above; L = 4-cyanopyridine or 4-acetylpyridine) may be formed in when using the respective pyridines as solvents. These show a similar bias towards the windmill configuration even in anhydrous conditions enabling the effect of hydration to be determined

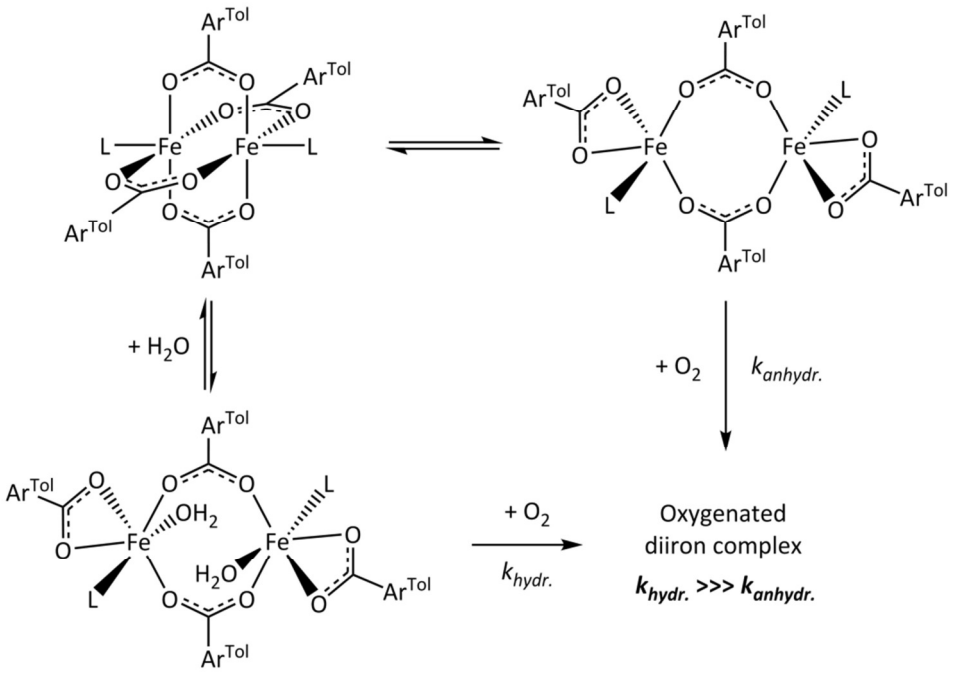

Figure 1.10.3 – The impact of hydration on the rate of dioxygen activation.

Kinetics experiments following the rate of oxygenation of these complexes may be monitored by observation of the intensity of the associated metal to ligand charge transfer (MLCT) band in the UV-vis region. Such studies show that water exposure had the effect of increasing the rate of oxidation by an order of magnitude relative to the anhydrous control (Figure 1.10.3).[210]

1.10.2.2 Protein environment mimics

In addition to providing the exact conformational and structural environment for metallocenters to perform their required function, proteins provide a protective, encapsulating shield that protects the reactive dimetal core. Without this shield, as is often observed with attempts at synthesising functional mimics, these metallocenters may undergo deleterious hydrolysis or polymerisation reactions leading to their subsequent deactivation or decomposition. This can to an extent be alleviated through diligent and deliberate choice of ligand *(vide supra)*, however such ligands often only serve to loosely shield the immediate core. Even then such shielding may also be negated when the model complex is able to interconvert into differing, less well shielded conformations as is the case with *m*-terphenyl carboxylates (Figure 1.10.3).

In order to improve upon the shielding afforded by existing *m*-terphenyl ligands it becomes necessary to increase the overall size of the ligand, building outward from the central *m*-terphenyl motif. Increasing the steric bulk of such ligands however is not without issue, practicably only the central phenyl ring of the *m*-terphenyl unit may be modified as modifications to the pendant phenyl rings causes a marked preference toward mononuclear Fe species (See Section 1.10.1). The addition of excessive steric bulk, in addition to introducing solubility issues, also has the potential to place significant steric constraints on the active metallocenter. In some instances this may effectively deactivate the complex by forbidding the conformer inter-conversion (Figure 1.10.2) required for catalyst activity. Consequently, a degree of flexibility in the added steric bulk was noted to be a critical requirement.

Engineering flexible bulky ligands to encompass the dimetallic core does however have serious downsides. Unlike a protein which may gate substrate access to the active site at the

dimetal core such behaviour cannot be achieved easily in smaller molecules. As such, the use of very bulky ligands may also unintentionally shield the dimetal core from intended substrates, severely hindering overall catalyst operation and utility. A balance between these competing considerations is then necessary in order to achieve a workable compromise.

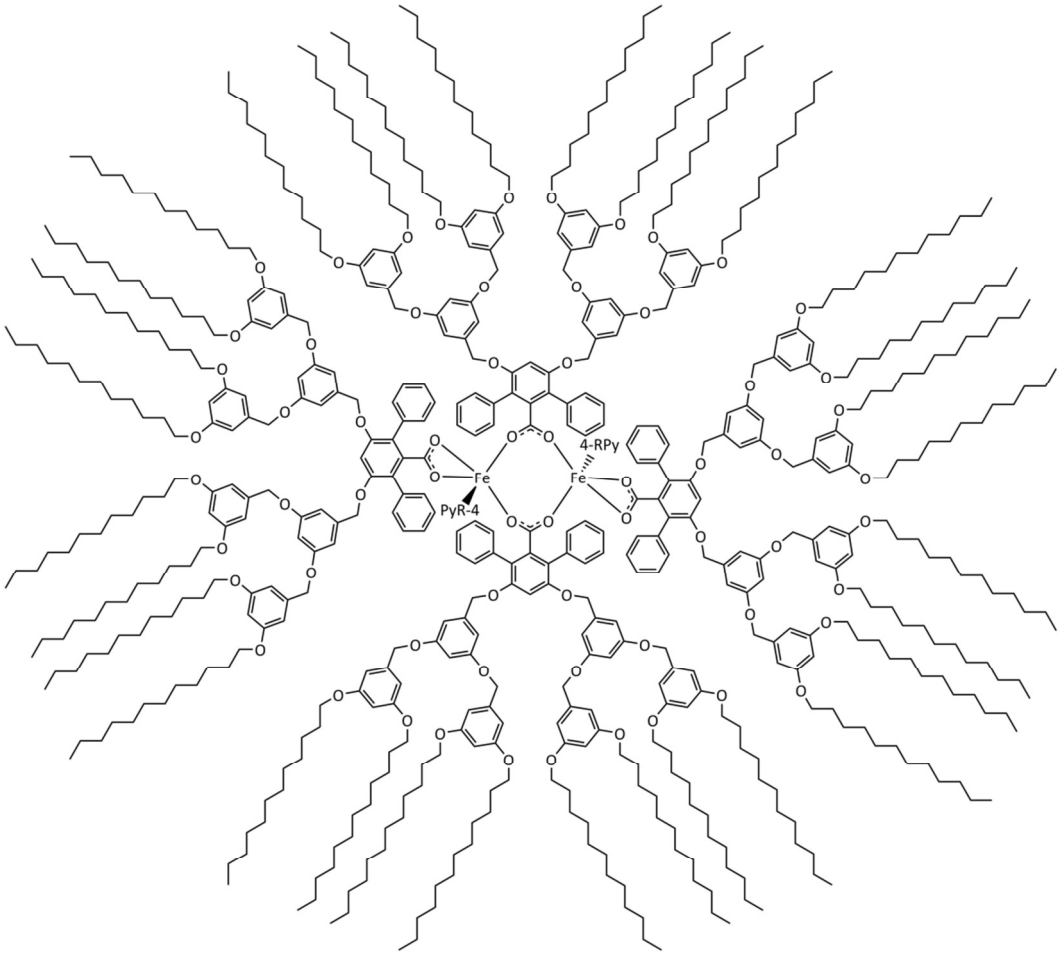

Figure 1.10.4 – Structure of $[Fe_2(\mu\text{-}O_2C\text{-}[G3])_2(O_2C\text{-}[G3])_2(4\text{-}RPy)_2$ where O_2C-[G3] = 3,5-bis[[3,5-bis[(3,5-didodecoxyphenyl)methoxy]phenyl]methoxy]-2,6-diphenyl-benzoate, a third generation dendritic poly(benzylether) ligand as developed by Lippard *et al.*

One class of molecules which presents an attractive option as shielding ligands are dendrimers. Such ligands have been of proven utility in the modelling of other haem enzymes[169] and have been increasingly used in modelling of non-haem systems[170] including sMMO.[168] The inherent flexibility, both in their physical structure and in the variability of their construction make these incredibly useful ligands. They readily facilitate catalytic activity and whilst still allowing some substrate access,[211] and even stabilise some otherwise unstable intermediates and oxygen adducts.[212]

Lippard *et al*. in particular championed the application of dendritic ligands (Figure 1.10.4) to Fe carboxylate MMOH mimics, synthesising a number of dendritically encapsulated versions of earlier reported *m*-terphenyl complexes with a view to studying the effects of such encapsulation.[168] As expected, whilst the dendritic shell markedly affected the oxygenation kinetics, decreasing the rate of gas uptake by over 300-fold,[168] the resultant oxygenated superoxo- adduct was significantly stabilised. In the naked complexes such intermediates are often too unstable to be detected via standard spectroscopic techniques. In contrast this method afforded oxygenated species that were stable indefinitely below -5°C. This facilitated characterisation of the generated intermediate *in-situ* via: Mössenbauer, UV-vis, Electron paramagnetic resonance (EPR), and X-ray absorption techniques. The ability to observe such oxygenated intermediates is of critical importance to the synthetic model chemist as their identification and characteristic spectra provide significant insight to the mechanisms by which natural systems may proceed.

1.10.3 Catalysis with carboxylate mimics

Despite the availability of a number of methodologies to obtain spectroscopically observable oxygenated species of the general form $Fe_2(O_2CR)_4L_2$ *(vide infra)*, the use of such species for bulk catalysis has yet to be satisfactorily demonstrated. Whilst a number of published examples of oxidative behaviour for these species have been reported to date, these either involve the use of incorporated substrates as part of the overall ligand framework or proceed via stoichiometric rather than catalytic means.

There are a number of reasons posited, pertaining to both steric and electronic considerations, for the elusive nature of such expected catalytic behaviour. The main steric argument suggests that substrate access is either largely hindered by the ligand shell or that, where such access is possible, the rate at which it occurs is insufficient to achieve catalytic activity prior to high valent Fe (IV) re-oxidative decomposition. Additionally, an electronic argument posits that intermolecular electron transfer in the bulk state may have the effect of largely quenching the population of the active species on a prohibitively short timescale, thereby eliminating the possibility of catalytic activity.

In order to investigate the oxidative properties of species such as $Fe_2(O_2CR)_4L_2$ a range of suitably substituted N-donor ligands (L) were devised including N,N-dibenzyl-ethylenediamine[213] (A) and a range of ortho substituted pyridines[214,215] (B) and their oxidative properties investigated (Figure 1.10.3).[216]

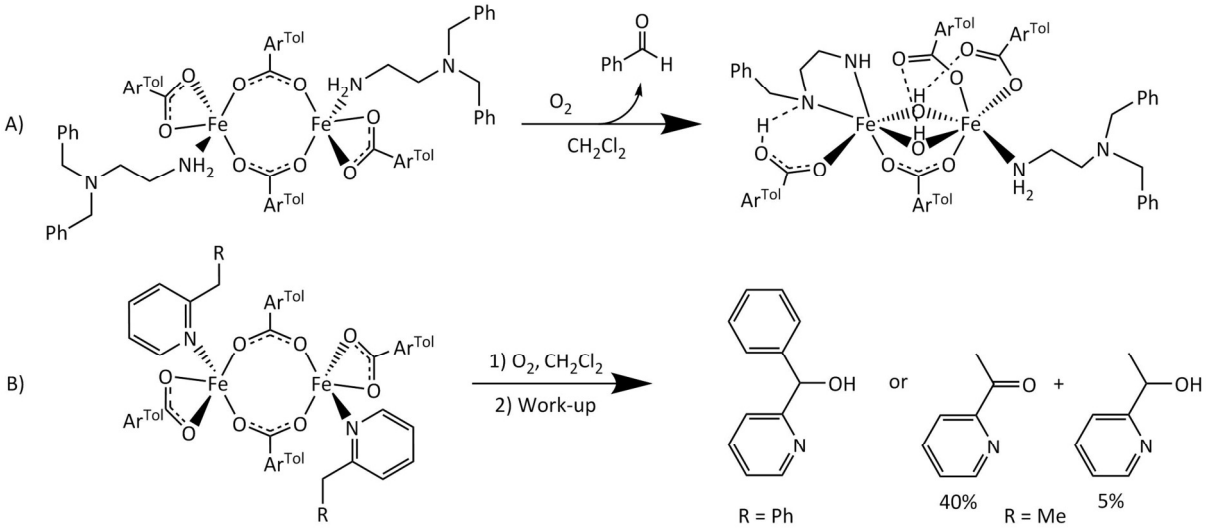

Figure 1.10.5 - Partial oxidation and C-H activation of ligand tethered substrates.

From these studies it was observed that the degree of substrate oxidation was primarily dependent on the proximity of the substrate to the diiron core. A marked decrease in yield was observed for systems substituted in the meta and para positions of the pyridyl ligand. Additionally it was observed that the use of sterically equivalent, but more electron-donating carboxylate and pyridyl ligands, increased the degree of conversion. This would indicate that such modifications may be required to better stabilise a particularly electrophilic intermediate.[214–216]

1.10.3.1 Other related examples of catalytic behaviour

Whilst bulk catalysis with non-bound substrates has not been forthcoming, a number of closely related complexes have displayed novel catalytic properties. For example it was noted that of the early mixed carboxylate and pre-organised N-donor backbone diiron complexes $[Fe_2(\mu\text{-}OC_2CAr^{Tol})_2(Me_3TACN)_2](OTf)_2$ (where TACN = 1,4,7-trimethyl-1,4,7-triazacyclononane) displayed what was initially thought to be bulk catalytic oxidation. This however was not the case; instead a novel means of coupling the catalytic conversion of aryl

phosphines to their corresponding oxides and the catalytic ring-opening of THF was discovered (Figure 1.10.6).[217]

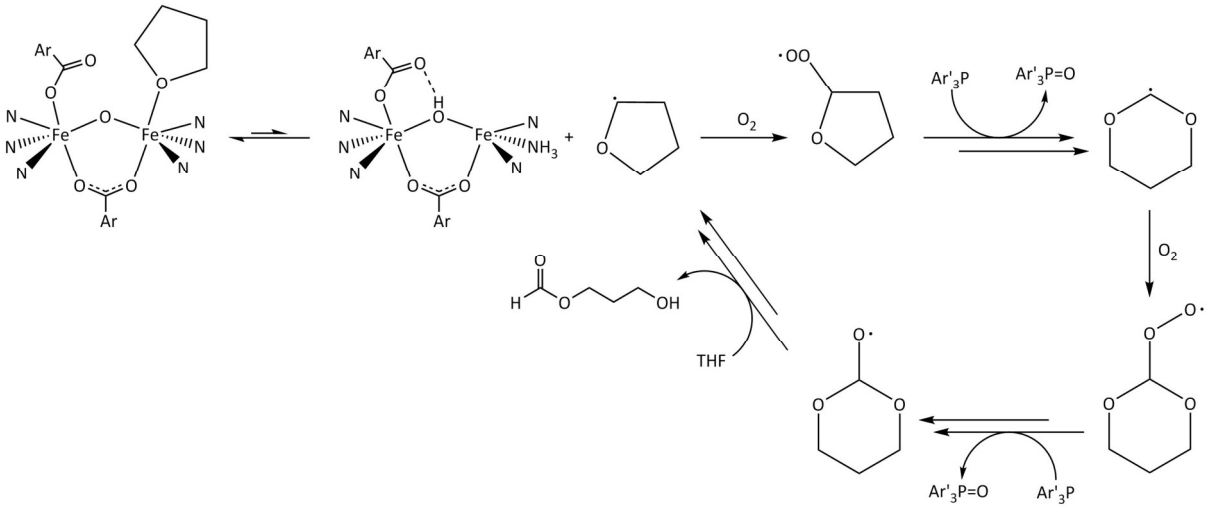

Figure 1.10.6 - Catalytic cycle for the coupled oxidation of aryl phosphines and novel ring-opening of THF

In so far as catalytic oxidative behavior of related species is concerned, save bound substrate models the closest reported example is that of a related triiron complex also reported by Lippard. This complex facilitated the catalytic conversion of cyclohexane to cyclohexanol, but initial studies indicate that the observed triiron cluster was itself not the active species.[218] The search for this elusive active species however formed the prelude to Lippard's later work on sMMO and related mimics.[219]

1.10.4 Diiron complexes containing pre-organised N-donor ligands

Whilst a significant number of diiron carboxylate complexes have been reported in the literature over the course of several decades of research into sMMO, there are relatively few examples of complexes containing predominantly N-donor ligands. MMOH itself contains only two N-donor imidazole ligands coordinated to its dimetal core (Figure 1.9.3). Consequently, most attempts to model MMOH have been restricted to the use of tetra-carboxylates and weak, typically functionalised pyridyl, N-donor ligands.

The inclusion of additional N-donor ligands results in complexes which are no longer strictly biomimetic with respect to MMOH and such complexes often show markedly different structural, spectral and electronic properties. These bioinspired complexes exhibit differing

coordination stoichiometry, relative orientation and geometry of their dimetal cores whilst ligand coordination through a less electronegative atom (N cf. O) results in markedly different molecular orbital (MO) energies, and by consequence ground states of different configurations.[220]

Changes in the distribution and population of MOs can result in a preference for low-spin iron complexes and intermediates (cf. high-spin iron as observed for carboxylate rich mimics and MMOH itself).[219,221] The observed change in spin markedly affects the chemistry of such complexes, leading to the formation of intermediates not observed for carboxylate rich complexes including the closest known synthetically derived analogue of MMOH intermediate Q.[219,221] In addition to the observation of this mechanistically important intermediate such complexes, despite their differing spin states and non-biomimetic structure, remain the only class of MMOH inspired models to achieve C-H and O-H activation and partial oxidation of small molecule substrates.[219]

1.10.4.1 Models of key intermediates synthesised using pre-organised N-donor ligands

In 2007, Xue and Que Jr. *et al.* reported a significantly more active biomimetic model of sMMO. The study of this model complex showed it to closely approximate the proposed electronic structure of intermediate Q in the catalytic cycle of sMMO (Figure 1.9.2). Initially this then saw the development of a synthetic precedent for the diamondoid $Fe^{II,II}_2(\mu\text{-}O)_2$ core that was proposed via bulk electrolysis of a secondary species and using substituted tris(2-pyridymethyl)amine (TPA) ligands giving the overall motif show below (Figure 1.10.7).[221]

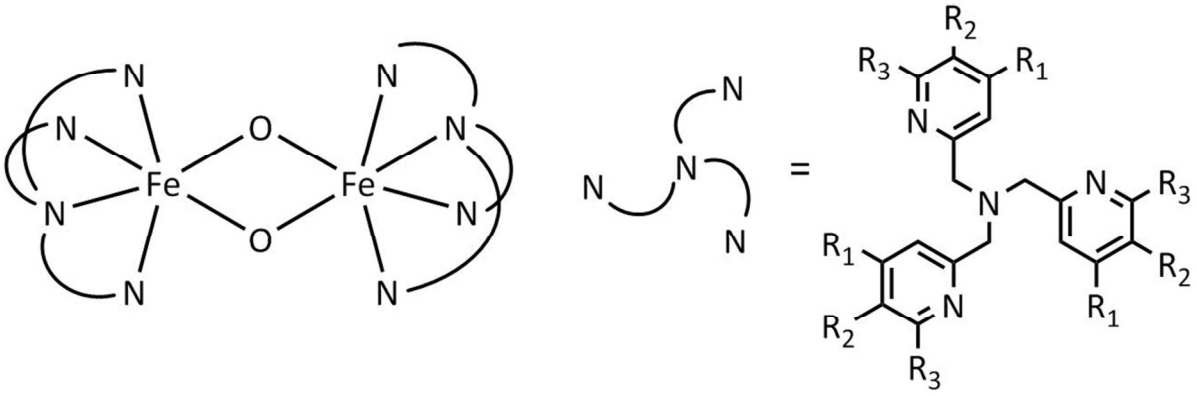

Figure 1.10.7 - Synthetic precedent of diamondoid $Fe_2^{II,II}(\mu\text{-}O)_2$ core supported by TPA ligands. R = H, Me, OMe, Et

Subsequent developments of this species saw its adaption to mimic the generation and chemical behaviour of the previous theorised intermediate in the catalytic cycle P, and its conversion to a Q-like species (Figure 1.9.2). The development of this model system afforded a complex with a limited degree of catalytic activity towards the desired substrates.[222] Rather than P itself, it is actually the generated peroxo- intermediate, termed P* that is thought to demonstrate this useful activity which is thought to proceed via the mechanism (Figure 1.10.8).

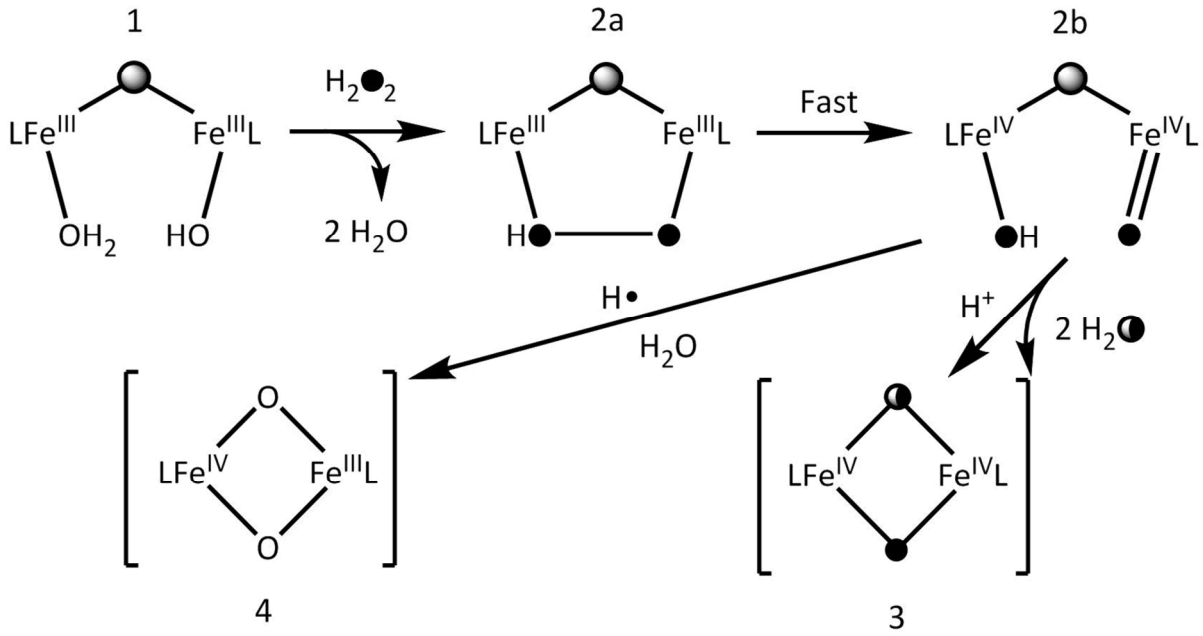

Figure 1.10.8 - Reaction scheme showing the synthetic route from model of intermediate P (1) to model of intermediate Q (3); shaded oxygen atoms were isotopically labelled to establish their origin and inclusion in products.

The use of larger, multi N-donor ligands such as TPA derivatives results in the generation of complexes that, whilst biomimetic in function, differ significantly from MMOH in structure (Figure 1.10.7 cf. Figure 1.9.3). Despite such differences in structure these complexes remains some of the most competent, and functional models, published to date.[219,221,223] This then validates the exploration of the use of other, related N-donor ligands and their complexes in augmenting our understanding of complex biological systems such as sMMO.

Unfortunately in the instance of the intermediate Q model cited, the catalytic activity reported is still three orders of magnitude lower than corresponding mono iron complexes utilising the same ligand backbone. [221,223] In addition the dimetal complex shows very limited thermal stability.[221,223]

Building on this collaboration Xue *and* Que Jr. *et al.* have since demonstrated that both C-H and even O-H activation can be achieved with activities 3 orders of magnitude higher than their previous system by moving towards a more open oxoiron $[HO–Fe^{IV}–O–Fe^{IV}=O]^{3+}$ species. Critically this introduces a terminal Fe=O mode which both opens up the core and also facilitates switching from the (S=1) $Fe^{IV}=O$ centre to a high-spin (S=2) state. As intermediate Q is also theorised to possess high spin, this change was then doubly beneficial, as it not only did it provide greater activity but also achieved this in a way that more closely mimics the biological system. In spite of such gains however, even the best of the current model complexes still utterly pales in comparison to the activity of sMMO itself.[223]

1.11 Formamidinate ligands

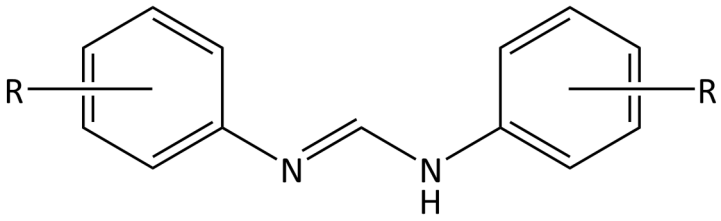

Figure 1.11.1 – General form of the diaryl formamidine backbone.

First synthesised in 1853 by Gerhardt,[224,225] the synthesis of these compounds has undergone a series of evolutions[226] culminating in their more convenient synthesis reported by Taylor in 1963[227]. As highly versatile ligands, diaryl formamidinates have been the subject of widespread use within organometallic and coordination chemistry,[225] and particularly in the emergent study of MM multiply bonded compounds.[228] Despite being iso-electronic to carboxylates, carboxamidates and triazenates, diaryl formamidinates have a proven ability to form paddlewheel type complexes with a far wider range of transition and S-block metals than any other known ligand, including carboxylates.[229]

1.11.1 Use as directing and capping ligands

Due to the highly substitutionally labile nature of carboxylates, many synthetic procedures for the generation of dimetallic complexes start with the parent tetracarboxylate, typically of the form $M_2(RCO_2)_4X_z$ (where X = counter ion, z = 0-2 as required). Softer, N donor ligands such as formamidinates are often then employed as a means to control and direct subsequent ligands substitution reactions.

Variation of reaction temperature and overall stoichiometry allows control of the degree of substitution of parent tetracarboxylate complexes to enable the isolation of the desired substitution product i.e. $M_2(RCO_2)_{4-y}(RNCNR)_yX_z$ (where y = 1-4; X = Counter-ion, if appropriate).[138,230–233] Similarly moderation of the steric bulk of the aryl substituent (Ar-R) of the ligand, can dictate the *cis*- or *trans*- substitution preference for the disubstituted product $M_2(RCO_2)_2(RNCNR)_2X_z$.[138] In combination, these strategies can be used to generate discrete bridged dimers, and 1-3D coordination polymers. The former strategy enabled the generation bridged dimers of the form $[M_2(RNCNR)_3]L_1$ was have found particular interest as bimetallic analogues of the Creutz-Taube ion.[231] The directing ability of the second strategy

has been used extensively in the investigation of molecular wires[234–238] and other supramolecular assembies.[138,233,239,240]

1.11.2 Coordination modes

As might be expected with a binding moiety that is iso-electronic with carboxylates the primary coordination modes of diaryl formamidinates are the same: monodentate (η^1-N), chelating (η^1, η^1-N,N'), and bridging (μ-η^1, η^1-N,N') modes (Figure 1.11.2). As with carboxylates, of these three chelating (μ-η^1, η^1-N,N') and bridging (η^1, η^1-N,N') are generally preferred. This is due to the $4e^-$ (cf. the $2e^-$ of the monodentate) binding interaction observed and the greater stability this provides to the resultant complex. It is further possible to strongly influence the predisposition toward bridging or chelating behaviour via modification of ligand steric demands and electronic donor/withdrawal effect(s) of the aryl substituents.[241]

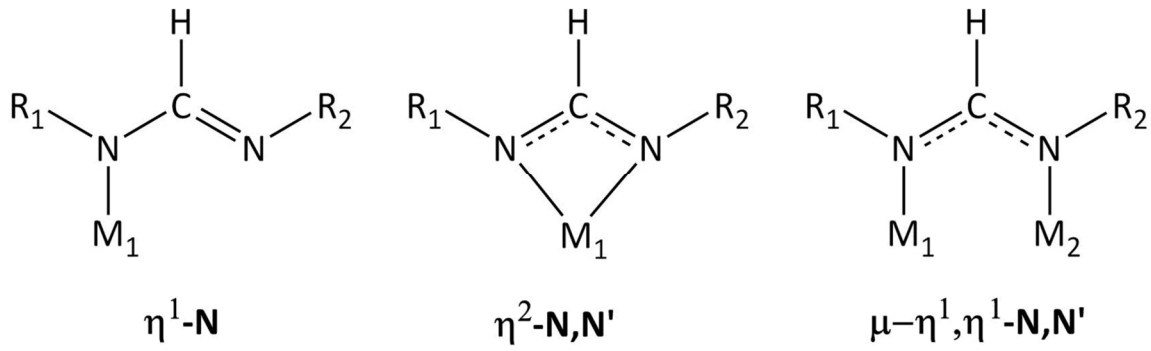

Figure 1.11.2 - Amidinate binding modes: monodentate (η^1-N), bidentate chelating (η^2-N,N') and bimetallic bridging (μ-η^1, η^1-N,N')

Despite their simplistic appearance, the coordination behaviour of diaryl formamidinates is however not non-trivial. This becomes particularly apparent when they are converted to their respective alkali metal salts, which is common practice for the subsequent synthesis of dimetallic transition metal formamidinate complexes.[103] These salts have been observed to display particular sensitivity the conditions used beyond that characteristic of typical organic-alkali metal salts.[241] It thought that such sensitivity is a consequence of the highly variable binding configurations these compounds can adopt *(vide infra)*. [241–246]

1.11.3 Unusual Coordination modes

Cotton reported the first structure of a formamidinate-alkali metal salt, $[Li_2(\mu\text{-}DTolF)_2(Et_2O)_2]$ (where DTolF = N,N'-bis(p-tolyl)formamidine) ,in 1997.[229] This came some 20 years after their widespread use in the synthesis of dimetallic complexes both by himself and others since the late 1970s. Cotton's sole rationalisation for the 20 year delay in the structural characterisation of these widely used reagents was the difficult in isolating a suitable crystal prior to rapid loss of associated ethereal solvent. It seems highly unlike that this presented the only barrier to the isolation of such complexes. More recently, the groups of Junk and Jones[241–246] have indicated that the coordinative flexibility of these species may have a significant negative impact on the stability of such salts.

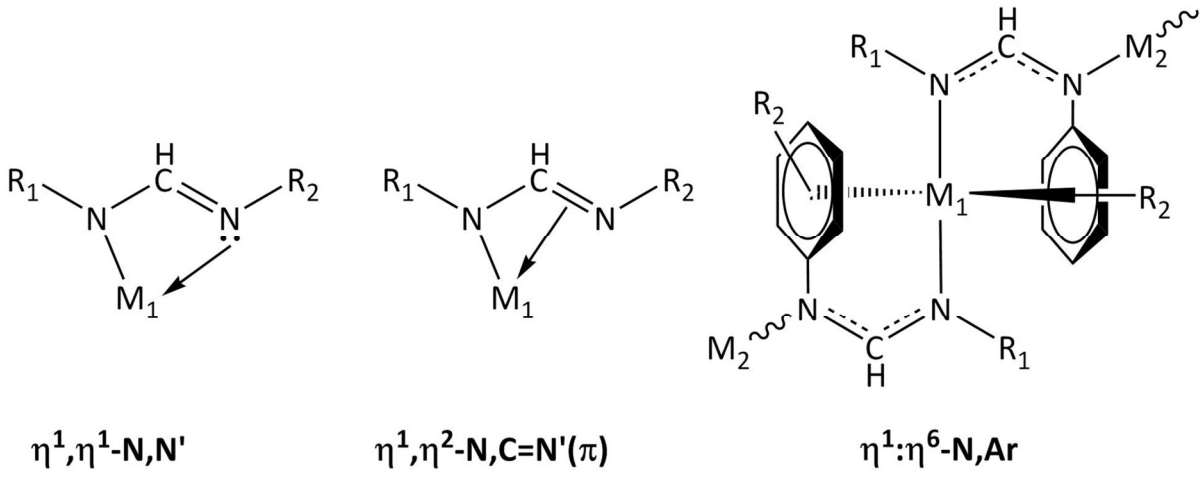

Figure 1.11.3 – Less common amidinate binding modes: Asymmetric N,N' chelation (η^1, η^1-N,N'); Asymmetric N,C=N(π) chelation (η^1, η^2-N,C=N'(π); and N,Ar-chelating, N'-bridging (η^1, η^6-N,Ar).

In addition to the more typical, expected binding modes shown previous (Figure 1.11.2) there are several published examples of formamidinates having adopted strained or otherwise unexpected binding modes in place of that expected (Figure 1.11.3). In most of the reported instances, these more unusual binding modes are chiefly observed with low valent alkali metals or where the coordination environment is already otherwise constrained.

The distortions observed are usual manifested via deviation from the expected symmetrical chelating (η^2-N,N') and bimetallic bridging (μ-η^1, η^1-N,N') modes as evident from bond distances in the solid state. These deviations typically include a break in the otherwise expected symmetrical N-C-N bonds of the amidinate backbone, indicative of retention of

the N=C-N' double bond observed in conjunction with elongation of one of the N-[metal] contacts. The configuration observed is then intermediate between a monodentate interaction (η^1-N), and that of a bidentate chelating (η^2-N,N') configuration. Differentiation of the N-C-N' bonds of the ligand implies that this requires a break in the charge delocalised configuration of the bound ligand, whilst retaining some formal donation. The source of this retained donation may be characteristic of the N' lone-pair (η^1,η^1-N,N') or from the now retained C=N'(π) bonding orbital (η^1, η^2-N,C=N'(π).[244] In the extreme case of the latter (η^1, η^6-N,Ar) from one of formamidinate aryl rings may be observed in preference to coordination of the N' nitrogen. The tantalum complex MeTaCl-$[C_6H_{11}NC(Me)NC_6H_{11}]_2$ provides perhaps the best example of the asymmetric, imino N-donating (η^1, η^1-N,N') binding mode (Figure 1.11.4).[247]

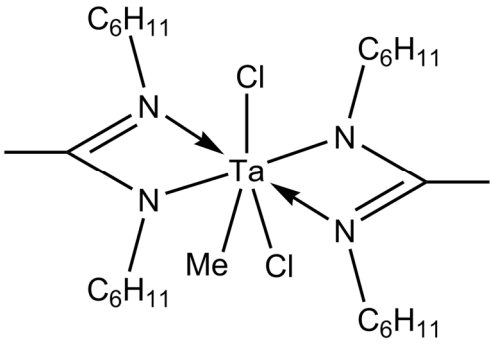

Figure 1.11.4 - Asymmetric N,N'-lone pair donation (η^1, η^1-N,N') in the complex MeTaCl-$[C_6H_{11}NC(Me)NC_6H_{11}]_2$

Structurally characterised examples of the related η^1, η^2-N,C=N'(π) coordination modality are significantly less well documented in the literature. Perhaps the best example of this behaviour is found in the complex [Li{N(2,6-$(R)_2C_6H_3$)C(H)N(2,6-$(R)_2C_6H_3$)}(pmdeta)] (where pmdeta = N,N,N',N'',N''-pentamethyldiethylenetriamine) reported by Junk and Jones.[244] For R = Me, two isomeric structures are observed within the asymmetric unit, (Figure 1.11.5) whilst for R = ^{i}Pr only the E-anti conformer is observed. In both instances the C=N(π) interaction is shorter than might be expected if no bonding interaction were present with C=N(π) – M distances of 2.448(15) (Me) and 2.596(13) (^{i}Pr).[244]

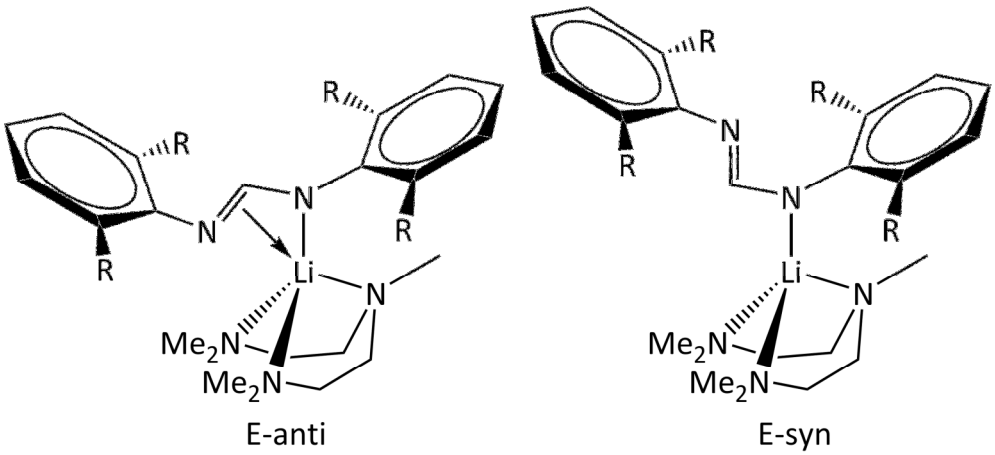

Figure 1.11.5 - Two observed isomeric structures of [Li{N(Ar)C(H)N(Ar)}(pmdeta)] observed within its crystallographic asymmetric unit.

The η^1, η^2-N,C=N'(π) binding mode is also observed for some mono- and diruthenium complexes, several examples of which are found in the work of Nagashima and coworkers. These include the diruthenium species [(η^5-C_5Me_5)Ru(μ_2-^{i}PrNC(Me)=N^{i}Pr)Ru(η^5-C_5Me_5)][X] (where X= $B(C_6F_5)_4$ or PF_6)[248–250] (Figure 2.1.6), and the related mono ruthenium complexes of the form (η^5-C_5Me_5)Ru(amidinate).[251] This then serves to demonstrate the capacity of these unorthodox binding modes to significantly contribute to the stabilisation of larger transition metals and that such behaviour is not merely restricted to alkali metals. What makes these examples of particularly interest however that they are formally Ru_2^{4+} and as such this has potential to impact those compounds reported herein (Chapter 3).[103,249,250]

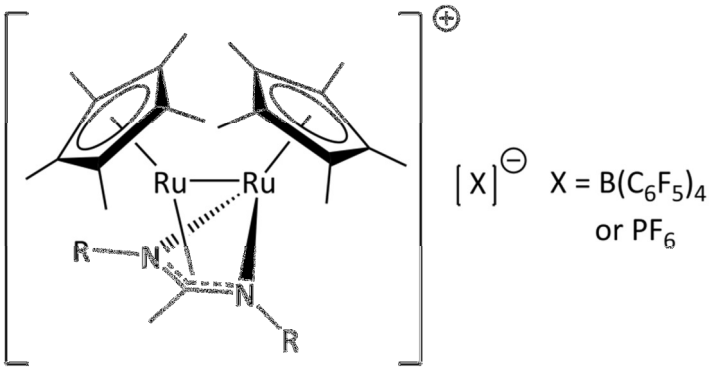

Figure 1.11.6 - Structural example of N-C-N(π) - Metal donation in the complex [(η^5-C_5Me_5)Ru(μ_2-^{i}PrNC(Me)=N^{i}Pr)Ru(η^5-C_5Me_5)][X]

The last of these three rarely-observed binding modes, (η^1, η^6-N,Ar), is particularly unusual in that it demonstrates that significant complex stabilisation also may be inferred from persistent π–Ar interactions. Whilst π–Ar are not uncommon with some ligands it remains

unusual to observed this mode of coordination in preference for the N,N' modes typically observed. Adoption of this coordination mode has typically only been noted when using ligands of significant steric bulk with smaller metals.[243] The example shown previously (Figure 1.11.3) is that of the complex $[K(\eta^6:\eta^1\text{-Ar})(\eta^6:\eta^1\text{-Ar})][K(THF)_2]$ (Where Ar = N,N'-di(mesityl)formamidine); this chemistry has since been extended to related potassium[246] and their sodium and lithium analogues.[243]

One of the downsides to this capacity of amidinates to adopt multiple binding modes, especially in low oxidation state metal complexes is that the nuclearity and nature of the coordination environments in resultant species are often very hard to predict. In many instances where conditions have not been optimised for a given product this results in a mixture of products being obtained. Cotton in particular observed this for a number of transition metal formamidinate complexes of V,[252,253] Ti,[254] Co,[255] Cr,[256] W,[256] Rh,[257] Fe[258–263] and Ru.[122,138,139,264] Such studies indicated that whilst one might expect a $M(L)_2$ or $M_2(L)_4$ configuration, others including $M(L)_3$, $M_2(L)_3$, $M_2(\mu\text{-}L)_2(L)_2$ and other higher order clusters may also commonly be formed.

1.12 Summary

In this introduction we have provided an overview of the wide range of themes that will be central to the content of this thesis. The industrial and societal context for this work is found in the need to both improve the efficiency of current industrial practise regarding critical highly energy intensive processes and to provide a means to diversify the supply of suitable fuels to society.

The previous research efforts to achieve significant gains in efficiency to current industrial practise have been summarised and the chemistry of dimetallic complexes introduced. Particular focus has been made of the chemistry of diruthenium complexes and the biological potential template for such chemistry provided in nature by MMOs.

Research efforts towards the development of functional small molecule mimics of sMMO are then summarised with a particular focus on the factors and features that both enable the isolation and function of these reactive compounds. Finally the chemistry of the formamidinate family of ligands is introduced along with its uses in inorganic transition metal coordination chemistry and the highly variable nature of its interactions with differing metal centres.

In subsequent chapters we will present a range of compounds inspired by the sMMO biological system, and intended to further the goal of achieving a functional catalytic mimic of this enzyme. The complexes reported will primarily (Chapters 2-3) contain formamidinate ligands as introduced herein, however Chapter 4 will address the diruthenium chemistry of the closely related amidate ligands.

2 Attempted synthesis of diiron (II,II) 'NN' tetra-formamidinate complexes

2.1 Aims

- To develop a synthetic methodology suitable for the general synthesis of a range of diiron (II,II) tetra-formamidinate complexes based on the two published literature examples. The general form of the target complexes is shown below (Figure 2.1.1):

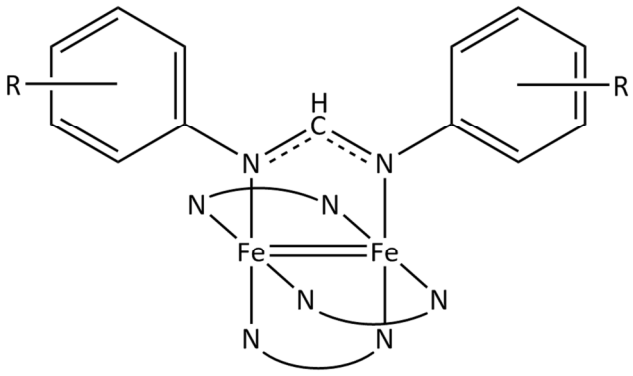

Figure 2.1.1 - General structure of the target diiron (II,II) tetra-formamidinate complexes; 3 of the 4 ligands are shown in a truncated form for clarity.

- To explore the impact of varying electron donating or withdrawing aryl substituents of the supporting formamidinate ligands on the resultant physical, spectroscopic and electronic properties of the diiron complexes formed.
- Where target species are isolated, to test their viability and activity of the as aerobic oxidation catalysts for the partial oxidation of simple organic substrates such as 9,10-dihydroanthracene.

2.2 Introduction

2.2.1 Developing biologically inspired diiron complexes

The previous work of Xue, Que Jr. and others in developing functional models of the key reactive intermediates Q and P* (Section 1.10.4) has demonstrated the value of N-donor ligands to better understand the function of sMMO (Figure 1.9.2). [202,221–223,265]

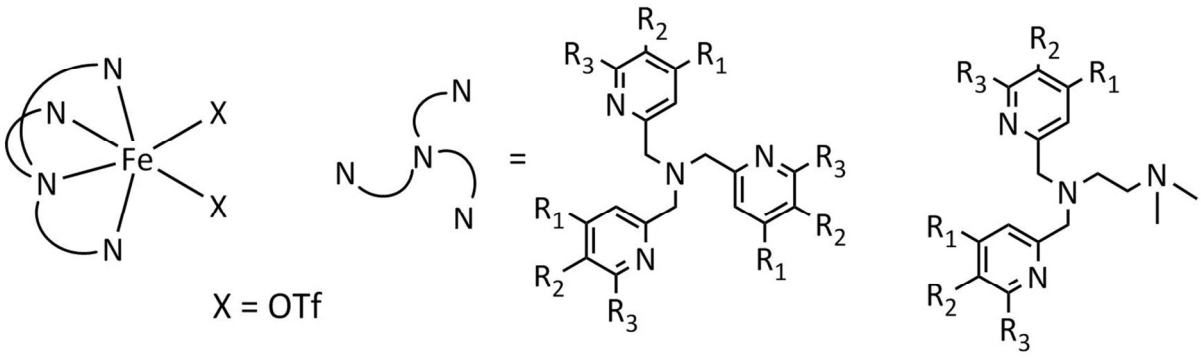

Figure 2.2.1 - Mono iron (II) complexes that show catalytic activity towards alkane supported by pre-organised tetra-dentate N-Donor ligands such as TPA (Left) and 'iso-bpmen' (Right) (where bpmen = $(CH_2Pyr)MeN(CH_2CH_2)NMe(CH_2Pyr)$)

Mono-iron complexes (Figure 2.2.1) closely related to their previous dimetallic analogues (Figure 1.10.7) utilise similar pre-organised ligands but have further been shown to be effective catalysts for the oxidation of alkanes.[266–270] These mono-iron complexes retain the best published catalytic activity for iron (II) alkane oxidation to date.[270]

Despite being more bio-inspired rather than biomimetic these complexes provide both excellent models of key intermediates and also allow replication of intended catalytic functionality. The proven utility of these complexes provides a precedent to explore the chemistry of other related N-donor coordinated diiron Fe_2^{4+} systems, such as those incorporating amidinate ligands.

Biological systems such as sMMO require a significant degree of coordinative flexibility from their ligand environment in order to achieve their function[207,210,219] (Section 1.10.2.1). Consequently, the use of other highly adaptable ligands such as amidinates presents a particularly attractive synthetic target. Amidinates are isoelectronic to carboxylates, yet have a greater proven utility as a ligand with a wider range of metals,[229] behaviour which is

a potential consequence of the highly variable coordinative binding modes they can adopt (Section 1.11.2).

2.2.2 Previous synthetic precedents

To date the literature only contains two structurally characterised $Fe_2^{II,II}$(formamidinate)$_4$ complexes: $Fe_2(DPhF)_4$, where HDPhF = N,N'-Diphenylformamidine and $Fe_2(\mu\text{-}DPhBz)_2(\eta^2\text{-}DPhBz)_2$, where HDPhBz = N,N'-diphenylbenzamidine.[258,259] The former, $Fe_2(DPhF)_4$, is synthesised via the related $FeCl_2$(H[amidinate])$_2$ di-adduct by addition of MeLi. The latter, $Fe_2(\mu\text{-}DPhBz)_2(\eta^2\text{-}DPhBz)_2$, by contrast is synthesised directly by combination of $FeCl_2$, H[amidinate] and MeLi in one step.[258,259] Both of these compounds are highly distorted in the solid state, yielding structures significantly different to most transition metal paddlewheel structures.

In the solid state the $Fe_2(DPhF)_4$ contains two pairs of trans-orientated ligands each biased towards opposing ends of the metal-metal vector whilst the Fe-N bond lengths display contraction between on ligand pair and elongation towards the other (Figure 2.2.1). This results in a pseudo-tetrahedral coordination environment at the iron centres and serves to reduce the overall symmetry from D_{4h} to D_{2d}. A recent computational study by Berry suggests this is the probable product of Jahn-Teller distortion of a proposed orbitally degenerate π^3 ground state as would be observed for $Fe_2(DPhF)_4$ under D_4 symmetry.[271]

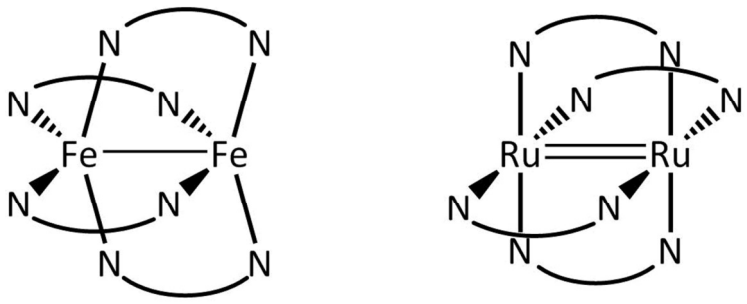

Figure 2.2.2 – Distorted geometries of diiron (II,II) tetraformamidinate complexes 1. (Left) Distorted paddlewheel structure as observed for $Fe_2(DPhF)_4$; (Right) A more typical paddlewheel complex, as observed for related complexes Ru_2^{4+} reported in chapter 3.

The use of the more bulky HDPhBz ligand in $Fe_2(\mu\text{-}DPhBz)_2(\eta^2\text{-}DPhBz)_2$ had been intended to favour a more regular paddlewheel structure than had been observed previously for $Fe_2(DPhF)_4$. In place of a more regular paddlewheel structure however a second highly

distorted structure was instead obtained (Figure 2.2.3) that shows closer relation to a windmill-type (Figure 1.10.2) configuration.

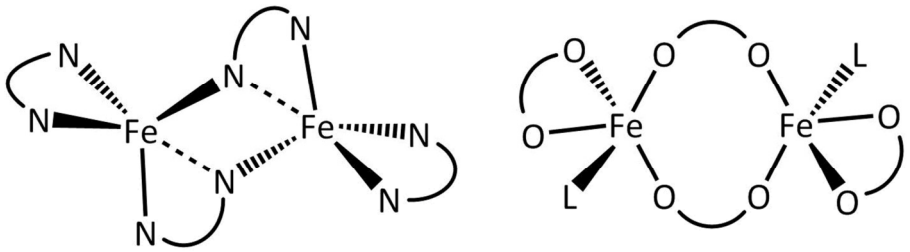

Figure 2.2.3 - Distorted geometries of diiron tetraformamidinate complexes 2. (Left) The distorted diiron core of $Fe_2(\mu\text{-DPhBz})_2(\eta^2\text{-DPhBz})_2$. The bonding interactions shown as dashed bonds were deemed intermediate in character.

The bonding in this distorted structure differs significantly from that typically seen in square pyramidal or trigonal bipyramidal 5-coordinate environments and is contorted such that the only symmetry element it possessed in the reported structure is a centre of inversion.[259] Four of the Fe-N contacts are approximately equidistant at 2.065(3) Å whilst the fifth contact (shown dashed) is considerably longer at 2.477(4) Å, yet still clearly contributes to the overall coordination environment of the iron centre.[259]

Modification of the steric bulk of the ligand backbone has been noted by others to heavily influence both the observed binding mode of the ligand and the nuclearity of the product obtained.[272–277] Suitable examples of this may be found in the work of Hessen and Sciarone who have reported a range of mono-iron $Fe^{II}(amidinate)_2$ compounds with related but more sterically demanding benzamidinate ligands.[272,274–277] Similar examples of even more bulky bis(amidinate) complexes incorporating a meta-terphenyl backbone have also been reported by Arnold and Schmidt.[278] In reference to the targeted synthesis of $Fe_2(DPhBz)_4$ however it is clear that modification of the steric bulk of the ligand alone is still insufficient to selectively obtain the target $Fe_2^{II,II}(formamidinate)_4$ in a paddlewheel configuration complex. Consequently the effects of changes to other reaction variables need be considered if this configuration is to be obtained selectively.

2.2.3 Formation of unwanted by-products

The chemistry of iron (II) salts in combination with amidinates and their low valent alkali metal salts has been observed to be highly complex,[262,263,272] with wide ranging products

dependant on reaction conditions, stoichiometry, ligand steric constraints and choice of alkyllithium reagent used.[225,258,259,261,262,272,274–277,279]

During previous work by Cotton towards the synthesis of diiron paddlewheels of the form $Fe_2(amidinate)_4$,[258,259] he reported on a range of unwanted additional products may be obtained under non-optimal conditions. These by-products included:

The mono-nuclear products $Fe^{II}(amidinate)_2$[272,274–277] and $Fe^{III}(amidinate)_3$;[225,261,279] the dinuclear $Fe_2^{I,II}(amidinate)_3$ lantern[260,280,281] (Figure 1.10.1) and $Fe_2^{II,II}(\mu\text{-}L)_2(L)_2$ windmill complexes[259] (Figure 2.2.3); and other higher order clusters such as $Li_2(amidinate)_2Fe_4O_4(amidinate)_6$[262] and $Fe_4^{II}(O)(amidinate)_6$[263] (Section 2.3.5.3). The last two of these were observed on exposure to excess lithiation and moisture/oxygen respectively.

Of these the most interesting are perhaps the lantern complex product $Fe_2^{I,II}(DPhF)_3$ and the cluster product $Fe_4^{II}(O)(amidinate)_6$. The former of these despite similarities in appearance to the target species $Fe_2^{II,II}(DPhF)_4$ differs very significantly, but both are remarkable high spin (HS) complexes with very different electronic structures. $Fe_2^{II,II}(DPhF)_4$ shows an overall spin of S=4, but its' electronic structure remains poorly understood despite recent efforts at modelling it.[271] The electronic structure of $Fe_2(DPhF)_3$ was not discussed in the initial publication of its synthesis but subsequent DFT modelling[103,281] has shown it to adopt a majority $\sigma^2\pi^4\pi^{*2}\sigma^{*1}\delta^2\delta^{*2}$ ground state with a rather exceptionally high spin configuration of S = 7/2 in agreement with that originally proposed by Cotton on the basis of EPR.[280] these are some of the highest spin diiron complexes known in the literature.[281]

The cluster species of the form $Fe_4^{II}(O)(amidinate)_6$ that have been adopts a distorted basic beryllium acetate structure which are curiously unevenly bridged about the edges of the Fe_4O tetrahedron at its core. Such arrangements have more generally been compared to that of diamond in connectivity and are observed for a range of transition metal.[103,282] This diamondoid structure, by comparison with other coordinative arrangements such as the paddlewheel or lantern appears to be significantly more thermodynamically stable. Considering the greater shielding of the metal core this configuration provides such determination does not seem reasonable. That such species have been reportedly form on

exposure to oxygen and/or moisture would also tend to indicate that were it unstable it would most probably decay further monomeric products as is typically observed on the oxidative decay of other configurations such as the paddlewheel. Similar exposure of $Fe_2^{II,II}(DPhF)_4$ was noted to result in an immediate deep burgundy colour followed almost immediately by decomposition to an intractable brown solid. The identity of this decomposition species is however highly unlike to resemble that of this cluster, which retains iron as iron (II) despite the postulated presence of dioxygen in its formation.

2.2.4 Development of other synthetic routes to $Fe_2^{II,II}$(formamidinate)$_4$ complexes

2.2.4.1 General considerations

A survey of the literature provides evidence of a wide range of potential factors that are thought to influence the formation of the products obtained by reactions between amidinates, their alkali metal salts and the corresponding salts of iron (II). However, the action of many of these factors remains poorly understood. The products obtained typically display extreme sensitivity to air, moisture, temperature and the use of many common non-donor solvents.[103,258,259,262,263,275,283] In addition the study of related mono-iron (II) amidinate species, some of which are postulated to be potential intermediates to the target $Fe_2^{II,II}$(formamidinate)$_4$ complexes, have also further strongly suggested many such species display significant sensitivity towards ambient light.[272]

Amongst the transition metal amidinates he studied, Cotton indicates that the chemistry of diiron amidinates is amongst the most complex seen.[103] Such comment was made in regard to both the highly varied nature of the products obtained and the often extreme impact on selectivity observed on minor changes in the conditions and reagents used. Cotton proposed for example, that selectivity was influenced by both the alkylating agent used to generate the formamidinate salt,[258–260] the effects of non-stoichiometric lithiation, and the presence of even trace amounts of water or oxygen.[262,263] He noted that switching lithiating agent from *n*-butyllithium to methyllithium was sufficient to favour the formation of the $Fe_2^{II,II}$(amidinate)$_4$ paddlewheel geometry as opposed to the $Fe_2^{I,II}$(amidinate)$_3$ trigonal lantern (Figure 1.10.1) The formation of the latter was thought to be the result of

nucleophilic attack of the iron centre by the alkyllithium resulting in further reduction of the iron and β-elimination of a alkene.[258,260] Despite this however, a later revised synthesis toward the same reported lantern complex utilises MeLi under closely related conditions indicating the alkyllithium choice probably is not the sole determining factor for his earlier observation.[280]

The study of related compounds such as diiron tetracarboxylates[284] has similarly indicated that the use of different metal salts, or even differing morphologies of the same metal salt, can have a profoundly affect the products obtained. Similar investigation with formamidinates has not been reported in the literature, however this may reasonable be considered as another potential variable with which to improve selectivity. Whilst Cotton chiefly used $FeCl_2$ many more contemporary reports suggest better results are often obtained with iron (II) triflate.[266,268–270,284,285]

2.2.4.2 Consideration of kinetics effects

Relative to later transition elements such as ruthenium the kinetics observed for reactions of iron (II) are very fast, with reactions typically proceeding readily at room temperature.[229,258] Whilst this has the advantage of potentially enabling rapid synthesis, it also has a logical and more negative impact on the stability of products on isolation and storage at similar temperatures. This was observed previously as both a tendency towards further reaction and equally in the extremely rapidly decomposition of such species on exposure to unfavourable conditions.[258,259,262,272,274–277]

The rapid kinetics observed similarly frustrates synthetic efforts in limiting the lifetime of potentially critical reaction intermediates. Where the isolation of such intermediates is critical, as reported for the synthesis of $Fe_2^{II,II}(DPhF)_4$ (Section 2.3.3) this may limit the utility of some synthetic methods but reports of related compounds indicate this isolated instance.

The more rapid kinetics of the generation of diiron complexes also predisposes such complexes to a similarly enhanced rate of decomposition in unfavourable conditions relative to later transition metal congeners, often rendering their analysis more difficult. The short-lived nature of such intermediates species similarly frustrates efforts to improve the mechanistic understanding of this chemistry.

Most synthetic methods for the generation of $M_2(amidinate)_4$ transition metal complexes require the use elevated temperatures; most commonly this is achieved as either solid state melt reaction or via high temperature ligand metathesis reactions in solution. This is typically required to provide many of the somewhat more kinetically inert later transitions metals to react. The low thermal stability of the iron (II) products however precludes the use of such approaches and necessitates the devising of suitable low temperature alternatives.

The most commonly practised alternative is to use alkali metal salts of the intended ligands in combination with the metal salt directly. However, such efforts are often then greatly complicated by the presence of highly reactive alkali metal species present in solution. [258,259,262,263,275,283]

2.3 Results and discussion

2.3.1 Ligand synthesis

2.3.1.1 General synthetic considerations

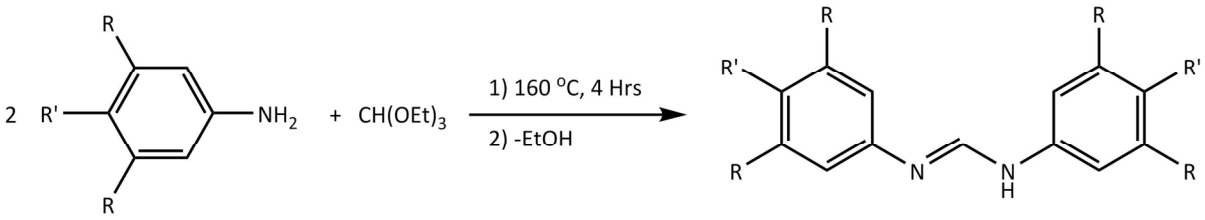

Figure 2.3.1 - General scheme for formamidinate synthesis. H[DMOPhFm]: R = OMe, R' = H; H[4FPhFm]: R = H, R' = F; H[3,5-$(CF_3)_2$PhFm]: R = CF_3, R' = H; H[TMOPhFm]: R = R' = OMe.

The chemistry of formamidinates is well established,[225,226] with the literature precedent[227] for their synthesis not having seen significant development since the 1960s.[225–227] A typical contemporary synthesis of formamidinates may proceed as shown (Figure 2.3.1).[286,287] The synthesis of some amidinates with more strongly electron withdrawing functionality often cite the need for the addition of a catalytic amount of acetic acid.[286,287]

The role of acid catalysis in the synthesis of amidinates was studied extensively in the 50s and 60s by Roberts[288–291] and latterly Taylor[227] who both sort to rationalise these disparate approaches though study of the involved reaction kinetics (Figure 2.3.2).[225,227]

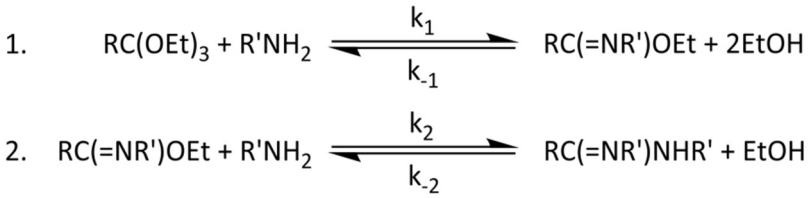

Figure 2.3.2 – Rate constants of forward and reverse reactions during amidinate synthesis.

In the absence of acid catalysis two equivalents of most amine substrate are rapidly and exclusively converted to the N,N'-disubstituted formamidine indicating the rate constants k_2 and k_1 are fast and show no strong dependence on $[H^+]$. The inclusion of excess orthoformate does not affect the observed selectivity which would further suggest that $k_2 >> k_1$. The reverse reaction rate k_{-2} for the reformation of the imido ester by contrast was found to be slow but showing high dependence on $[H^+]$.

Under non-acid catalysed conditions where $k_2 > k_1 >>> k_{-2}$ kinetic control was observed, with the second reaction (2) proceeding effectively irreversibly. The removal of liberated the ethanol from (2) by boiling the reaction mixture to dryness further serves to drive the equilibrium of reaction (2) in favour of the amidinate.

The inclusion of acid catalysis is of great utility in synthesising N,N'-disubstituted formamidinates for which the un-catalysed yield are unexpectedly low[227,292] such as those of highly fluorinated anilines.[286,287,293,294] Acid catalysis renders reaction (2) highly reversible with $k_{-2} \approx k_2$ resulting in thermodynamic control. Isolation of the target amidinate in good yield shows strong dependence on the selective and progressive removal of liberated ethanol. Exclusive selectivity towards the amidinate is lost under acid conditions and some formation of the imido ester is consistently observed.[227]

2.3.1.2 Choice of formamidinate ligands

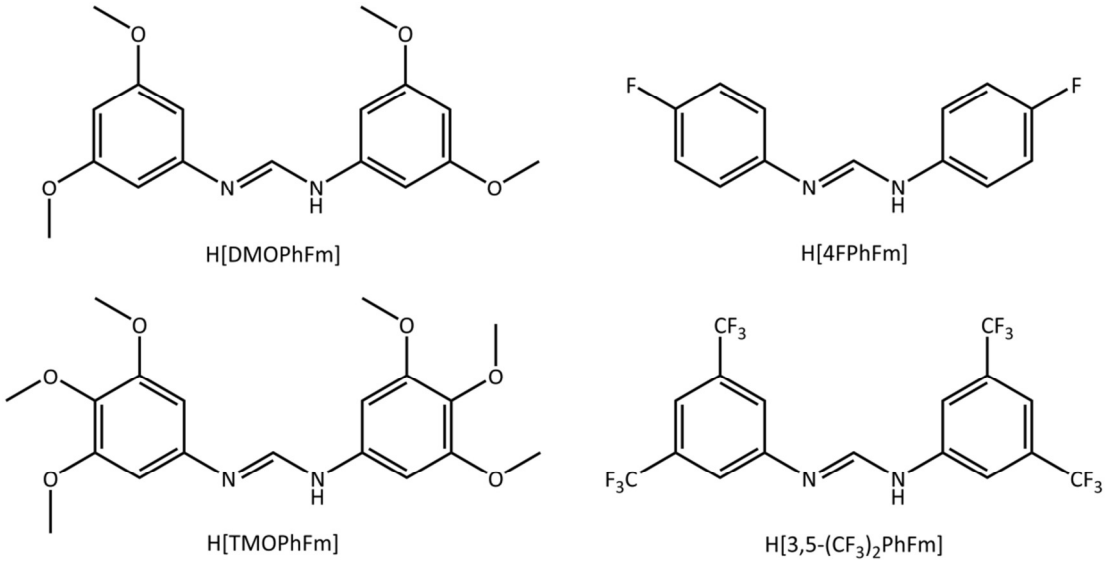

Figure 2.3.3 - Formamidinate ligands synthesised.

Choice of ligands was informed by a comprehensive review of the literature with the intention of providing a range of electron withdrawing and donating substituents which have not been utilised previously with Fe_2^{4+}, Ru_2^{4+} or Ru_2^{5+} complexes. It was intended that this novel range of ligands would allow a direct comparison between complexes of both metals, and separately between the two differing oxidation states of ruthenium.

Similar independent studies of the effects of ligand substitution on molecular properties have been conducted previously for a wide range of related metal tetra-formamidinates such as those of Mo_2^{4+},[295] Rh_2^{4+},[296] Ni_2^{4+},[297] Cr_2^{4+},[298] and Ru_2^{5+}.[228] However, corresponding data for Fe_2^{4+} and Ru_2^{4+} formamidinates is notably absent from the literature.[103,228]

2.3.1.3 Synthesis of formamidinate ligands

The synthesis of all required ligands was readily achieved in good to excellent yield (Section 2.5.4) via direct reaction of 2 equivalents of the suitably substituted aniline with 1 equivalent of triethyl orthoformate at reflux (160 °C) for a period of 4 hours (Figure 2.3.1). All of the ligands synthesised are novel with the exception of ***H[4FPhFm]*** which has been reported previously. Since their initial synthesis the ligand ***H[3,5-(CF$_3$)$_2$PhFm]*** has since been reported elsewhere.[299]

Despite the literature precedent[286] for the required inclusion of acid catalysis with highly fluorinated aniline substrates, this was not observed to be necessary for those synthesised and used in this study.

Formally solventless, the only liquids present are the orthoformate and the ethanol liberated in the course of the reaction. Once the reflux has completed both of these may be readily boiled off by removal of the reflux condenser which serves to simplify the work up and increase overall yield due to the added thermodynamic drive in favour of the intended products.

Isolation of the product formamidinates was achieved via recrystallisation of the residual solid from the reaction using hot hexane. This afforded ***H[DMOPhFm]*** and ***H[4FPhFm]*** as large off-white crystalline blocks in excellent yield. Both ligands were then further purified by sublimation at reduced pressure.

The remaining ligands including the bulky ***H[TMOPhFm]*** and the highly fluorinated ***H[3,5-(CF$_3$)$_2$PhFm]*** showed significantly reduced solubility in most solvents and necessitated some variation from the work described previously. The fluorinated ligand ***H[3,5-(CF$_3$)$_2$PhFm]*** required recrystallisation from hot toluene due to its low solubility in hexane and its high

melting point limited the utility of sublimation in further purification. In practice sublimation was only effective in removal of more volatile starting materials.

The most bulky ligand ***H[TMOPhFm]*** despite differing from the related ***H[DMOPhFm]*** by only two Ar-OMe groups (Figure 2.3.3) was unexpectedly insoluble in all common solvents. It displayed show only very sparing solubility in MeCN and DMSO. It is postulated that the additional Ar-OMe functionality serves to sterically inhibit Ar-O-Me bond rotation, limiting both conformational freedom and disrupting intermolecular hydrogen-bonding. Added steric pressure may lower the ability of the oxygens of the pendant methoxy- groups to act as H-bond acceptors lowering solubility in polar solvents whilst

The insolubility of ***H[TMOPhfm]*** rendered all attempts at recrystallisation ineffective. Attempts at purification by sublimation were frustrated by its low volatility and simply resulted in decomposition at temperatures in excess of 250 °C. However, Mass spectrometry and elemental analysis indicate the intended product was cleanly obtained *(vide infra)*.

2.3.1.4 Ligand characterisation

Compounds were identified and chiefly characterised via ^{1}H, ^{13}C ^{19}F NMR spectroscopy and HR-ESI-MS, whilst individual batch purity was assessed via determination of variations in M_p. IR data were found to be of little diagnostic utility and is subsequently only provided for new compounds.

Observed M_p deviation between batches was well within experimental error, typically <0.15 °C and in accordance with literature values where present. The exception to this was ***H[4FPhFm]*** which was consistently observed to have a M_p of 146.1 +/- 0.1 °C which is significantly higher than the reported literature value of 99-100 °C.[286] This disparity is attributed to the reference sample being of lower purity, as has been noted previous for other related formamidinate samples produced via differing methods.[289,290] Samples produced via acid catalysed synthetic routes are often contaminated by small quantities of the imido ester which serves to depress the reported M_p value relative to an authentic sample.

2.3.1.5 X-Ray crystallography

Crystal structures of the ligands employed were not routinely obtained as those of similar compounds are prevalent throughout the literature. However, crystals of the novel ligand ***H[DMOPhFm]*** suitable for X-Ray diffraction were adventitiously isolated from recrystallisation mixtures intended to isolated the targeted dimetallic products. These crystals were obtained from DCM/*n*-pentane mixtures via vapour diffusion on storage at -18 °C for one week.

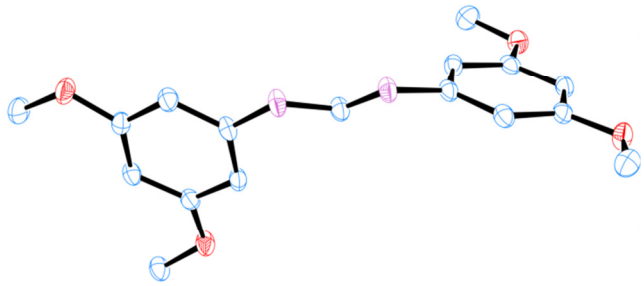

Figure 2.3.4 - Crystal structure of H[DMOPhFm]. Hydrogen atoms are omitted for clarity and thermal elipsoids are drawn at the 50% probability level.

In good accord with a great number of similar reported formamidinates, H[DMOPhFm] forms a distantly H-bonding dimer in the solid state.[300–303] As is generally observed for such compounds neither of the aryl rings is co-planar with the R-NCN-R bridge, giving the compound a significant distinct torsion of 73.3° between the planes of the aryl rings. Observed C=N (1.286(2) Å) and C-NH (1.349(3) Å) bond lengths are in well within the ranges typically observed for closely related compounds[300–303] and show close particularly good agreement to that reported for the related *m*-OMe substituted compound.[303] Complete crystallographic information for ***H[DMOPhFm]*** is included in appendix B-1.

2.3.2 Synthesis and characterisation of $FeCl_2(H[amidinate])_2$ diadducts

The primary utility of $FeCl_2(H[amidinate])_2$ di-adducts is as more soluble forms of the corresponding parent M^{2+} salts, and as starting materials for the synthesis of related dimetallic complexes.[103,255,304,305] As starting materials the pre-coordination of the formamidinates serves as a means to control overall stoichiometry and influence the coordination mode of the ligand.[305] This synthetic approach to dimetallic complex synthesis has seen the development of analogous formamidinate di-adducts of a range of other metals including cobalt,[255,304,305] nickel[103,304] platinum[305] and manganese[103,304] for subsequent use in the targeted synthesis of their dimetallic tetraformamidinate analogues.

2.3.2.1 Synthetic methodology

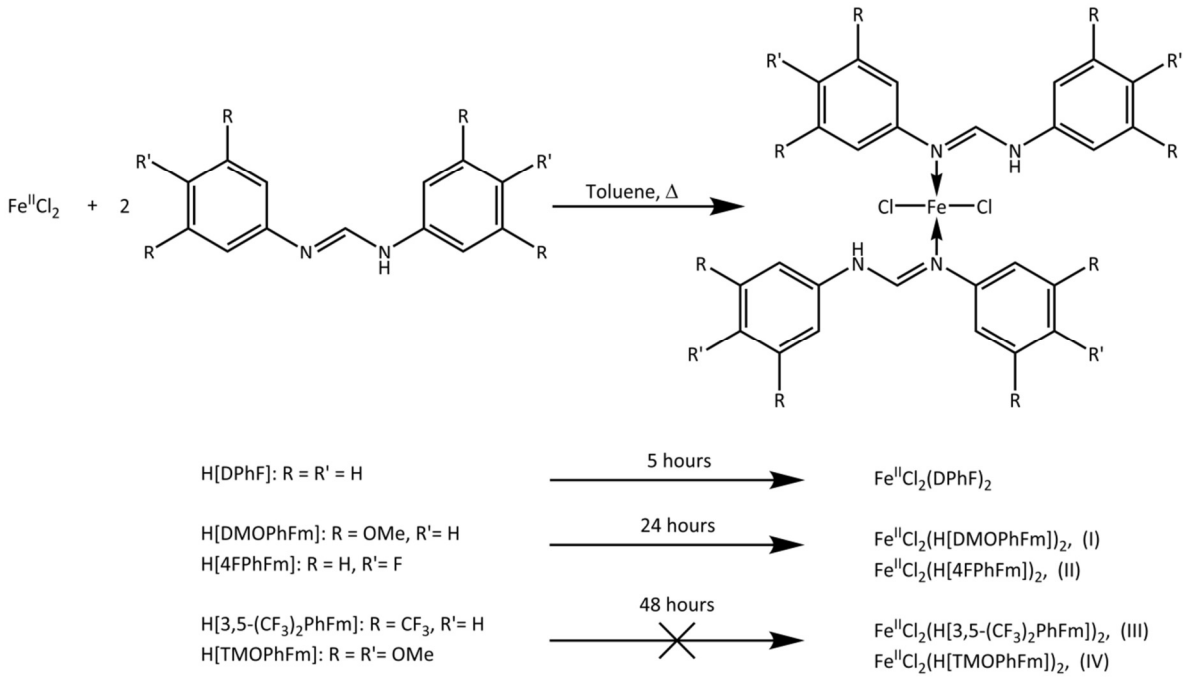

Figure 2.3.5 - General scheme for the synthesis of $FeCl_2(H[amidinate])_2$ di-adducts

With a view to replicating the synthetic procedure for $Fe_2^{II,II}(DPhF)_4$ published by Cotton[258,259] which utilises the mono iron species $Fe^{II}Cl_2(DPhF)_2$ as its starting material a range of analogous $FeCl_2(H[amidinate])_2$ di-adducts were synthesised using the previously described ligands ***H[DMOPhFm]***, ***H[4FPhFm]***, ***H[TMOPhFm]*** and ***H[3,5-(CF$_3$)$_2$PhFm]***. A general scheme for the formation of these adducts is provided above (Figure 2.3.4)

The formation of the target diadducts proceeds via reflux of a suspension of $FeCl_2$ and the appropriate ligand in toluene for 24-48 hours. The progress of the reaction was monitored via the mass spectrometry technique MALDI-TOF-MS (see Section 2.3.2.2). The previously reported length of time for which this suspension was held at reflux (5 hours) was found to be insufficient for generation of the target species with the ligands employed. After 5 hours the reaction mixtures were observed by MS to contrain the corresponding mono-adduct in addition to the intended products ***$FeCl_2$(H[DMOPhFm])$_2$ (I)*** (Figure 2.3.6) and ***$FeCl_2$(H[4FPhFm])$_2$ (II)***.

Extension of the time the suspensions were held at reflux from 5 to 24 hours facilitates the complete conversion to the intended di-adducts. Any remaining residual free ligand was then removed via sublimation under reduced pressure to yield ***$FeCl_2$(H[DMOPhFm])$_2$ (I)*** and ***$FeCl_2$(H[4FPhFm])$_2$ (II)*** cleanly. These products were obtained in good (>80%) yield as an off-white/cream coloured solids. Further heating of the reaction mixture was not found to provide any further increase in the yield.

It is noted that attempts to generate similar di-adducts via alternative methods such as the use of melt reactions, have been previously reported for other formamidiante ligands but were found to present additional complications due to the inclusion of oily by-products.[258] In contrast no such complications were observed using the modified methodology described above.

The attempted synthesis of ***$FeCl_2$(H[TMOPhFm])$_2$ (III)*** and ***$FeCl_2$(H[3,5-(CF_3)PhFm])$_2$ (IV)*** provided some additional complications, arising chiefly from the significantly lower solubility of the parent ligands in toluene even at elevated temperatures. The lower solubility of both ligands and products caused a significant reduction in the observed rate of adduct formation and effectively precluded clean isolation of ***(III)*** or ***(IV)*** from reaction mixtures containing residual ligand and mono-adduct impurities via post-synthetic work-up.

Extension of the reflux period to 48 hours provides some further degree of conversion in favour of the di-adduct products ***(III)*** and ***(IV)*** but a mixture of the mono- and di- adduct products is still consistently obtained for both ***(III)*** (Appendix A-1-2) and ***(IV)***. Further

extension of the reflux conditions is not observed to result in significant further change prior to eventual decomposition of the products.

The use of more soluble forms of $FeCl_2$, such as $Fe_4Cl_8(THF)_6$ was explored as a means to improve upon results obtained with commercial $FeCl_2$. However, this was not observed to have a significant effect on the product distribution obtained implying that ligand solubility plays a more significant role in the progress of the reaction.

2.3.2.2 Choice of Mass spectral technique - MALDI-TOF-MS

MALDI-TOF-MS (Matrix Assisted Laser Desorption Ionisation Time Of Flight Mass spectrometry) was used extensively in the work reported herein as its features provides one of the valued and well suited means of analysing air sensitive species of which we are aware.

Most of our target compounds are neutral, non-volatile, and cover a wide 200-2500 m/z range. The use of a 'soft' ionisation method also enables the identification of the parent ions of the analysed specie, which in turn then in turn greatly aids in the monitoring and optimisation of reaction conditions. Avoiding the use of hard ionisation techniques also avoids the complications of fragmentation and also provides higher sensitivity than alternative techniques such as FAB and ESI.

Unlike some other methods the ability to introduce samples in the solid state is also of great advantage as this allows the preparation of solid, matrix-incorporated samples on the metal target within the protective environment of the glovebox. Combination of this and the ability to transport the target under argon (in a secondary sealed vessel) served to minimise the potential for samples to decompose prior to analysis.

2.3.2.3 Characterisation of $FeCl_2(H[amidinate])_2$ diadducts

The products obtained were identified primarily via MALDI-TOF-MS and the isotopic distributions of the product parent ions compared to those calculated using IsoPro 3.1 (a freeware isotopic distribution calculator).[306]

$FeCl_2(H[DMOPhFm])_2$ (I) and ***$FeCl_2(H[4FPhFm])_2$ (II)*** were obtained as free flowing off-white microcrystalline solids and identified by MALDI-TOF-MS by their [M-Cl] ions at m/z = 723.4 and 555.2 respectively. The isotopic distribution patterns obtained for ***(I)*** (Figure 2.3.6) and ***(II)*** by MALDI-TOF-MS spectra agree very closely with that calculated with IsoPro *(vide supra)*. As ***(I)*** and ***(II)*** were chiefly intended as intermediates species rather than particular target compounds of interest they were not subjected to further analysis.

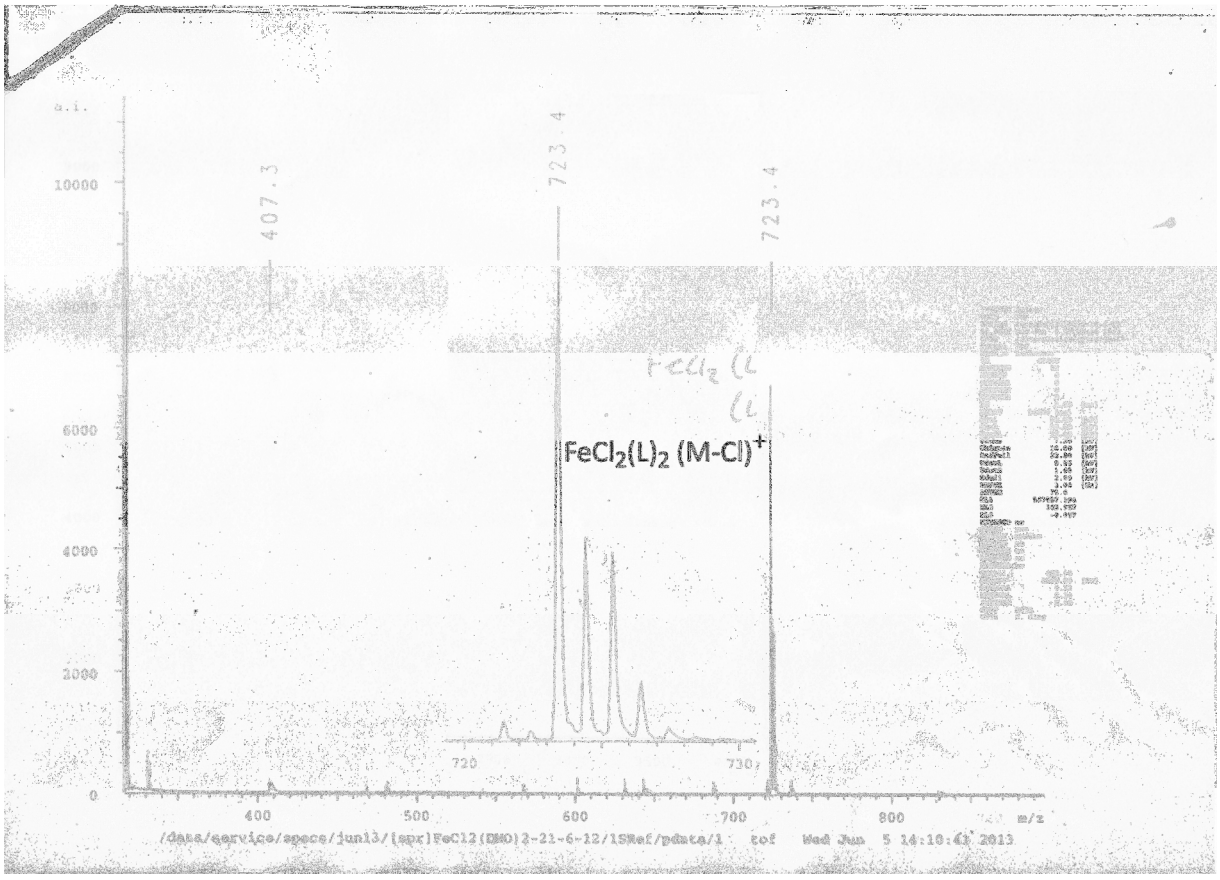

Figure 2.3.6 - Complete conversion to the target di-adduct (I) under extended reflux for 24 hours. Expansion shown of the target m/z.

As discussed previously neither ***$FeCl_2(H[TMOPhFm])_2$ (III)*** nor ***$FeCl_2(H[3,5\text{-}(CF_3)_2PhFm])_2$ (IV)*** were cleanly isolated but the presence of the target species was identified via MALDI-TOF-MS (e.g. Appendix A-1-1) as the $[M\text{-}Cl]^+$ ion at m/z = 843.5 and 1026.9 respectfully. In

addition to the intended parent ions the presence of significant free ligand and the corresponding mono-adducts was also observed.

2.3.3 Attempted synthesis of $Fe_2^{II,II}$(formamidinate)$_4$ complexes via $FeCl_2$(H[amidinate])$_2$ intermediates

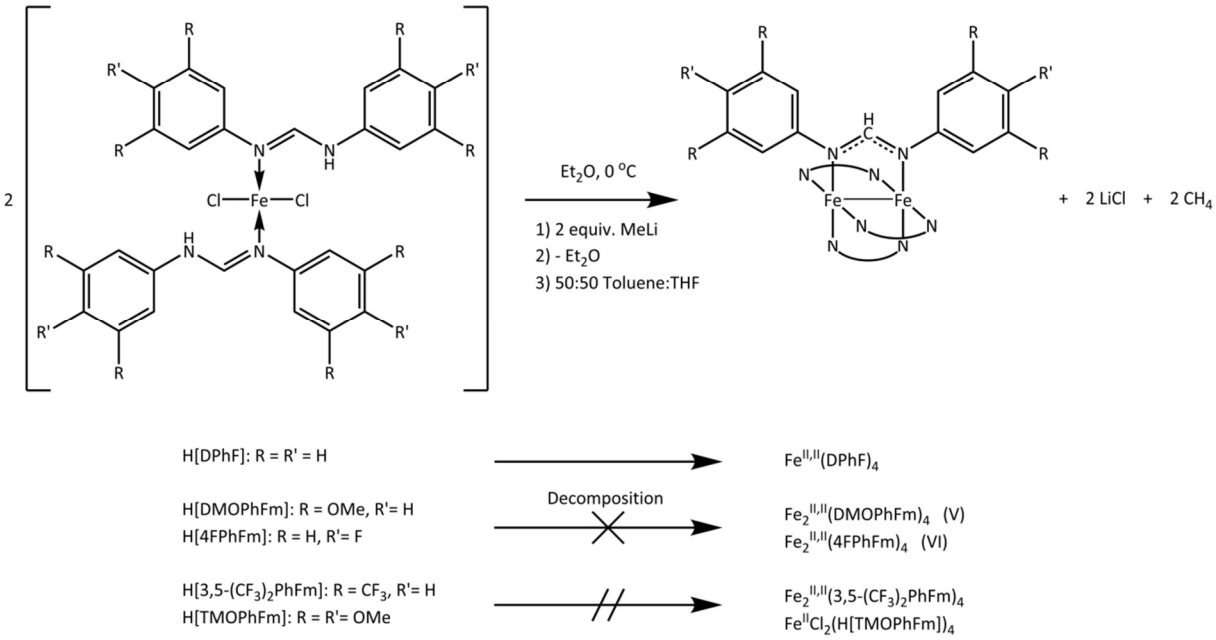

Figure 2.3.7 - Reaction scheme for the attempted synthesis of *Fe_2(DMOPhFm)$_4$ (V)* and *Fe_2(4FPhFm)$_4$ (VI)*. The synthesis of the analogous compounds utilising the last two ligands was not attempted due to issues with synthesis of the associated starting materials (vide infra).

The methodology published by Cotton for the synthesis of Fe_2(DPhF)$_4$, (where HDPhF = N,N'-Diphenylformamidine)[258] and synthetic efforts to replicate this chemistry with other ligands are summarised in Figure 2.3.7. For Cottons published example, that of H[DPhF] (where R = R' =H) on addition of 2 equivalents of MeLi a fine microcrystalline precipitate of an undefined but synthetically critical intermediate was reported. Successful isolation of the target compound Fe_2(DPhF)$_4$ was indicated to be contingent on the timely isolation and immediate re-dissolution of this intermediate in a 50:50 THF:toluene mixture. The reactive intermediate was noted to be unstable both in the initial ethereal reaction mixture on standing and on isolation in the solid state.[258,259]

2.3.3.1 Synthetic methodology

The synthesis of ***$Fe_2(DMOPhFm)_4$ (V)*** and ***$Fe_2(4FPhFm)_4$ (VI)*** was attempted in a similar fashion to that reported for $Fe_2(DPhF)_4$, utilising the previously synthesised diadducts ***$FeCl_2(H[DMOPhFm])_2$ (I)*** and ***$FeCl_2(H[4FPhFm])_2$ (II)***.

Attempts to synthesis the target tetra-formamidinates ***(V)*** and ***(VI)*** start with the suspension of the diadduct starting materials ***(I)*** and ***(II)*** respectively in diethyl ether and the cooling of these suspensions to 0 °C in an ice bath. Addition of MeLi to these suspensions did not result in the generation of a precipitate of the unstable intermediate observed by Cotton. Attempts were made to isolate the intermediate by removal of solvent, but MALDI-TOF-MS of the resultant solid indicated decomposition to unidentified low mass species.

As noted by Cotton for the HDPhF analogue, the intermediate formed after addition of MeLi is highly unstable and its precipitation is integral to the success of this reaction under the reported procedure. Small differences in the aryl substitution between the ligands used (Figure 2.3.8) appear sufficient to adversely increase the solubility of the ligands and preclude the isolation of the reactive intermediate.

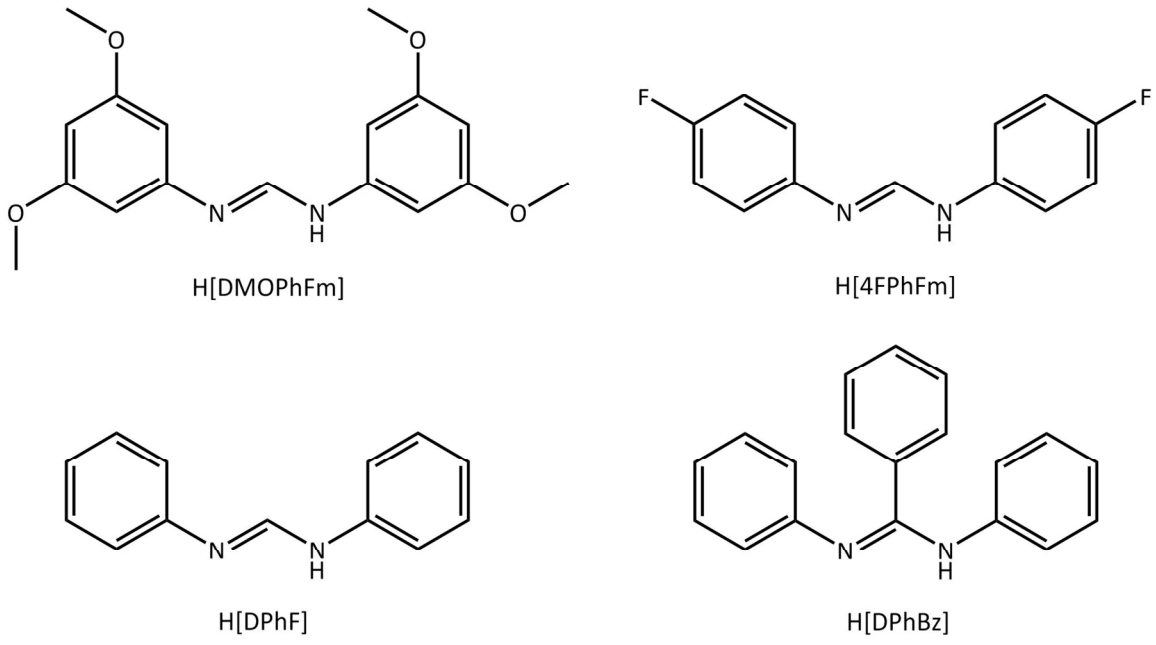

Figure 2.3.8 - Comparison of formamidinate ligands used, herein (top) and previously by Cotton (bottom).

Attempts were made to induce precipitation of the critical intermediate via use of minimal initial solvent (<5 ml total volume) and the further cooling of the reaction to -78 °C following addition of MeLi similarly failed to yield the described precipitate.

Further modifications to the procedure including the use of different the reaction solvent systems and the attempted use of other alkyllithium reagents such as ^{n}BuLi compounds similarly failed to provide an evidence of a precipitate.

In the absence of observable precipitation the reaction procedure was modified to enable monitoring of the reaction via mass spectrometry. Samples were taken for MALDI-TOF-MS immediately after addition of MeLi, at 10 minute intervals thereafter, and on removal of all volatiles *in vacuo* at the end of the experiment.

The residual solid from the reactions was then immediately extracted into a minimal volume of 50:50 THF:toluene and layered with *n*-pentane with the intention of inducing re-bulk crystallisation. Despite continued and repeated efforts the only crystals suitable for structural characterisation via X-Ray crystallography obtained were those of the parent free ligand of ***(I)*** and ***(V)*** **-** H[DMOPhFm].

2.3.3.2 Characterisation of resultant product mixtures

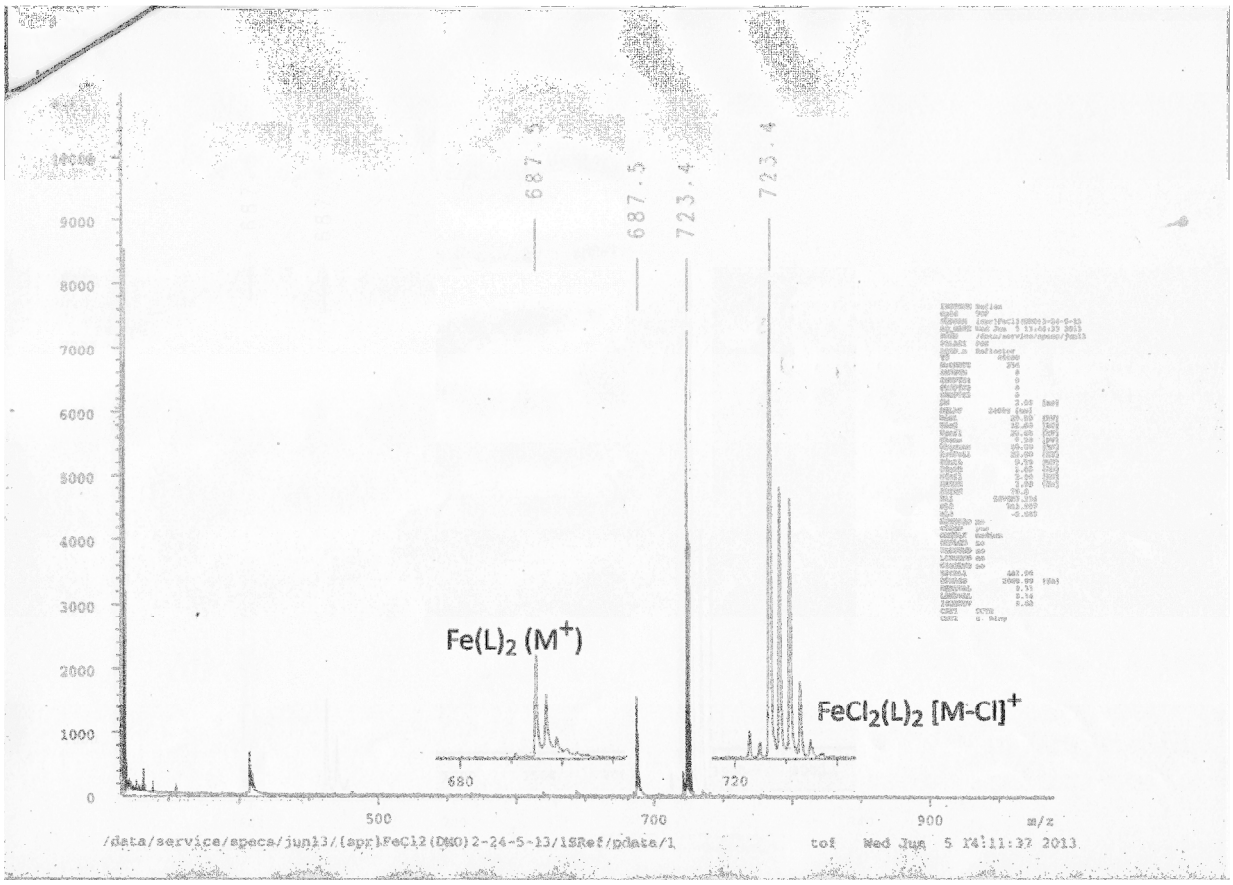

Figure 2.3.9 - FeCl2(H[DMOPhFm])$_2$ (I) after addition of MeLi at t=0 showing the formation of a new lower mass ion corresponding to a m/z loss approximating that of a further –Cl loss.

MALDI-TOF-MS samples taken immediately after the addition of the alkyllithium reagent, indicate that the peaks corresponding to the starting diadducts ***(I)*** and ***(II)*** respectively begin to rapidly decay in the initial few minutes of the reaction whilst a new secondary peak indicative of loss of chlorine from the parent ion was briefly observed at the slightly reduced m/z values of m/z = 686.2 and 520.1 respectively. After 2 hours, the only observed m/z ions in MS are those of low mass decomposition products indicating that the species corresponding to these new m/z ions are similarly unstable in the reaction media, and on attempted isolation in the solid state.

Cotton proposed that the unknown reactive intermediate was likely of the form [Fe(amidinate)$_2$Cl$_2$]$^{2-}$, but owing to the instability of the species was unable to provide and structural characterisation to support this.[283] As there is no indication of the new parent m/z ion having broadened or doubled to indicate the formation of a M^{2+} species it was

postulated that this species may instead be that of the corresponding bis(amidinate) (Figure 2.3.9).

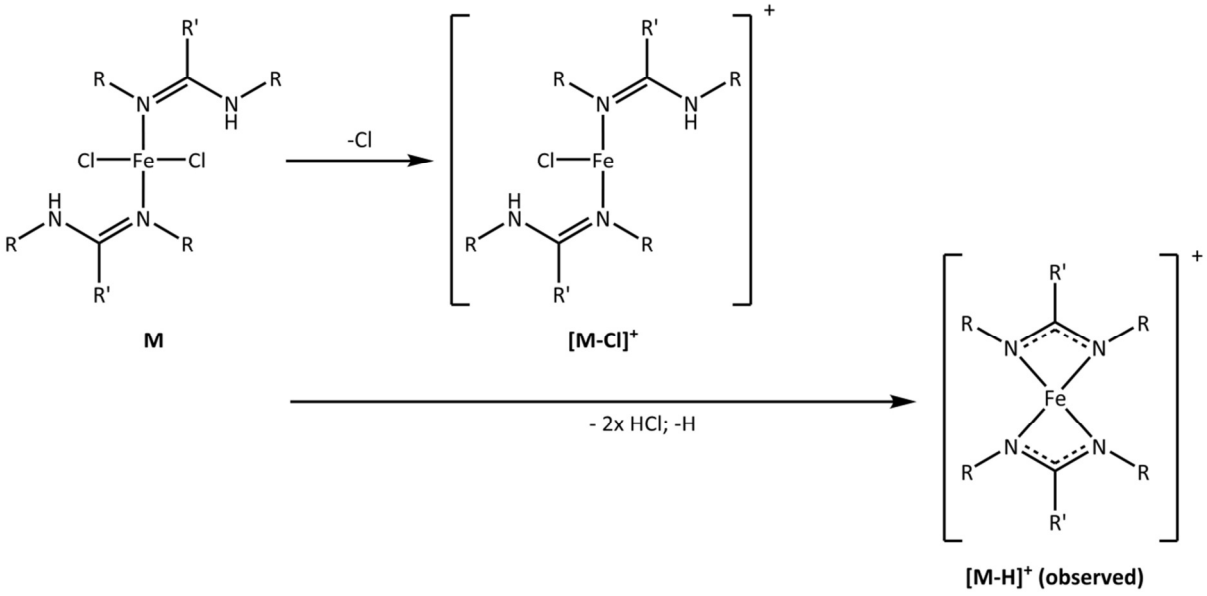

Figure 2.3.10 - Postulated unstable reactive intermediate as inferred from MALDI-TOF-MS spectra following MeLi addition

It is postulated that the interconversion of the diadduct to the bis(amidinate)may proceed via abstraction of two N-H protons, followed by the elimination of LiCl, both of which might reasonably be expected to occur on addition of suitably non-hindered alkyllithium reagents. The effective change in ligand binding mode from monodentate η^1-N to chelating η^2-N,N' (Figure 2.3.11) also allows iron to adopt a pseudo-tetrahedral configuration for which it shows a distinct preference.[103,258,259,272,274–277] Further, the decomposition of bis(amidinate) iron complexes of this type in solution is not without precedent, as similar complexes such as $Fe^{II}[^tBuC(NCy)]_2$ are known to display significant light sensitivity.[272]

Subsequent work by the groups of Hessen and Sciarone would tend to support the theory that the bis(amidinate presents a more plausible rationalisation of the observed unstable intermediate. Since Cotton's initial publication Hessen and Sciarone have identified and structurally characterised a range of closely related mono-iron amidinate compounds that exhibit comparable coordination environments (Figure 2.3.11).[272,274,275,277] This work also serves to further highlight the extreme reactivity and instability of these compounds, which in most instances was what lead to the adventitious isolation of these novel species.

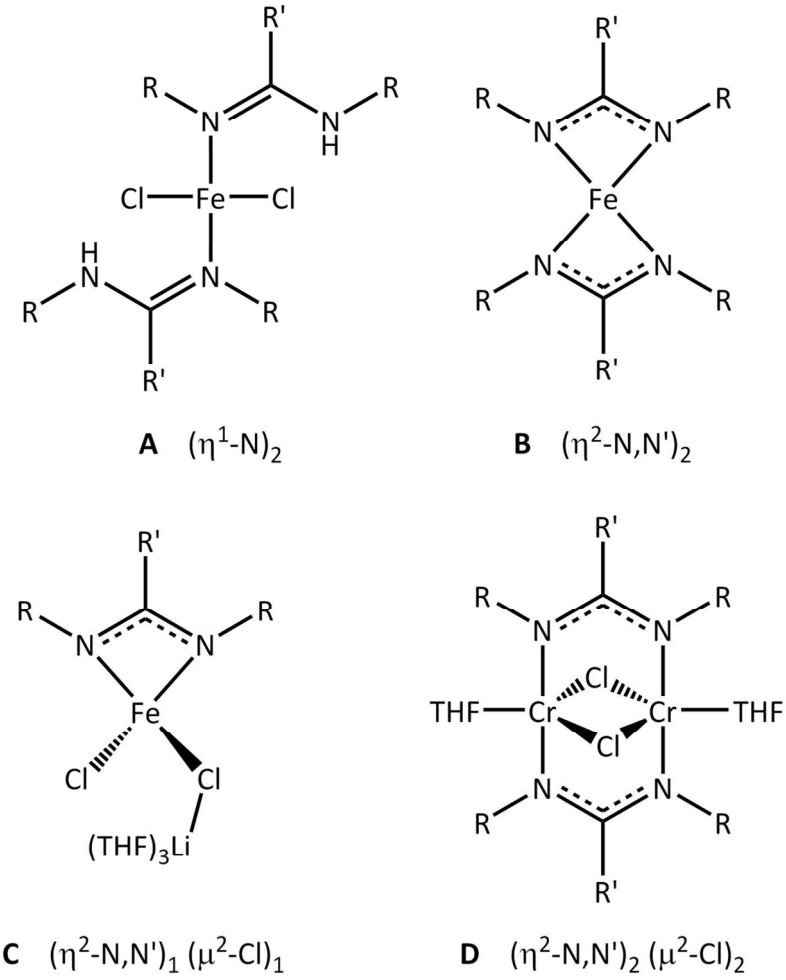

Figure 2.3.11 – Illustration of differing hapticity and bridging connectivity reported for intermediates towards the formation of M^{II}_2(amidinate)$_4$ complexes for iron and chromium. Aryl (R) and amidinate backbone (R') functionality is omitted for clarity.

Cottons di-adducts (**A**) have been described previously *(vide supra).* Hessen reported the related paramagnetic complex $Fe^{II}[^tBuC(NCy)]_2$ (**B**) for which both synthesis and products displayed significant sensitivity to ambient light.[272] Hessen and Sciarone later reported complexes such as $[\{PhC(NAr)_2\}Fe^{II}Cl(\mu^2\text{-}Cl)Li(THF)_3]$ which maybe isolated only in donor solvents, decaying to the related (**B**) type compound on standing in non-donor solvents or by reaction with some alkylating agents such as $LiCH(SiMe_3)_2$.[275] Similarly, Cotton reported that the complex $Cr_2^{II,II}(\mu^2\text{-}Cl)_2(DXylF)_2(THF)_2$ (where DXylF = N,N'-bis(2,6-xylyl)-formamidinate) may be isolated utilising THF as the reaction solvent, whilst again a (**B**) product is obtained where toluene is utilised instead.[283]

Both the initial (**B**) complex and those later described by Hessen and Sciarone such as $Fe^{II}[Dipp)]_2$ (where Dipp = N,N'-Bis(2,6-diisopropylphenyl)benzamidinate) are also highly

paramagnetic, matching that observed by Cotton. Hessen and Sciarone further showed that these compounds are capable of supporting highly strained geometries and high spin state iron. Square planar[274] and 5-coordinate complexes[277] high spin (S = 2) Fe^{II} complexes of this form have since been reported and structurally characterised. In both instances the steric demands of the ligands are thought to be central both to the enforcement of such conformers and relative selectivity and stability of the target products.[274,277]

2.3.4 Attempted synthesis of $Fe_2^{II,II}$(formamidinate)$_4$ complexes via direct methods

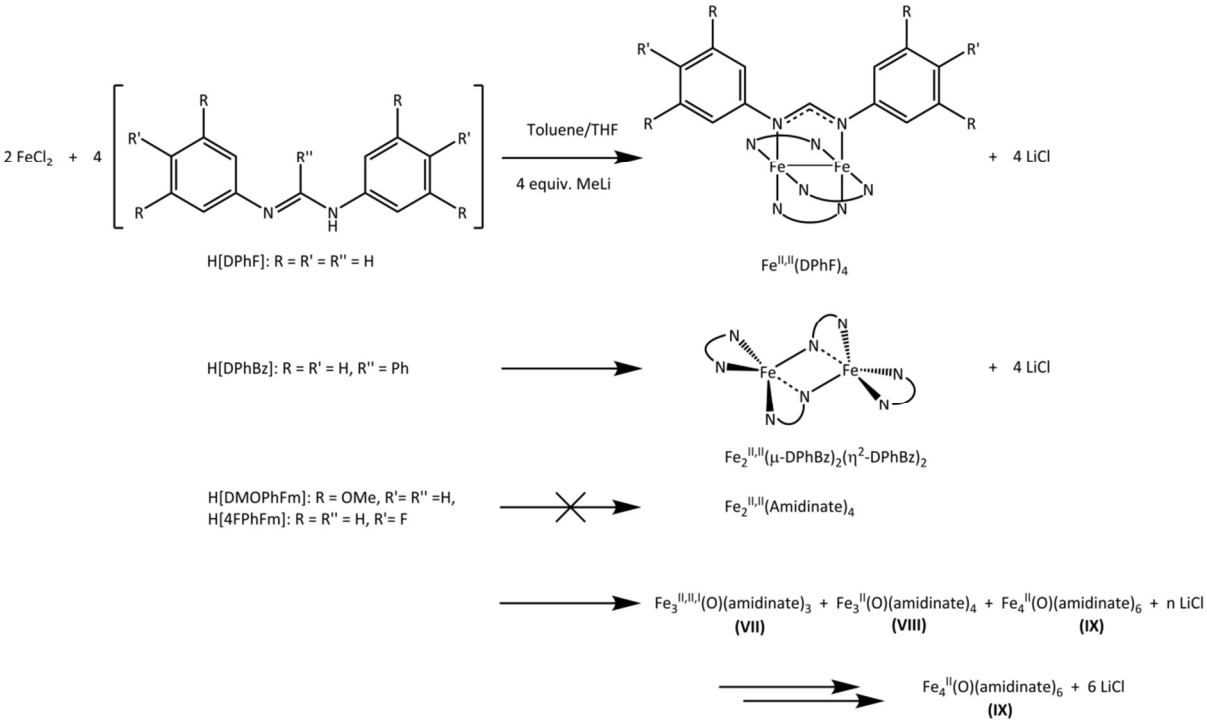

Figure 2.3.12 - Summary of synthetic efforts towards the generation of novel diiron (II) tetra-amidinates

In his attempts to reduce the distortion observed in the diiron core of $Fe_2(DPhF)_4$ Cotton proposed the synthesis of the more bulky benzamidinate complex of $Fe_2(DPhBz)_4$ (where HDPhBz = N,N'-diphenylbenzamidine)[259] Unexpectidly however, in place of the intended paddlewheel complex the distorted windmill species $Fe_2(\mu\text{-}DPhBz)_2(\eta^2\text{-}DPhBz)_2$ was obtained instead.

In contrast to the published procedure for $Fe_2(DPhF)_4$ however, the published synthesis of $Fe_2(\mu\text{-}DPhBz)_2(\eta^2\text{-}DPhBz)_2$ shows no dependence on the isolation of a precipitated reactive

intermediate. Consequently, this was deemed the most suitable synthetic on which to base further attempts towards the generation of ***$Fe_2(DMOPhFm)_4$ (V)***.

Cotton's reported synthesis of $Fe_2(\mu\text{-DPhBz})_2(\eta^2\text{-DPhBz})_2$ proceeds via direct combination of $FeCl_2$ and the free benzamidinate followed by the addition of MeLi at -77 °C. On addition a sharp colour change from yellow to red/brown was observed, and the reaction then slowly allowed to warm to room temperature. It is indicated that it is necessary to remove a small amount of an unknown solid on warming, followed by the need to rapidly filter the mixture prior to generation of an unknown precipitate. However, as the nature of these species and a more precise indication of the required timings of these steps is not well defined these elements complicate efforts to accurately replicate the procedure.

Attempts to synthesis ***$Fe_2(DMOPhFm)_4$ (V)*** under the conditions published by Cotton were unsuccessful and did not induce a similarly rapid colour change to a red/brown mixture, but a distinct yellow -> orange/brown colour change was noted. Further, on warming to room temperature and prolonged standing no particulate solid or precipitate formation was observed and as such it was not possible to remove these species as indicated in the methodology.

Analysis via MALDI-TOF-MS provided the primary means to follow and characterise the residual solid from the reactions which was consistently observed to contain a mixture of disparate products. These mixtures included a species at m/z = 1444.4 that was consistent with a postulated THF solvate of ***(V)***, $Fe_2(DMOPhFm)_4(THF)$ ($M_{monoisotopic}$ = 1444.5). This product was consistently observed in combination with several other products whose m/z ions ranging from 1000-2135 but the identity of which could not be readily resolved. Further characterisation was precluded as it was not possible to cleanly isolate individual products from the mixtures obtained and synthetic efforts moved to optimise the reaction conditions in favour of the postulated THF solvate of ***(V)***.

2.3.4.1 Optimisation of product conditions

Despite attempts to optimise a wide range of reaction variables the same series of products was consistently obtained, with only differences in their relative proportions noted. As

intractable product mixtures were obtained, no yields for these reactions could be determined.

On replication of published conditions the product mixtures were initially thought to include $Fe_2(DMOPhFm)_4(THF)$, a solvate of ***(V)*** observed by MALDI-TOF-MS with m/z = 1444. Efforts to optimise the reaction conditions to favour the clean isolation of this product were unsuccessful.

Subsequent experimentation using 2-Me THF, and in the absence of THF, eventually disproved the initial assignment of the m/z = 1444 peak as $Fe_2(DMOPhFm)_4(THF)$. A tentative alternative assignment is therefore provided (Section 2.3.6) for all major product species (m/z = 1129, 1444, and 2131) as representing a series of increasingly large poly-iron (II) cluster products.

The products obtained are postulated to be the result of thermodynamic control trending towards the largest and most thermodynamically stable cluster species (m/z =2131) ***$Fe_4^{II}(O)(DMOPhFm)6$ (IX)***. The identity of this species was confirmed by X-Ray crystallography and was observed to adopt the known low energy basic beryllium acetate structure.[263,282] Unlike previously reported structures of this type for iron amidinates[263] the observed structure is not distorted and shows regular bridging behaviour as has been previously reported for related Zn, Co and Mn complexes.[263] Two separate structures of ***(IX)*** were determined; however only one was of sufficient quality for publication.

Despite variation of iron (II) salt and alkyllithium used no clear dependence of any of the major product m/z species was observed. This contrasts strongly with that previously reported for the related complex $Fe_2^{II}(DPhF)_4$[258,259] and with other previously reported complexes utilising the same HDPhF ligand.[258–263,280,281] In the chemistry examined herein reaction temperature and time were ultimately observed to have the most significant impact on the distribution of the cluster products obtained.

Prolonged exposure to donor solvents and trace moisture was noted to significantly alter the distribution of the products obtained. Product mixtures containing predominantly the lower mass products at m/z = 1129 and 1444 assigned as ***$Fe_3^{II,II,I}(O)(amidinate)_3$ (VII)*** and ***$Fe_3^{II}(O)(amidinate)_4$ (VIII)*** respectively were observed to favour the formation of ***(IX)*** on

extended contact with THF. It was further noted that exposure of such reaction mixtures to trace moisture similarly favoured the formation of ***(IX)*** even in samples isolated in the solid state. Trace water content has been cited as a driving force towards clusters of similar form to ***(IX)*** from dizinc tetra-amidinates, however iron analogues are by contrast proposed to form via exposure to oxygen.[263] Conduction of solvent sensitivity studies (Section 2.3.5.7) within a securely oxygen free glovebox environment indicate that such chemistry proceeds does in fact proceed via H_2O rather than O_2 as previously reported.[263] Such transformation has never previously been noted to proceed in the solid state, nor on prolonged contact with other donor solvents such as THF however a precedent for such sensitivity can be found in related bis(amidinate chemistry) of iron[275] and dichromium tetra-amidinates.[283]

With a view to aiding further development of synthetic method development towards $Fe_2^{II,II}$(formamidinate)$_4$ complexes a comparative analysis of the reaction variables test with the previous available literature is provided in the following sub-sections.

2.3.4.2 Variation of the iron (II) salt starting material

Attempts to modify the reaction to utilise alternative metal salts such as $Fe_4Cl_8(THF)_6$,[307] $Fe(OTf)_2 \cdot xMeCN$[284] and $Fe(OAc)_2$[308,309] were then attempted with the intention of providing a means to selectively isolate a single product associated with the 1444.4 m/z (Figure 2.3.12).

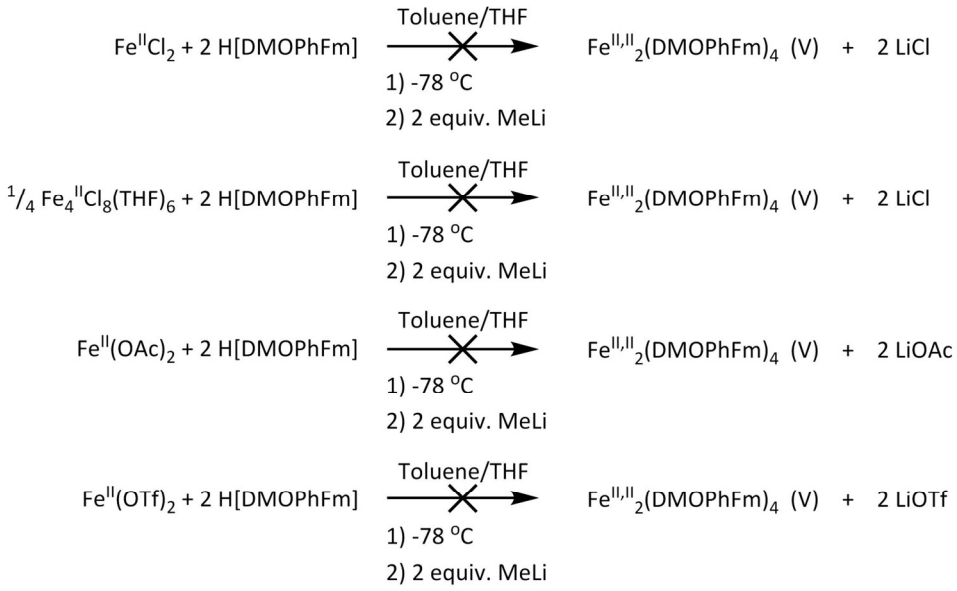

Figure 2.3.13 - Initial reaction conditions utilised for initial metal variation studies.

The use of $Fe_4Cl_8(THF)_6$ or $Fe(OTf)_2$·xMeCN was not found to significantly alter the major products formed compared to $FeCl_2$ nor the relative distribution in which they were obtained. The use of $Fe(OAc)_2$ by contrast yielded only low m/z decomposition products. The drying of $Fe_4Cl_8(THF)_6$ yields a more soluble polymorph of $FeCl_2$. As the use of this polymorph showed no significant advantage over commercial $FeCl_2$ however its use was discontinued in favour of the commercial alternative.

The use of $Fe(OTf)_2$·xMeCN was noted to result in the formation of few lower valent low m/z species compared to the other salts. For example, no indication of the formation of the corresponding mono-iron diadduct $Fe^{II}(OTf)_2(DMOPhFm)_2$ was observed via MALDI-TOF-MS. Deliberate attempts to form diadducts analogous to ***(I)*** by refluxing of the free ligand with $Fe(OTf)_2$·xMeCN or $Fe(OAc)_2$ further fail to yield such species and instead yield the bis(amidinate) (Figure 2.3.13).

In agreement with that noted in the study of diiron tetracarboxylates by Lippard, the most synthetically useful iron starting materials are $Fe(OTf)_2$·xMeCN and $FeCl_2$. The former shows comparable utility to metal perchlorates without the associated safety implications[284,310] whilst the latter has been shown in related mono iron bis(amidinate chemistry to facilitate the formation of otherwise unstable reactive intermediates.[274]

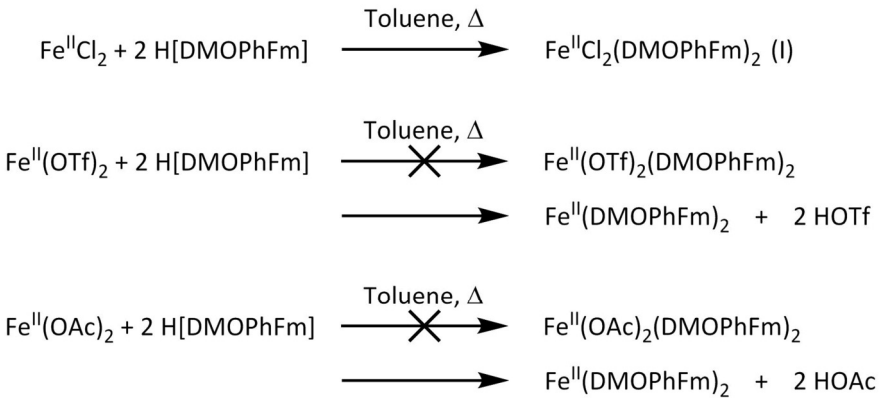

Figure 2.3.14 - Scheme of attempted synthesis of analogues of (I) using different metal salts

2.3.4.3 Pre-formation of lithium amidinate salts

The first major deviation from the published method that was explored was the generation of the alkali metal formamidinate salt prior to addition of the iron (II) salt rather than the reported one-pot synthesis.[259] This was done to minimise the potential for nucleophilic attack by the RLi on the Fe (II) centre and the formation of reduced species containing Fe_2 (I,II)[260,280] or Fe(0)[275] via reductive β-elimination of an alkene.

Synthetic attempts conducted in this manner have previously been reported[261,279] to yield the oxidised tris-substituted mono-iron species $Fe^{III}(DPhF)_3$. In contrast to such reports no evidence of the analogous species $Fe^{III}(DMOPhFm)_3$ was observed in synthetic attempts towards ***(V)*** (Figure 2.3.14).

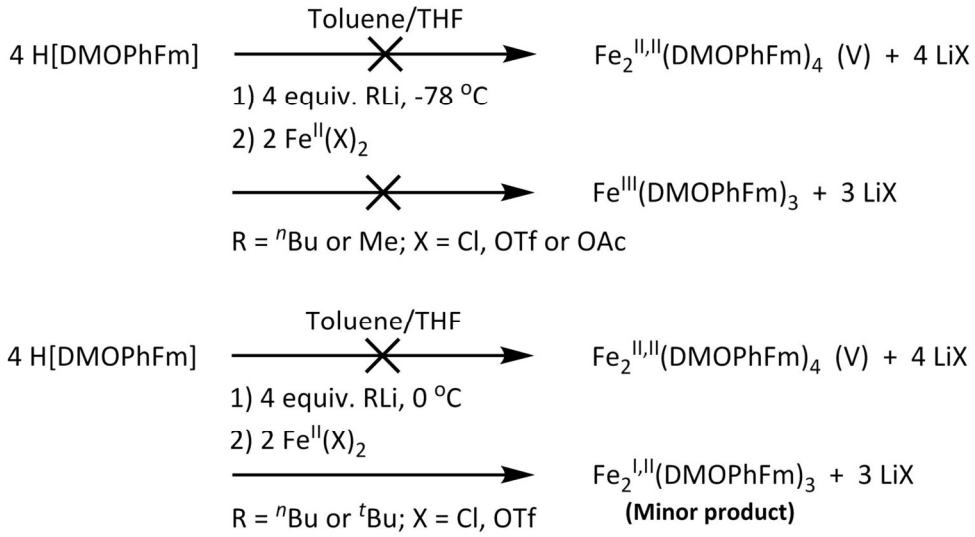

Figure 2.3.15 - Scheme of initial reactions utilising differing alkyllithium reagents. (Top) The formation of the mono-iron tris-substituted species $Fe^{III}(DMOPhFm)_3$. (Bottom) The formation of the reduced diiron (I,II) trigonal lantern product $Fe_2^{I,II}(DMOPhFm)_3$. Excess starting materials present after the reactions generating unintended side-products are omitted for clarity.

2.3.4.4 Variation of the Alkyl lithium reagent

The use of MeLi, ^{n}BuLi or ^{t}BuLi in combination with H[DMOPhFm] was not observed to significantly alter the identity, or distribution, of the major products obtained under the vast majority of conditions tested contrasting strongly with previous reports by Cotton.[258–260,262,280]

Under deliberately aggressive conditions, (e.g. addition of ^{n}BuLi or ^{t}BuLi at 0 °C cf. -78 °C,) the inclusion of a species with a m/z ion consistent with the β-elimination product $Fe_2^{I,II}(DMOPhFm)_3$ was observed in the product mixture (Figure 2.3.15). This was however only ever noted as a minor product (Appendix A-2-2), even under conditions further modified to intentionally favour its formation (e.g. use of a 3:2 ligand:metal stoichiometry.) No formation of the β-elimination product $Fe_2^{I,II}(DMOPhFm)_3$ was observed where the addition of the alkyllithium was conducted under more typical conditions at -78°C. This contrasts with an initial report by Cotton for the synthesis of $Fe_2^{I,II}(DPhF)_3$ from $Fe^{II}Cl_2(DPhF)_2$ conducted under very similar conditions.[260] A subsequent report however provides a revised synthetic approach to this complex which eschews the use of ^{n}BuLi entirely in favour of MeLi.[280]

More recent reports from the groups of Hessen and Sciarone on related bulky mono-iron bis(benzamidiante) complexes suggest that sensitivity towards some alkyllithium reagents such as ^{n}BuLi,[274,276,277] and MeLi[272] may be offset by provision of sufficient steric bulk from the ligand. In some instances they also report the use of other more bulky non-nucleophilic bases such as lithium diisopropylamide (LDA) and lithium bis(trimethylsilyl)amide (LiHMDS) which despite their non-nucleophilic nature do in some instances still result in the formation of β-elimination products.[275]

2.3.4.5 Impact of the use of sodium amidinate salts

In addition to the use of differing alkyllithium reagents, the corresponding sodium salt Na[DMOPhFm] was also generated via reaction with NaH in THF and its impact on the products obtained explored Figure (2.3.15).

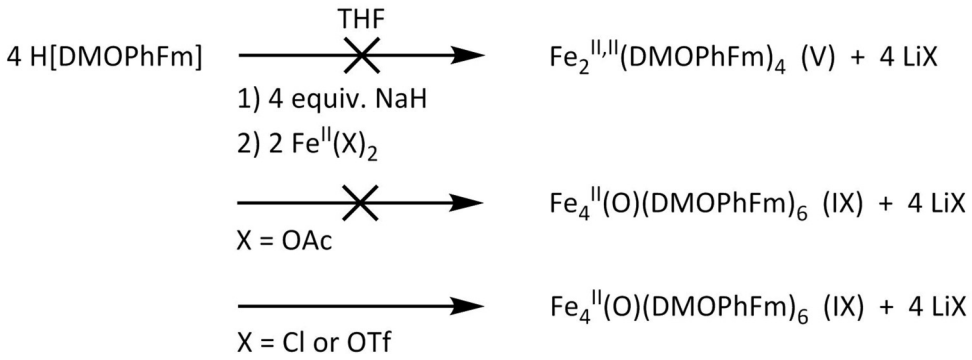

Figure 2.3.16 - Reaction scheme for the attempted failed synthesis of X and synthesis of Y using Na[DMOPhFm].

As might be expected for these more reactive species the largest poly-iron species ***$Fe_4^{II}(O)(DMOPhFm)_6$ (IX)*** is obtained almost exclusively in combination with $FeCl_2$ or $Fe(OTf)_2$·xMeCN. Attempts to replicate similar chemistry with $Fe(OAc)_2$ show only low mass products postulated to be indicative of decomposition.

The two starting materials $FeCl_2$ and $Fe(OTf)_2$·xMeCN despite both showing the singular presence of ***(IX)*** by MALDI-TOF-MS vary significantly in appearance. Reactions using the former display and immediate yellow -> deep green colour change on addition of the sodium salt. The latter retains its initial yellow colour, turning orange over the course a few minutes in a manner consistent with the generation of ***(IX)*** observed with alkyllithium reagents.

The identity and nature of the strongly green coloured species obtained via use of $FeCl_2$ is not readily apparent by MALDI-TOF-MS which shows only ***(IX)***. Experimental observations however match closely with reports of the formation of $Fe^{III}(amidinate)_3$ species as published by Kilner[279] and later by Cotton[261] potentially indicating that the Fe (II) present may have been oxidised to a corresponding Fe (III) species. Despite repeated attempts no crystals of this green product suitable for X-Ray diffraction could be obtained.

2.3.4.6 Achieving control of the product distribution obtained

During extended reactions where the yellow/orange mixture of iron and alkali amidinate salts were allowed to stir for 16-24 hours, the higher mass product ***(IX)*** was observed to dominate the product distribution obtained. Reactions stopped by evacuation of all volatile components *in vacuo* and extraction into DCM after shorter time periods (1-16 hours) showed increased population of the lower mass products proposed as ***$Fe_3^{II,II,I}(O)(amidinate)_3$ (VII)*** and ***$Fe_3^{II}(O)(amidinate)_4$ (VIII)***. Selectivity for ***(VII)*** was further enhanced by extension of the time taken to warm the reaction mixture from -78 °C to room temperature to 1-3 hours and the use of 1:1 metal:ligand stoichiometry.

Preventing further reaction of isolated samples mixtures containing mostly ***(VII)*** and ***(VIII)*** proved more difficult that expect as both readily react further to yield ***(IX)*** as the primary product on prolonged exposure to donor solvents such as THF. This may be observed by comparison of MALDI-TOF-MS spectra for the same sample made and allowed to stand in THF and DCM (Appendix A-2-3 + Appendix A-2-4) for 3-4 hours. The authenticity of the DCM sample was confirmed by comparison to a MALDI-TOF-MS sample prepared in toluene with which it was consistent.

A similar trend towards ***(IX)*** was observed for samples isolated in the solid state that were subject to contact with trace moisture over the course of 1 month (Appendix A-2-5). The source of this trace moisture was thought to be residual moisture adsorbed on the glass of the some sample vials. Removal of such trace water was common practise with reaction vessels by heating via blow-torch under high vacuum but such rigorous drying was not always possible with sample storage vials.

Similar trends have previously been reported for analogous transition metal $M_2^{II}(amidinate)_4$ complexes (where M = Zn, Mn or Co) which interconvert to their corresponding $M_4(O)(amidinate)_4$ on exposure to oxygen or moisture.[263] Where such efforts have been applied to diiron analogues of these however, differing distorted structures were obtained.[263] In contrast to such reports, we report the structure of the first symmetrically bridged iron (II) complex of this form ***(IX)*** (Section 2.3.6.3).

The presence of donor solvents such as water and THF is known to facilitate the rapid coordinative reconfiguration of diiron carboxylate complexes; this was shown by Lippard to significantly enable reactivity with biologically relevant substrates such as dioxygen.[210] Consequently, the potential to undergo coordinative rearrangement is of critical importance for biological modelling. In the instance of ***(IX)*** such rearrangements appear irreversible as the product obtained shows greater thermodynamically stability than the parent species ***(VII)*** and ***(VIII)***.

2.3.5 Characterisation of poly-iron (II) cluster species obtained during the attempted synthesis of $Fe_2(DMOPhFm)_4$ (V)

2.3.5.1 MALDI-TOF-MS

Assigned compound ID	$M_{average}$	$M_{monoisotopic}$ [M+]	[M-Cl]
$Fe^{II}(DMOPhFm)_2$	686.5	**686.2**	-
$Fe^{II}Cl_2(H[DMOPhFm])_2$	757.5	756.1	**721.2**
$Fe^{III}(DMOPhFm)_3$	1001.9	**1001.3**	-
$Fe_2^{I,II}(DMOPhFm)_3$	1057.7	**1057.3**	-
$Fe_3^{II,II,I}(O)(DMOPhFm)_3$	1129.6	***1129.2***	-
$[Li(THF)_4][Fe^{II}(DMOPhFm)_3]$	1297.3	**1296.6**	-
$Fe_2^{II,II}(DMOPhFm)_4$	1373.1	**1372.4**	-
$Fe_2^{II,II}(DMOPhFm)_4(THF)$	1445.2	**1444.5**	-
$Fe_3^{II}(O)(DMOPhFm)_4$	1444.9	**1444.3**	-
$Fe_4^{II}(O)(DMOPhFm)_5Cl$	1851.6	1850.4	**1815.4**
$Fe_4^{II}(O)(DMOPhFm)_6$	2131.5	**2130.5**	-
$Fe_4^{III}O_4(DMOPhFm)_6Li_2(H[DMOPhFm])_2$	2826.1	**2824.8**	-

Table 2.3.1 – Predicted mass ions for analogues of previously reported species and postulated cluster products in order of increasing m/z. Expected mass ions are highlighted in bold.

The products mixtures obtained in the attempted synthesis of ***$Fe_2(DMOPhFm)_4$ (V)*** from by direct combination of iron (II) and alkali metal formamidinate salts were noted to all contain a small number of identical m/z ions. These species were consistently observed at m/z = 1129, 1444, and 2131. A number of additional species were also commonly, but not consistently observed at m/z = 1057, 1550, 1575 and 1816. Assignments for these m/z ions are provided above (Table 2.3.1) and an example of a typical un-optimised product mixture is given overleaf (Figure 2.3.16) with inserts showing expansions of the isotopic distribution of the parent ions.

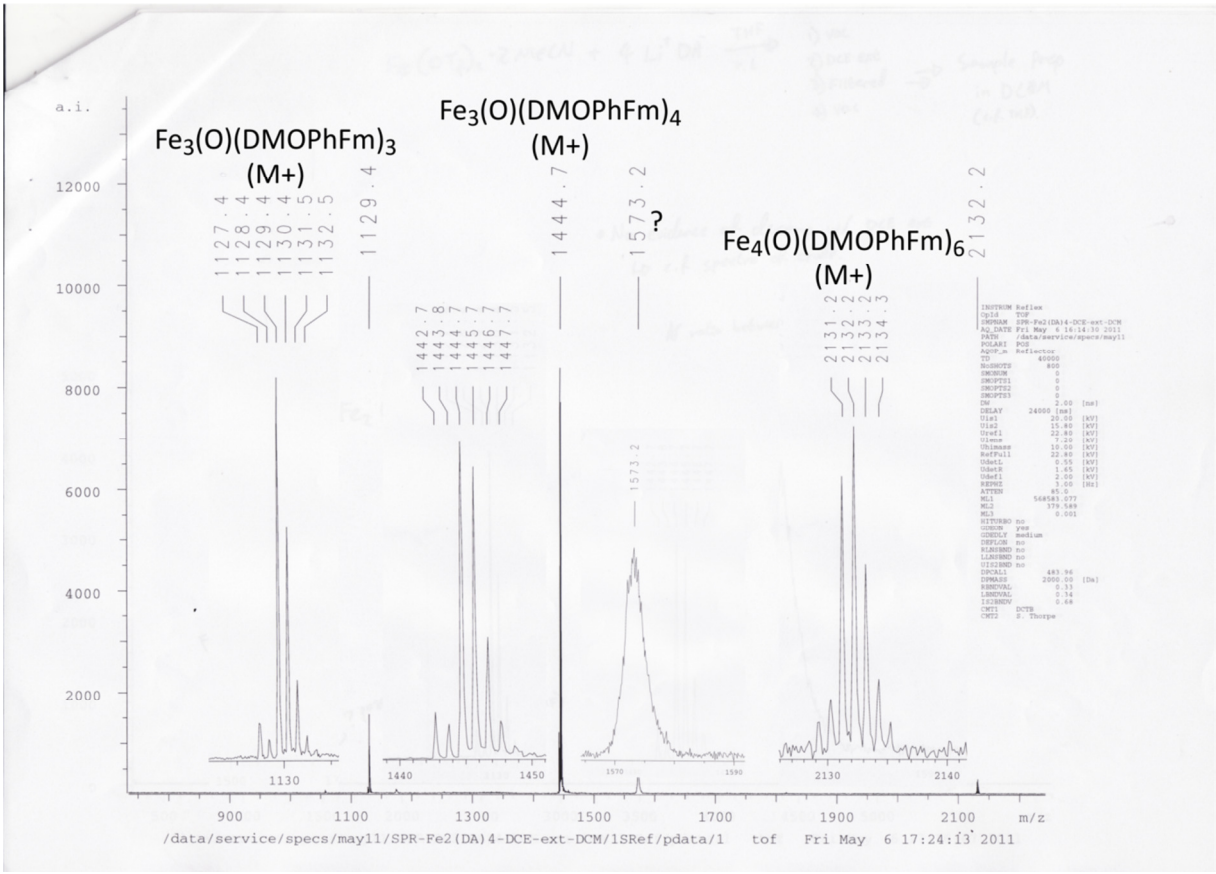

Figure 2.3.17 - A typical un-optimised product mixture obtained during attemtpts to synthesise (V). Assignments are given above for ions for which an identity was determined. The doubly charged mass ion at m/z = 1573 was could not be assigned.

The m/z ion observed at m/z = 1444 was observed as the major product in initial testing (Figure 2.3.16) and was tentatively assigned as the THF solvate of the intended tetra-substituted product $Fe_2^{II,II}(amidinate)_4(THF)$ with $M_{monoisotopic}$ = 1444.2. Later experiments substituting 2-methyl THF as an alternative co-solvent to however still yielded the same species at 1444 disproving this initial assignment.

Consideration of other previously reported related species such as the partial reduction product $Fe_2^{I,II}(amidinate)_3$ enabled the assignment of some further m/z ions. In this way the infrequently observed species at m/z = 1057 was assigned as the corresponding β-elimination product $Fe_2^{I,II}(DMOPhFm)_3$ (Appendix A-2-2). As this species was however both uncommonly observed and had no discernible impact on the distribution of the more common products it was not thought not to be a probable intermediate in their formation.

Application of similar comparative analysis to previously cited products[263] led to the tentative assignment of the m/z ion at m/z = 2130 to the tetra-iron cluster species

$Fe_4^{II}(O)(DMOPhFm)_6$ (IX). This assignment was then subsequently confirmed by the structural characterisation of ***(IX)*** by X-Ray crystallography.

In light of the identification of the major product at m/z = 2130 as a poly-iron cluster species, similar formulations were proposed for the remaining major product m/z ions at m/z = 1129 and 1444. These two species were proposed as being ***$Fe_3^{II,II,I}(O)(DMOPhFm)_3$ (VII)*** and ***$Fe_3^{II}(O)(DMOPhFm)_4$ (VIII)*** respectively however no firm evidence to support these assignments could be obtained.

Attempts made to optimise the reaction conditions to favour ***(VII)*** (Appendix A-2-3) and ***(VIII)*** (Figure 2.3.16) increased selectivity but despite this neither was isolated exclusively. The observed trend of further reactivity toward the formation of ***(IX)*** (Section 2.3.5.7) provides some explanation of this behaviour.

2.3.5.2 Isotopic distribution as a diagnostic indicator of product nuclearity

Compounds containing metals with a number of highly abundant isotopes show corresponding complex m/z ions. In many instances the complexity of these isotopic distributions provides significant diagnostic utility in facilitating the determination of nuclearity of a given metal within the observed species where the likely components are known (Section 3.3.2).

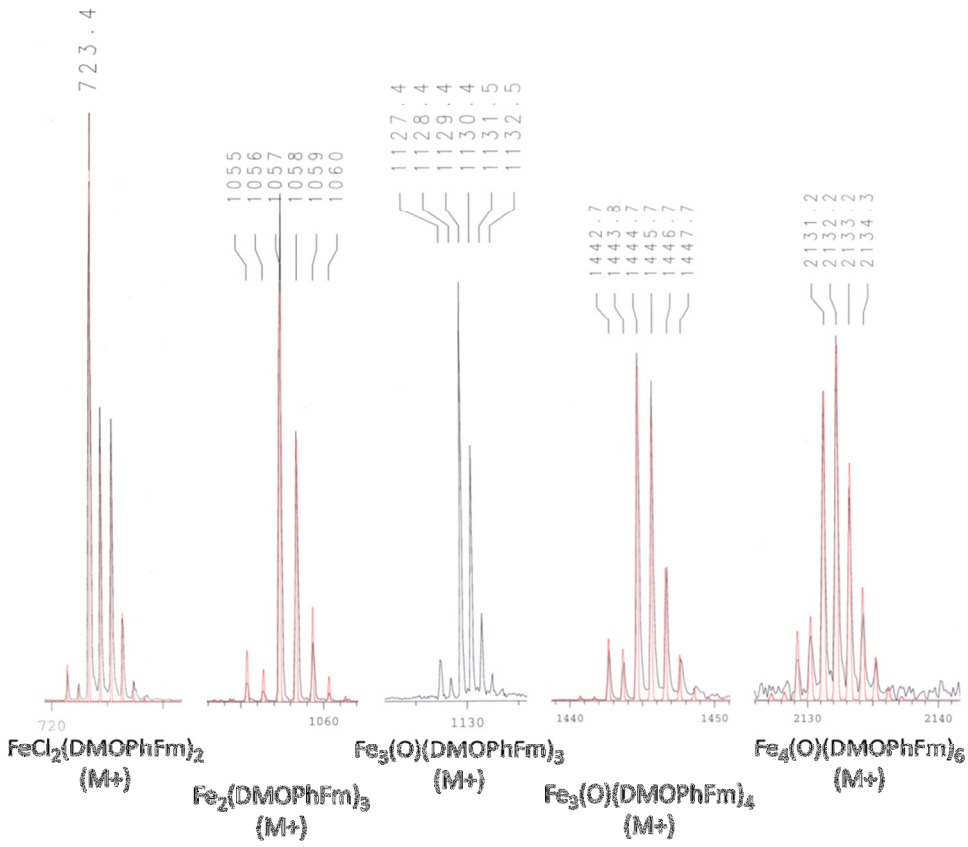

Figure 2.3.18 - Examination of isotopic distribution observed for the m/z ions of a range of iron amidinate species. Calculated isotopic distributions using Isopro 3.1

In contrast to more isotopically rich later transition metals such as ruthenium however, iron contains comparatively few abundant isotopes which severely limits the application of this practice to its complexes. Low isotopic variation observed for the metal results in contributions from the more numerous non-metallic elements (C, N, H, O) of the supporting ligands dominating the shape of the m/z ions of observed. Consequently, there is very little observable difference between species containing Fe_1, Fe_2 and Fe_3 and only a small difference for M_4 (Figure 2.3.17).

2.3.5.3 X-Ray crystallography

Crystals of ***$Fe_4^{II}(O)(DMOPhFm)_6$ (IX)*** were obtained via vapour diffusion of *n*-pentane into a saturated solution of DCM at -18 °C over one week. Subsequent attempts to grow crystals of ***(VII)*** and ***(VIII)*** from product mixtures in which they were the predominate product only yielded an additional structures of ***(IX)*** (Section 2.3.5.7) and ***H[DMOPhFm]*** (Section 2.3.1.5).

The crystals of ***(IX)*** obtained were extracted from the crystallisation vessel and initial crystal selection was conducted with the crystals under argon immersed in dried, de-gassed fomblin® oil. Suitably sized crystals were then mounted atop a mylar® tip in a small glob of oil and rapidly transferred to the diffractometer wherein they were held within a cooled stream of nitrogen at 100 K.

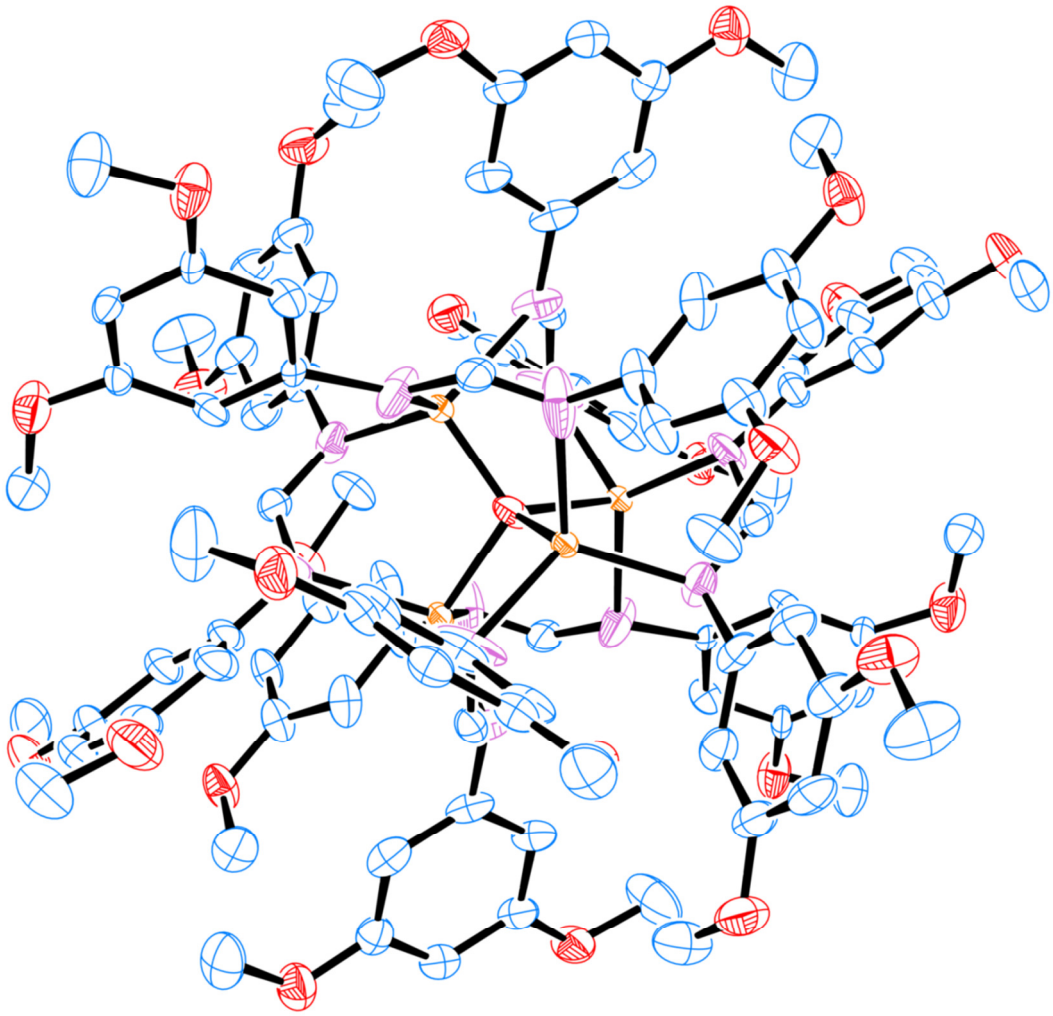

Figure 2.3.19 Solid state structure of $Fe_4^{II}(O)(DMOPhFm)_6$ (IX). Hydrogens and modelled disorder of one phenyl ring are omited for clarity. Thermal elipsoids are drawn at the 50% probability level. Selected bond lengths are provided in table 2.3.2; Complete X-Ray difraction tables are provided elsewhere in appendix B-2.

The structure of the complex ***$Fe_4^{II}(O)(DMOPhFm)_6$ (IX)*** (Figure 2.3.18) resembles both that of the basic beryllium acetate[282,311–313] $Be_4O(OAc)_6$ (from which this structure type derives its name) and similar amidinate complexes of Fe, Mn, Co and Zn.[263]

The central $(\mu^4\text{-}OFe_4)^{6+}$ core of ***(IX)*** was disordered across two configurations (Figure 2.3.19) and the free-refinement of the occupancy of these disordered elements affords a 50:50 observed split in occupancy.

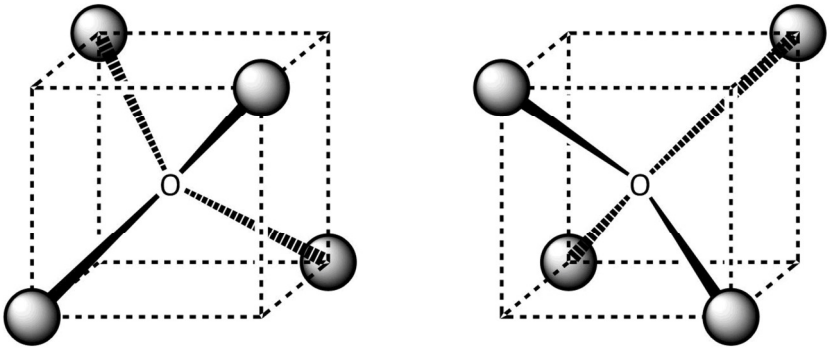

Figure 2.3.20 - Illustration of the two different occupied configurations of $(M_4O)^{6+}$ core

The immediate coordination environment of the $(Fe_4O)^{6+}$ core is more apparent where phenyl substituents are further omitted (Figure 2.3.20). Each Fe atom was observed to coordinate to 3 surrounding ligand nitrogen atoms forming a $\mu\text{-}\eta^1,\eta^1$-N,N' bridge to each of its other Fe neighbours (Figure 2.3.20).

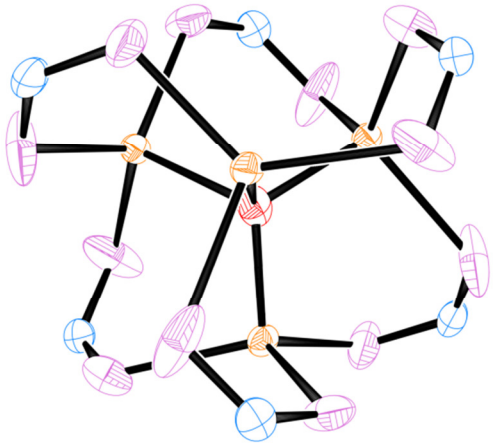

Figure 2.3.21 - Immediate coordination environment of the u4-OFe4 core. Ligand phenyl substitutions are omitted for clarity and thermal elipsoids are drawn at the 50% probability level.

Only two related iron to ***(IX)*** are known in the literature: $Fe_4(O)(DPhF)_6$ and $Fe_4(O)(DBiPhF)_6$ (where DBiPhF = N,N'-bisbiphenylformamidinate).[263] Despite in one instance using the same

ligand the related complex $Mn_4(O)(DPhF)_6$ which also shows similar connectivity[263] and the same disordered core as ***(IX)***, the reported iron complexes are significantly different.

In providing a rationalisation of the difference in the observed structures of ***(IX)*** and the previous reported relate iron complexes $Fe_4(O)(DPhF)_6$ and $Fe_4(O)(DBiPhF)_6$ it is helpful to visualise the core of (IX) showing both disordered components of its $(\mu^4\text{-}OFe_4)^{6+}$ core. The sum of these two disordered configurations can be considered to collectively define a Fe_8 cube which greatly aids visualisation of the core structure and the relative arrangement of the supporting ligands (Figure 2.3.19 + Figure 2.3.21).

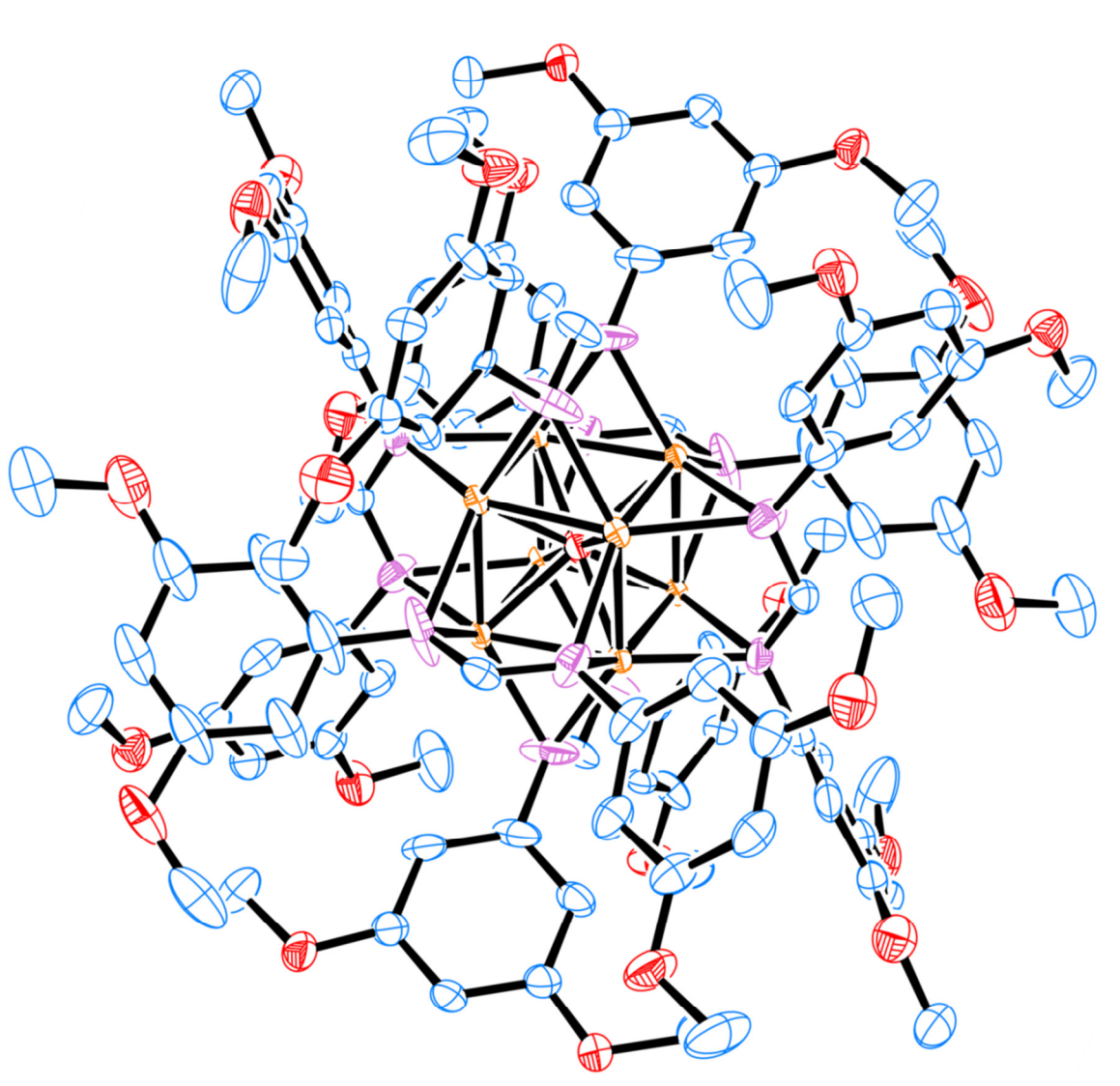

Figure 2.3.22 -- Solid state structure of $Fe_4^{II}(O)(DMOPhFm)_6$ (IX). Hydrogens and modelled disorder of one phenyl ring are omited for clarity. Both disordered components of the $(\mu^4\text{-}OFe_4)^{6+}$ tetrahedral core are shown. Thermal elipsoids are drawn at the 50% probability level.

The bridging formamidinate ligands in ***(IX)*** occupy positions directly bisecting each face of the imagined Fe_8 cube (Figure 2.3.21 + 2.3.22 – Left), presumably so as to minimise the energy of bonding interacts between ligand and either arrangement of the disordered core. The thermal ellipsoids of the bridging nitrogen atoms were observed to elongate in plane defined the Fe-Fe' edges of the cube, further suggesting that only small variations in position are needed to bind to both core configurations. Similar elongation in not observed in the carbon of the RN-C(H)-NR amidinate backbone which appears to behave as a pivot point. Such distortions in the ligand orientation have been similarly reported previously[263] for the related complex $Mn_4(O)(DPhF)_6$ which shares the same kind of disordered core as ***(IX)*** and the associated averaging of the ligand position (2.3.22- Left).

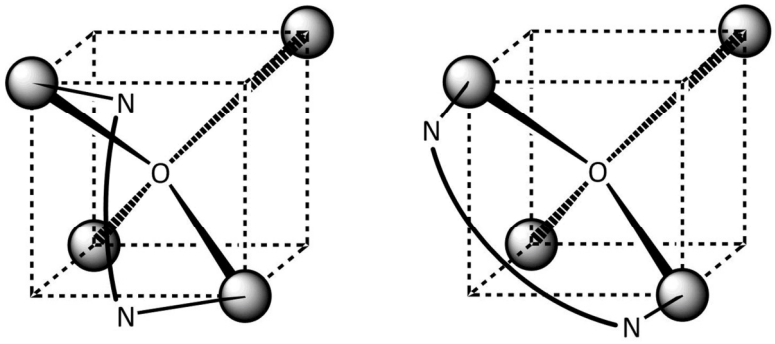

Figure 2.3.23 - Differing relative orientation of bridging ligands in: (Left) Disordered M_4O cores such as for (IX) and $Mn_4(O)(DPhF)_6$; and (Right) ordered M_4O cores like that of $Fe_4(O)(DPhF)_6$.

Only two related iron to ***(IX)*** are known in the literature: $Fe_4(O)(DPhF)_6$ and $Fe_4(O)(DBiPhF)_6$ (where DBiPhF = N,N'-bisbiphenylformamidinate).[263] Despite in one instance using the same ligand as the Mn complex isostructural with ***(IX)*** these iron complex however differ significantly from ***(IX)*** in connectivity**.**

The previously reported complexes in contrast to ***(IX)*** possess well-defined Fe_4O cores *(vide infra)* and display a more typical vertex-to-vertex orientation of the bridging ligands (Figure 2.3.22 – Right). The distribution of these bridging ligands around the core however provides the most significant change relative to ***(IX)***. Both previous complexes were asymmetrically bridged about tetrahedral Fe_4O core (Figure 2.3.23 – Right). In contrast the bridging ligands in ***(IX)*** are symmetrically arranged about each edge (Figure 2.3.23 – Left + Figure 2.3.20).

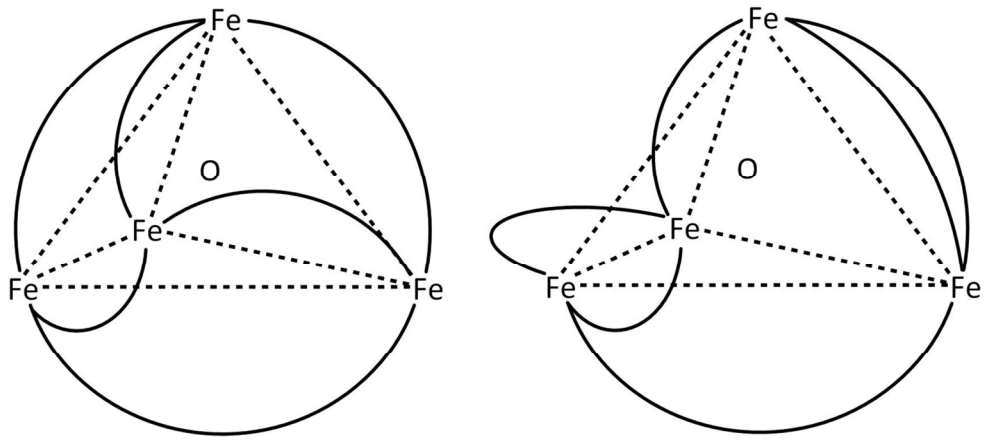

Figure 2.3.24 - Differing bridging configurations: (Left) Symmetrically bridged about each edge; (Right) Asymmetically bridged, 2 doubly bridged, 2 singly bridged and 2 non-bridged edges.

These difference in reported structure make ***(IX)*** the first example symmetrically bridged example of a $Fe_4^{II}(O)(formamidinate)_6$ within the literature and finally provide a suitable tetra-iron comparator to known analogous structures of Mn, Co and Zn amindinate clusters.[263]

Despite showing a more regular ligand bridging arrangement the tetrahedral core of ***(IX)*** still shows some deviation from an ideality, which may again best visualised as a cube defined by the combined atomic positions of the iron atoms in both core configurations. This may be oberved by elipsing the equivilent Fe1-Fe4' and Fe4-Fe1' vectors as shown, resulting in the overlay of the differing remaining Fe-O bonds (Figure 2.3.24).

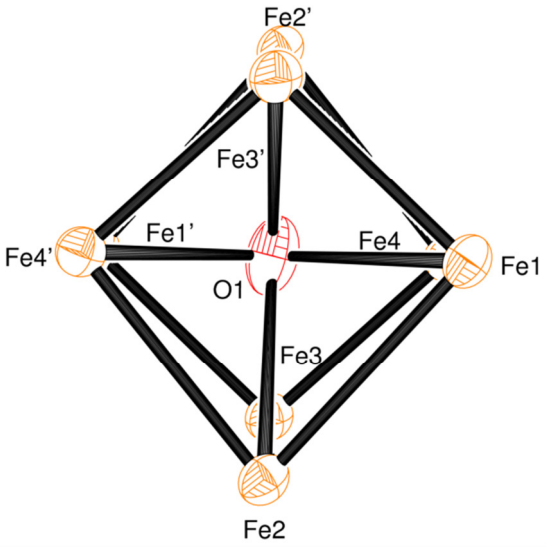

Figure 2.3.25 - Illustration of the distortions to the M_4O caused by sym elongation for the Fe2-O1 bond and contraction of the Fe3-O bond.All non-core atoms have been omitted for clarity.

Elongation of the Fe2-O1 bond to 2.084 Å and contraction of the Fe3-O1 bond to 1.839 Å relative to the average Fe-O distance of 1.947 Å (Table 2.3.2-B) serves to further distort the core slightly from an ideal tetrahedral configuration (Figure 2.3.20). As might be expected this then also leads to slight lengthening of the corresponding Fe3-N bonds (2.272-2.196 Å) over the average Fe-N bond length of 2.171 Å (Table 2.3.2-A).

Bond ID	Bond length /Å
Fe1-N1	2.067(5)
Fe1-N3	2.109(5)
Fe1-N6	2.259(6)
Fe2-N2	2.280(6)
Fe2-N4	2.120(5)
Fe2-N6	2.174(6)
Fe3-N1	2.216(3)
Fe3-N4	2.272(5)
Fe3-N5	2.196(4)
Fe4-N2	2.090(4)
Fe4-N3	2.216(5)
Fe4-N5	2.049(4)
Fe-N (Average)	2.171

Bond ID	Bond length /Å
O-Fe1	1.9598
O-Fe2	2.084
O-Fe3	1.839
O-Fe4	1.906
Fe-O (Average)	1.947

Bond ID	Distance /Å
Fe1-Fe2'	3.226
Fe1-Fe3	3.129
Fe1-Fe4'	3.139
Fe2'-Fe3	3.293
Fe2'-Fe4'	3.199
Fe3-Fe4'	3.080
Fe-Fe (average)	3.178

Table 2.3.2 - (A - Left) Fe-N bond lengths; (B – Right top) Fe-O bond lengths; (C – Right bottom) Fe-Fe distances

The observed Fe-Fe distances are too long to be considered bonding and do not show any considerable variation from the average of 3.178 Å (Table 2.3.2-C). These distances do however contrast strongly with the previous reported structures of $Fe_4(O)(DPhF)_6$ and $Fe_4(O)(DBiPhF)_6$ where far closer Fe-Fe contacts of as little as 2.85 Å were observed.[263]

Both instances are considerable longer than the already long Fe-Fe bond observed in the previously reported structures of $Fe_2^{I,II}(DPhF)_3$[260,280] and $Fe_2^{II,II}(DPhF)_4$[258,259] at 2.232(8) Å and 2.462(2) Å respectively. The latter of these is itself very close to that observed in metallic iron at 2.52 Å.

2.4 Conclusions

The synthesis of a range of formamidinate ligands is reported, ***H[DMOPhFm]*** and ***H[TMOPhFm]*** of which are novel. The first of these was also adventitiously structurally characterised via X-Ray crystallography and showed good agreement with the previously reported structures of related formamidinates.

Of the ligands synthesised 2 are converted to their respective $FeCl_2$(H[amidinate])$_2$ diadducts ***$FeCl_2$(H[DMOPhFm])$_2$ (I)*** and ***$FeCl_2$(H[4FPhFm])$_2$ (II)***. Attempts to use ***(I)*** and ***(II)*** under reported literature conditions[258,259] to generate compounds ***Fe_2(DMOPhFm)$_4$ (V)*** and ***Fe_2(4FPhFm)$_4$ (VI)*** were unsuccessful. In contrast to the reported account a reactively critical intermediate could not be isolated. Failure to isolate this intermediate is attributed to the difference in solubility between the ligands in use herein and that presented in the literature. Further, by review of the surrounding literature a probable identity of this previously unknown intermediate is reported as that of the related bis-amidinate complex Fe^{II}(amidinate)$_2$. This determination is supported by limited Mass spectrometry (MS) evidence of the generation of such species *in-situ*.

The attempted synthesis of ***Fe_2(DMOPhFm)$_4$ (V)*** was then attempted under a second set of literature conditions[259] but was similarly unsuccessful. The products obtained in all instances were mixtures of which only the largest component, that of ***Fe_4(O)(DMOPhFm)$_6$ (IX)*** was able to be structurally characterised. This complex adopts the basic beryllium acetate and is the first reported instance of such an iron complex to display symmetrical bridging about the Fe_4O core.

Extensive attempts to optimise the reaction conditions to synthesis ***Fe_2(DMOPhFm)$_4$ (V)*** were made, but were ultimately unsuccessful. Examination of the reaction variables indicated that, in contrast to previous reports, the most significant degree of selectivity obtained over the product distribution was achieved by variation of reaction temperature and time. Products were further observed to interconvert from lower order clusters toward ***(IX)*** on prolonged exposure to donor solvents or even by exposure to trace moisture when stored at room temperature in the solid state.

2.5 Experimental

2.5.1 Physical measurements

^{1}H and ^{13}C NMR spectra were collected at room temperature on Bruker Avance 250, 400 or DRX500 spectrometers as indicated. Chemical shifts were assigned relative to the residual solvent peak and are given to 0.01 ppm for ^{1}H and 0.1 ppm for ^{13}C.

Mass spectra were obtained either by ESI or MALDI-TOF-MS as indicated. ESI spectra were collected on a Waters Premier LCT operating in ESI mode whilst MALDI-TOF-MS spectra were obtained using a Bruker Reflex III mass spectrometer operating in reflectron, positive ion mode using an N_2 laser. MALDI samples were prepared as solutions in THF (unless otherwise indicated) and using the matrix DCTB (trans-2-[3-(4-tert-Butylphenyl)-2-methyl-2-propenylidene]malononitrile). Calculated monoisotopic mass values were obtained via use of the IsoPro 3.1 isotopic calculator and are cited to 2 decimal places.[306]

Electrochemical measurements were conducted using an Metrohm Autolab PGSTAT100 potentiostat-galvanostat in a nitrogen purged 0.1M solution of $[^{n}Bu_4N][PF_6]$ in the stated solvent using a standard three electrode system. This consisted of a polished Pt microdisc working electrode, Pt wire counter electrode, and an Ag/AgCl pseudo reference electrode; all quoted values are given relative to the $FeCp_2/FeCp_2^{+}$ redox couple of ferrocene a small amount of which was added at the end of data collection and used as an internal standard.

UV-Vis-NIR spectra were recorded using a Varian Cary 5000 spectrophotometer equipped with a 0.5mm path length quartz cuvette. Infrared spectra were obtained using either as solid samples with a Perkin-Elmer Spectrum RX I FT-IR spectrometer equipped with a DuraSamplIR II diamond ATR probe and universal press; or as solutions in a stated solvent using a Perkin-Elmer Spectrum One FT-IR spectrometer in a quartz glass cell.

Elemental analysis was conducted by the Microanalytical Service of the University of Sheffield Department of Chemistry using a Perkin-Elmer 2400 Series II CHNS/O Analyser. This data is provided for synthesised ligands only. Attempts to use this technique for the analysis of dimetallic complex products consistently resulted in immediate visual sample decomposition on exposure to air and/or moisture prior to the start of the analysis. The

data subsequently obtained was irreproducible and due to the visible decomposition could not be considered representative of the initial sample.

Melting points were obtained using a Linkam HFS91 heating stage with a TC92 controller, and are uncorrected.

2.5.2 X-ray Crystallography

X-ray crystallography was conducted using either a Bruker APEX II Smart 4000, or APEX II Kappa system as indicated, both utilising CCD detectors and MoK radiation at λ= 0.71073 Å in conjunction with an Oxford Cryosystems cryostat set to 100 K. Raw data was integrated, equivalent reflections merged and an empirical absorption correction applied (SADABS) based on comparison of symmetry-equivalent measurements.[314] Structures were solved using direct methods, unless otherwise stated, using the SHELXS-97 suite of programs (2008 revision)[315] and refined by full-matrix least squares on weighted F^2 values for all reflections using SHELXTL (Bruker 2008).[316] All expected hydrogens were included in the models generated and were input at calculated positions using a riding model as follows: U(H) = 1.5 x Ueq (C) for methyl hydrogen atoms and U (H) = 1.2 x U_{eq} (C) for methine, methylene and aromatic hydrogen atoms. Where possible disordered solvent was modelled and its inclusion in the structure noted; however where the location of solvent on special positions prohibited is accurate modelling the electron density associated with it was removed via PLATON/SQUEEZE[317,318]

2.5.3 Materials

All manipulations were conducted under an inert atmosphere of argon using standard Schlenk-line techniques or in a MBraun glovebox. Reagents were obtained from Strem, Sigma-Aldrich Chemical Co., Apollo Scientific Ltd, Fluorochem Ltd, Fischer Scientific Ltd and Alfa Aesar and unless otherwise indicated reagents were used as received.

All solvents used were dried in accordance with standard procedures:[319] Tetrahydrofuran (THF) was purified by distillation over sodium wire and benzophenone where possible, but otherwise dried over CaH_2; acetonitrile, 1,2-dichlorobenzene (DCB), 1,2-dichloroethane (DCE), dichloromethane (DCM), hexanes, mesitylene, *n*-pentane, toluene, and *o*-xylene were

dried by fractional distillation over CaH_2; methanol was dried over Mg/I_2 and fractionally distilled. Solvents were stored in Schlenk-type glassware and where appropriate over pre-dried 4Å molecular sieves. All solvents were additionally degassed thoroughly with argon immediately prior to use.

The metal salt starting materials $Fe_4Cl_8(THF)_6$,[307] $Fe(OTf)_2 \cdot xMeCN$[284] and $Fe(OAc)_2$[308,309] were all synthesised according to established literature procedures.

2.5.4 Ligand synthesis

2.5.4.1 Formamidinate ligands (RNC(H)NR)

Synthetic procedures for N,N'-bis(4-fluorophenyl)formamidine,[287] hereafter H[4-FPhFm], and N,N'-bis[3,5-bis(trifluoromethyl)phenyl]formamidine,[320] hereafter H[3,5-$(CF_3)_2$PhFm] are known, as are general procedures for non-fluorinated analogues.[227,290,292,321] The modified procedure proposed by Fackler *et al.*[286] for highly fluorinated formamidines was found to be unnecessary in the case of the above compounds; consequently all formamidines used were synthesised via the same modified, scaled up procedure outlined below. N,N'-bis(3,5-dimethoxyphenyl)formamidine, hereafter H[DMOPhFm], and N,N'-bis(3,4,5-trimethoxyphenyl)formamidine hereafter H[TMOPhFm] are novel compounds.

To a round-bottomed flash containing 27 mmol of the substituted aniline was added 14 mmol of anhydrous triethyl orthoformate and the flask was then fitted with a reflux condenser. The mixture was then heated to reflux for a period of 3 hours, after which time the condenser was removed and the mixture boiled to dryness. The resultant solid was then isolated by recrystallization from minimal volume of hot toluene. Where required, products were then further purified by sublimation *in vacuo*. Products were obtained in high purity with first crop yields of 79-93%.

H[DMOPhFm] – N,N'-bis(3,5-dimethoxyphenyl)formamidine

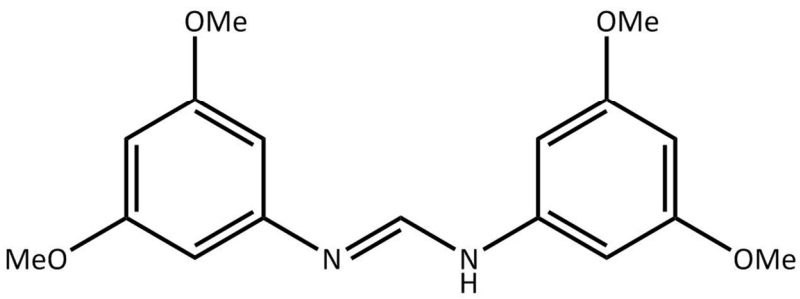

Yield = 87 %. M_p: 149.1 °C. ^{1}H NMR ($CDCl_3$, 400 MHz): δ 3.72 (s, 12H, ArO*CH*$_3$), 6.19-6.23 (m, 6H, *Ar*H), 8.25 (s, 1H, NC(*H*)N), 9.84 (s, 1H N*H*). ^{13}C NMR ($CDCl_3$, 250 MHz DEPTQ/CPD): δ 55.3 (s, *m*-O*C*H$_3$), 95.9 (s, *o-ArC*), 97.5 (s, *p-ArC*), 147.2 (s, *i-ArC*), 149.8 (s, N=*C*(H)-N), 161.6(s, *m-ArC*). HR-ESI-MS: calcd. monoisotopic MW for $C_{17}H_{20}N_2O_4$ m/z: 316.1423, found m/z: 316.13 (M^+, 100%). IR (cm^{-1}): 3342w, 2997w, 2938w, 2840w, 1664s, 1580s, 1513m, 1456m,

1423m, 1317m, 1281m, 1243m, 1191s, 1143s, 1062s, 1001s, 958m, 940m, 812s, 794s, 740m, 667s. Elemental analysis calcd. for $C_{17}H_{20}N_2O_4$: C, 64.54%; H, 6.37%; N, 8.86%; found: C, 64.35%; H, 6.39%; N, 8.79%.

H[TMOPhFm] – N,N'-bis(3,4,5-trimethoxyphenyl)formamidine

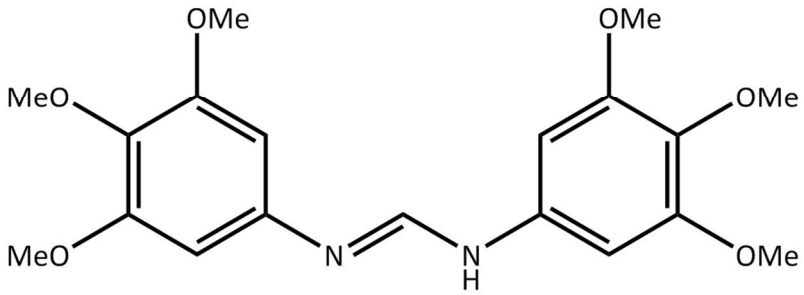

Yield = 85 %. M_p: 256.2 °C. ^{1}H NMR ($CDCl_3$, 400 MHz): δ 3.80 (s, 12H, m-OC*H*$_3$), 3.86 (s, 6H, p-OC*H*$_3$), 6.28 (s, 4H, *o-ArH*), 8.13 (s, 1H, NC(*H*)N). ^{13}C NMR ($CDCl_3$, 400 MHz DEPTQ/CPD): δ 56.1 (s, *m*-OCH_3), 61.0 (s, *p*-OC*H*$_3$), 96.8 (s, *o-ArC*), 134.5 (s, *m-ArC*), 129.7 (s, p-ArC),149.6 (s, *i-ArC*), 153.9 (s, N=*C*(H)-N). HR-ESI-MS: calcd. monoisotopic MW for $C_{19}H_{24}N_2O_6$ m/z: 376.1634, found m/z: 376.11 (M^+, 100%). IR (cm^{-1}): 3337w, 2987w, 2965w, 2924w, 2838w, 1668s, 1583s, 1503s, 1458s, 1414s, 1323m, 1283s, 1222s, 1124s, 1006s, 984s, 832s, 755m, 716m, 634m. Elemental analysis calcd. for $C_{19}H_{24}N_2O_6$: C, 60.63%; H, 6.43%; N, 7.44%; found: C, 60.37%; H, 6.42%; N, 7.48%.

H[4-FPhFm] – N,N'-bis(4-fluorophenyl)formamidine

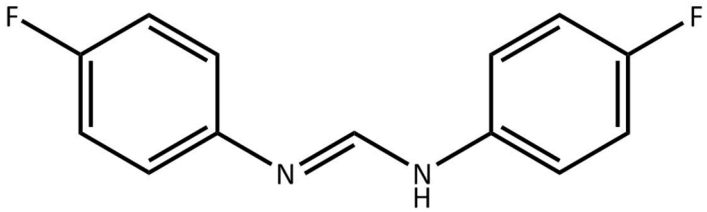

Yield = 93%. M_p: 146.1 °C. ^{1}H NMR (DMSO, 400 MHz): δ 7.02-7.45 (br m, 8H, *ArH*), 8.10 (s, 1H, NC(*H*)N), 9.72 (s, 1H N*H*). ^{13}C NMR (DMSO, 400 MHz DEPTQ/CPD): δ 115.9 (d, *m*-Ar*C*), 120.8 (br s, *o-ArC*), 148.6 (s, *i-ArC*), 157.3 (s, N=*C*(H)-N), 159.7 (s, *p-ArC*-F). ^{19}F NMR (DMSO, 400 MHz): δ 121.67 (s, 1F, *Ar-F*). HR-ESI-MS: calcd. monoisotopic MW for $C_{13}H_{10}F_2N_2$ m/z: 232.0812, found m/z: 233.09 (M^+, 100%). With the exception of M_p (lit. value is 99-100 °C) data correlates with that published in the literature.[286]

H[3,5-(CF_3)$_2$PhFm] – N,N'-bis(3,4,5-trimethoxyphenyl)formamidine

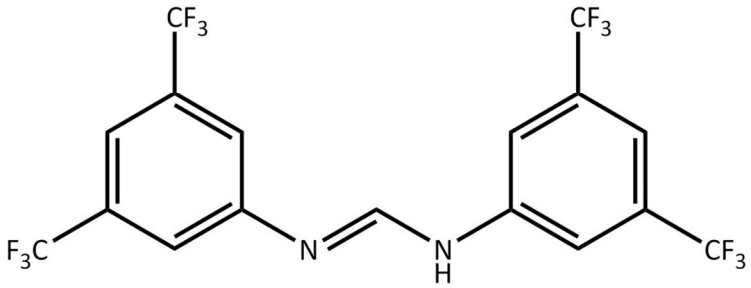

Yield = 79%. M_p: 263.8 °C (decomp.). ^{1}H NMR (DMSO, 400 MHz): δ 7.62 (br m, 4H, *o-ArH*), 7.83 (br m, 2H, *p-ArH*), 8.68 (s, 1H, NC(*H*)N), 10.59 (s, 1H N*H*). ^{13}C NMR (DMSO, 400 MHz DEPTQ/CPD): δ 115.7 (m, *ArC*), 119.4 (br m, *ArC*), 123.8 (q, Ar-*C*F_3), 131.4 (q, *ArC*), 151.4 (s, *p*- N=*C*(H)-N). ^{19}F NMR (DMSO, 400 MHz): δ 61.71 (s, 1F, *Ar*-C*F$_3$*). HR-ESI-MS: calcd. monoisotopic MW for $C_{17}H_8F_{12}N_2$ m/z: 468.0496, found m/z: 469.06 (M^+, 100%). Data correlates with published values.[320]

2.5.5 Synthesis of $FeCl_2(H[formamidinate])_2$ intermediates

The synthesis of these mono-iron intermediates was conducted via a modified version of the procedure published by Cotton[258] for $FeCl_2(DPhF)_2$. Below is an example of the general procedure used.

$FeCl_2(H[DMOPhFm])_2$ (I)

A 25ml Schlenk was charged with 0.51 g (4 mmol) of $FeCl_2$ and 2.56 g (8.1 mmol) of H[DMOPhFm] and 15 ml of toluene then added via cannula. The resultant mixture was then heated at reflux for 24 hours, rapidly filtered through a fine sintered glass frit whilst hot and then allowed to cool slowly to room temperature. Addition of 20 ml of cold (~5 °C) *n*-pentane to the orange filtrate caused the immediate precipitation of the target compound which is the isolated by filtration. The yellowish white solid obtained on the frit is then carefully washed with a further 2x 5ml of cold *n*-pentane and dried *in vacuo*. Target species were primarily identified by MALDI-TOF-MS spectrometry with samples prepared in a toluene/DCTB solution.

Yield: 2.60 g, 86 %. MALDI-TOF-MS: calcd. monoisotopic MW for $FeC_{34}H_{40}N_4O_8Cl_2$ m/z: 758.16, found m/z: 723.18 (M-Cl, 100%)

$FeCl_2(H[4FPhFm])_2$ (II)

Yield: 1.94 g, 82 %. MALDI-TOF-MS: calcd. monoisotopic MW for $FeC_{26}H_{20}N_4F_4Cl_2$ m/z: 590.04, found m/z: 555.07 (M-Cl, 100%.)

Attempted synthesis of $FeCl_2(H[TMOPhFm])_2$ (III)

Length of reflux increased to 48 hours. It was not possible to cleanly isolate the intended product. Low solubility of the ligand and it's adducts frustrated efforts at recrystallisation and further optimisation of reaction and work-up conditions.

Yield: N/A. MALDI-TOF-MS: calcd. monoisotopic MW for $FeC_{38}H_{48}N_4O_{12}Cl_2$ (di-adduct) m/z: 878.19, found m/z: 843.23 (M-Cl, 100%.);

Attempted synthesis of $FeCl_2(H[(3,5\text{-}CF_3)PhFm])_2$ (IV)

Length of reflux increased to 48 hours. It was not possible to cleanly isolate either intended product ***(IV)*** or the mono-adduct ***$FeCl_2(H[(3,5\text{-}CF_3)PhFm])_1$ (IVa)***. Low solubility of the ligand and it's adducts frustrated efforts at recrystallisation and further optimisation of reaction and work-up conditions.

Yield: N/A. MALDI-TOF-MS: calcd. monoisotopic MW for $FeC_{17}H_7N_2F_{12}Cl_2$ (mono-adduct) 592.91 m/z:, found m/z: 557.92 (M-Cl, 100%.)

2.5.6 Attempted synthesis of $Fe_2^{II,II}$(formamidinate)$_4$ complexes via $FeCl_2$(H[amidinate])$_2$ intermediates

Using the method reported by Cotton,[258,259] both as stated, and in a modified form as outlined below the synthesis of the compounds ***Fe_2(DMOPhFm)$_4$ (V)*** and ***Fe_2(4FPhFm)$_4$ (VI)*** was attempted. An example of the modified synthetic procedure is provided below:

A small 25ml Schlenk was charged with 0.190 g (0.25 mmol) of $FeCl_2$(H[DMOPhFm])$_2$ and 10 ml of diethyl ether then added via syringe. The mixture was then cooled to 0 °C and 0.32 ml (0.51 mmol) of a 1.6M solution of methyllithium in Et_2O added via micro-syringe. The reaction mixture was then allowed to stir for 5 minutes before removal of all volatiles *in vacuo*. Once removal of volatiles was complete the resultant orange/yellow residual solid was extracted into 5 ml of 50:50 THF:toluene, transferred via a filter cannula to a second Schlenk. Crude samples were taken for MS analysis and the remaining sample layered with 20 ml of *n*-pentane and stored at -18 °C to facilitate crystallisation.

Further modifications to the above procedure included variation of:

- Alkyllithium reagent used: MeLi; ^{n}BuLi;
- Reaction solvents: THF; 50:50 THF:toluene; 50:50 THF:Et_2O; toluene
- Reaction temperature on alkyl base addition: 0 °C; -78 °C
- Reaction length after alkyl base addition: 5 min; 15 mins; 30 mins; 1 hour; 24 hours

Neither ***Fe_2(DMOPhFm)$_4$ (V)*** nor ***Fe_2(4FPhFm)$_4$ (VI)*** were successfully isolated via this method or variations thereon.

2.5.7 Attempted synthesis of $Fe_2^{II,II}$(formamidinate)$_4$ complexes via alternative methods

Utilising a more traditional organometallic synthetic approach[103] the direct synthesis of the target compounds was attempted from a range of Iron (II) salts. A typical example of synthetic approach employed is outlined below:

Attempted synthesis of Fe_2(DMOPhFm)$_4$ (V)

A small, 25 ml Schlenk was charged with 0.192 g (0.61 mmol) of H[DMOPhFm] and 10 ml of THF before being cooled to -78 °C. Once cooled 0.25 ml (0.62 mmol) of a 2.5M solution of *n*-butyllithium in hexanes was added via syringe and the resultant clear yellow solution was allowed to stir for 10 minutes.

A second 25 ml Schlenk was charged with 0.131 g (0.3 mmol) of $Fe(OTf)_2 \cdot 2MeCN$. The cold solution in the first Schlenk was then transferred via cannula into the second and an immediate clear yellow -> cloudy orange colour change observed. The second Schlenk was then allowed to warm to room temperature and an initial (time = 0) sample taken for MALDI-TOF-MS analysis.

After stirring for 2 hours the orange/brown solution was filtered through a packed Celite plug to remove the fine suspension of LiCl and reduced to minimum volume *in vacuo*. A second MALDI-TOF-MS sample was then taken and the remaining solution layered with 25 ml of *n*-pentane and cooled to -18 °C to facilitate the growth of crystals for structural determination via X-Ray diffraction. Where crystals were obtained a sample of the recrystallisation solution was then resubmitted for MALDI-TOF-MS for verification purposes.

Further to the above outlined procedure a series of reaction variables were considered and modified with a view to affecting changes in the distribution of the observed products, these included:

- Metal salt used: $FeCl_2$, $Fe_4Cl_8(THF)_6$,[307] $Fe(OTf)_2 \cdot xMeCN$[284] and $Fe(OAc)_2$[308,309]
- Alkyllithium reagent used: MeLi; ^{n}BuLi; ^{t}BuLi
- Use of alternate alkyl metal bases: NaH; KH
- Reaction solvents: THF; 50:50 THF:Et_2O; 2-Methyl THF; Toluene

- Reaction temperature on alkali base addition: 0 °C; -20 °C; -78 °C
- Rate of warming to room temperature: immediate; over 1 hour.
- Rate of alkyl base addition: single addition at once; addition over 10 minutes via syringe pump.
- Reaction length after alkyl base addition: 5 min; 15 mins; 30 mins; 1 hour; 24 hours
- Work up solvents: THF; 50:50 THF:Et_2O; 2-Methyl THF; Toluene; MeOH; ^{i}PrOH; *n*-pentane, hexanes, MeCN, DCM; DCE; DCB.

Fe_2(DMOPhFm)$_4$ (V) was not successfully synthesised via this method and a mixture of products was consistently obtained. The synthesis of ***Fe_2(4FPhFm)$_4$ (VI)*** by this method was not attempted.

2.5.7.1 Structural determination of $Fe_6(O)(DMOPhFm)_6$

Crystals of the related cluster species ***Fe_4(O)(DMOPhFm)$_6$ (VII)*** were obtained from two reactions both utilising $Fe^{II}(OTf)_2$ and ^{n}BuLi as described in the previous section with the following modifications:

Reaction stirring time (after addition of all reagents) was extended to 24 hours after which all volatiles were removed *in vacuo*. The resulting solid was then extracted into DCM, filtered through Celite and reduced to minimum volume. Crystals suitable for X-ray diffraction were grown by vapour diffusion of *n*-pentane at -18°C over a period of 1 week. MALDI-TOF-MS: calcd. monoisotopic MW for $Fe_4C_{102}H_{114}O_{25}N_{12}$ m/z: 2130.5415, found m/z: 2131.7 (M^+, 100%).

3 Structural, electronic and computational studies of diruthenium 'NN' formamidinate complexes

3.1 Aims

- To synthesise a range of diruthenium (II,II) tetra-formamidinate complexes using ligands with varied electron donating or withdrawing aryl substituents. The general form of these complexes is shown below in Figure 2.1.1.

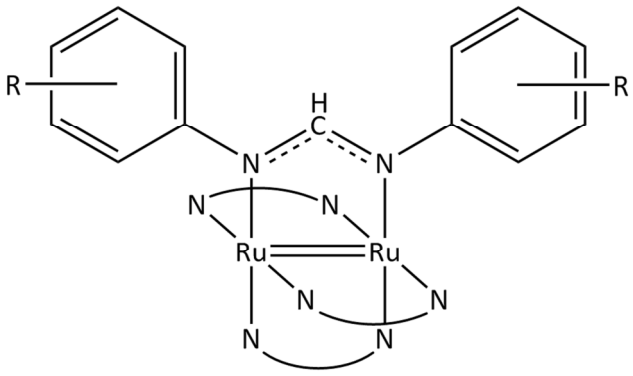

Figure 3.1.1 - General structure of a diruthenium (II,II) tetra-formamidinate complex; 3 of the 4 ligands are shown in a truncated form for the sake of clarity.

- To determine the physical, spectroscopic and electronic properties of these compounds.
- To generate a series of computational model complex for these compounds using the hybrid functionals B3LYP and PBE0 and examine the accuracy the predictions of these models make vs. experimental data.
- To test the viability and activity of the synthesised complexes as aerobic oxidation catalysts.

3.2 Introduction

3.2.1 Previous catalytic applications of related dimetallic Ru_2 (II,III) and Ru_2 (II,II) complexes

Beyond sMMO, dimetallic systems have been the subject of extensive investigation for their potential to catalyse a wide array of industrially and synthetically important processes.[103] In this respect, diruthenium species have proven of particular interest due to their potential to conduct a wide range of chemistries comparable to those of the multitude of other iron based catalysts observed in nature.

The mixed valence complexes of Ru_2 (II/III) have been of particular interest due to both their formally intermediate oxidation state of +2.5, offering chemical potential not present in monometallic species and additionally their ability to incorporate useful functionality into the axial position, with respect to the M-M vector, by substitution for Cl^-.

Other related diruthenium complexes have also been shown to display catalytic activity towards a diverse range of substrates. One noteworthy formamidinate bearing example being that of that of the C-H amination catalyst $Ru_2^{II,III}(D(3,5\text{-}Cl_2)\text{-}PhF)_4(N_3)$ (where D(3,5-Cl_2)-PhF = N,N'-bis(3,5-dichlorophenyl)formamidinate) as reported by Berry[322,323] (Figure 3.1.1). The axial transfer behaviour of these complexes has since also been extended to include related 'NO' bridging species such as $[Ru_2(chp)_4N_3]$ (where chp = 2-chloro- 6-hydroxypyridinate).[324] In addition, the group of Du Bois has recently published a related 'NO' bridged complex, $Ru_2^{(II,III)}(hp)_4Cl$ (where hp = 2-oxypyridinato) which is able to conduct this chemistry on an intramolecular level.[325]

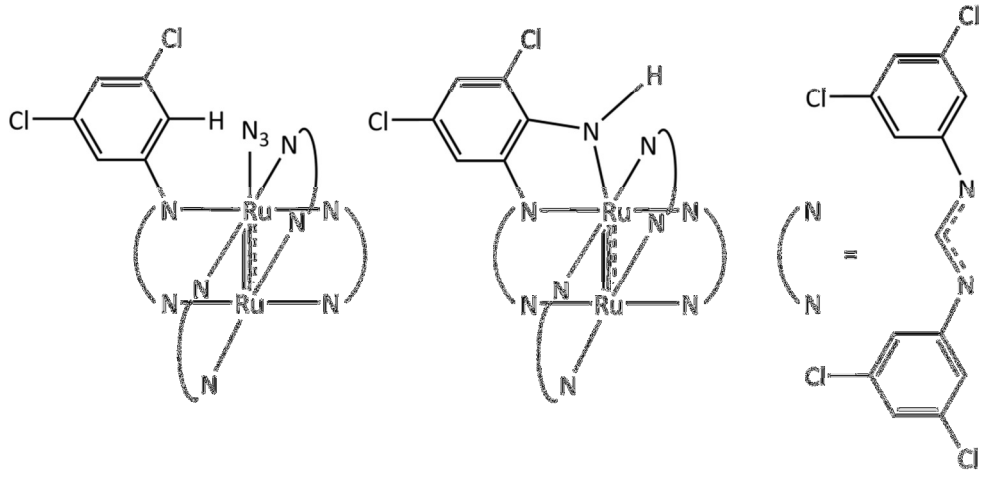

Figure 3.2.1 - Berry's Axial C-H amination in the complex $Ru_2^{II,III}(D(3,5\text{-}Cl_2)\text{-}PhF)_4(N_3)$ (Left), to generate the species $Ru_2^{II,III}(D(3,5\text{-}Cl_2)\text{-}PhF)_3(D(3,5\text{-}Cl_2\text{-}2NH)\text{-}PhF)$ (right)

3.2.1.1 Related catalytic active oxidation catalysts

The group of Ren recently reported that catalytic sulphide oxidation may similarly be accomplished via used of the closely related tetra-carboxylate complexes $Ru_2(esp)_2Cl$ (where esp = tetramethyl-1,3-benzenedipropionate), its $[BF_4]$ salt and even the common starting material $Ru_2(OAc)_4Cl$[326] (Figure 3.2.2).

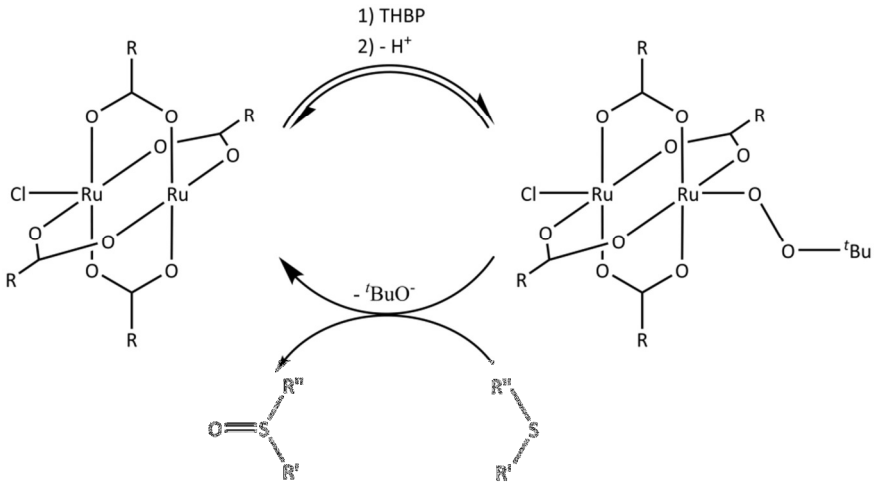

Figure 3.2.2 - Ren's $Ru_2^{(II,III)}(RCO_2)_4$ catalysised oxygenation of organic sulfides by tert-butyl hydroperoxide

Looking towards their closely related Ru_2 (II,II) tetra-carboxylates, separate reports from the groups of Jasra[327] and Naota[328] have reported $Ru_2^{(II,II)}(OAc)_4$ and $Ru_2^{(II,III)}(RCO_2)_3(CO_3)$ were catalytically active aerobic alcohol oxidation catalysts.

3.2.1.2 Catalysts for water splitting

One of the more actively pursued areas of current catalysis research is the facile division of water into molecular oxygen and hydrogen. Many of the recent reports in this area have emerged from the group of Nocera who has focused on utilising photo-activated catalysts to drive the oxidation half-cell reaction.[329–338]

As collective understanding of diruthenium systems has developed in recent years, catalytic examples of both the required anodic/cathodic have been separately reported, making diruthenium complexes one of the few classes able to perform both functions.

The reductive catalytic system for the generation of H_2 was provided by the group of Mori, who reported this behaviour for the complex $[Ru_2^{(II,III)}(p\text{-BDC})_2Br]_n$ (Where *p*-BDC = 1,4-benzenedicarboxylate) supported within a larger metal organic framework (MOF).[339]

The catalyst proposed in a recent publication by Dunbar *et al.* for the corresponding water oxidation half-cell reaction was, rather surprisingly one that has been known in the literature since 1984, $Ru_2(OAc)_4$. This is particularly interesting not just because it has been known for 30 years, but due to the fact that in Wilkinson's subsequent publication in 1985 it was noted that the dihydrate was sufficiently stable to afford crystals for structural determination by X-ray crystallography.[140] That this potentially provides proof of the ability of Ru_2 (II,II) complexes to activate their axial ligands towards useful reactivity is of great interest.

3.2.2 Focusing on Ru_2 (II/II) formamidinates

Our work, presented in this chapter will consider $Ru_2^{(II,II)}(amidinate)_4$ complexes, which despite the proven chemical utility of Ru(II) in mono metallic complexes (see chapter 1), have yet to receive significant attention.[103] Of the less a dozen examples of these complexes present in the literature, only an isolated few are directly synthesised and isolated. Most reported instances of these species are generated and studied in-situ by bulk-electrolysis[136,137] or chemical reduction[154,340] of their related Ru_2 (II,III) analogues. In addition when utilising methanol as the solvent, there have been a number of reported

instances of generation of Ru_2 (II,II) complexes via disproportionation of the parent Ru_2 (II,III) analogue; however no mechanism for this behaviour has yet been confirmed.[138,146]

3.2.3 Synthetic precedent for the direct synthesis of $Ru_2^{(II/II)}$(amidinate)$_4$ complexes

The first direct synthesis of a $Ru_2^{(II,II)}$(amidinate)$_4$ complex was provided by Cotton in 1991[139] for the complex $Ru_2^{(II,II)}(DFM)_4$ (where DFM = N,N'-bis(*p*-tolyl)formamidinate), which proceeds via the combination of the corresponding tetra-acetate $Ru_2^{(II,II)}(OAc)_4$ and the lithium formamidinate salt. In the reported synthesis a number of pertinent observations are made relating to the isolated product including the extreme air sensitivity of the species; the rapid colour change from red -> purple on exposure to air and the apparent reactivity with some common solvents including chloroform. In addition, despite the report of methanol inducing disproportionation in some related Ru_2 (II, III) species coming in the same year from Cottons lab,[146] and the noted solvent sensitivity of the product obtained, the reported procedure still utilises methanol during the work-up.

The reported characterisation of this complex was conducted in reference to the previously reported, structurally similar and better studied triazenato complex $Ru_2^{(II,II)}(RNNNR)_4$ (where RNNNR = N,N''-bis(*p*-tolyl)triazenate).[257,341] It was expected that $Ru_2^{(II,II)}(DFM)_4$ would exhibit very similar properties, however this was not observed experimentally for UV-Vis or CV data.[139] Calculations conducted for the model complex $Ru_2(HNCN(H)NH)_4$ at the SCF-Xα level of theory,[139] and based on assumptions dervived from the parallel study of the related triazenato complex were found to be insufficient to fully describe it the electronic structure beyond a qualitative assignment. The level of theory used provided a good estimation of the relative order of the complex MOPs but was unable to provide satisfactory predictions for the experimentally observed UV-vis or IR spectra.

The assumption that the triazenate complex should be sufficiently similar to allow the use of a common model was later shown by Cotton be invalid, as the ground state configuration is poorly defined for the formamidinate complexes and variations allow to the relative re-organisation of the energies of the π* and δ* orbitals.[103,342] Finally the reported cyclic voltammogram reported that assigned the two redox processes as a reduction and

oxidation respectively could not account for the apparent reactivity toward oxygen.[122,139] Despite this inconclusive nature of the characterisation reported, no significant follow-up work on these compounds was published making this one of only two papers that address the characterisation of this class of compounds within the literature.

Only two papers have been published directly concerning such complexes since 1991; the first of which, also by Cotton compares $Ru_2^{(II,II)}(DFM)_4$ to its $Ru_2^{(II,III)}$ analogue.[122] This report similarly comments the CV data warrants further investigation, but fails to ever deliver this or any further characterisation data on the $Ru_2^{(II,II)}$ analogue to which the papers' title alludes.[122] The second subsequent report concerning $Ru_2^{(II,II)}(form)_4$ complexes, whilst related is of little synthetic utility and concerns the isolation of the CO adduct of the electrolysis generated species $Ru_2^{(II,II)}(dpf)_4$ (where dpf = N,N'-bis(phenyl)formamidinate).[136]

One additional complex, $Ru_2(DAniF)_4$ (where DAnif = N,N'-bis(*p*-anisyl)formamidinate), was generated via the adventitious, solvent dependant disproportionation of $Ru_2(O_2CMe)_4Cl$ in MeOH during work relating to similar Ru_2 (II,III) species. Despite their apparent efforts however, this behaviour was found to be isolated to this specific ligand / tetracarboxylate pair. $Ru_2(DAniF)_4$ in conjunction with $Ru_2(DFM)_4$ and the related axial CO adduct $Ru_2^{(II,II)}(dpf)_4(CO)$ remain the only three discrete, monomeric and structurally characterised $Ru_2^{(II,II)}$ tetra formamidinates in the literature.

Beyond the initial work by Cotton and the singular report concerning the CO adduct by Kadish, $Ru_2^{(II,II)}$ formamidinate complexes have not been the subject of significant further intentional synthetic work until recent years.[103] The Creutz-Taube analogue study by Cotton *et al.*, in 2004 provided some renewed interest in the area but then chemistry of $Ru_2^{(II,II)}$ formamidinate complexes still remains poorly understood. In this they remain a noteworthy exception to the otherwise broad scope of transition metal formamidinate complexes reported in recent decades including those of V,[252,253] Ti,[254] Co,[255] Cr,[256] W,[256] Rh,[257] Fe[258–263] and $Ru_2^{(II,III)}$.[122,138,139,264] A review of more general trends in transition metal formamidinate complexes was provided in a by Tong Ren, an ex-student of Cotton, in 1998.[228]

3.3 Results and discussion

3.3.1 Ligand synthesis

The synthesis of the formamidinate ligands used is discussed in the preceding chapter (Section 2.3.1)

3.3.2 Attempted synthesis of $Ru_2^{II,II}$(formamidinate)$_4$ complexes using alkali metal formamidinate salts

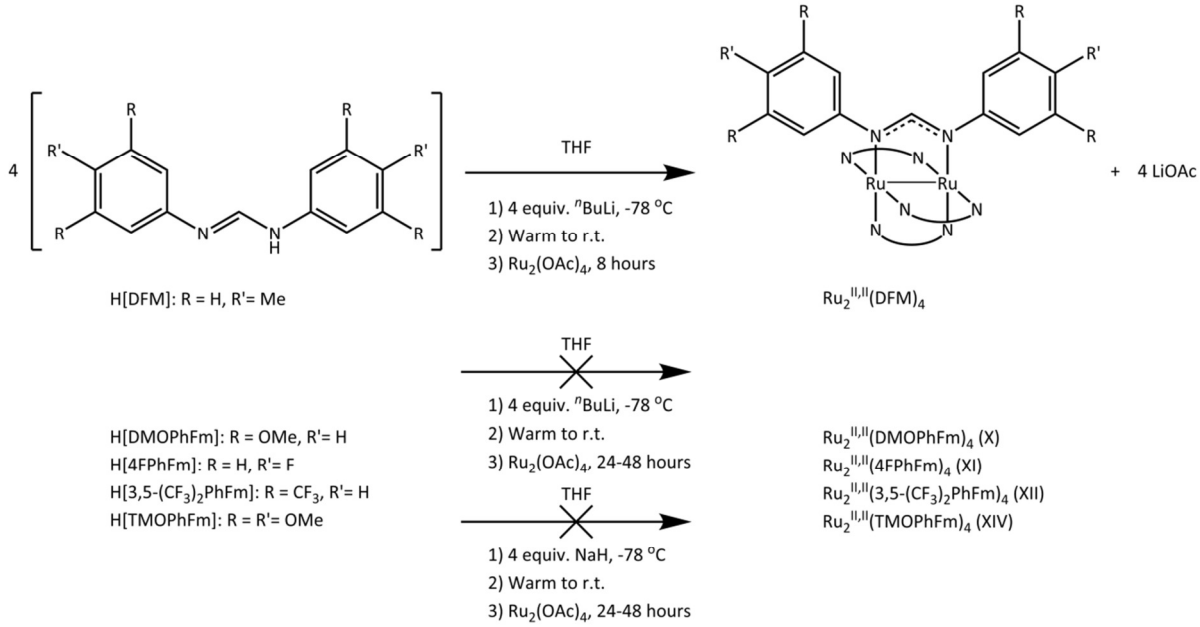

Figure 3.3.1 - General procedure for the attempted synthesis of diruthenium tetraformamidinates via akali metal salts

Cotton reported the synthesis of the diruthenium tetraformamidinate complex $Ru_2^{II,II}(DFM)_4$ (where DFM = N,N'-bis(p-tolyl)formamidinate) as generated via direct reaction ligand metathesis reactions between the *in-situ* generated lithium formamidinate salt and $Ru_2^{II,II}(OAc)_4$ (Figure 3.3.1).[139]

In contrast to related diiron analogues the use of specific alkyllithium reagents is not indicated as necessary and the lithium salts are generated in a routine manner. ^{n}BuLi in is added to a solution of the free ligand in THF at -78 °C, generating a yellow solution and the resultant salt solution allowed to warm to room temperature. Addition of a solution of $Ru_2^{II,II}(OAc)_4$ was then noted to induce a colour change to deep red over 30 minutes under stirring and the reaction stopped by removal of all volatile components after 8 hours.

Subsequent washing with methanol and then hexane was reported to facilitate the clean isolation of the desired tetra-kis product.

Attempts to synthesise ***X, XI, XII*** and ***XIV*** via this reported procedure (Figure 3.3.1) were unsuccessful. MALDI-TOF-MS analysis indicated that the product mixtures obtained consistently showed the presence of the intermediate bis- and tris- substituted partial metathesis products, i.e. $Ru_2^{II,II}(OAc)_{4-n}(amidinate)_n$ (n = 2 or 3 respectively). The desired tetrakis- compound was also observed, never as the sole product under the reported conditions.

Attempts were made to optimise the reaction conditions to enable the isolation of the tetra-kis product in isolation including: extension of the reaction time to up to 48 hours; inclusion of a significant ligand excess; the use of differing alkyllithium reagents (MeLi, ^{n}BuLi, ^{t}BuLi), and the use of other alkali bases such as NaH to generate the corresponding sodium salts. Despite the use of these modified conditions however, these attempts to isolate the tetra-kis product exclusively were ultimately unsuccessful.

3.3.3 Synthesis of $Ru_2^{II,II}$(formamidinate)$_4$ complexes by direct metathesis

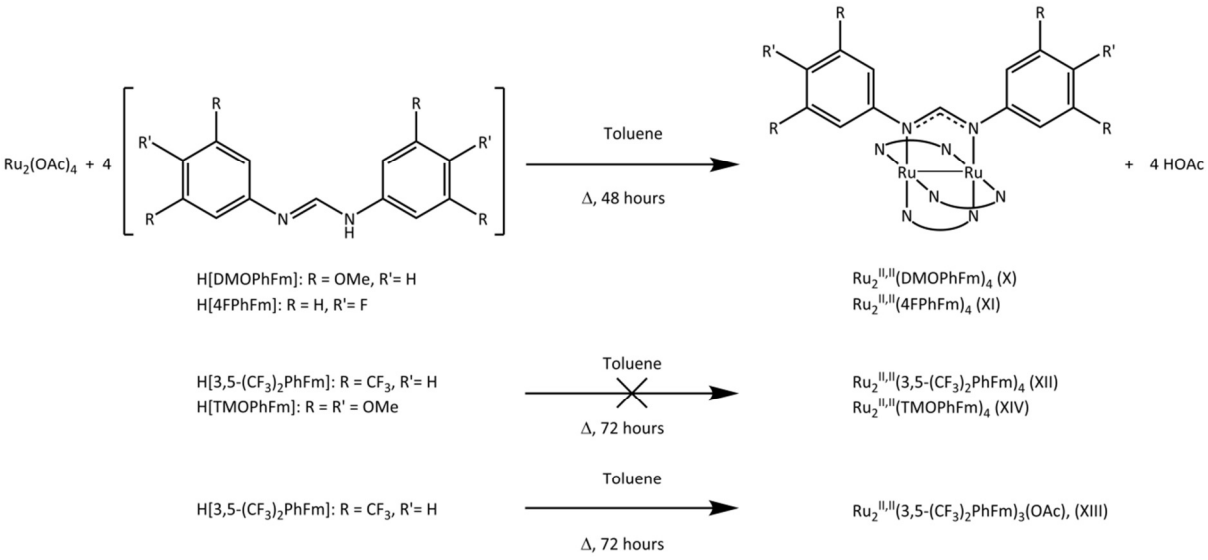

Figure 3.3.2 - General scheme for the synthesis of X, XI and XIII

The tetrakis- products ***$Ru_2^{II,II}$(DMOPhFm)$_4$ (X)*** and ***$Ru_2^{II,II}$(4FPhFm)$_4$ (XI)*** may be synthesised from $Ru_2^{II,II}(OAc)_4$ via refluxing of the protonated ligand in either THF or toluene for 48 hours

(Figure 3.3.2).Further prolonged reflux was not observed to result in significant changes in yield prior to eventual thermal decomposition of the target products.

Attempts to synthesise the more bulky tetrakis- products ***$Ru_2^{II,II}$(3,5-$(CF_3)_2$PhFm)$_4$ (XII)*** and ***$Ru_2^{II,II}$(TMOPhFm)$_4$ (XIV)*** do not proceed under the stated conditions, and prolonged reflux beyond results in eventual decomposition. However, the tris- substituted product of the former, ***$Ru_2^{II,II}$(3,5-$(CF_3)_2$PhFm)$_3$(OAc) (XIII)***, may be obtained as the sole product by where the reflux step to is extended to 72 hours. The synthesis of ***$Ru_2^{II,II}$(3,5-$(CF_3)_2$PhFm)$_4$ (XII)*** and ***$Ru_2^{II,II}$(TMOPhFm)$_4$ (XIV)*** requires more forcing conditions (Section 3.3.4).

This new synthetic route to ***$Ru_2^{II,II}$(amidinate)$_4$*** complexes presents a more optimal means to generate these highly reactive species. The removal of additional reagents serves to both simplify the methodology and to the remove the potential range of alkali metal inclusion by-products that may be formed. In contrast to the previously published procedure where the by-products are primarily alkali salts, direct metathesis as described proceeds via the liberation of acetic acid. Due to the high temperature at which the reflux step is conducted however, more volatile by-products such as acetic acid are effectively excluded from the reaction and lost into the inert gas manifold. Any remaining acetic acid may similarly easily removed in conjunction with any excess ligand present upon completion of the reaction *in vacuo*. Where necessary, the reflux may stopped part way and this evacuation step conducted to further drive the reaction equilibria (Figure 3.3.2) towards the intended tetra-kis product.

3.3.3.1 Alternative method utilising THF

The use of non-donor solvents is generally preferred in the synthesis and study of highly reactive species due to negative interactions commonly observed with donor solvents.[103] These range from reductive moderation of observed redox behaviour[141] to promoting unexpected reactivity e.g. disproportionation in methanol,[138,146] or even catalytic ring opening (Figure 1.10.6) as observed in some diiron (II,II).complexes.[217] Consequently the use of toluene is preferable but as donor solvents such as THF may also provide some utility in stabilising some related complexes[275,283] an alternative method utilising THF is also

reported. This will be discussed in greater detail in Section 3.3.8. There was no significant difference between products obtained via either method based on the analysis conducted.

3.3.4 Synthesis of bulky $Ru_2^{II,II}$(formamidinate)$_4$ complexes under harsh conditions

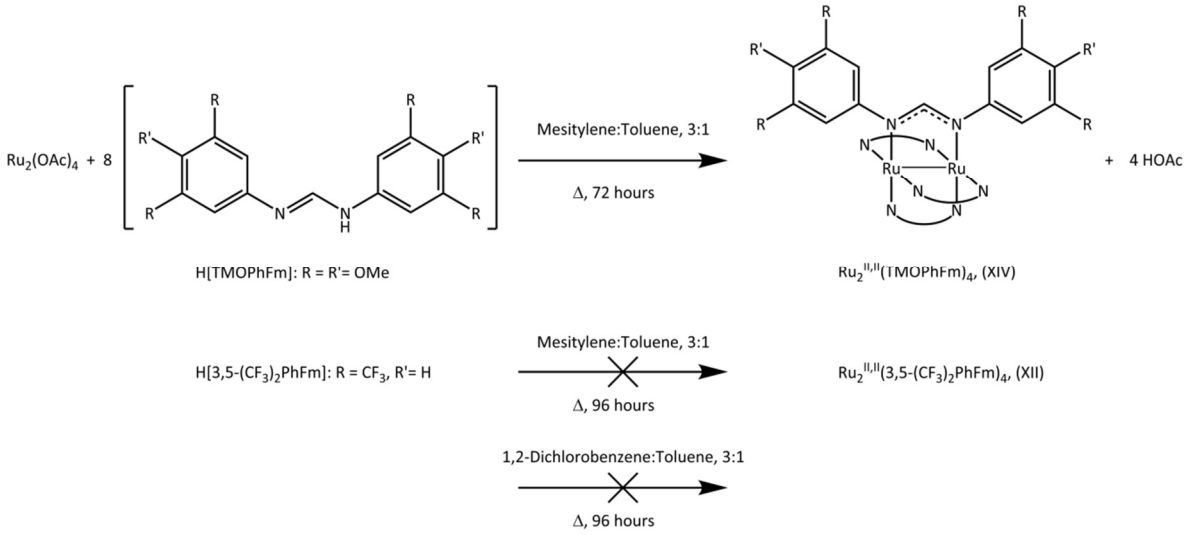

Figure 3.3.3 – Synthesis of XIV and the attempted synthesis of XII under more extreme conditions

The synthesis of ***$Ru_2^{II,II}$(TMOPhFm)$_4$ (XIV)*** and ***$Ru_2^{II,II}$(3,5-(CF$_3$)$_2$PhFm)$_4$ (XII)*** presented some additional challenges. Significantly elevated conditions were required to prevent the metathesis reactions from stopping at the tris- substituted products such as ***XIII***. However, synthetic efforts were also limited by the thermal stability of the reactant/product mixture over prolonged periods (>72 hours). Modification of the procedure described previously for ***X, XI*** and ***XIII*** to utilise a higher boiling solvent system was therefore explored as a means to generate these compounds.

After 72 hours ***$Ru_2^{II,II}$(TMOPhFm)$_4$ (XIV)*** was observed as the sole product by MALDI-TOF-MS however, as was noted in the synthesis of both related iron complexes (Section 2.3.2.2) and the parent ligand (Section 2.3.1.4), these species are almost completely insoluble in most common solvents, and only very sparingly soluble in the best instance. Consequently, there was no immediate way to remove the significant excess of ligand present or to otherwise isolate ***XIV*** cleanly to facilitate further characterisation.

By contrast to ***XIV***, even on prolonged reflux for 96 hours, the tetra-kis product ***$Ru_2^{II,II}$(3,5-$(CF_3)_2$PhFm)$_4$ (XII)*** was only ever obtained in small quantities and as part of binary mixtures with the related tris- product ***XIII***. The use of higher boiling solvents such as 1,2-DCB was tested but either solvent or reflux temperature in that instance was observed to greatly increase the observed decomposition rate at which the reaction mixture decomposed.

For both ***(XII)*** and ***(XIV)*** the combination of unwanted products, intractable excess ligand, very low solubility and the presence of significant decomposition products greatly frustrated attempts to characterise the products generated by methods other that MALDI-TOF-MS. Consequently, subsequent analysis shall focus on the more soluble products ***$Ru_2^{II,II}$(DMOPhFm)$_4$ (X)*** and ***$Ru_2^{II,II}$(4FPhFm)$_4$ (XI)*** and to a lesser extent the tris- substituted product ***$Ru_2^{II,II}$(3,5-$(CF_3)_2$PhFm)$_3$(OAc) (XIII)***.

3.3.5 Computational studies of Ru_2(amidinate)$_4$ complexes and a proposed oxo-adduct.

In order to better understand the complex electronic structure of the products obtained DFT calculations were conducted on the model complex $Ru_2(dmf)_4$ (dmf = N,N'-diphenylformamidinate).

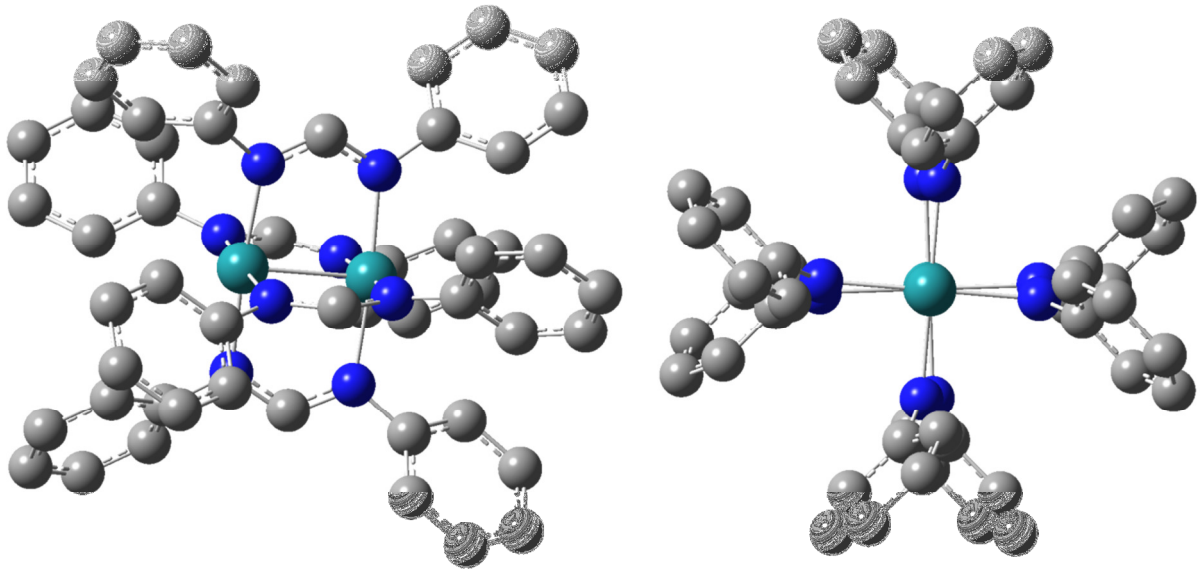

Figure 3.3.4 - The model complex $[Ru_2(dmf)_4]^0$

To date the only reported theoretical calculations for complexes of the form $Ru_2^{II,II}$(amidinate)$_4$ are those provided by Cotton in his published synthesis of $Ru_2^{(II,II)}(DFM)_4$ (where DFM = N,N'-bis(*p*-tolyl)formamidinate).[122,139] These calculations were conducted utilising the Self-Consistent Field-Xσ-Scattered Wave (SCF-Xσ-SW) methodology, an early implementation of DFT which has seen been superseded by other methodologies[343] for the simplified complex $[Ru_2^{(II,II)}(HNC(H)NH)_4]^{0/+1}$. Justification for the validity of this simplification was afforded by comparison to a parallel study of the related complex $[Ru_2^{(II,II)}(HNNNH)_4]^{0/+1}$ wherein the energy of the δ* >> π*.[139] A subsequent comparison with the related Ru_2 (II,III) analogue $Ru_2^{(II,III)}(DFM)_4Cl$ by Cotton in 1995[122] demonstrated that this assumption is invalid with the (II,II) -> (II,III) oxidation invoking extensive change of the electronic structure from $\sigma^2\pi^4\delta^2\pi^{*4}\delta^{*0}$ in the (II,II) to $\sigma^2\pi^4\delta^2\pi^{*2}\delta^{*1}$ for the (II,III). Having established that the prior calculations were conducted under now proven invalid assumptions however, no further investigation was made into $Ru_2^{II,II}$(amidinate)$_4$ complexes.

SCF-Xσ-SW is a less computationally expensive alternative to traditional *ab initio* Hartree-Fock and Post-HF methodologies which included a limited implementation of electron correlation and spin. This provided a simple approximation of HF that could be conducted in a greatly reduced computational timeframe.[343] This methodology was often sufficient to provide a qualitative description of M-M bonding interactions, and was successfully applied to complexes of Mo,[344–346] Rh[347] and Ru[145,257,341,348] by Norman et al. Despite this early precedent however, the accuracy of calculated values for experimentally determinable properties, such as calculated UV/Vis spectra, was generally very poor.[343]

During the 1990s Becke published both the foundation for[349–351] and perhaps most widely used example of a hybrid functional – B3LYP[350–352] (Becke, 3-parameter, Lee-Yang-Par). Both this and other hybrid functionals such as PBE0 have since served to vastly improve the quality of the results that may be obtained from DFT calculations, often offering far better agreement with experimental properties that those conducted using SCF-Xσ-SW.[343,353]

This allows for the better modelling of many molecular properties, which are otherwise poorly defined in traditional *ab initio* functionals and in a less computationally intense manner. This results in a methodology that is both computationally easier to conduct whilst still showing comparable or better correlation with experimental results.[354,355]

3.3.5.1 Limitations of B3LYP

Of the hybrid functionals proposed by Becke, the most widely used is B3LYP[350–352] (Becke, 3-parameter, Lee-Yang-Parr). B3LYP is not without its limitations however, yet it remains a very widely used benchmark.[343]

Of its limitations the most notable is in how B3LYP models exchange and correlation energy in metals especially in extended systems[356] This is the primarily a limitation of the LYP functional as it does not provide distinct treatment of opposite- and parallel-spin correlations.[356,357] Consequently, it lacks the ability to adequately describe such interactions over moderate ranges and may this may in turn be attributed to similar limitations in the Salvetti theory from which B3LYP is derived.[358,359]

In practise this has meant that B3LYP is not always the most practical choice of hybrid functional for metallic systems as has been noted in the observations in many recent computational studies of closely related diruthenium[156,360–363] and diosmium[364,365] complexes. In these instances the related Perdew–Burke–Ernzerhof exchange correlation functional (PBE0)[353,366,367] affords results more consistent with experimental evidence for these types of system. [156,360–362,364,365] PBE0 similarly has its limitations, most notably a tendency to disproportionally stabilise higher energy excited states.[368,369] Despite this, PBE0 remains a preferable alternative to B3LYP for dimetal systems including Ru and Os.[156,356,360–362]

3.3.5.2 Computational methodology

Geometry optimisation was conducted for the model complex $Ru_2(dmf)_4$ in gas phase and the singlet state under both B3LYP[350–352] and PBE0[353,366,367] functionals with the relativistic SDD basis set for ruthenium[370] and 6-31G*(5d) Pople basis set[371] (For C, H, N, O) using the Gaussian09 suite of programs (revision A.02). This was conducted under C4 (B3BLP) and D4 (PBE0) symmetry constraints and Structures were confirmed to be minima on the potential energy surface by frequency analysis. The electronic absorption spectra was calculated using the time-dependent DFT (TD-DFT) method[372–374]

Unrestricted open–shell calculations were conducted in every instance. Where calculations require description of singul`ar occupancy molecular orbitals and/or the of independent spin states, the electronic description of the molecular orbitals is conducted independently for both alpha and beta spin states resulting in separate alpha and beta manifolds.[375]

3.3.5.3 $[Ru_2(dmf)_4]^0$

A comparison of selected key calculated physical properties under the two different functionals with those determined crystallographically for ***Ru_2(DMOPhFm)$_4$ (X)*** is given below in Table 3.3.1.

	B3LYP	PBE0	$Ru_2(DMOPhFm)_4$
Ru–Ru	2.518	2.494	2.4998(5)
Ru–N (average)	2.07	2.042	2.05
N–C{H} (average)	1.33	1.324	1.329
N–Ru–Ru–N (average)	6.5	6.1	5.8

Table 3.3.1 - Comparison of calculated and experimental crystallographic data for *Ru_2(DMOPhFm)$_4$ (X)*

As can be seen from the above, calculations conducted utilising PBE0 provided the best approximation of the experimental physical data and modelling the geometry of the dimetal core. Consequently, subsequent discussion shall focus primarily on calculations conducted using this hybrid functional.

The electronic structure of the converged models was determined as $\sigma^2\pi^4\delta^2\pi^{*4}\delta^{*0}$ and is shown in the frontier MO diagram overleaf for PBE0 (Figure 3.3.5), whilst cartoons of the shapes of the bonding MOs eigenstates are provided on the following page (Figure 3.3.6).

The frontier MO diagram shown for the neutral model $[Ru_2(dmf)_4]^0$ in Figure 3.3.5 is shown with just the HOMO populated for the sake of visual clarity, however it should be implicit that all lower energy MOs are fully populated. Those combinations that are non-bonding with respect to the metal- metal bond or which arise from ligand-π combinations have been included for completeness but are shown in grey.

The HOMOs are a degenerate pair of Ru_2- π* combinations, separated from the LUMO and LUMO+1 combinations (Ru_2- δ* and Ru_2- σ*) by 2.45 eV and 3.51 eV respectively. Overall then it can be seen that the Ru_2- δ* has been significantly destabilised by the Ru-ligand nitrogen lone pair anti-bonding interactions (grey) resulting in the observed overall $\sigma^2\pi^4\delta^2\pi^{*4}\delta^{*0}$ electronic configuration.

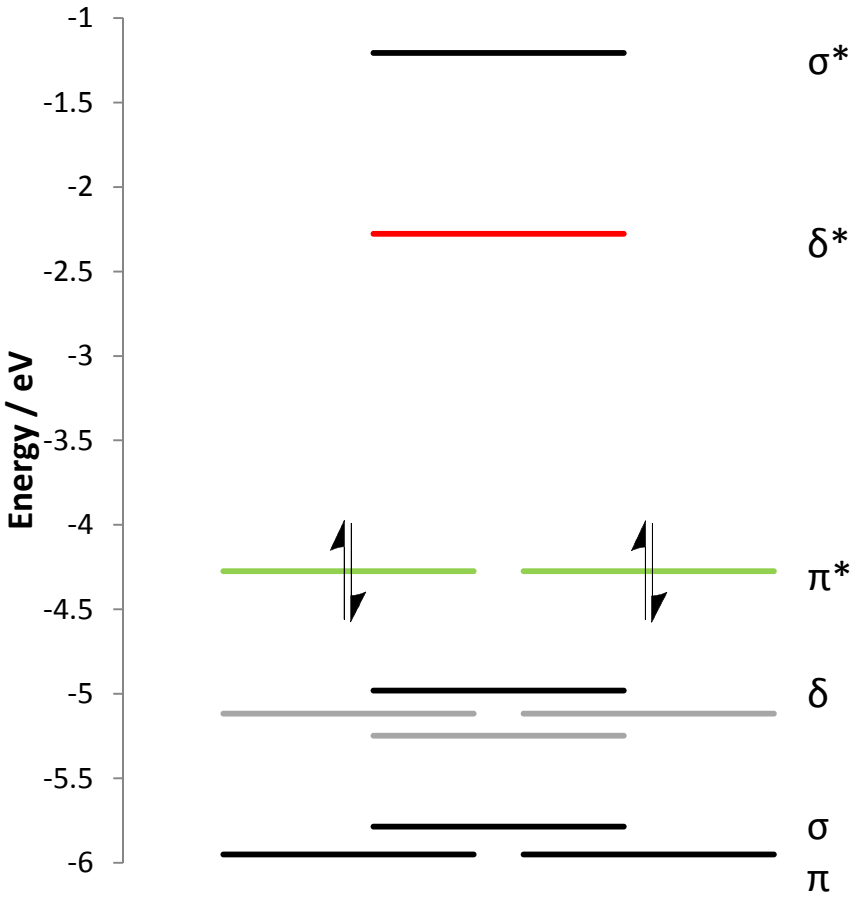

Figure 3.3.5 - Diagram of frontier MOs of $[Ru_2(dmf)_4]^0$, HOMO, LUMO; HOMO is populated in isolation for clarity and ligand based orbitals, whilst included for completeness, are shown in grey.

Application of TD-DFT allows this model to calculate the allowed optical transitions that might be observed experimentally in the UV-Vis region. However, as might be expected for compounds with such complex electronic structures there are a large number of predicted transitions many of which with very low associated oscillatory strength (*f*). For the sake of brevity only those transitions with f > 0.04 are show below in Table 3.3.2

Energy (eV)	Wavelength (nm)	Molar Absorptivity (M^{-1} cm^{-1})	Assignment
1.64	755	0.0092	Ru_2-π* -> Ru_2-δ*
2.02	613	0.0688	Ligand-π -> Ru_2-δ*
2.26	548	0.0052	Ru_2-δ -> Ru_2-δ*
2.92	424	0.1946	Ru_2-π/ Ligand-π -> Ru_2-δ*
3.06	405	0.0174	Ligand-π -> Ru_2-σ*
3.28	378	0.0086	Ru_2-π* -> Ligand-π*

Table 3.3.2 - Predicted UV-Vis transitions generated via TD-DFT for the model complex $[Ru_2(dmf)_4]^0$

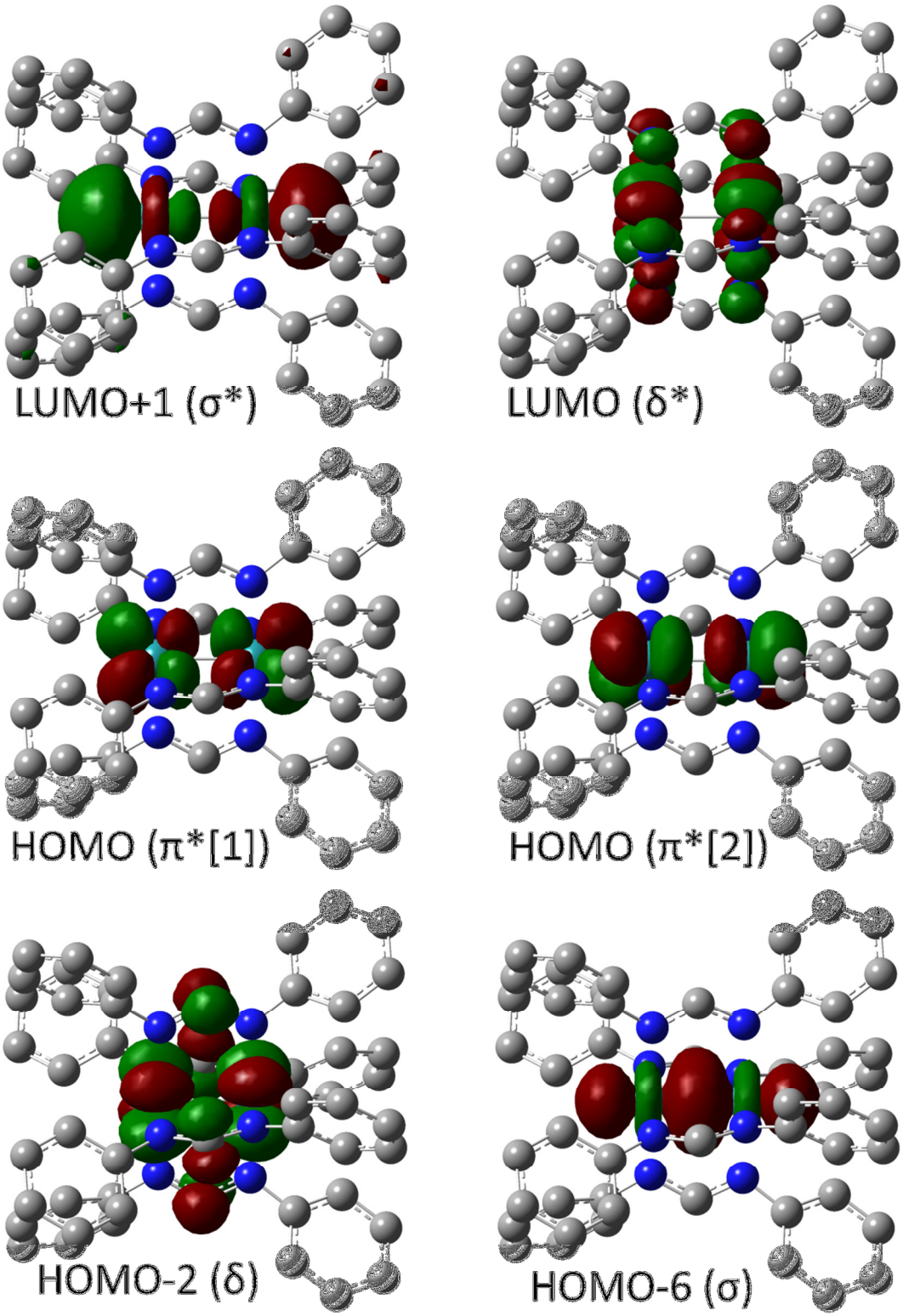

Figure 3.3.6 – Molecular orbital surfaces for $[Ru_2(dmf)_4]^0$ drawn at the 0.03 isovalue

The cartoons shown above in Figure 3.3.6 provide a very visual indication of the description of the bonding interactions present within the dimetal core.

Of the transitions shown previously, (Table 3.3.2) it is probably that only those corresponding to the LCMT at 613 nm and the MLCT at 424 nm will be observed with any significant intensity. Despite this however, as a significant number of the remaining transitions involve ligand π combinations it is noteworthy to consider the impact of the inclusion of the modelled phenyl rings. Many of these ligand- π combinations such as HOMO-3 show a distribution of electron density across the aryl rings of the ligand to varying degrees (Figure 3.3.7). Similarly many of the metal dominated MOs at lower energy such as the Ru_2-π combinations HOMO-7, HOMO-8 also display a degree of ligand-π character. This validates the inclusion of the phenyl rings into the computational model and provides stark contrast to the previous study wherein these were modelled as simple hydrogens. It is clear even from the below, that delocalisation of electron density to these rings provides a significant contribution to the overall electronic structure of the complex.

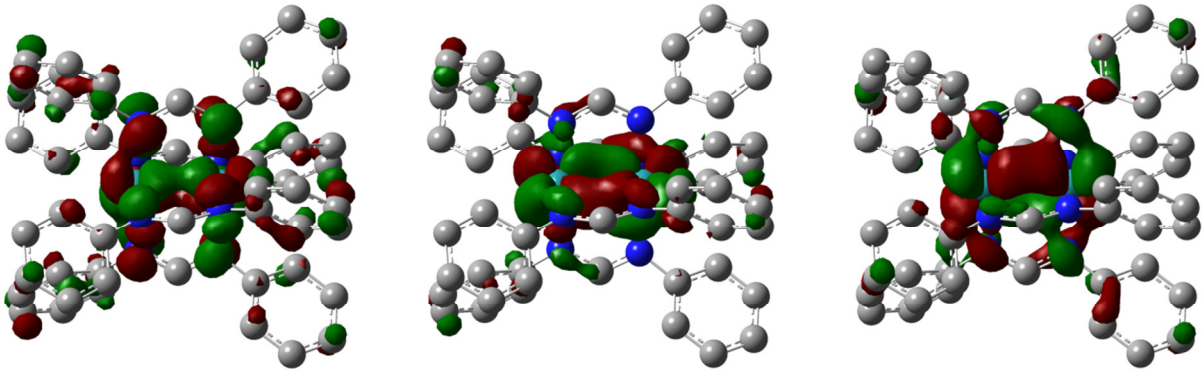

Figure 3.3.7 - MO surfaces for [Ru2(II,II)(PhNC(H)NPh)4]^0 drawn at the 0.03 isovalue; L->R, these are: HOMO-3 (Ligand π); HOMO-7 (δ*); HOMO-8 (π*[1]); HOMO-1 (π*[2]) as referred to in the above text

3.3.5.4 $[Ru_2(PhNC(H)NPh)_4]^+$

The structure of the 1+ charged model, which equates to Ru_2 (II,III), was minimised under the presumption of C_4 symmetry and within a DCM solvent mask as with the neutral model. As in the previous study by Cotton the converged model possesses an electronic structure consistent with $\sigma^2\pi^4\delta^2\pi^{*2}\delta^{*1}$ (Figure 2.3.15) and the greater stability of this confirmation readily displayed in the relative energies of the frontier MOs cf. those observed for the neutral model.

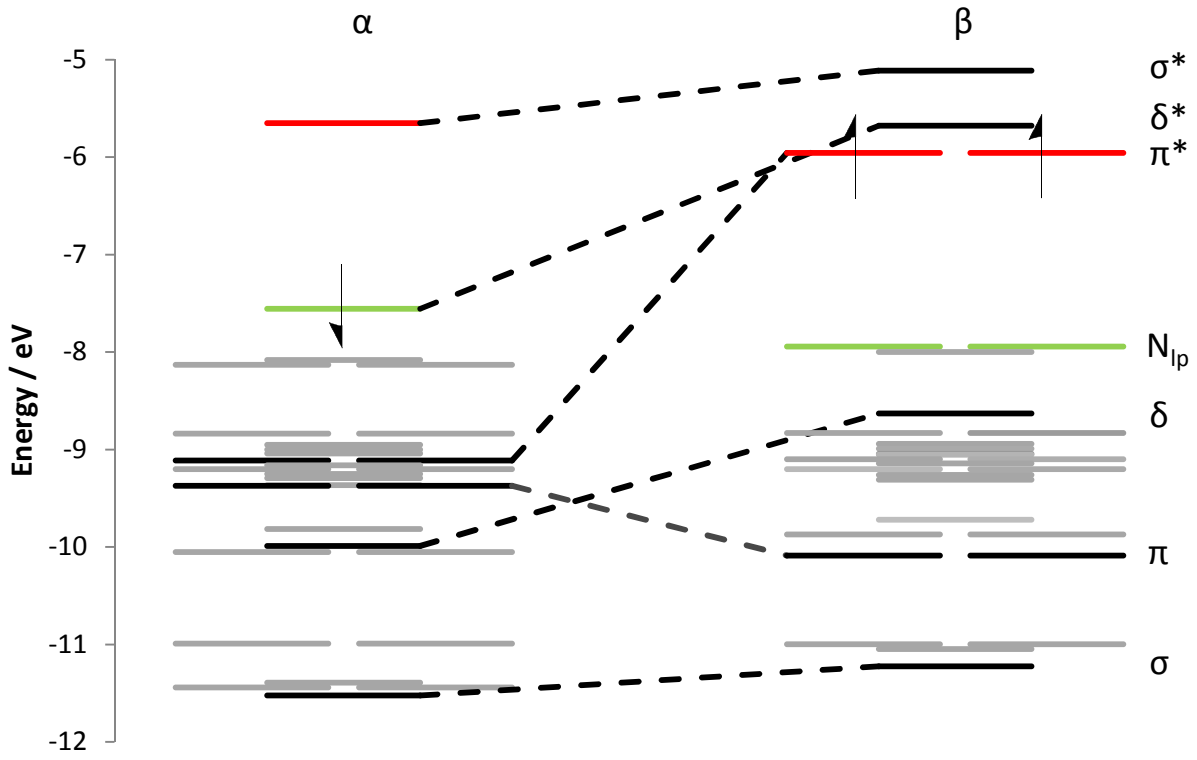

Figure 3.3.8 - Diagram of frontier MOs of $[Ru_2(PhNC(H)NPh]^+$, HOMO, LUMO; SOMOs (δ* in α, and π* in β) are populated in isolation for clarity and ligand based orbitals, whilst included for completeness, are greyed out.

By contrast to the neutral model, the contributions from ligand orbitals, many of which exhibit π character and are delocalisation across the aryl rings, are clearly of greater significance than in the neutral (II,II) model. This is exemplified within a charged species where it becomes necessary to model both spin manifolds. In the β spin manifold for example just such a combination is now formally the HOMO. This combination, in distinct from many of the ligand π character MOs in that is it predominately centred on the donor nitrogen π combination similar to that observed for the HOMO-3 combination for the neutral species (Figure 3.3.6).

Comparison of the respective α and β spin manifolds affords the singularly occupied $\delta^{*1}\pi^{*2}$ set of SOMOs which are now notably closer in energy than the neutral model at an average separation of 0.9 eV [1.6(α), 0.28(β)] as compared to 2 eV in $[Ru_2(dmf)_4]^0$. What might otherwise be expected to be the facile addition of a single electron in the transition from (II,III) → (II,II), then clearly also necessitates a comprehensive rearrangement of the wider electronic structure.

This determination provides significant potential insight into the commonly noted difficulty in isolation of (II,II) formamidinate species generated from their (II,III) analogues.[103] It may further provides some rationalisation to the apparent thermodynamic preference towards the Ru_2(II,III) oxidation state.

Conversion of the (II,III) → (II,II) is likely disfavoured due to the need to not just populate a presumed $(II,III)^-$ transition state approximating $\sigma^2\pi^4\delta^2\pi^{*2}\delta^{*2}$, but also to facilitated the complete electronic reconfiguration to the higher energy $\sigma^2\pi^4\delta^2\pi^{*4}\delta^{*0}$ ground state of the (II,II) $[Ru_2(dmf)_4]^0$ model.

The reverse process, that of (II,II) → (II,III) by contrast requires no change in overall electronic configuration, merely the loss of $1e^-$ from the π*, and is thermodynamically favoured by subsequent relaxation of the probable $\sigma^2\pi^4\delta^2\pi^{*3}\delta^{*0}$, $(II,II)^+$ transition state to the $^2\pi^4\delta^2\pi^{*2}\delta^{*1}$ of (II,III). The differentiation in the reversibility of these processes following on presumption of the generation of electronically intermediate transition states, if a valid description, should then be reflected in the electrochemistry of respective (II,II) and (II,III) compounds.

3.3.5.5 Generation of a dioxygen adduct model of $[Ru_2(dmf)_4(OO)]$

Attempts to model the interaction between dioxygen and the diruthenium tetraamidinate complexes ***X*** and ***XI*** present a number of very significant challenges both practical and computationally.

Firstly the nature of the interaction is poorly defined. Experimental evidence from electrochemistry indicates that the interaction is both week and distorts rather than fundamentally alters the electronic structure of the dimetal core. This then presents two practical challenges, defining the orientation of the oxo-adduct to peroxo- or superoxo- and simultaneously considering how to model such a distant, potentially anti-ferromagnetically coupled interaction. This is a direct consequence of combination of the un-paired spin from triplet oxygen and a dimetallic core able to reconfigure into a range of differing electronic configurations as seen for the II,II and II,III states.

It was concluded that the most likely orientation of the oxo-adduct would be as a peroxo due in part to steric considerations but this then provides a high degree of rotational freedom to the O-O vector which renders attempts to optimise the geometry of the model complex far more challenging.

Several iterative scenarios were considered which reflected the likely nature of the ground state, however as many of these failed to converge during geometry optimisation it became readily apparent that predetermination of the state was not a realistic option. Consequently attempts were made to optimise the geometry of the singlet, triplet and quartet ground states assuming no overall change in charge, which on observation of the lack of change observed in the electrochemistry seems a reasonable assumption. In order to facilitate convergence it was necessary to implement an ultra-fine mesh potential energy surface as the stabilisation observed for the global energy minima was notably small.

Of these geometry optimisations the only one to converge and permit further analysis was that of the quartet ground state and only in the absence of any solvent mask or other additional considerations. Consequently the PBE0 calculations for NN^0 and NN^+ were similarly repeated in the absence of a solvent mask, as reported in the previous section to better facilitate a comparative analysis.

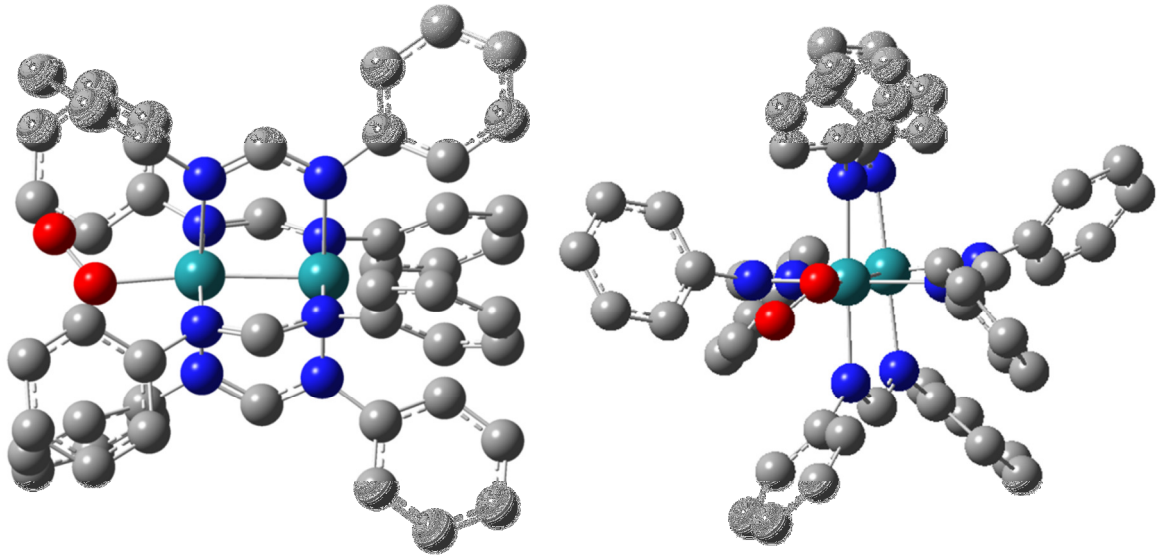

Figure 3.3.9 – Peroxo- adduct model NN-OO complex [$Ru_2(dmf)_4(OO)$]

Using the minimised structure it is then possible to generate qualitative MO cartoons to show the localisation of the MOs within the model as show overleaf in Figure 3.3.11, whilst MO energies are summarised in Table 3.3.8 that follows thereafter.

The model for the peroxo-adduct does not differ massively from that seen in the neutral free tetraformamidinate but it can readily be seen (Figure 3.3.11) that the new calculated LUMO+1, LUMO and HOMO (shown top, L ->R) have significant contributions from the bound dioxygen adduct.

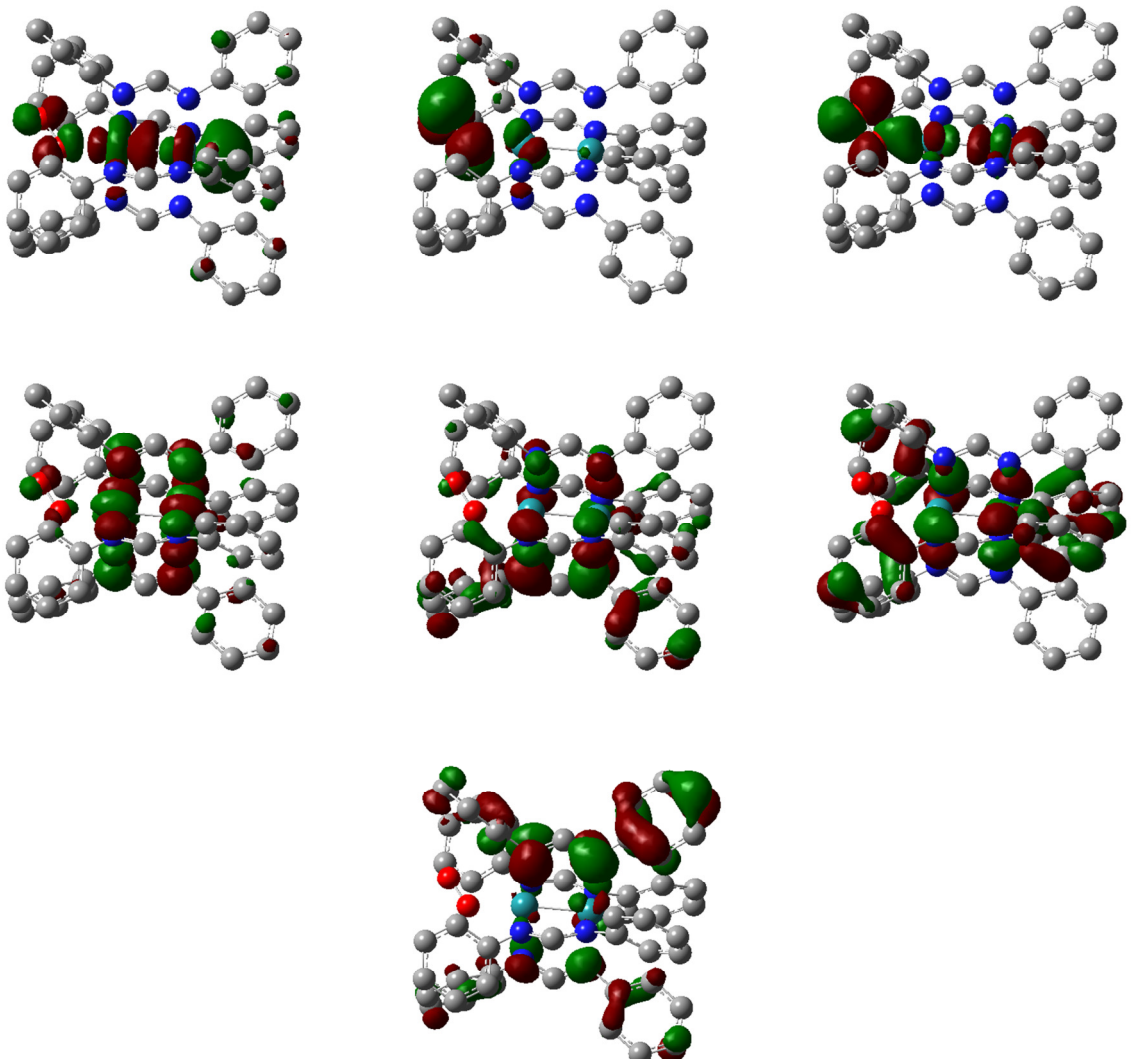

Figure 3.3.10 - MO surfaces for the α-manifold of the model NN-OO, drawn at the 0.03 isovalue. L->R, by row these are: LUMO+1 (M_2 σ* + O_2 π*); LUMO (O_2 π*); HOMO (O_2 π*); HOMO-1 (M_2 δ*); HOMO-2 (Ligand π); HOMO-3 (Ligand π); HOMO-4 (Ligand π); HOMO-5 (M_2 π*)

Where previously ligand-π contributions were observed to dominate many of the frontier MO combinations it is clear that under this model the inclusion of O_2 renders it the as intrinsic to almost every MO combination. The impact of the introduction of a peroxo-adduct can therefore, on the basis of this modelling exercise be reasonably expected to have a very considerable impact of the electronic configuration of the dimetal core. Its introduction induces a similar re-configuration to that observed on transitioning from the Ru (II,II) to (II,III) and further underlines the configuration flexibility of these dimetallic units.

α manifold

MO #	Character	PBE0 (eV)	Assignment
236	LUMO+4	-0.37	Ligand π*
235	LUMO+3	-0.43	Ligand π
234	LUMO+2	-0.63	Ligand π*
233	LUMO+1	-1.02	M_2 σ* + O_2 π
232	LUMO	-1.16	O_2 π*
231	HOMO	-4.91	O_2 π*
230	HOMO-1	-5.01	M_2 δ*
229	HOMO-2	-5.77	Ligand π
228	HOMO-3	-5.82	Ligand π
227	HOMO-4	-5.89	Ligand π
226	HOMO-5	-6.39	M_2 π*

Table 3.3.3 - MO assignements of the α manifold of NN-OO

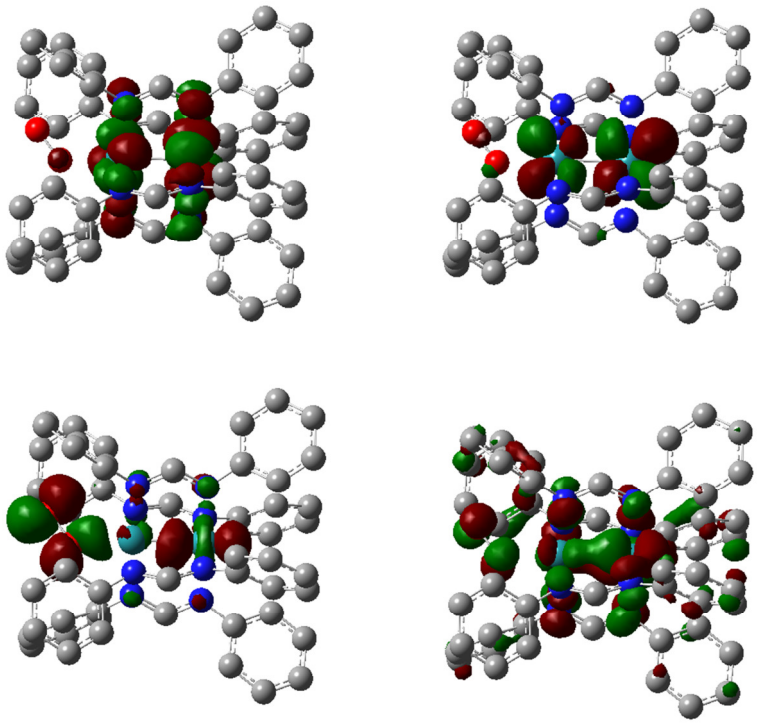

Figure 3.3.11 - MO surfaces for the β-manifold of the model NN-OO, drawn at the 0.03 isovalue. L->R, by row these are: LUMO+1 (M_2 δ*); LUMO (M_2 π*); HOMO (O_2 π*); HOMO-1 (Ligand π);

β manifold

MO #	Character	PBE0 (eV)	Assignment
234	LUMO+4	-0.43	Ligand π
233	LUMO+3	-0.69	M_2 σ*
232	LUMO+2	-2.4	M_2 π*
231	LUMO+1	-2.41	M_2 δ*
230	LUMO	-2.48	M_2 π*
229	HOMO	-5.35	O_2 π*
228	HOMO-1	-5.5	Ligand π
227	HOMO-2	-5.59	Ligand π
226	HOMO-3	-5.65	Ligand π
225	HOMO-4	-5.67	M_2 δ
224	HOMO-5	-5.99	O_2 π*

Table 3.3.4 - MO assignements of the β manifold of NN-OO

3.3.5.6 Comparison of UV-Vis-NIR and IR spectra generated via PBE0 calculations

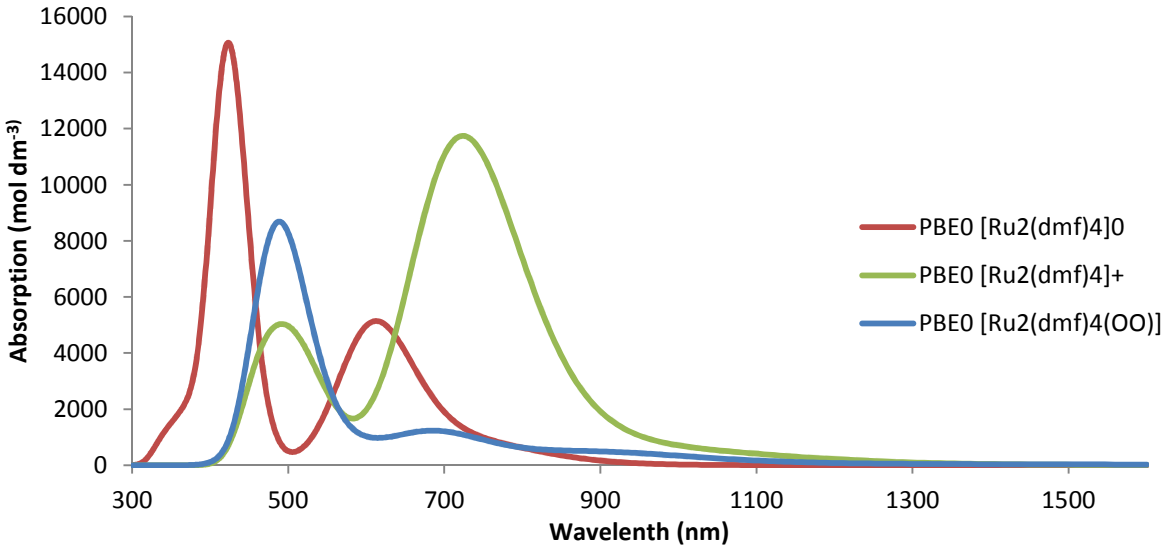

Figure 3.3.12 - Predicted electronic excitation spectra for the modelled complexes

Figure 3.3.13 Provides a visual summation of the output for the TD-DFT modelling process. This graph shows the predicted UV-Vis spectra for the 3 modelled states. The free neutral complex, that of the corresponding (II,III) state wherein a single electon has been lost, and the modelled peroxo-adduct complex. It was intended that visual comparision between the predicted spectra and that seen for X or XI in the UV-Vis on exposure to dioxygen might provide some insight into the potential nature of the observed interaction. However, due to the complexities inherent in modelling such a poorly defined and understood species as the

proposed peroxo-adduct it is not immediately clear how much can readily be concluded from such a comparison.

On the one hand, the UV-vis spectra predicted for the modelled peroxo-adduct does not correlate at all with that seen experimentally but it remains unclear if this is due to the model having been devised based on flawed assumption – or – if the model simply does not possess the required descriptive power to model this interaction. PBE0 like any hybrid functional provides a compromise between complexity, descriptive rigor and the required computational time to run the calculations. As in this case the modelled dimetal core is readily able to quite fundamentally re-configure itself due to small overall changes as is seen between II,II and II,III configurations. In this instances PBE0 may not be sufficient to effectively model the variety of potential outcomes sufficiently, and like is observed with B3LYP the construction of these functionals does itself provide a significant bias in the predictions that they provide. The peak data from the above figure are collated below in Table 3.3.10.

	Wavelength (nm)	Absorption (mol dm-3)
NN^0	423	15064
	613	5142
NN^+	723	11741
	492	5036
NN-OO	685	1233
	489	8686

Table 3.3.5 - Peak data for calculated electronic excitation spectra for the three computed models

As can be seen from comparison of this data to that obtained experimentally, (section 3.3.8) there is unfortunately no strong correlation between the experimental and calculated spectra, with no predicted transition occurring in close proximity to the 542 nm excitation observed for the O_2 generated species experimentally. Consequently what can be concluded from this computational study is that whilst a model has been successfully obtained, this does not provide a suitable description for the species generated experimentally.

3.3.6 Characterisation of diruthenium complexes

Characterisation of the synthesised complexes was primarily conducted via MALDI-TOF-MS, and where possible, X-Ray crystallography. Computation calculations were used in addition to complement and rationalise the observed transitions in the UV-Vis-NIR spectrum, and structural properties observed crystallographically.

The diamagnetic nature of the complexes obtained was confirmed for **(X-XIV)** via ^{1}H and ^{13}C NMR spectroscopy, which in conjunction with MALDI-TOF-MS was used during optimisation of reaction conditions as a means to identify the presence of remaining free ligand via the small, observed shift, (<0.25 ppm), on coordination to the metal centre.

IR spectra of the compounds obtained are dominated via vibrational modes of the common Ar-NCN-Ar ligand backbone with IR spectra of the complexes only differing from that of the corresponding ligand in the fingerprint region (1000-750 cm^{-1}) and by the notable loss of the N-H transition. The IR spectra of the complexes then predominantly reflected the identity of the ligand used.

3.3.6.1 MALDL-TOF-MS

Assigned compound ID	$M_{average}$	$M_{monoisotopic}$ [M+] (Calcd.)	$M_{monoisotopic}$ [M+] (obs.)
$Ru_2^{II,II}(DMOPhFm)_4$ (X)	1463.5	**1463.7**	**1464.3**
$Ru_2^{II,II}(4FPhFm)_4$ (XI)	1127.0	**1128.1**	**1128.2**
$Ru_2^{II,II}(3,5\text{-}(CF_3)_2PhFm)_3(OAc)$ (XIII)	1662.9	**1664.0**	**1664.0**
$Ru_2^{II,II}(TMOPhFm)_4$ (XIV)	1703.7	**1704.4**	**1704.4**
$Ru_2^{II,II}(3,5\text{-}(CF_3)_2PhFm)_4$ (XII)	2071.1	**2072.0**	**2072.1**

Table 3.3.6 – Predicted mass ions for analogues of isolated and non-cleanly isolated products in order of increasing mass. Expected mass ions are highlighted in bold

Initial experiments utilising alkali metal formamidinate salts commonly saw the inclusion of additional lower m/z species consistent with either low-valent lithium bridged dimers of the form $Li_2(amidinate)_2$ or other non-ruthenium containing species. As discussed, one of the advantages of the new proposed reaction methodology is that the mass-spectra obtained for the crudes products are notably free of such unwanted species.

In contrast to the mixed products observed previously with diiron (Section 2.3.5) and when utilising alkali metal salts (Section 3.3.2) products ***X-XIV*** are, with the exception of ***XII,*** all observed as single m/z ions. Even under the harshest conditions tested ***XII***, as previously discussed, wass observed as a binary mixture of the tris- and tetra-kis products. A typical mass spectra for the cleanly isolated complexes is included below for ***X*** (Figure 3.3.5) along with an expansion of the isotopic distribution of the parent ion at 1464.3 m/z.

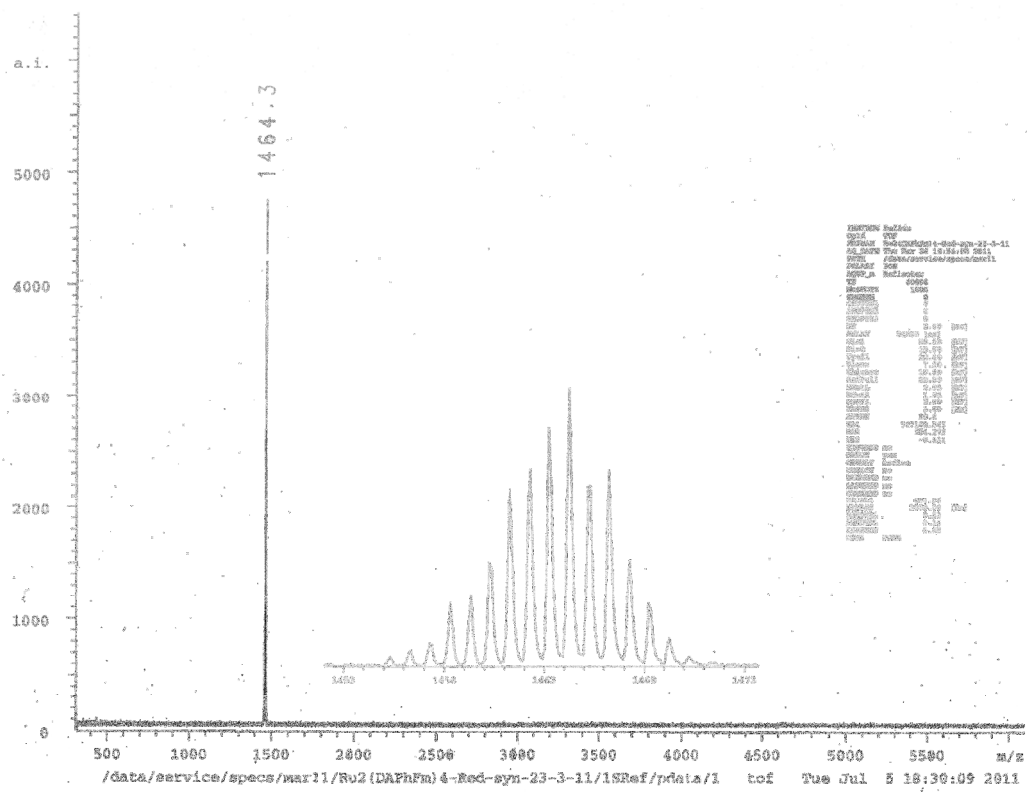

Figure 3.3.13 - MALDI-TOF-MS spectrum of $Ru_2^{(II,II)}(DMOPhFm)_4$ prepared in DCTB matrix using DCM. Inset – magnification of parent m/z ion peak and associated isotopic distribution.

The small deviation between calculated and observed mass for ***X*** in the example given is within the error associated with the calibration of the instrument. Internal calibration is conducted on a per-use basis that provides a calibrated m/z range of 500-5000 over 5 points and as such provides a compromise between usable range and accuracy. However, as this is conducted on a per-use basis repeat analysis of samples serves to ensure the accuracy and validity of the results obtained. Typical precision across disparate analytical runs is more typically +/- 0.5 m/z.

As was briefly discussed previously for the related diiron chemistry (Section 2.3.5.2), the isotopic distribution of the parent ion provides a great deal of useful information. With

heavier, more isotopically rich elements such as ruthenium and Molybdenum (Chapter 5) this provides a fingerprint that can be compared against that calculated with an isotopic calculcator. This allows a very facile means to determine the nuclearity of the originating species with respect to the included metal (Figure 3.3.5).

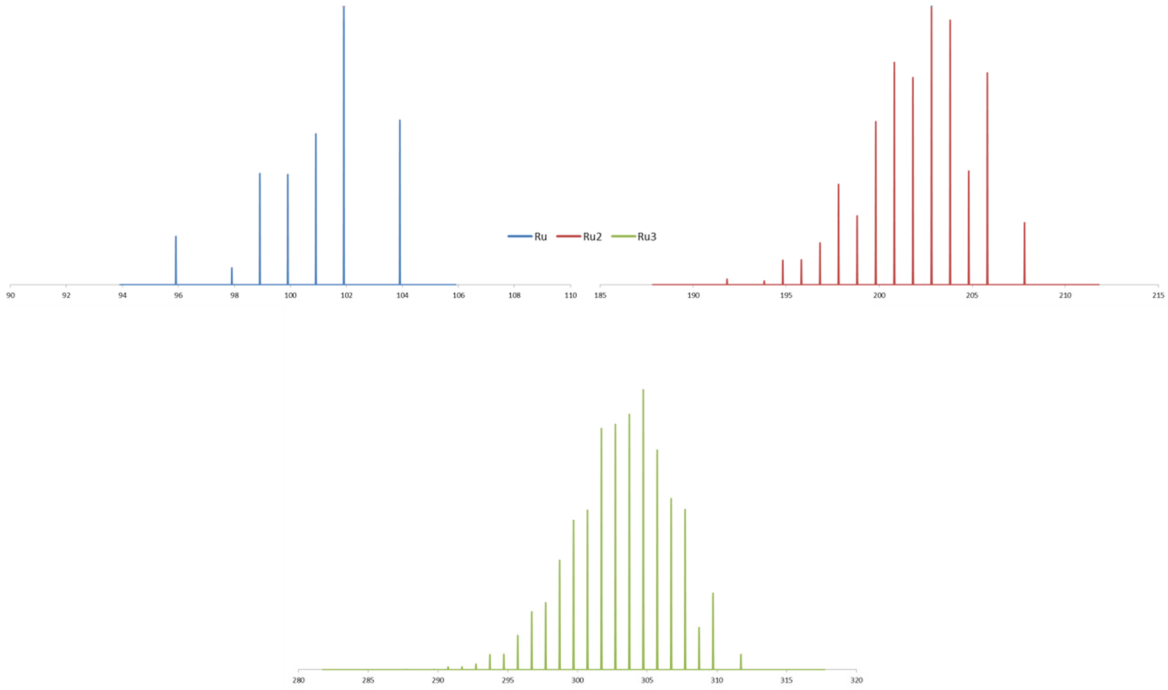

Figure 3.3.14 - Isotope m/z distribution pattern of Ru1 (Blue), Ru2 (Red), and Ru3 (Green)

Many programs provide this functionality such as Chemdraw™, but that used herein is the comparable freeware calculator IsoPro v3.1 as this provided the more useful interface.[306] To give some indication of the power this simple approach provides consider the comparison provided overleaf (Figure 3.3.6) for the isotopic distribution of ***X*** (left), with that calculated (right).

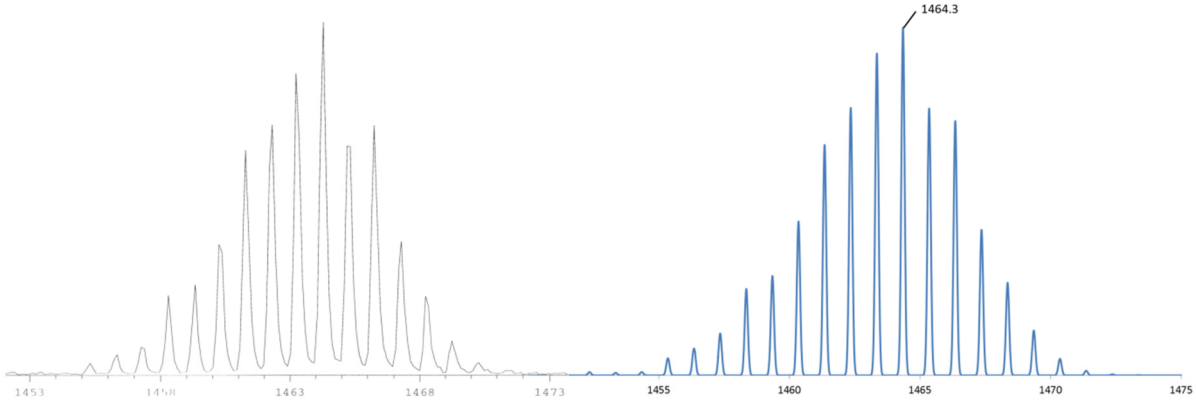

Figure 3.3.15 - (Left) Expansion of m/z peak of $Ru_2^{II,II}(DMOPhFm)_4$ (X) (from Figure 3.3.4); (Right) Isotopic distribution calculated for $C_{68}H_{76}N_8O_{16}Ru_2$ using IsoPro v3.1

As can be readily seen from the above that calculated shows very close accord with experimental data and by comparison to those patterns for $Ru_{1\text{-}3}$ (Figure 3.3.5) the species in question contains at least Ru_2. In practice the added complexity seen for ***X*** arises from isotopic contributions from other non-metallic elements in the ligand and is readily distinguishable from that calculated for any Ru_3 product.

3.3.6.2 X-Ray crystallography

Crystals suitable for X-Ray diffraction of ***$Ru_2^{II,II}(DMOPhFm)_4$ (X)*** and ***$Ru_2^{II,III}(3,5\text{-}(CF_3)_2PhFm)_3(OAc)_2$ (XIII-b)*** were grown by layering of *n*-pentane on saturated solutions in DCM at -18 °C over the course of a week. Suitable crystals of ***$Ru_2^{II,II}(OAc)_4(HDMOPhFm)_2$ (XV)***.were obtained by vapour diffusion of *n*-pentane into a saturated solution in THF at -18 °C over the course of several days. Despite repeated attempts crystals of ***XI-XIV*** could not be obtained.

$Ru_2^{II,II}(DMOPhFm)_4$ (X)

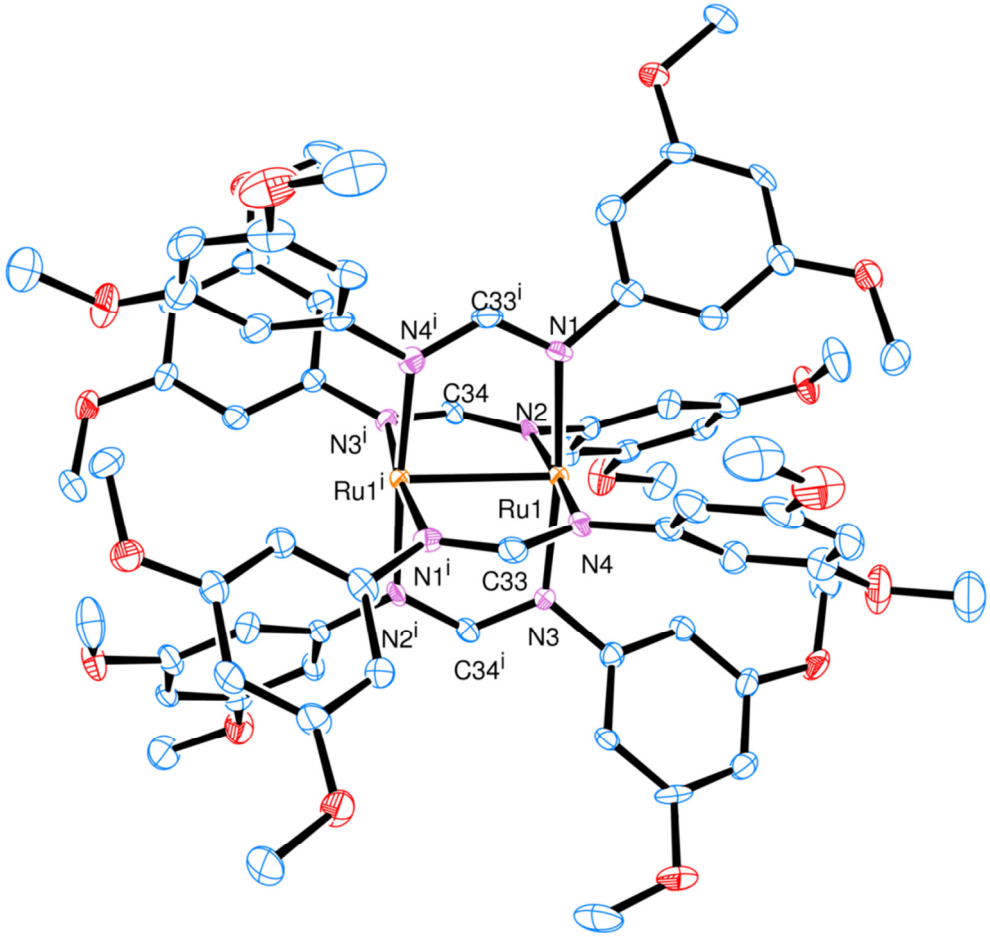

Figure 3.3.16 - Crystal structure of the complex $Ru_2^{II}(DMOPhFm)_4$. Disordered pentane occupying a special position about the edge of the unit cell is not shown for clarity. Thermal ellipsoids are drawn at the 50% probability level.

Synthesis of ***(X)*** provided multiple batches of crystals suitable for analysis from a range of solvents including pyridine, THF and DCM. Of these three, the first two provided relatively poor diffracting crystals that provided structures of similar quality (R_{int}>15%).The third

structure finally yielded a crystal structure suitable for publication.[376] All of the solved structures were functionally identical in form and features.

The asymmetric unit consists of only one Ru coordinated to 4 amidinate nitrogen atoms and one of the two formamidinate phenyl rings with the remainder of the structure being generated by symmetry operations to yield the structure as shown (Figure 3.3.7). Notable bond lengths and distances are provided below (Table 3.3.2), and full cif tables provided in the appendix (Appendix B-4). The cited structure has had a single disordered pentane solvate (located bisecting the unit cell edge) removed via the squeeze function of Planton. For the sake of clarity and completeness the .cif table for the structure preceding this operation is also provided (Appendix B-3) but will not be addressed further herein.

Bond ID	Bond length /Å
Ru-Ru'	2.4998(5)
Ru-N1	2.064(3)
Ru-N2	2.033(3)
Ru-N3	2.075(3)
Ru-N4	2.029(3)
Ru-N (average)	2.05

Bond ID	Bond length /Å
N1-C33	1.333(5)
N4-C33	1.331(5)
N2-C34	1.320(5)
N3-C34	1.328(5)

Torsion	Angle /°
N1-Ru1-Ru'-N4'	6.1(1)
N2-Ru1-Ru'-N3'	5.6(1)

Table 3.3.7 - Selected bond lenths and torsions for $Ru_2^{II,II}(DMOPhFm)_4$ (X).

In comparison to closely related tetracarboxylates which have a typical Ru-Ru bond length of 2.23-2.31 Å the observed Ru-Ru bond length for ***X*** is significantly longer at 2.4998(5) Å. Tetracarboxylate complexes adopt a $\sigma^2\pi^4\delta^2\delta^{*2}\pi^{*2}$ electronic structure, with a formal Ru-Ru bond order of two, whilst tetraamidinates are proposed to adopt a $\sigma^2\pi^4\delta^2\pi^{*4}$ configuration in which the strongly antibonding π* orbitals are populated in preference to the δ*. Consequently, Relative to equivalent tetracarboxylates, tetraformamidinates show significant expected elongation of the Ru-Ru bond.

The two complexes of the same form as ***X*** published previously by Cotton, $Ru_2^{II,II}(DTolF)_4$ and $Ru_2^{II,II}(DTolF)_4$, show Ru-Ru bond lengths of 2.454(1) and 2.474(1) Å, respectively. These are

in good agreement, if slightly shorter, than that determined for ***X.***[139] The longest known example of a Ru_2^{4+} bonding interaction remains that of the related mono-carbonyl complex $Ru_2(DPhF)_4(CO)$, with a Ru–Ru bond length of 2.554(1) Å.[136]

There is a notable deviation from the expected D_{4h} symmetry clearly present upon looking down the Ru-Ru vector with an observed N-Ru-Ru-N torsion angle averaging 5.9°. This torsion is largely a consequence of the steric bulk of the ligand which is minimised by partial deviation from D_{4h} symmetry. Previous work within our group[155,156] has described the propensity for more bulky carboxylate ligands to favour the increased internal rotation about the M-M bond to relieve steric tension; however such treatment considers the involvement of populated δ* orbitals which are unpopulated in the case of $Ru_2(II,II)(form)_4$ complexes.[155,156]

Another notable feature of this structure is the unusually long c axis of the unit cell (52.4 Å) which due to the inclusion of an α-helical twist in the packing arrangement of the asymmetric unit. Tetra-kis substituted paddlewheel complex are known to commonly deviate from co-planarity about the L-M-M-L vector and typically due to the steric demands of the ligand backbone.[103,156] In many instances these slight dihedral twists are localised the ASU, but where, as with ***X***, these effects are driven by steric bulk at the periphery of the ligands these effects may cause wider crystal packing effects as was observed for ***X***.

This effect is particularly notable with increasing aryl substituent bulk in formamidinates. The twist seen between the phenyl rings of the formamidinate with respect to the –N–C–N– backbone is directly driven by the need to accommodate this added bulk. In some instances this can even be sufficiently severe to effectively block further ligand substitution as seen for ***XIII*** *(vide infra)*.

$Ru_2^{II,III}$(3,5-$(CF_3)_2$PhFm)$_3$$(OAc)_2$ (XIII-b).

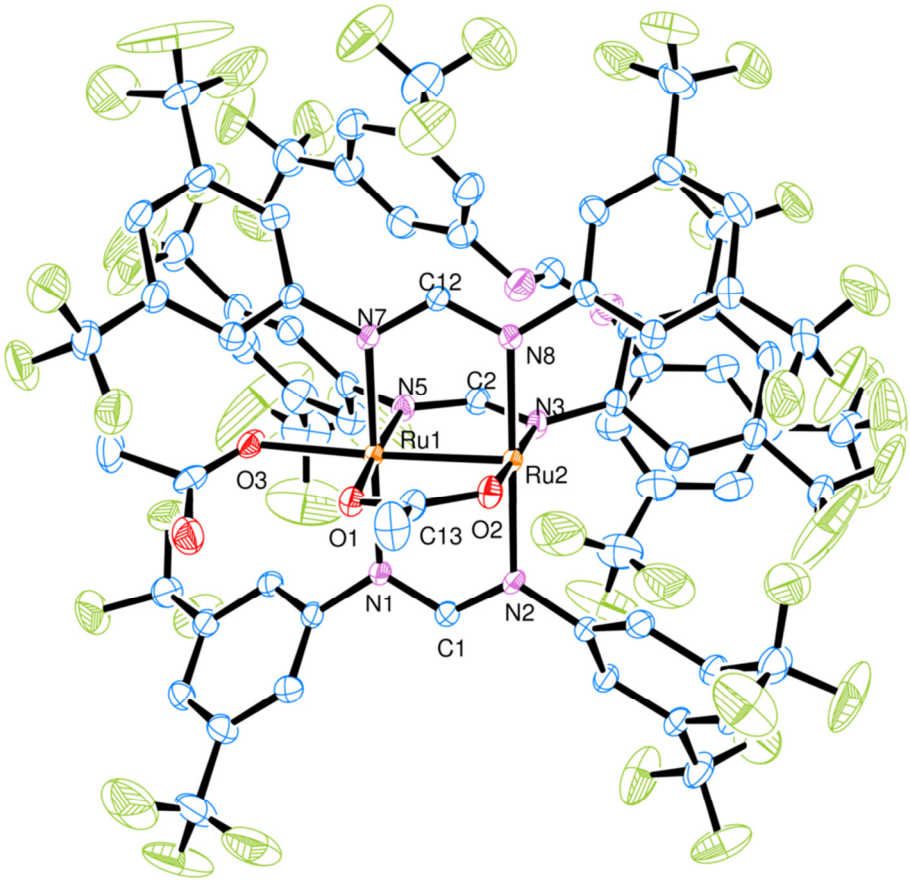

Figure 3.3.17 - Crystal structure of $Ru_2^{II,III}$(3,5-$(CF_3)_2$PhFm)$_3$$(OAc)_2$ (XIII-b). Hydrogens are omitted for clarity and thermal ellipsoids are drawn at the 50% probability level.

Bond ID	Bond length /Å
Ru-Ru	2.3043(4)
Ru1-N1	2.076(2)
Ru1-N5	2.062(2)
Ru1-N7	2.078(2)
Ru2-N2	2.048(2)
Ru2-N3	2.021(2)
Ru2-N8	2.048(2)
Ru-N (average)	2.06

Bond ID	Bond length /Å
Ru1-O1	2.068(2)
Ru1-O3	2.097(2)
Ru2-O2	2.039(2)

Torsion	Angle /°
O1-Ru1-Ru2-O2	6.67(8)
N1-Ru1-Ru2-N2	6.28(9)
N3-Ru2-Ru1-N5	5.2(1)
N7-Ru1-Ru2-N8	8.9(1)

Table 3.3.8 - Selected bond lengths and torsions of $Ru_2^{II,III}$(3,5-$(CF_3)_2$PhFm)$_3$$(OAc)_2$ (XIII-b).

Whilst attempts to grow crystals of the tris-subtituted product ***XIII*** were unsuccessful, crystals of the closely related Ru_2^{5+} species ***XIII-b*** (Figure 3.3.8) were adventitiously obtained from a toluene/*n*-pentane layer of a residual aliquot of the crude reaction mixture.

The Ru-Ru bond length of 2.3043(4) Å ***XIII-b*** is short by the standards of other comparable Ru_2^{5+} formamidinates, which are typically observed in the range of 2.305-2.506 Å. However, in such instances variation of the axial ligand is known to have considerably greater impact than changes in aryl functionalisation.[103] In ***XIII-b*** it is further apparent that this interaction is significant from the Ru1-O3 axial bond length at 2.097(2) Å. This very closely approximates that seen for the bound bridging acetate at 2.039(2)-2.068(2) Å indicating the strength of the axial interaction. The increased ability of the axial acetate ligand to act as a π-acceptor allows electron density to be effectively shifted from M-M anti-bonding combinations to the M-L π resulting in the observed shortening of the Ru-Ru bond.

Disproportionation products are not uncommon in the chemistry of related species, and indeed this been previously been used as a synthetic strategy to generate target Ru_2^{4+} compounds from Ru_2^{5+} starting materials.[103,138,340] However, despite not being representative of ***XIII***, which can be shown to be a Ru_2^{4+} complex electrochemically (vide infra), the structure of ***XIII-b*** still provides a critical insight into the complications in synthesising the related target tetra-kis product ***XII***.

The three initially bound $[3,5\text{-}(CF_3)_2PhFm]^+$ ligands are sufficiently bulky that the ligand arrangement about the dimetal core distorts significantly. This distortion of the ligand environment is most evident from the L-M-M-L torsion angles which, as can be seen in Table 3.3.3, differ quite markedly even between ligands that might reasonably be expected to be otherwise equivalent. The ligand shown top in Figure 3.3.8 displays a torsion angle almost ~50% greater than that seen for both the equivalent ligand diametrically opposing it (shown bottom), and that observed in less hindered complexes such as ***X*** (vide supra). In addition to steric considerations, the highly fluorinated nature of the ligand also introduces significant electrostatic repulsion between proximal fluorine atoms further favouring a more distorted ligand arrangement. This contrasts with less distorted systems like ***X*** where rather than repulsion, stabilising inter-ligand hydrogen bonding are clearly evident within the packing of the crystal lattice.

The distortion in the ligand configuration in ***XIII-b*** serves to effectively shield the remaining potential substitution site, occupied by an acetate ligand against further attack. In this way, formation of the intended product ***XII*** is severely limited and serves to explain why under lower temperature methods ***XIII*** was isolated as the major product.

Complete cif tables for ***XIII-b*** are provided in appendix B-5

$Ru_2^{II,II}(OAc)_4(H[DMOPhFm])_2$ (XV).

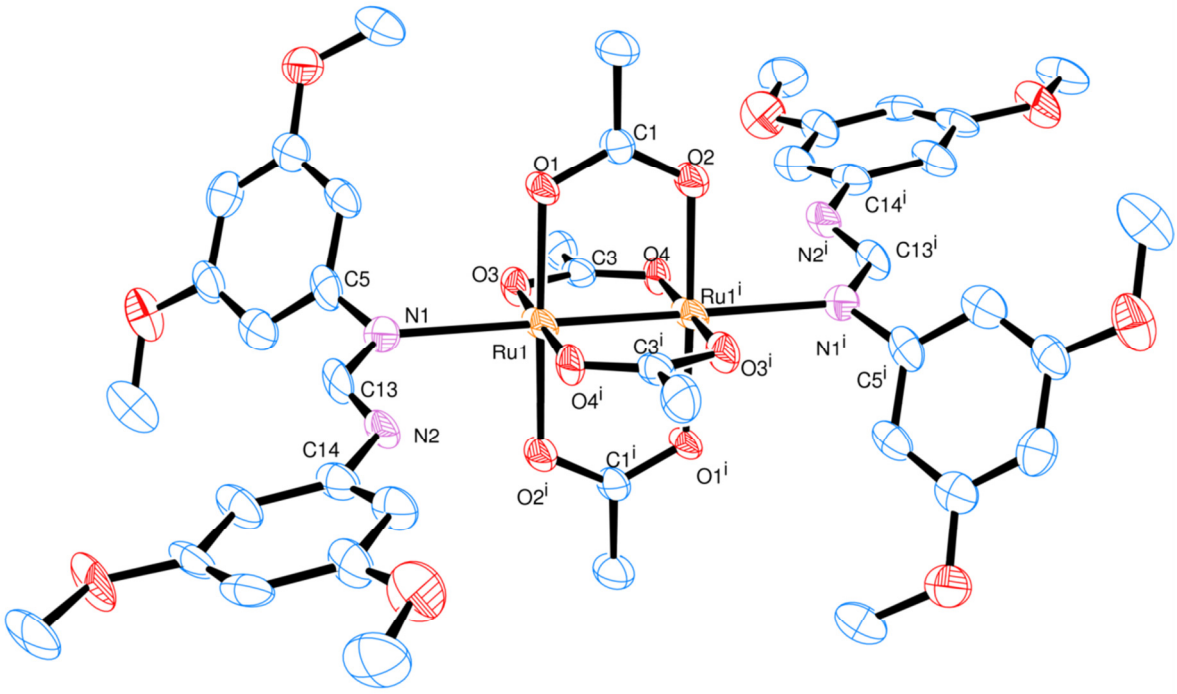

Figure 3.3.18 - Crystal structure of intermediate $Ru_2^{II,II}(OAc)_4(H[DMOPhFm])_2$ (XV). Hydrogens are omitted for clarity and thermal ellipsoids are drawn at the 50% probability level.

Bond ID	Bond length /Å
Ru-Ru	2.289(1)
Ru1-O1	2.085(6)
Ru1-O2	2.087(6)
Ru1-O3	2.061(5)
Ru1-O4	2.080(5)
Ru1-N1	2.370(7)
N1-C13	1.31(1)
N2-C13	1.32(1)

Bond ID	Bond length /Å
O1-C1	1.26(1)
O2-C1	1.27(1)
O3-C3	1.27(1)
O4-C3	1.27(1)
Ru-O (Average)	1.27

Torsion	Angle /°
O1-Ru-Ru'-O2	0.0(2)
O3-Ru-Ru'-O4	0.7(2)

Table 3.3.9 - - Selected bond lengths and torsions of $Ru_2^{II,II}(OAc)_4(H[DMOPhFm])_2$ (XV).

Crystals of ***XV*** were obtained adventitiously whilst attempting to elucidate the structure of an unknown purple by-product as isolated from the synthesis of ***X*** conducted in THF. This alternative method is detailed in the experimental, but proved less robust than the reported procedure using toluene as the reaction solvent. Crystals suitable for X-Ray diffraction were

grown by layering the filtrate from completed reactions, from which ***X*** could be successfully isolated, with *n*-pentane and storage at -18 °C for 1 week.

It is critical to note that this species is chemically distinct from the purple oxidative products that were generated reversibly during oxidative studies. Unlike these oxidative products that will be discussed further in a subsequent section (Section 3.3.8) this purple product was stable for prolonged periods provided an inert atmosphere was rigorously maintained.

The Ru-Ru bond length observed for ***XV*** of 2.289 Å is typical for Ru_2^{4+} tetracarboxylate complexes, which have reported with bond lengths of 2.252-2.311 Å. In contrast to formamidinates these complexes typically show no significant dependence on the nature of the axial ligand and as such ***XV*** is comparable to $Ru_2^{II,II}(OAc)_4(H_2O)_2$ which has a Ru-Ru distance of 2.262(3) Å.

The structure of ***XV*** whilst of limited utility to this study provides some insight into the probable associative mechanism by which the intended tetra-kis products ***X-XIV*** are formed in THF. Following initial axial coordination of the ligands, it is proposed that the intended substitution products are obtained by concerted loss of acetate and formamidinate ligand migration.

The equivalence of the N1-C13 and N2-C13 bonds in the –N–C–N– amidinate backbone suggests that the formamidinate is delocalised but still present in its protonated H[amidinate] form. Further, the observed N1-Ru1 bond length is still relatively long at 2.370(7) Å compared to that seen in ***X*** at an average of 2.06 Å.

Complete cif tables for ***XIII-b*** are provided in appendix B-6

3.3.6.3 Electrochemistry

The CV spectra of $Ru_2^{II,II}$(formamidinate)$_4$ complexes has only featured twice in the literature to date as despite the small handful of these complexes that have been reported many were themselves generated by bulk electrolysis of other related species.

In the initial publication of its synthesis by Cotton $Ru_2^{II,II}(DFM)_4$ was found to display two redox processes at 0.713 and -0.568 V (versus Fc/Fc+), which were assigned as the $Ru_2^{4+/5+}$ oxidation and $Ru_2^{3+/4+}$ reduction, respectively. In both this initial publication and a related report concerning an axial CO adduct published by Kadish[136] these CV spectra are assigned by reference to a better studied triazenate complex, $Ru_2^{(II,II)}(PhNNNPh)_4$. It was a stated assumption that these were expected to be approximately equivalent for the purpose of the analysis conducted.[122,136,139] However, Cotton also noted in his initial report that this assignment failed to adequately explain the extreme air sensitivity observed for these complexes,[139] and later recognised the proposed equivalence to triazenates to be flawed assumption.[122] Despite this however, no alternative analysis or subsequent assignment was presented.

The cyclic voltammogram recorded for ***$Ru_2^{II,II}$(DMOPhFm)$_4$ (X)*** and ***$Ru_2^{II,II}$(4FPhFm)$_4$ (XI)*** (offset above) in dichloromethane containing a 0.1M solution of $^nBu_4NPF_6$ are shown overleaf in Figure 3.3.21. For ***X*** two reversible redox processes are observed at -0.584 V and 0.643 V. Based upon the results of the UV–Vis spectroelectrochemical study, vide infra, we assign both of these observed processes as consecutive oxidations corresponding to the $Ru_2^{4+/5+}$ and $Ru_2^{5+/6+}$ redox couples, rather than an oxidation and reduction.

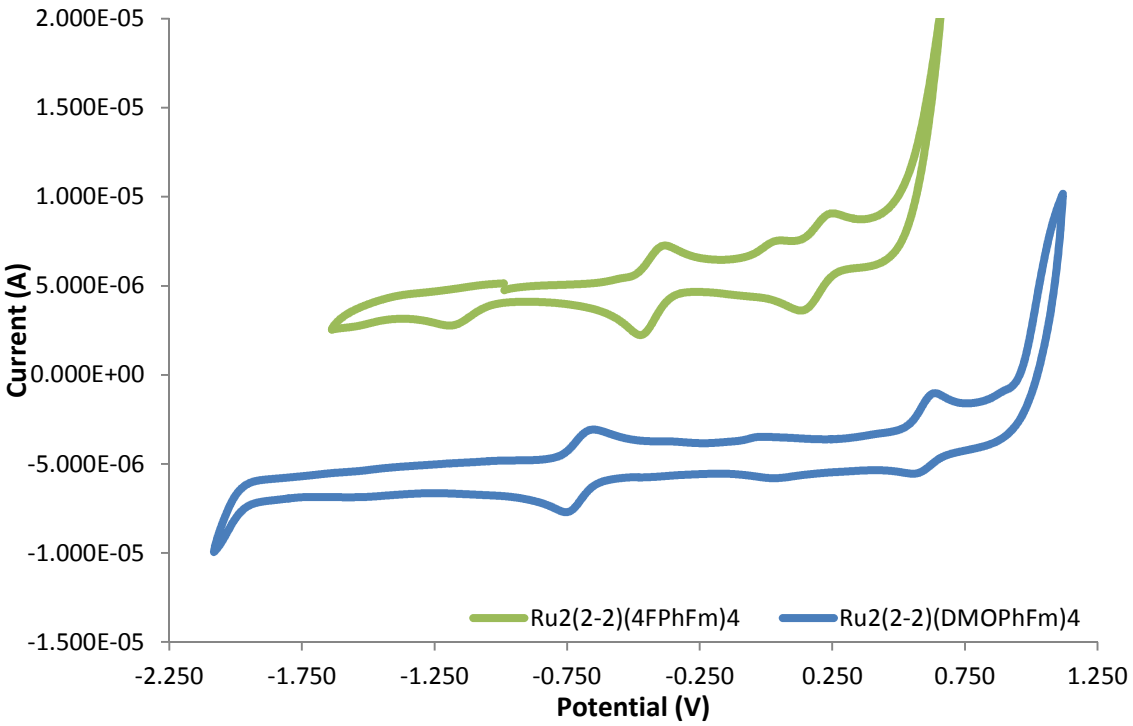

Figure 3.3.19 - Cyclic voltammogram of $Ru_2^{(II,II)}(DMOPhFm)_4$ (X) and $Ru_2^{(II,II)}(4FPhFm)_4$ (XI) recorded in in a 0.1M solution of $^nBu_4NPF_6$ in DCM, with a scan rate 100 mv s^{-1}. (Traces are offset by 5x10-6 Amps above/below zero on the Y-axis to aid readability.)

In each instance, two separate $1e^-$ redox couples are observed, which were then internally refererenced to the Fc/Fc^+ couple and are sumerised in below (Table 3.3.15).

Oxidative couple	2-2 to 2-3				2-3 to 3-3			
	E_{pc} (V)	E_{pa} (V)	$E_{1/2}$ (V)	ΔE_P	E_{pc} (V)	E_{pa} (V)	$E_{1/2}$ (V)	ΔE_P
$Ru_2^{II,II}(DMOPhFm)_4$	-0.75	-0.65	-0.70	0.11	0.55	0.64	0.60	0.09
$Ru_2^{II,II}(4FPhFm)_4$	-0.47	-0.38	-0.43	0.09	0.13	0.25	0.19	0.12

Table 3.3.10 - Electrochemical data for $Ru_2^{II,II}(DMOPhFm)_4$ (X) and $Ru_2^{II,II}(4FPhFm)_4$ (XI)

Whilst we report the CV data for **(X-XI)** it is noteworthy that attempts to obtain satisfactory data for the related tris-substituted product **(XIII-XIV)** despite repeated attempts were unsuccessful. This was in due in part to the very low current response obtained in the solvents tested (DCM,THF, MeCN, MeOH) which is itself a reflection of the very low solubility of these more bulky complexes.

In addition to the two observed redox couples observed in **(X-XI)**, a small unknown current response was noted at ca. 0.05 V in **(X-XI)**, which is most evident in **(X)**. It was initially thought that this was due to the inclusion of residual ferrocene but was found to persist despite thorough washing, over multiple samples, differing batches and even with a

completely new set of electrodes. A similar peak is visible, but not reported or otherwise assigned in the CV of $Ru_2^{II,II}(DFM)_4$ reported by Cotton.[139] The identity of this is not immediately clear but appears to be largely non-variant between the 3 complexes despite other processes showing significant variance. It is postulated that this may represent the formation and disassociation of an axial adduct of the (II,III) species observed in this region of the CV as this behaviour has been previously noted for such species.[103]

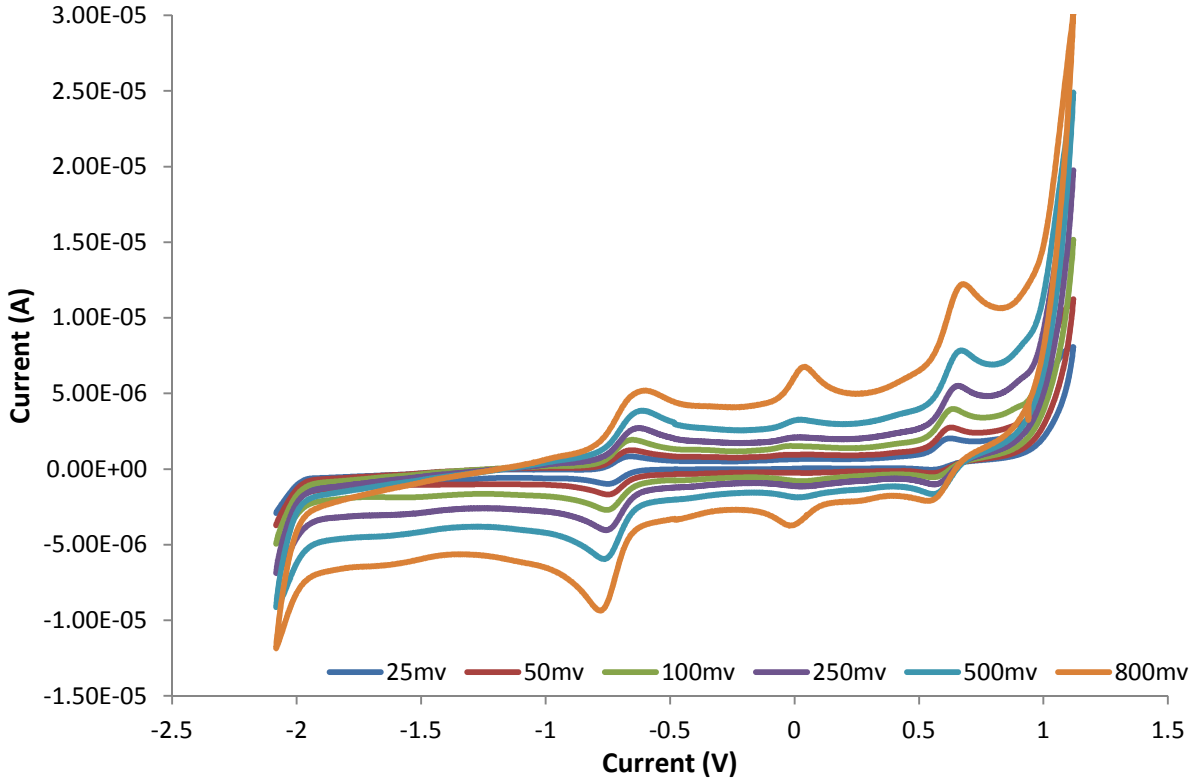

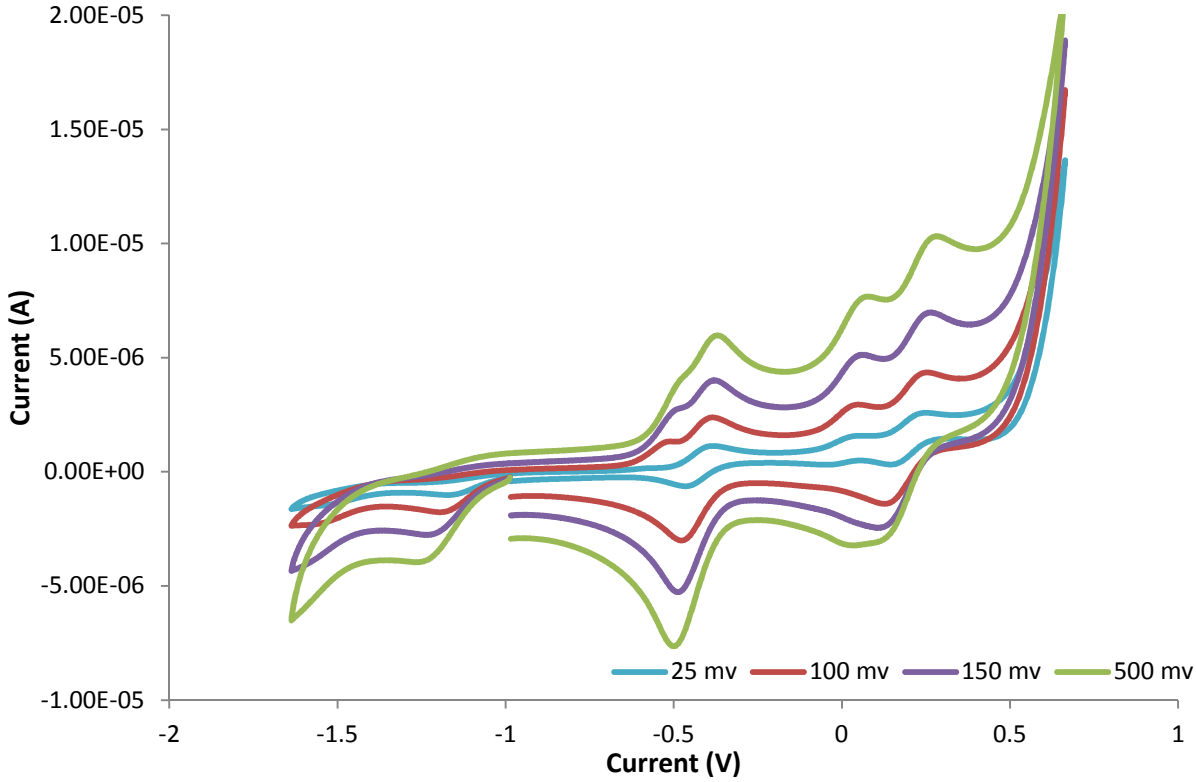

Figure 3.3.20 - Effect of variable scan rate in CV of (top) $Ru_2^{II,II}(DMOPhFm)_4$ and (bottom) $Ru_2^{II,II}(4FPhFm)_4$.

3.3.6.4 Reversibility of observed redox processes

The CV of both **(XI)** proceeds from the left and may be readily oxidised from (II,II) to (II,III) at $E_{1/2}$ = -0.70 V **(X)** and -0.43 V **(XI)** respectively, with a corresponding colour change, in both instances, from a deep red to a dark purple. The redox wave associated with the process shows a high degree of both chemical and electrochemical reversibility as shown by the small observable deviation in ΔE_P with increasing scan rate (Figure 3.3.22). In **(X)** there is also some indication of potential absorption of the (II,II) species onto the electrode surface resulting in the introduction of the hump observed on the upper oxidative half-wave..

That this redox couple appears to represent the (II,II) to (II,III) oxidation cf. the previous reported reduction has important implications, most notably in potential interactions with dioxygen. It has been repeatedly[103,122,136,139] noted that these species are extremely sensitive towards dioxygen and the potential of this oxidative redox couple could potentially explain this behaviour as it is more than sufficient to reduce O_2. The nature of this interaction will be considered in greater detail in a subsequent chapter.

The second oxidative redox process observed in the CV of **(X-XI)** representing the (II,III) to (III,III) couple also appears to demonstrate a significant degree of electrochemical reversibility; however in the case of **(X)** this does not appear to be as chemically reversible as observed in **(XI)**. In **(XI)** there is what appears to be a second oxidative wave just preceding this second redox process; as described above however this is most likely derived from the unknown process at 0.05 V overlapping cf. a probable indication of absorptive behaviour at the electrode surface. This distinction is however not one that can be made empirically based on the spectra of **(XI)** in isolation.

On comparison of **(X)** and **(XI)** it is clear that the general reported trend[103,228] for the functionalization of formamidinate, in affording chemical tunability to a dimetal core also extends to Ru_2 (II,II) as well. Variation from *m*-OMe to *p*-F affords a 200 and 300 mv variation in the observed $E_{½}$ values of the (II,II) to (II,III) and (II,III) to (III,III) respectively. That such variation in ligand electron donor/acceptor behaviour facilitates such behaviour in these species, whilst not-unexpected had until now yet to be proven.

3.3.6.5 UV-Vis-NIR spectroscopy

3.3.6.6 Initial UV-Vis-NIR studies

The UV-vis-NIR spectrum of the isolated compounds **X, XI** and **XIII,** was recorded in DCM under protective atmosphere of argon and corrected for molar absorptivity to generate the comparative plot shown in Figure 3.3.23; peak data and relative assignments are provided in table 3.3.16

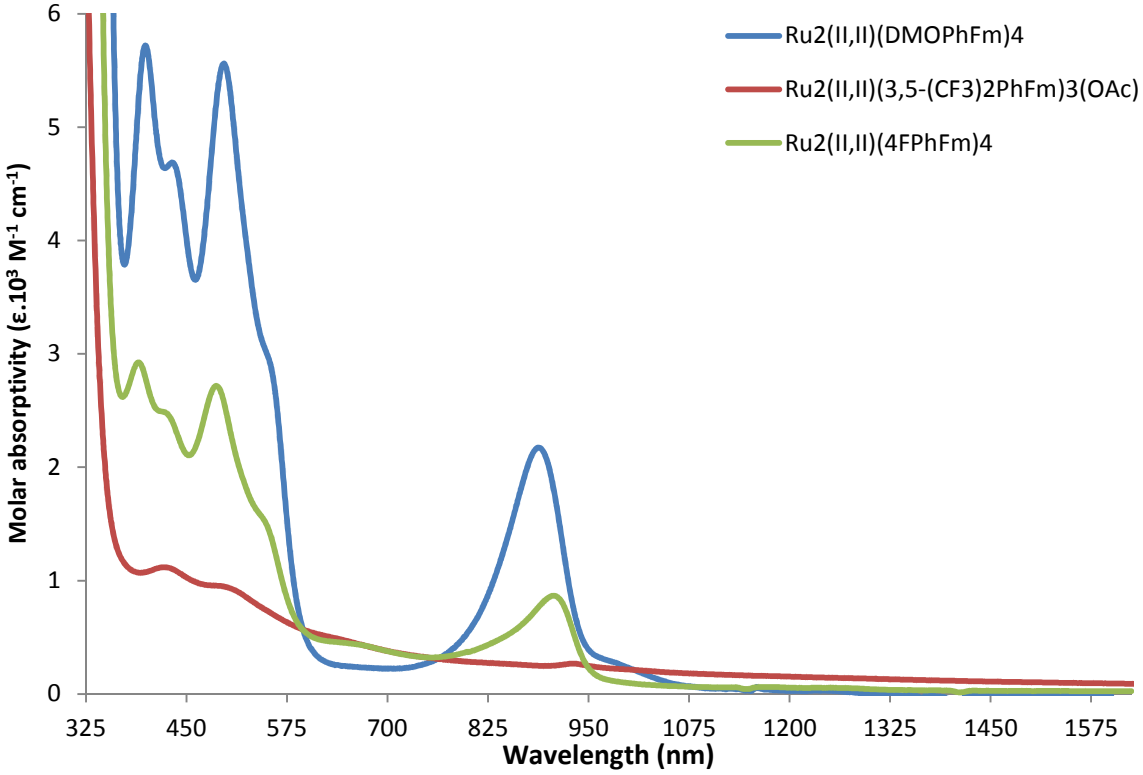

Figure 3.3.21 - Relative intensity of observed electronic transitions of compounds (X, XI, XIII), corrected for molar absorptivity

With the aid of TD-DFT calculations for the model complex $Ru_2(dmf)_4$, the results of which are summarised in Table 3.3.2 of the DFT section it is possible to make tentative assignment of the nature of the transitions observed as is shown for **(X)** in Figure 3.3.24 overleaf. Such assignments do however make the assumption that trends observed in the solid state persistent in solution.

Complex	Peak wavelength (λ)	molar absorptivity ε·103(m-1 cm-1)
$Ru_2^{(II,II)}(DMOPhFm)_4$	399	5720
	432	4688
	497	5560
	548	3039
	888	2174
$Ru_2^{(II,II)}(4FPhFm)_4$	390	2925
	420	2460
	487	2718
	545	1551
	907	868
$Ru_2^{(II,II)}(3,5\text{-}(CF_3)_2PhFm)_3(OAc)$	423	1118
	490	953
	650	468
	929	269

Table 3.3.11 - UV-Vis-NIR peak data for compounds (1-3)

$Ru_2(DMOPhFm)_4$ (1)

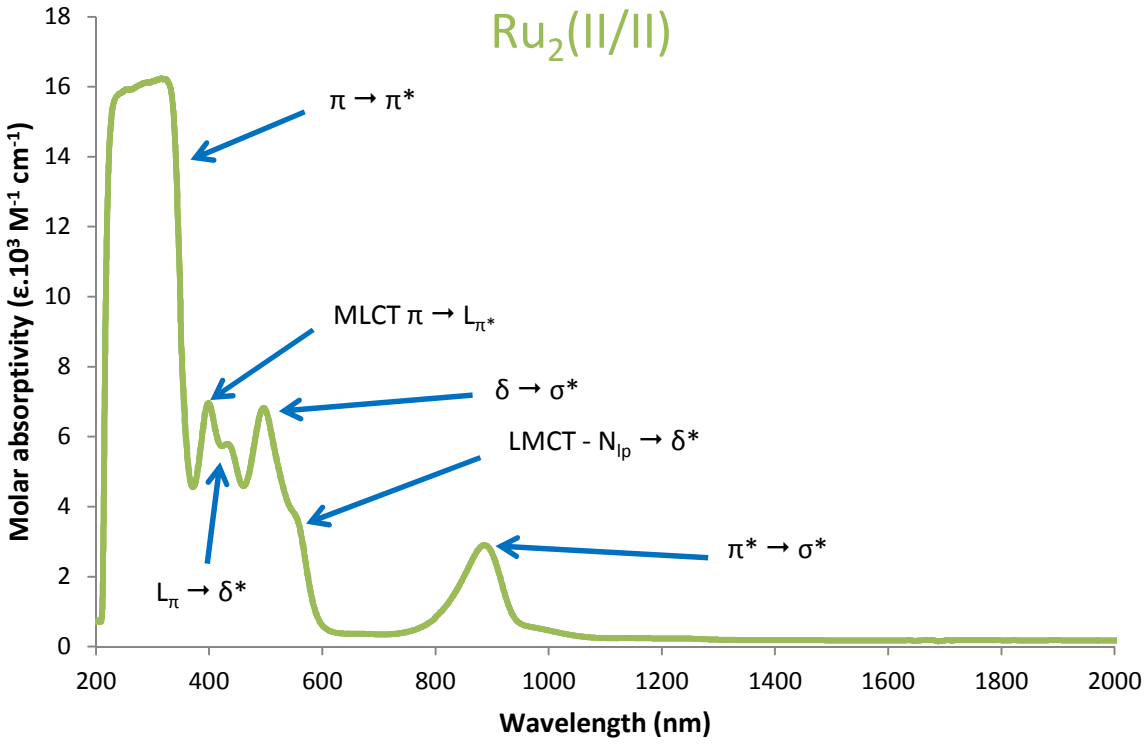

Figure 3.3.22 - Assignment of observed electronic transitions by comparison to TD-DFT derived predictions

$[Ru_2^{(II,II)}(PhNCHNPh)_4]^0$

Wavelength (nm)	Oscillator strength (f)	Assignment	Description
789	0.0035	π* → σ*	M_2 π* to σ* (HOMO/HOMO-1) to (LUMO +1)
663	0.0347	LMCT Lπ → δ*	Ligand π to M_2 δ* (HOMO-3/HOMO-4) to (LUMO)
571	0.0055	δ → δ*	M_2 δ to δ* (HOMO-2) to (LUMO)
455	0.098	π → δ*	M_2 π to δ*(HOMO-7/HOMO-8) to (LUMO)
431	0.0049	LMCT Lπ → σ*	Ligand π to M_2 σ* (HOMO-3/HOMO-4) to (LUMO+1)
394	0.0051	LMCT Lπ → σ*	Ligand π to M_2 σ* (HOMO-5) to (LUMO+1)
388	0.0041	MLCT π* → Lπ*	M_2 π* to Ligand π* (HOMO/HOMO-1) to (LUMO+3)
365	0.0033	LMCT Lπ → δ*	Ligand π to M_2 σ* (HOMO-10/HOMO-11) to (LUMO)
338	0.0405	LMCT Lπ → δ*	Ligand π to M_2 σ* (HOMO-13) to (LUMO)
332	0.0025	π → δ*	M_2 π to δ*(HOMO-7/HOMO-8) to (LUMO)

Table 3.3.12 - - Calculated electronic transitions for $[Ru_2(PhNC(H)NPh)_4]^0$ (where oscillator strength, f > 0.0025)

As can be seen from comparison of tables 2.3.4 and 2.3.5, not all predicted transitions are observed and some, most notable the predicted transition at 789 nm, show strong variation due to ligand induced electronic effects. Despite these variations it can be seen that the model complex $[Ru_2^{(II,II)}(PhNCHNPh)_4]^0$ provides a good approximation to what is experimentally observed.

Of the transitions observed that which gives the compound its characteristic brick red colour observed at 885.5 nm represents is, as one might expect that from the HOMO -> LUMO (π* -> δ. At higher energy and just below the solvent window at 394.9nm can be seen the MCLT from the metal π -> L_{π^*} to one of the many ligand π* combinations whilst a LMCT from a MO largely nitrogen lone pair in character back to the metal delta star can be seen as a shoulder at 553.3nm (N_{lp} -> δ*). The most dominant of the remaining two transitions observed, just greater in oscillator strength than the MLCT, is that of the delta to sigma star (δ -> σ*). The last observed transition involves another LMCT originating from a ligand π character MO back to the δ*.

3.3.6.7 Spectroelectrochemistry

Spectroelectrochemistry is the practise of combining the powerful techniques of cyclic voltammetry and UV-Vis-NIR spectroscopy allowing the probing of electrochemically generated species.

As the UV-Vis-NIR spectra of **(X)** is known, collection of UV-Vis-NIR spectra in the three regions defined by the two redox couples observed for **(X)** in its corresponding CV (Figure 2.3.16), the facile identification of the potential range in which the neutral complex exists may be achieved. In this instance the unperturbed (II,II) UV-Vis-NIR spectra is observed in for hold potentials below the -0.7 v redox couple strongly indicating that this does in fact represent an oxidation cf. the previous assignment provided by Cotton.[122,139]

Once the initial spectra observed in the absence of a applied potential has been established the applied potential is then swept beyond the first redox couple and the observed changes recorded by sequence of recorded spectra (Figure 2.3.20).

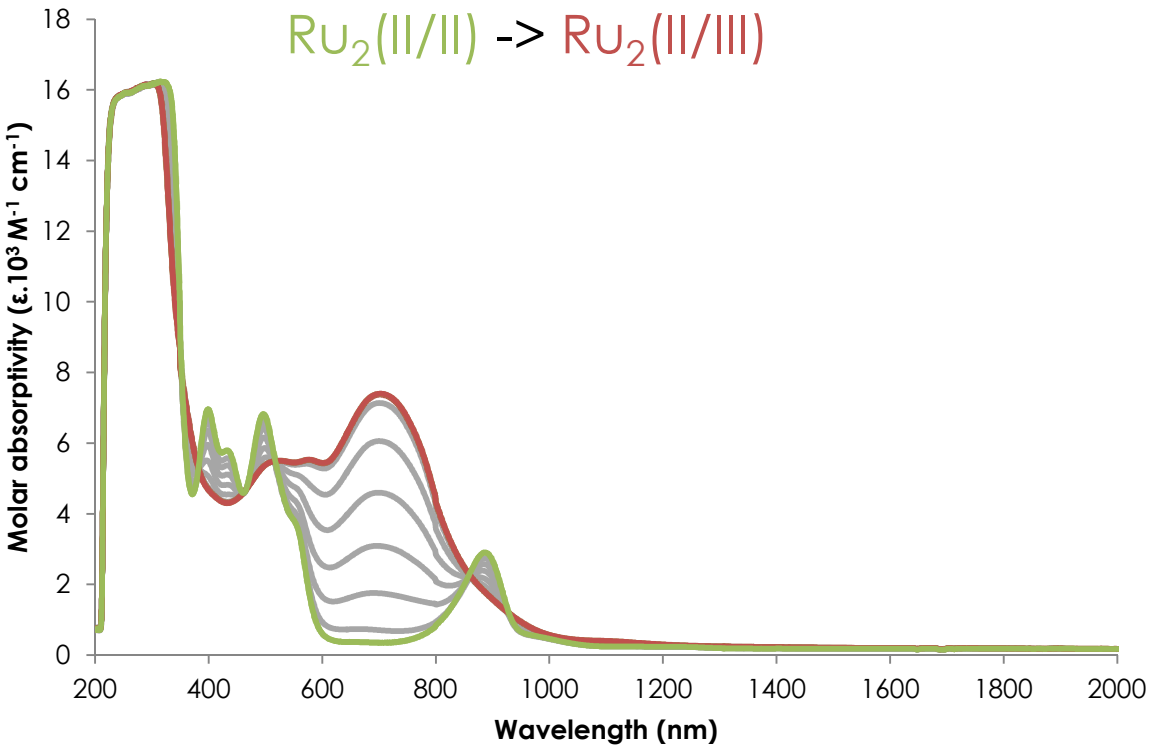

Figure 3.3.23 - Observed changes afforded to the UV-Vis-NIR spectra of (1) on modification of the applied potential from -0.8 v to -0.6v corresponding to the previously assigned (II,II) to (II,III) redox couple

As can be seen from Figure 2.3.20, the transition from Ru_2 (II,II) to (II,III) is accompanied by the loss of the fine structure previously observed between 350-520 nm and the transition 888 nm, replaced by a plateau from 516 -620 nm and a new transition growing in at 701 nm with comparable molar absorptivity of 7400 M^{-1} cm^{-1}.

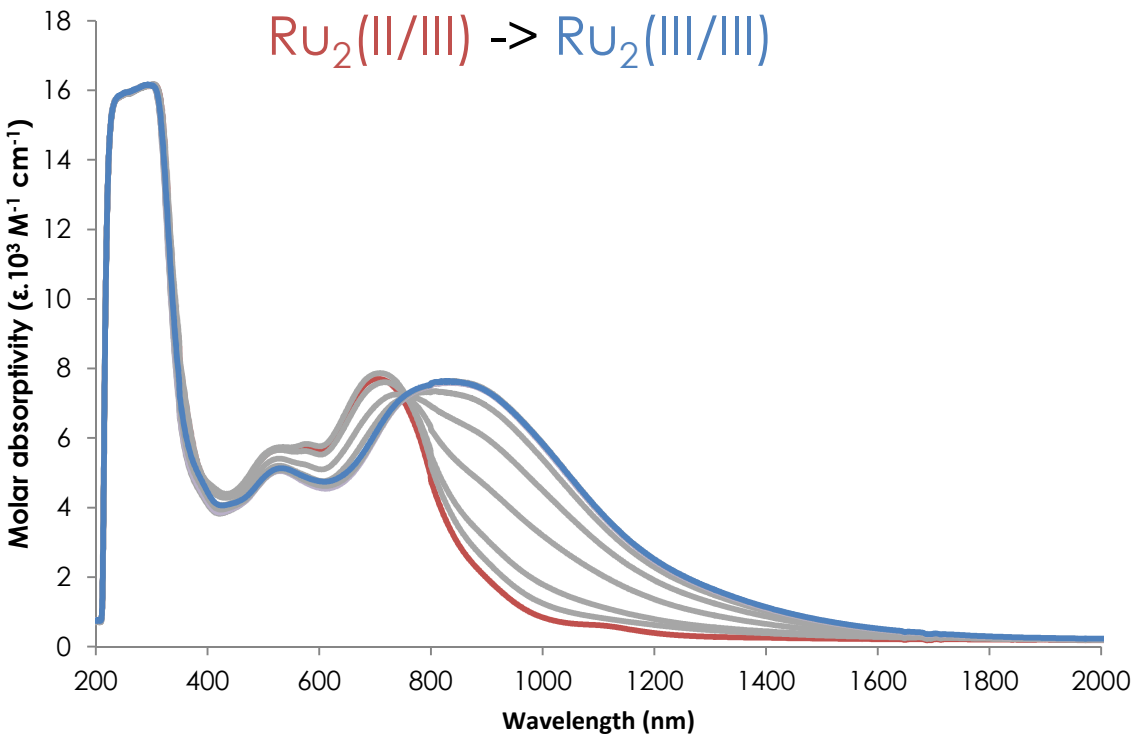

Figure 3.3.24 - Observed changes afforded to the UV-Vis-NIR spectra of (1) on modification of the applied potential from 0.4 v to 0.8v corresponding to the previously assigned (II,III) to (III,III) redox couple

As seen, the species present at -0.6 v now undergoes a second transformation with the UV spectra reflecting this in a loss of the previous plateau in the 500-600 nm region to reveal a peak at 535 nm (5016 M^{-1} cm^{-1}) and a second, more broad transition growing in at 853 nm (7571 M^{-1} cm^{-1}).

The progressive conversion of the electrochemically generated species shown in Figures 2.3.20-21 are however, as reflected by the redox wave shape in the electrochemistry highly reversible allowing the regeneration of the original (II,II) species by re-application of a suitable (-0.8 V) potential with no observable degradation loss or bleaching as is shown in Figure 2.3.22 below.

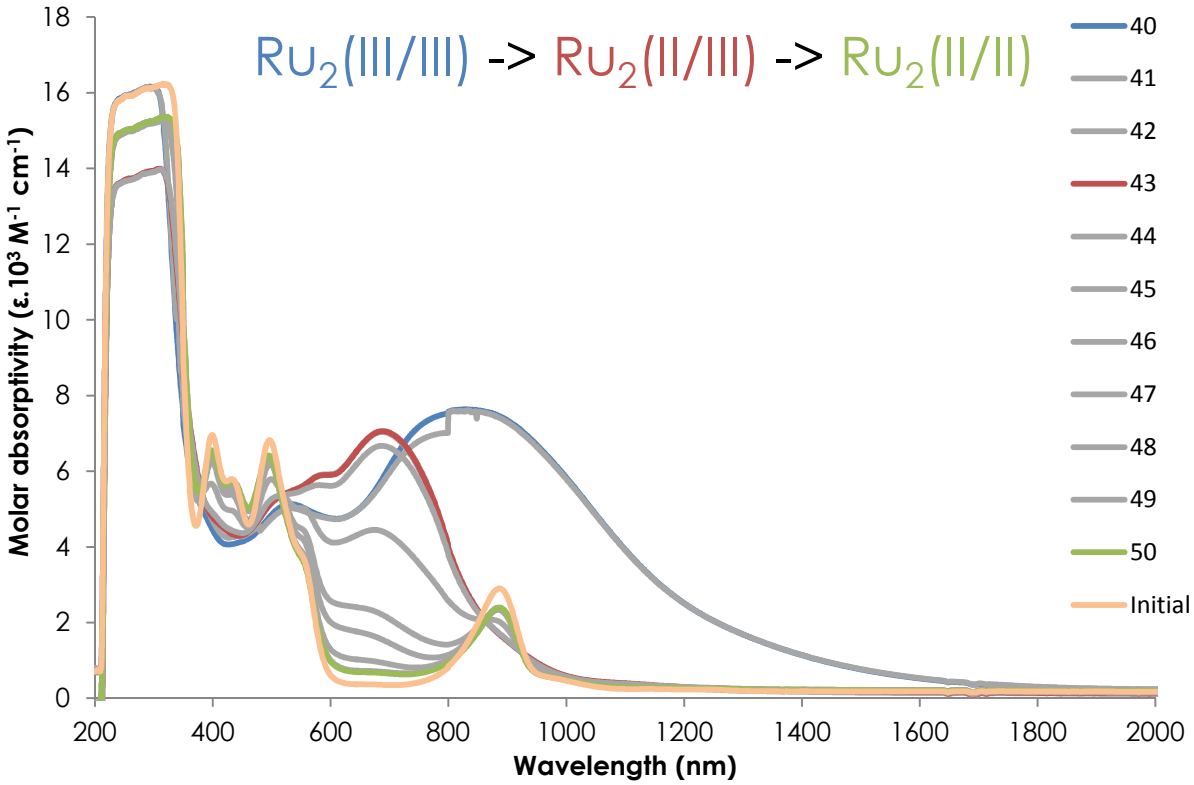

Figure 3.3.25 - UV-Vis-NIR spectra of reverse process, affording the regeneration of Ru2 (II,II)

3.3.7 Aerobic oxidation studies

3.3.7.1 Initial catalyst screening

In light of the successful aerobic oxidation studies conducted by Jasra[327] and Naota[328] utilising diruthenium tetraacetates to conduct simple alcohol oxidation, the conditions used were replicated of the study of the oxidative behaviour of ***X*** an ***IX***.

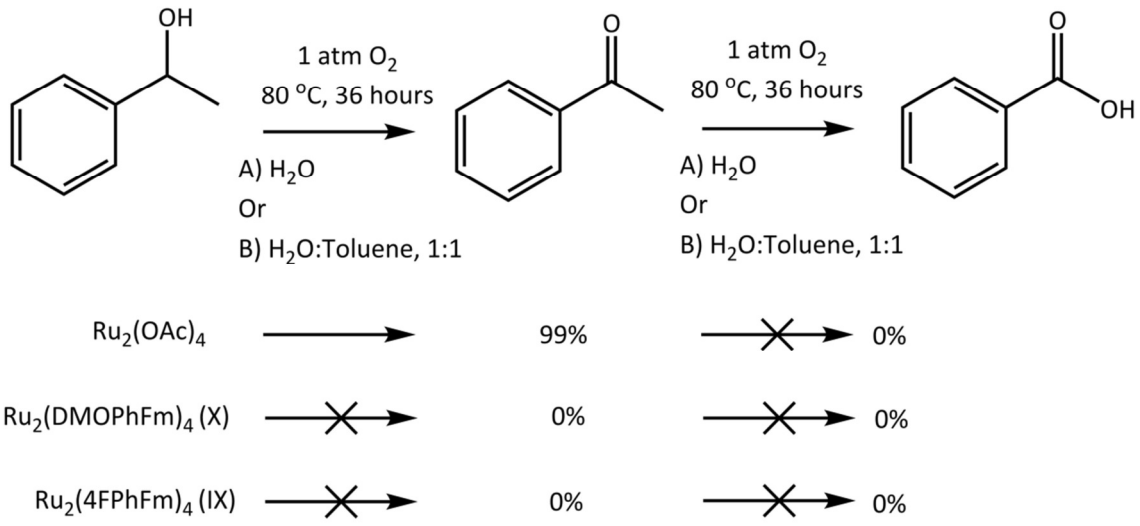

Figure 3.3.26 - Catalysis screening with benzyl alcohol under the conditions reported by Naota et al. percentages shown indicate degree of conversion after the alloted time.

All catalytic activity reactions were assessed via two methods, ^{1}H NMR and GC-MS. GC-MS allowed the following of reaction progress and an approximation of analyte concentration by calibration of the TIC readout count associated with a target eluent verses a set of pre-made internal standards. These standards contained pre-set concentration ratios of products from 0-100% of the concentrations used in the catalyst tests. On completion of the reaction a sample was taken for ^{1}H NMR to determine if any observable change had occurred. Control reactions were additionally run at ambient temperature to validate the need for thermal input.

Initial tests conducted using benzyl alcohol (Figure 3.3.28) showed zero measurable conversion after 36 hours under the conditions used by both GC-MS and ^{1}H NMR. This indicated that despite the rapid colour change on exposure of ***X*** or ***XI*** to molecular oxygen that the generated species is not active towards the oxidation of the target substrate. In

addition to the reported conditions a range of other solvent systems were also tested in order to rule out the impact of particular solvent and donor/non-donor solvent effects:

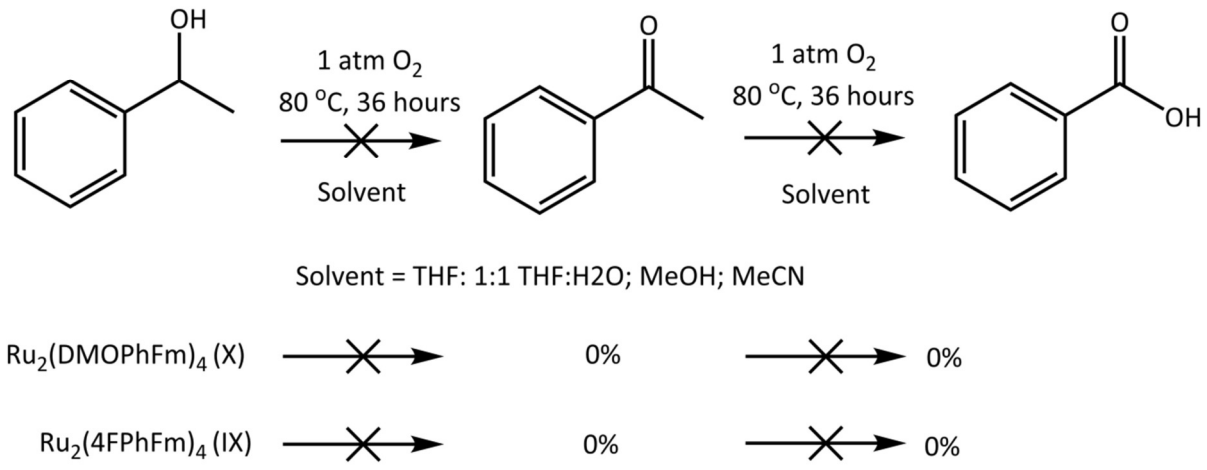

Figure 3.3.27 - Degree of substrate conversion after 36 hours at 80 °C with X or XI and a range of different solvents as indicated.

All of the other tested solvents showed the same behaviour as that observed for the initial solvent systems with the exceptions of MeOH and MeCN. Methanol causes the accelerated decomposition of the catalyst in < 1hour whilst MeCN solutions displayed the opposite effect and retained the deep purple colour of the exposed solution for considerably longer often up to 24 hours. In light of this considerable effort was taken to utilise this to obtain crystals of the species generated but such efforts we unsuccessful. It is not known why or how MeCN partially stabilises this meta-stable species.

With attempts to replicated the conditions previously reported a range of alternative readily oxidised substrates were tested including 9,10-dihydroanthracene and cyclohexene. Duplication of the above described test screening was similarly unsuccessful at obtaining measurable conversion to either partially oxidised products. In all instance the target substrate was retained and unmodified.

3.3.7.2 Use of oxo-transfer and peroxo-reagents

As the nature of the interaction between O2 and ***X*** or ***XI*** was not well understood a series of tests were conducted to assess the impact of other co- oxidants on the catalyst-substrate mixtures. Reports from the Ren group for related diruthenium (II,III) tetraamidinates in combination with such reagents as tert-Butyl hydroperoxide have been reported to useful

catalytic behaviour towards biologically important substrates such as organic sulphides.[129,326]

	X	XI
mCPBA	Immediate decomposition	
PhIO		
H_2O_2		
TBHP		

Table 3.3.13 - Table of interaction results between Ru2(formamidinate)4 and oxidatant

As can be seen from Table 3.3.17 exposure of ***X*** or ***XI*** to common oxidants like hydrogen peroxide and tert-butyl hydrogen peroxide (TBHP) and other nucleophilic oxidants like meta-chlorobenzoic acid and Iodosylbenzene results in immediate decomposition to a black intractable mixture of low mass products.

3.3.8 Reversible interaction with dioxygen

3.3.8.1 UV-Vis-NIR spectra of dioxygen exposed $Ru_2(DMOPhFm)_4$

The UV-Vis-NIR spectra of $Ru_2(DMOPhFm)_4$ was recorded in DCM and the effects bubbling both inert and reactive gasses though the sample cuvette on the resultant UV-Vis spectra was probed.

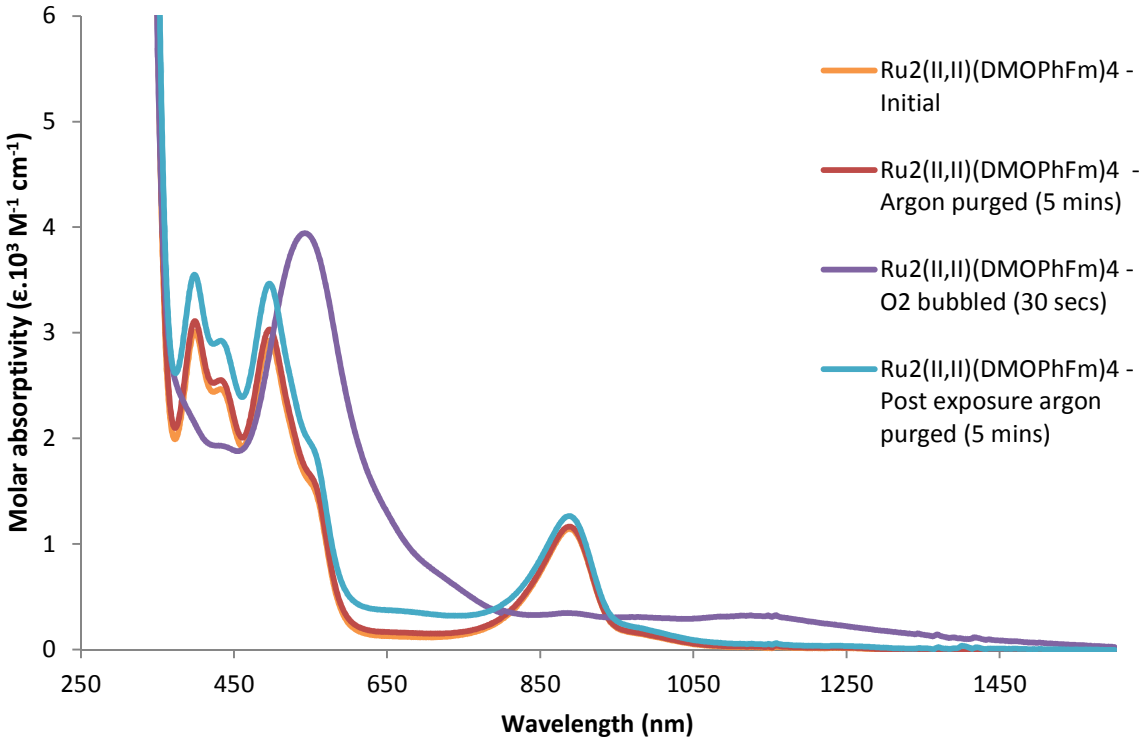

Figure 3.3.28 - UV-Vis-NIR spectra of O_2 exposure experiment with Ru2(DMOPhFm)4. Identity of traces provided is indicated in the legend.

As can be seen in Figure 3.3.30 aboveon exposure to oxygen exposure the UV spectrum obtained bears similarities to that obtained for the Ru_2 (II,III) analogue generated in the spectroelectrochemical conducted in Section 3.3.6.4. This Ru (II,II) to (II,III) transition was observed to result in the loss of the lower wavelength fine structure and the transition at 888 nm; whilst a new peak grew in at 701nm.

The spectrum obtained for this oxygen interaction species, whilst similar that of the Ru_2 (II,III), it remains notably different in several key respects indicating in originates from a different species. Whilst it shares the loss of lower wavelength fine structure in the 390-510

nm region and the single higher wavelength peak (888 nm), the new observed transition that grows in occurs at the significantly shorter wavelength of 542 nm compared to 724 nm for the generated Ru_2 (II,III) species. This is more readily apparent when the two spectra are over-laid as shown below in Figure 3.3.31.

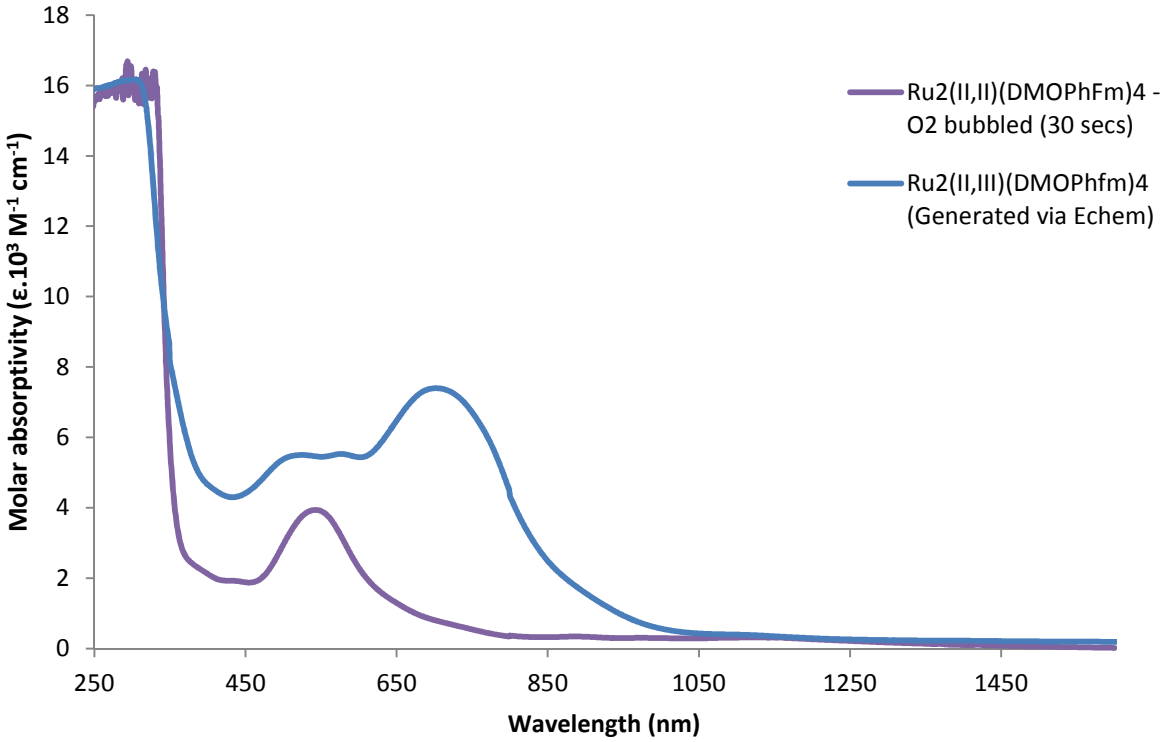

Figure 3.3.29 – Comparison of UV-Vis-NIR spectra of O2 exposure product of $Ru_2^{(II,II)}(DMOPhFm)_4$ and the Ru_2(II,III) species of the same complex previously generated via electrochemistry.

That these two species differ significantly implies that the product of exposure of $Ru_2^{(II,II)}(DMOPhFm)_4$ to air cannot merely be the discreet $Ru_2^{(II,III)}$ analogue. Instead it suggests that that observed is distinct and is representative of a new species entirely.

The literature contains numerous examples of the effects of axial ligation on the properties of diruthenium complexes,[103,147,148,152,228,234–238,377–379] more than sufficient for a sizable Chem. Rev. article, however several publications are of particular note to the present problem. These include the effects of replacement of the axial halides in Ru_2 (II,III) complexes with phenylacetylides and exploiting of their strong π-acceptor ability. to facilitate the generation of stabilised Ru_2 (III,III) species. In this way the axial ligand may be used to stabilise chemical transformations that might otherwise lead to immediate decomposition. In the instance of synthetic routes to Ru_2 (III,III) species this often via

proceeds via deliberate aerobic oxidation.[236] In this way what would otherwise be a decomposition process may be turned into a useful synthetic tool and further highlights the criticality of understanding how axial ligand interactions affect the chemistry of the dimetal core.

The deliberate aerobic oxidation of some related Ru_2 (II,III) formamidinates using suitably designed axial ligands, [235,236,378]and in complexes incorporating related non-formamidine NCN donor ligands provides a suitable proof of concept for the utility of this methodology.[379] From consideration of the UV-Vis-NIR spectrum in isolation it is impossible to draw any immediate conclusions, however it is apparent from the electrochemistry that the impact of oxygen exposure is a weak interaction rather than representative of a chemical redox process or wider change[235,236,380] (See Section3.3.8.2).

Whilst the examples of Ru_2 (III,III) species are relatively rare outside of those supported by conjugated aromatic π-systems, recent reports from the group of Berry and separately by Ren infer the possibility of a simpler (II,III)-oxo adduct may not be an unreasonable theory. In his recent report regarding the use of $Ru_2^{(II,III)}(OAc)_4$ as a sulphide oxidation catalyst, in conjunction with TBHP, Ren invokes a proposed an axial M-M-peroxo adduct as the active species. Similarly, recent work in the Berry group regarding axial nitrides has ably demonstrated the significant impact such M-L interactions can have on the properties and reactivity of diruthenium formamidinates specifically.[322–324,381]

3.3.8.2 Electrochemistry of dioxygen exposed $Ru_2(DMOPhFm)_4$

As with the UV-Vis-NIR exposure study, the electrochemistry of $Ru_2(DMOPhFm)_4$ was first replicated as conducted in chapter two, followed by the examination of the oxygen exposure generated species followed by the attempted regeneration of the parent (II,II) complex (Figure 5.3.3).

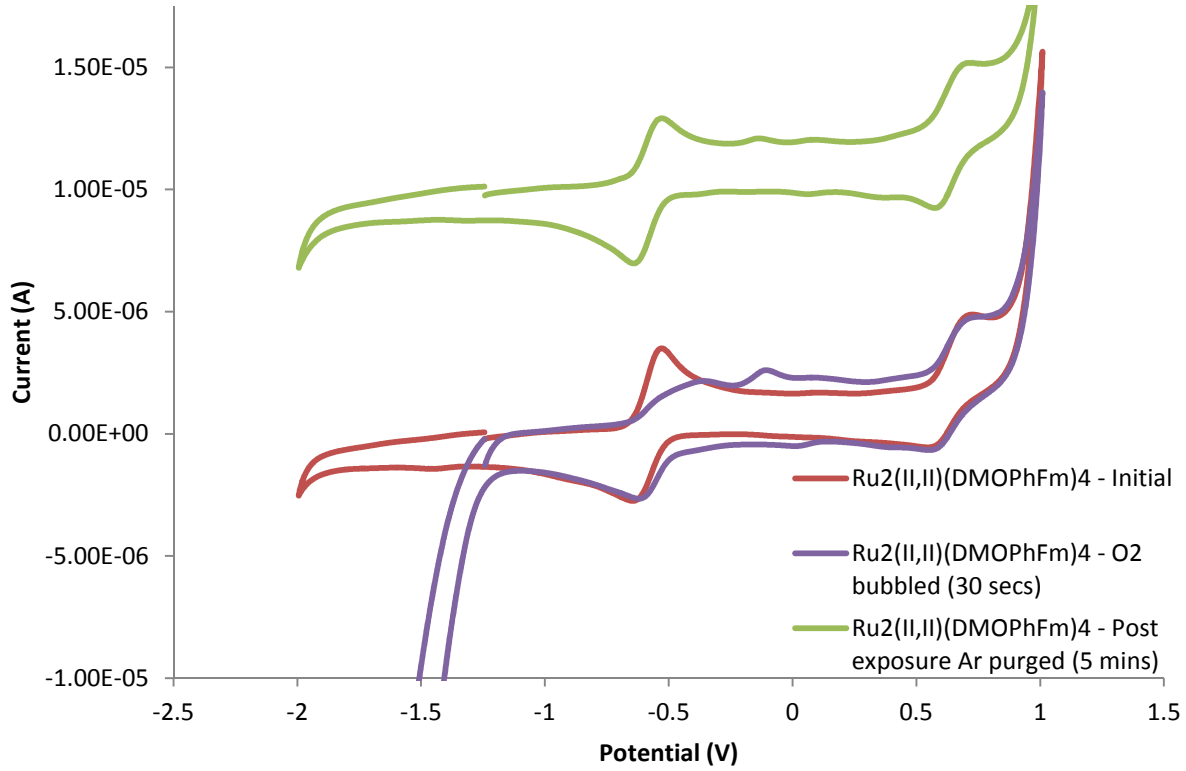

Figure 3.3.30 - Cyclic voltammogram of Ru2(II,II)(DMOPhFm)4 and Ru2(II,II)(4FPhFm)4 recorded in in a 0.1M solution of nBu4NPF6 in DCM, with a scan rate 100 mv s-1. (Trace of regeneration product offset by 1x10-5 Amps above zero on the Y-axis for ease of readability.

The important thing to grasp from figure 3.3.32 is that all the obtained voltammograms contain the same fundamental redox processes. The potentials and which all but one of these processes occur remains unchanged despite exposure of the solution to dioxygen. What is observed to change between the red, initial CV and that post exposure, shown in purple is that the oxidative half of the first redox wave is retarded by almost half a volt! The corresponding reduction half-wave remains unchanged, indicating that the electronic structure has not fundamentally changed as might be expected if oxygen exposure had oxidised the complex. Instead what is seen is that oxygen exposure serves to stabilise the tetra-amidinate complex, significantly towards further oxidation to the II,III state. What makes this particularly interesting is that this occurs in the absence of evidence of irreversible change. On re-purging of the solution with inert gas, the green CV trace is obtained showing that the original species ***X*** has been re-generated with minimal losses

It is proposed that shift in the oxidative process is a reflection of the raising of the oxidation potential that might be expected if a stabilising interaction were made with dioxygen via a probable axial interaction. The transient, labile nature of this adduct would explain the

observed increase in stability towards further oxidation but similarly explain our present difficulty in obtaining a significant analytical handle on the nature of this species. If the interaction itself is weak there is no reason why it might be expect to be visible via MS, and indeed no indication of such a species has been observed. Similarly whilst attempts to observe this species via exploiting any potential magnetic properties arising from the inclusion of triplet oxygen were hoped to provide some diagnostic information, however the species was both EPR silent and showed not notable shift in any chemical shifts during repeated Evens NMR experiments.

Whilst informative as to the lack of probable chemical change, the UV-Vis-NIR and electrochemistry in isolation remain insufficient to facilitate the identification of the species generated. In an attempt to further probe the nature of this apparent oxo-adduct samples were analysed via a range of additional techniques including Evans NMR, magnetic susceptibility, EPR, and IR and .Raman.

3.3.8.3 Infrared spectroscopy

The IR spectra, as briefly noted in chapter two were not expected to offer much diagnostic information due to the dominance of the IR spectra by ligand based vibrational modes. The one asymmetric stretch that might afford some diagnostic information is that of the bridging NCN linkage. This is however rather central to then complex and surrounded on all sides with the mass of the aryl rings serving to obscure any active IR active vibrational modes such as V_{NCN} which might have been informative to a significant degree.

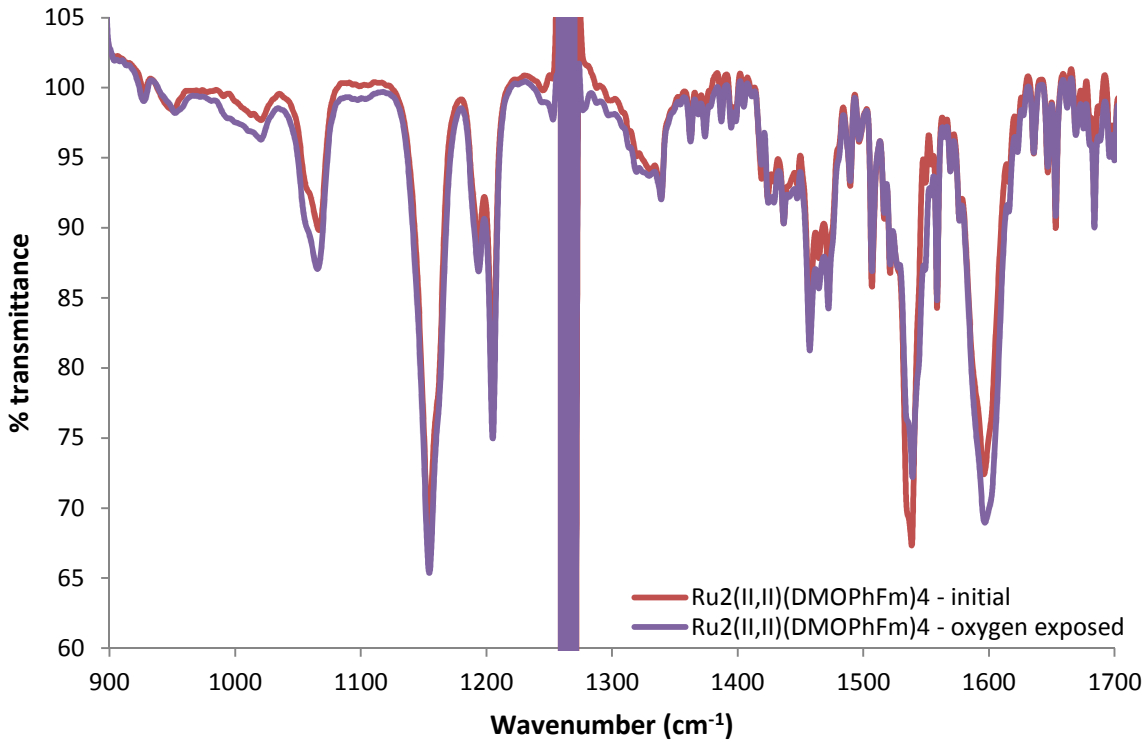

Figure 3.3.31 - IR spectrum of $Ru_2(DMOPhFm)_4$ and its oxygen exposure product collected as the thin films in DCM. Despite collection of data as a thin film cf. in bulk solution, high DCM concentration precluded the effective subtraction of solvent background in the narrow band of 1259-2171 cm^{-1}

DCM was not found to be the most well suited solvent for the collection of the IR spectra of the initial and peroxo-adduct of **(X)** due to the number of solvent associated bands this introduces to the spectra. Attempts to use other, more preferable solvents for this task such as carbon tetrachloride, or alternative methods such as Nujol mulls were frustrated by the apparent reaction of **(X)** with the former and the lesser clarity afforded with the later cf. DCM. At present we cannot explain the nature of the reactivity of **(X)** with CCL_4, but it is presumed decay occurs in a similar manor to that observed for $CHCl_3$ as previously noted by Cotton.[139]

3.3.8.4 Determination of magnetic susceptibility

The conduction of magnet susceptibility determinations was attempted via 3 established methodologies: Evans NMR,[382–385] EPR[386] and room temperature determination utilising a gouy balance.[342] Both the initial complex, and the proposed oxo-adduct were however found to show no magnetic moment or other indication of paramagnetism.

3.4 Conclusions

A range of diruthenium, tetra formamidinate complexes **(X-XIV)** have been successfully synthesised and a number of these and related species have been structurally characterised. The significant differences in the steric demands of the ligands used were observed to vastly alter the easy with which the intended tetra-kis products could be obtained and in some instances which evidence of the target species was obtained via MS, there was no practical way to extract or use some species e.g. ***XIV*** due to its incredibly low solubility.

The synthesis of these complexes was attempted via existing literature routes, which were found to be insufficient to obtain the target compounds. Consequently new synthetic routes were developed to obtain the target compounds and where possible these synthetic challenges were explained in reference to subsequent structural evidence. The attempted synthesis of XII provides a good example of this where synthetic efforts were frustrated by the bulk and electrostatic repulsion between adjacent ligands leading to the isolation of ***XIII*** as the preferred product.

Spectroelectrochemical analysis yielded an alternative assignment of the electrochemical processes in the CV of Ru_2(Formamidinate)$_4$ complexes. This suggested that in contrast to the one reductive and one oxidative redox processes that these were in fact representative of two successive oxidations. This then provides a more practical explanation of the extreme oxygen sensitivity of the species generated.

The potential for the use of X and XI as aerobic oxidation catalysts was explored extensively utilising common, readily accessible substrates such a 9,10-dihydroanthrecene and benzyl alcohols. Unfortunately the tested complexes showed absolutely no significant activity across the range of solvents, substrates and experimental conditions tested. Attempts to utilise further utilised these complexes with common oxidants such as H_2O_2 mCPBA, TBHP and PhIO in place of aerobic oxidation proved similarly unsuccessful and instead resulted in immediate decomposition of the dimetallic complex.

A DFT study of the model complexes $[Ru_2(dmf)_4]^0$, $[Ru_2(dmf)_4]^+$ and $[Ru_2(dmf)_4(OO)]$ utilising two differing hybrid functionals was conducted which demonstrated that calculations using PBE0 provides a better model of the experimentally observed structural data. The series of

DFT models was extended to include a proposed structure of an axial peroxo-adduct that might potentially present that seen experiementally on exposure of the target compounds to dioxygen. However, comparison between data obtained experimentally and that derived from this model showed that this model was not representative of the observed species. It is not immediately clear is this is a consequence of limitations of the model and the computational componentry used or a simply a consequence of this presenting a very difficult computational problem.

3.5 Experimental

For details of physical measurement procedures please refer to Section 2.5.1; for X-ray crystallographic details please refer to Section 2.5.2; for general information on the sourcing and pre-treatment of reactants and reagents please refer to Section 2.5.3 and the additional considerations outlined below:

$Ru_2(OAc)_4$,[140] was synthesised according to established literature procedures and its purity assessed via IR.[140,141]

3.5.1 Ruthenium formamidinate complexes

Synthesis of $Ru_2^{II,II}(DMOPhFm)_4$, (X)

Method A)

$Ru_2(OAc)_4$ 0.065 g (0.15 mmol), 0.195 g (0.615 mmol, 4.1 mol. equiv.) of H[DMOPhFm] and 20 ml of toluene were combined in a small, ca. 50ml Schlenk. The resultant mixture was then heated at reflux for 48 hours. Upon completion the reaction mixture was allowed to cool to room temperature, filtered through a fine Celite plug, reduced to minimum volume and the product precipitated from with hexanes as a bright, brick red solid which is then isolated by filtration. The recovered solid was then washed with 2x 5ml aliquots of *n*-pentane and dried *in vacuo*. Yield: 0.126 g, 57%

Crystals of $[Ru_2(DMOPhFm)_4 \cdot C_5H_{12}]$ obtained suitable for X-ray diffraction were grown from DCM / *n*-pentane by vapour diffusion in a freezer at -18°C over several days. MALDI-TOF-MS: calcd. monoisotopic MW for $Ru_2C_{68}H_{76}O_{16}N_8$ m/z: 1464.30, found m/z: 1464.31 (M^+, 100%). IR (DCM) [cm^{-1}]: 835.50 (w), 1066.44 (m), 1154.19 (s), 1194.20 (m), 1204.81 (s), 1338.84 (w), 1362.94 (w), 1394.76 (w), 1418.87 (w), 1424.18 (w), 1439.71 (w), 1456.96 (m), 1464.19 (m), 1472.38 (m), 1489.74 (w), 1506.62 (m), 1535.46 (s Sh), 1538.92 (s), 1558.68 (m), 1596.77 (s), 1653.18 (m), 1684.03 (m), 2310.78 (m Sh), 2321.87 (m Br), 2363.82 (m Br). UV-VIS-NIR (DCM; 345-3300) [λ_{max}, nm (ε, M^{-1} cm^{-1})]: 399 (5720); 432 (4688); 497 (5560); 548 (Sh. *ca.* 3039); 888 (2174).

Method B) A variation on A) utilising THF and incorporating a different work-up. Method A should be used in preference; this method is provided for reference only.

A solution of $Ru_2(OAc)_4$ 0.065 g (0.15 mmol), and 0.195 g, (0.615 mmol 4.1 mol. equiv.) of H[DMOPhFm] in 15 ml of THF was heated at reflux for 16 hours after which time it was allowed to cool. Volatiles components were removed *in vacuo* at 60°C for 1 hour followed by the addition of a solution of two further equivalents of H[DMOPhFm], 0.095 g, 0.3 mmol in 15ml of THF. The resulting solution was then heated at reflux for a further 24 hours. Upon completion the reaction mixture was allowed to cool to room temperature and was then filtered through a fine sintered frit to isolating a bright, brick red product mixture from the purple filtrate. The recovered solid was then recrystallized from DCM/n-pentane, re-isolated via filtration, was washed with 2x 5ml aliquots of *n*-pentane and dried *in vacuo*. Yield: 0.116 g, 53 %.

Synthesis of $Ru_2^{II,II}(4FPhFm)_4$, (XI)

Readily synthesised via either 1A or 1B without additional modification, resulting in the isolation of a bright orange/red powder. Via 1A – yield: 0.095 g, 56%; and via 1B – Yield: 0.099 g, 59%. Repeated attempts to grow crystals of ***(XI)*** suitable for X-ray diffraction utilising a range of solvents were ultimately unsuccessful. MALDI-TOF-MS: calcd. monoisotopic MW for $Ru_2C_{52}H_{36}N_8F_8$ m/z: 1128.10, found m/z: 1128.2 (M^+, 100%). UV-VIS-NIR (DCM; 345-3300) [λ_{max}, nm (ε, M^{-1} cm^{-1})]: 390 (2925); 420 (Sh ca. 2490); 487 (2718); 545 (Sh ca. 1551); 907 (868).

Synthesis of $Ru_2^{II,II}$ $(3,5\text{-}(CF_3)_2PhFm)_3(OAc)$, (XIII)

Whilst attempting to optimised the reaction conditions to generate the tetra-substituted complex ***(XII)***, $Ru_2(3,5\text{-}(CF3)_2PhFm)_4$, the tris-substituted complex ***(XIII)*** was isolated as the sole product utilising the procedure 1B and an extended 72 hour reflux. All attempts at generating crystals of ***(XIII)*** for further structural analysis failed. MALDI-TOF-MS: calcd. monoisotopic MW for $Ru_2C_{68}H_{28}N_8F_{48}$ m/z: 1663.95, found m/z: 1664.0 (M^+, 100%). UV-VIS-NIR (DCM; 345-3300) [λ_{max}, nm (ε, M^{-1} cm^{-1})]: 423 (1118); 490 (Sh ca. 953); 650 (Sh ca. 468); 929 (269).

Synthesis of $Ru_2^{II,II}(3,5\text{-}(CF_3)_2PhFm)_4$, (XII)

0.065 g (0.15 mmol) $Ru_2(OAc)_4$ and 0.561 g (1.2 mmol, 8 equiv.) of H[3,5-$(CF_3)_2$PhFm] are combined in a small, ca. 50 ml Schlenk which is then fitted with a high efficiency reflux condenser. 20ml of a 3:1 mixture of mesitylene:toluene is then added and the resultant mixtures heated to reflux for 72 hrs. Once complete cooling to 5 °C overnight effects the precipitation of excess ligand which is removed via filtration. The retained filtrate is then reduced to minimal volume, and the product ***(XII)*** recovered by precipitation with hexanes and subsequent filtration. Product is afforded as a deep orange-red powder which is washed with 2x 5ml aliquots of *n*-pentane and dried *in vacuo*. In most instances a secondary, hot recrystallization from toluene is typically required to remove excess residual ligand to afford the target product ***(XII)*** cleanly. Yield: 0.040g, 13%. Product was found to shown very low solubility in most common solvents which greatly frustrated attempts a further analysis and rendered attempts and growing crystals of **(4)** all but impossible. MALDI-TOF-MS: calcd. monoisotopic MW for $Ru_2C_{68}H_{28}N_8F_{48}$ m/z: 2071.98, found m/z: 2072.1 (M^+, 100%).

Attempted synthesis of $Ru_2^{II,II}(TMOPhFm)_4$, (XIV)

Synthesis of $Ru_2(TMOPhFm)_4$ does not proceed beyond the tris-substituted product $Ru_2(TMOPhFm)_3(OAc)$ (not isolated) under the conditions of method 1A) or 1B) and requires a similar modified procedure to ***(XII)*** which is outlined below.

0.065 g (0.15 mmol) $Ru_2(OAc)_4$, 0.451 g (1.2 mmol, 8 equiv.) of H[TMOPhFm] and 150 ml of a 3:1 mixture of mesitylene:toluene are combined in a large, ca. 250 ml Schlenk which is then fitted with a high efficiency reflux condenser. The resultant slurry is then heated to reflux for 72 hrs. On completion and the reaction mixture is immediately filtered hot and the recovered light red powder dried to *in vacuo* to afford the desired product ***(XIV)*** in low yield (<10%.) Subsequent attempts at recrystallization, or further purification to effect the removal of remaining excess ligand are greatly frustrated by its insolubility in all common solvents. Attempts to utilise higher boiling solvents in excess of 200 °C are similarly ineffective and simply results in complex decomposition. MALDI-TOF-MS: calcd. monoisotopic MW for $Ru_2C_{76}H_{92}N_8O_{24}$ m/z: 1704.43, found m/z: 1704.4 (M^+, 100%).

3.5.2 Aerobic oxidation

An example oxidative catalysis experiment for ***X*** was conducted as follows: A 10 ml was charged with 0.073 g (0.05 mmol) of ***Ru_2(DMOPhFm)$_4$ (X)***, a small stirrer bar and sealed under argon with a rubber septum within the glovebox. To this was added 7.5 ml of a degassed 1:1 H_2O:toluene mixture to give a bright, brick red, solution of ***X***. The solution was transferred to a stirrer hotplate fitted with ambient temperature water and allowed to stir for 2 minutes. After this time 9.65 ml (1.0 mmol) of benzyl alcohol was added via syringe and after 10 seconds under stirring a low bubble of molecular O_2 was introduced to the solution via needle. Addition of O_2 causes an immediate abrupt colour change of the solution from brick red to deep purple. The reaction was then warmed to 80 °C over the course of ~5 minutes and the mixture allowed to stir for 36 hours. Small 0.25 ml aliquots were removed at regular intervals and analysed via GC-MS. The reaction mixtures turned from purple to black over 1-3 hours.

On completion of the reaction a sample was submitted for ^{1}H NMR in DCM for the purpose of comparison to the non-exposed and non-substrate containing control samples.

4 Diruthenium complexes with bulky amidate ligands

4.1 Aims

- To develop a synthetic methodology suitable for the general synthesis of a range of diruthenium (II,II) and (II,III) bulky tetra-formamidate complexes of the form shown below (Figure 4.1.1)

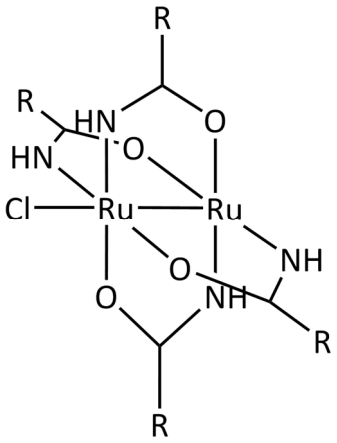

Figure 4.1.1- General form of diruthenium (II, III) amidates

- To explore the impact of varying electron donating or withdrawing aryl substituents of the ligand backbone on the resultant physical, spectroscopic and electronic properties of the diiron complexes formed.
- Where target species are isolated, to test their viability and activity of the as aerobic oxidation catalysts for the partial oxidation of simple organic substrates such as 9,10-dihydroanthracene.

4.2 Introduction

The chemistry of diruthenium complexes bearing 'NO' type bridging ligands, began in earnest in in the 1980s, with the publication of the electrochemical studies of the Ru (II, III) complex $Ru_2(HNOCCF_3)_4$ in 1983[125] particular drawing attention towards the amidate subset of these

In binding via a terminal, typically primary, amide, these complexes offer an intermediate mix of the better developed chemistries of both carboxylates and N donor ligands such as formamidinates. Initial reports of these species noted their propensity to often forego the common zig-zag arrangement often seen in Ru_2 (II,III) chloride bridged species, in favour of the formation of asymmetric dimers.[126,127] These dimers display significant variation in the Ru-Cl distances between and within adjacent dimers in an alternating fashion (Figure 4.2.1 overleaf).

It is particularly unusual that this pseudo-dimerisation appears to occur spontaneously within the polymeric zig-zag chains and in complexes without any appreciable steric pressure from the ligand backbone. Similarly, despite the formal capacity of the ligand to afford up to 4 distinct isomeric products, it is notable that all of the handful of structurally characterised complexes, exhibit the trans 2,2- regio isomer as the only observed product.[103]

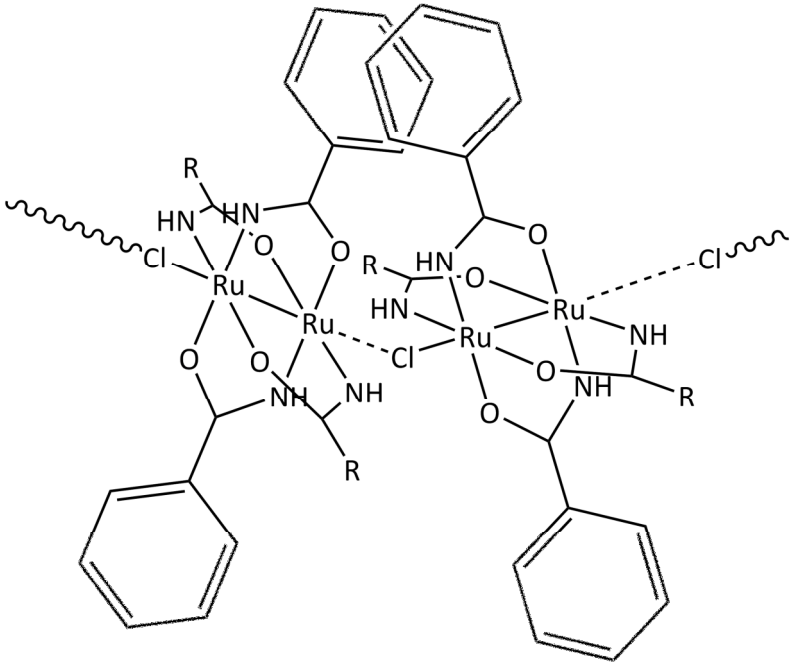

Figure 4.2.1 - Alternating long - short - long Ru - Cl distances observed in pseudo-dimeric zig-zag chains; R= Ph (omitted for clarity).

Amidate complexes also have a history of mediating some unorthodox ligand derived processes, such as ligand to metal arylation in interactions with aryl phosphines;[127,387–389] whilst more recent reports have shown they additionally have the capacity for oxidative catalysis.[129]

The amidate complexes within the literature to date are limited to those of simple substituted benzamide derivatives.[103,390] The recent attention drawn to the synthesis of such complexes[129,390] has however provided the impetus for our investigation of a wider range of more sterically bulky and encompassing ligand architectures. These include the *meta*-terphenyl- and 2,4,6-triisopropyl- substituted ligand backbones which have seen already seen widespread use to great effect in other carboxylate complexes of transition metals and are described herein.

In consideration of our wider work with Ru_2 (II,II) complexes, in addition to the exploration of Ru_2(II,III) amidates, we additionally report the first two examples of Ru_2 (II,II)(amidate)$_4$ complexes

4.3 Results and discussion

4.3.1 Ligand Synthesis

H[pTmtPhCO$_2$] – [2,6-bis(p-tolyl)benzoic acid]

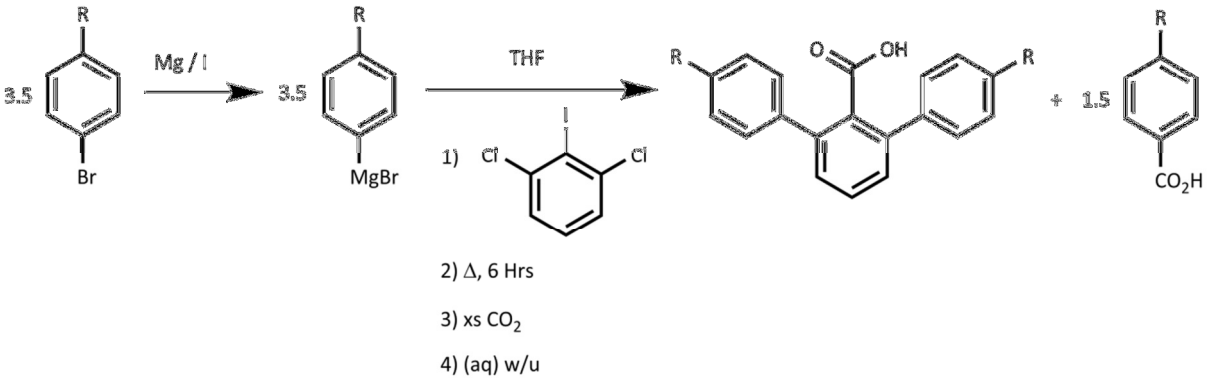

4.3.1.1 Amidation of corresponding carboxylic acid to primary amide via HATU mediated peptide coupling

Conversion of the carboxylic acid to its corresponding primary amide was conducted in excellent, near quantitative yield in all instances under mild conditions via HATU mediated coupling of the respective acid with aqueous ammonia. This approach had previously been proposed for more complex protected polypeptides using HOBt by Wang[391] for which traditional acid chloride formation conditions would lead to substrate degradation

Whilst it is quite possible to prepare these amides via the traditional route of formation of the acid chloride followed by amination under Schotten–Baumann conditions, this route was however found to be both more protracted and ultimately lower yielding. This was due in part of the hydrophobicity and bulk of the substrate which made clean isolation of the products via simple aqueous workup more challenging, practically mandating the need for column chromatography, which due to the >10g typical scale of these reactions was less than desirable.

In contrast the peptide coupling route is both more elegant and greatly simplifies the work-up required.

4.3.2 Synthesis of Ru_2(II/II)(amidate)$_4$ complexes

Synthesis of ***$Ru_2^{II,II}(Ben)_4$*** **(XVI)** and ***$Ru_2^{II,II}(pTPhAm)_4$*** **(XVII)** is readily achieved via combination of excess ligand, elevated temperature afforded by reflux in toluene and mesitylene respectively, and the active scrubbing of liberated acetic acid via use of the Soxhlet extraction assembly.

The use of the Soxhlet extractor to facilitate the removal of the liberated acetic acid provides an elegant solution to driving an otherwise very slow reaction towards the intended products. In the synthesis of amidate complexes from carboxylates one of the significantly retarding factors is the lower binding affinity of the amidate moiety often necessitating both harsh and protracted conditions to achieve complete substitution. On practical observation of the degree to which this impedes the progress of an un-Soxhlet scrubbed reaction it is perhaps unsurprising that the literature examples to date have been restricted to small, non-bulky functionalised benzamides. Utilisation of this methodology provides a practical and viable means to obtain tetra-substituted amidates even using such bulky ligands as the terphenyl amide H[pTPhAm].

Such synthetic approaches are not without their limitations however, and the synthesis of the Ru_2 (II,II) analogue of ***$Ru_2^{II,III}(TiPBAm)_4Cl$*** **(XX)** was not possible via this procedure as the ***H[TiPBAm]*** ligand to readily sublimed away under heating.

4.3.3 Synthesis of Ru_2(II/III)(amidate)$_4$ complexes

Synthesis of ***$Ru_2^{II,III}$(Ben)$_4$Cl (XVIII)***, ***$Ru_2^{II,III}$(pTPhAm)$_4$Cl (XIX)*** and ***$Ru_2^{II,III}$(TiPBAm)$_4$ (XIX)*** may be achieved in good to moderate yield via this procedure provided it is conducted in high concentration in minimal solvent. The use of more conventional sized Soxhlet extraction glassware showed a considerable >10% drop in yield cf. the smaller micro (~10 ml extraction volume) setup. This is likely due to the fact that total solvent volume is largely proscribed by the combination of Soxhlet extractor volume and relative reflux high temperature is required to achieve the effective operation of the Soxhlet with such high boiling solvents. Extensive use of insulating material was required to ensure effective operation of the extractor whilst the protracted reflux of ***$Ru_2^{II,III}$(pTPhAm)$_4$Cl (XIX)*** and ***$Ru_2^{II,III}$(TiPBAm)$_4$ (XIX*** necessitates the use of higher temperature heating media such as silicone oil. The propensity of this oil to spontaneously polymerise on addition of impurities and minor water contamination (e.g. condensation run-off from condenser tubing) is a legitimate concern in the 5 days synthetic procedure.

4.3.4 Characterisation

Characterisation of the complexes was primarily conducted via MALDI-TOF-MS, Electrochemistry and UV-Vis-NIR spectroscopy. The diamagnetic nature of complexes ***$Ru_2^{II,II}$(Ben)$_4$ (XVI)*** and ***$Ru_2^{II,III}$(pTPhAm)$_4$ (XVII)*** was confirmed via ^{1}H and ^{13}C NMR spectroscopy, but as with the Ru(II,II) complexes in chapter 2 NMR was otherwise found to be of limited diagnostic utility. NMR was used in conjunction with MALDI-TOF-MS during optimisation of reaction conditions as a means to identify the presence of remaining free ligand via the small, invariantly (<0.25 ppm) change in chemical shift observed on coordination to the metal centre.

4.3.5 Electrochemistry

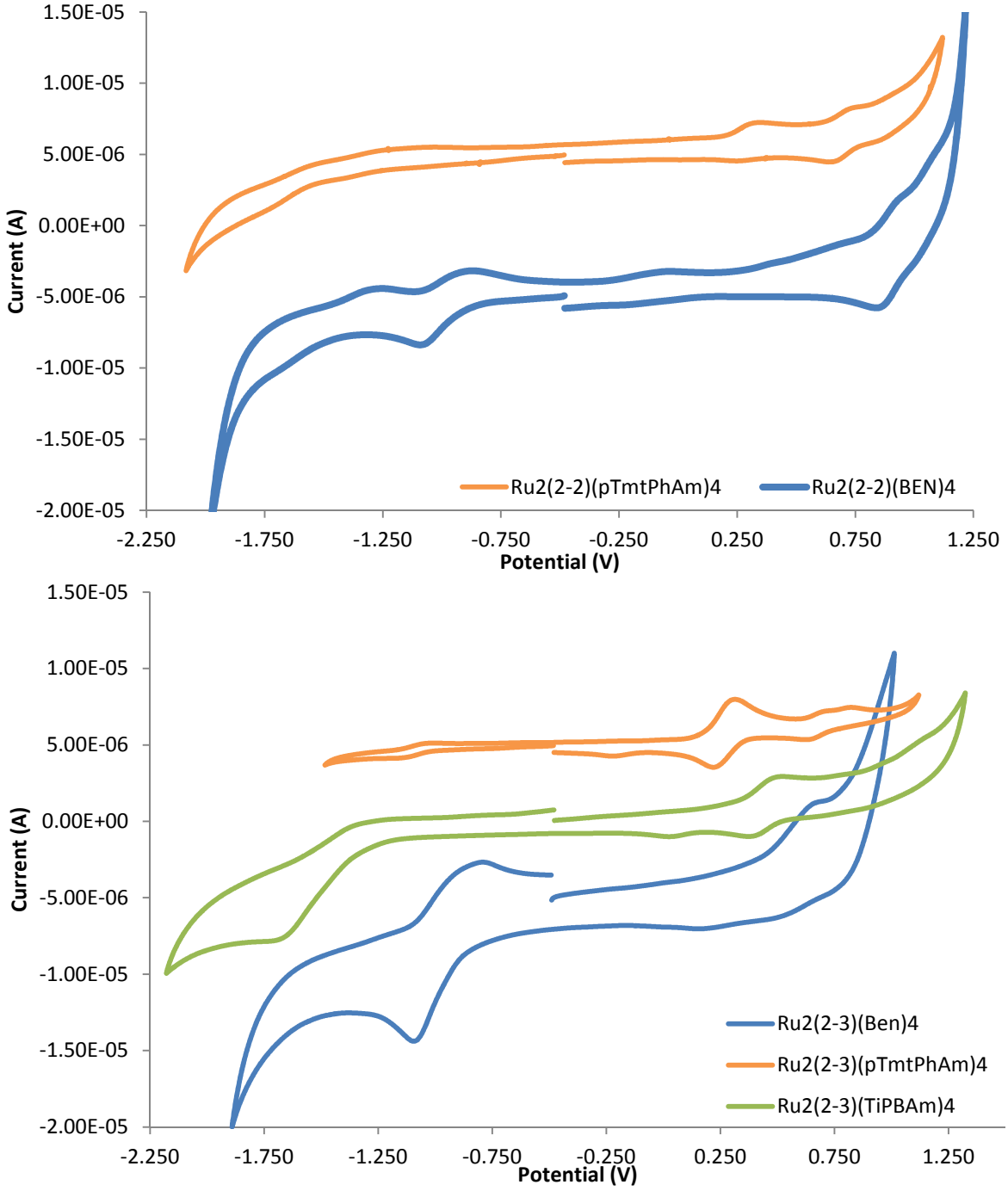

Figure 4.3.1 - Cyclic voltammograms for(top) $Ru_2(II,II)(amidate)_4$and (bottom) $Ru_2(II,III)(amidate)_4$ complexes recorded in in a 0.1M solution of $^{n}Bu_4NPF_6$ in DCM, with a scan rate 100 mv s^{-1}. (Traces are offset by 5x10-6 Amps above/below zero on the Y-axis for ease of readability.)

4.3.6 UV/Vis spectroscopy

4.3.6.1 $Ru_2(II,II)(amidate)_4$ complexes

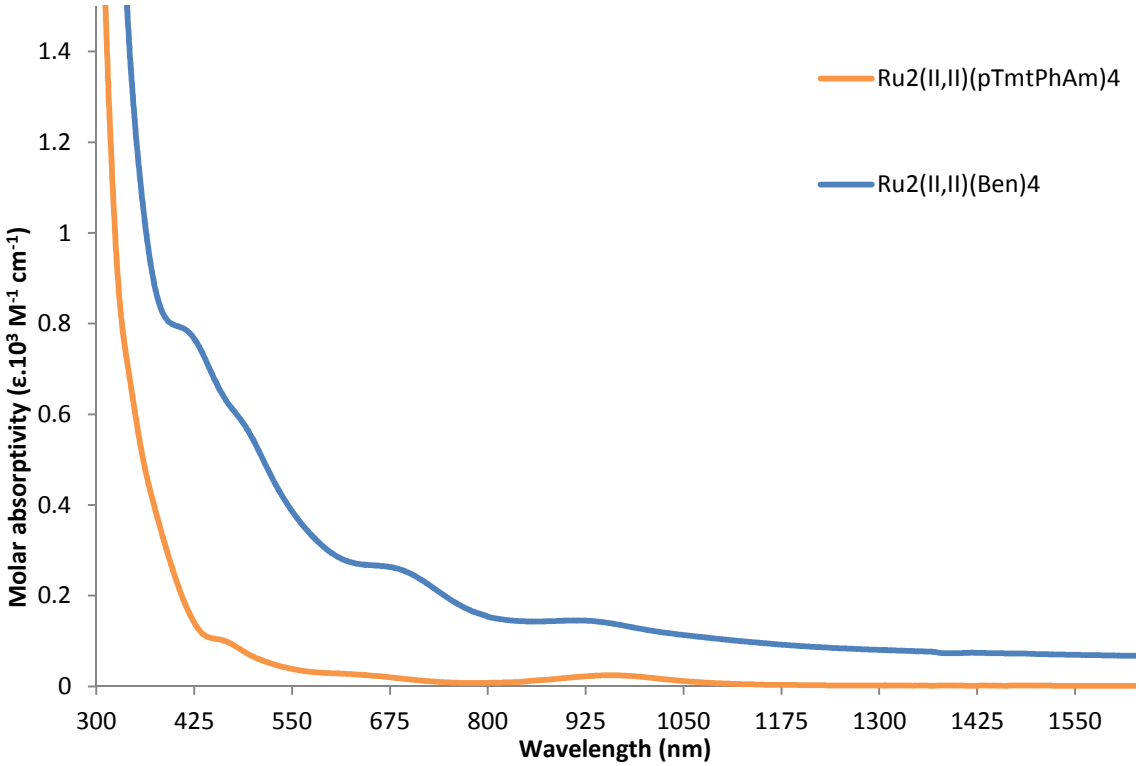

Spectra obtained in DCM. Relative to the spectra obtained by the related $Ru_2^{(II,II)}$(formamidinate)$_4$ complexes of chapter 3, the $Ru_2^{(II,II)}$(amidate)$_4$ complexes ***$Ru_2^{II,II}(Ben)_4$ (XVI)*** and ***$Ru_2^{II,III}(pTPhAm)_4$ (XVII)*** show far weaker absorbing spectra with little to no observable features, typical of amidate complexes in general, save for a series of smaller shoulders and weak transitions. Peak data is provided in Table 4.3.1

Complex	Peak wavelength (λ)	molar absorptivity $\varepsilon \cdot 10^3 (M^{-1}\ cm^{-1})$
$Ru_2^{(II,II)}(Ben)_4$	410	790
	682	260
	918	145
$Ru_2^{(II,II)}(pTPhAm)_4$	640	102
	957	24

Table 4.3.1 - Peak data for $Ru_2^{(II,II)}$(amidate)$_4$ complexes ***$Ru_2^{II,II}(Ben)_4$ (XVI)*** and ***$Ru_2^{II,III}(pTPhAm)_4$ (XVII)***

4.3.6.2 $Ru_2(II,III)(amidata)_4$ complexes

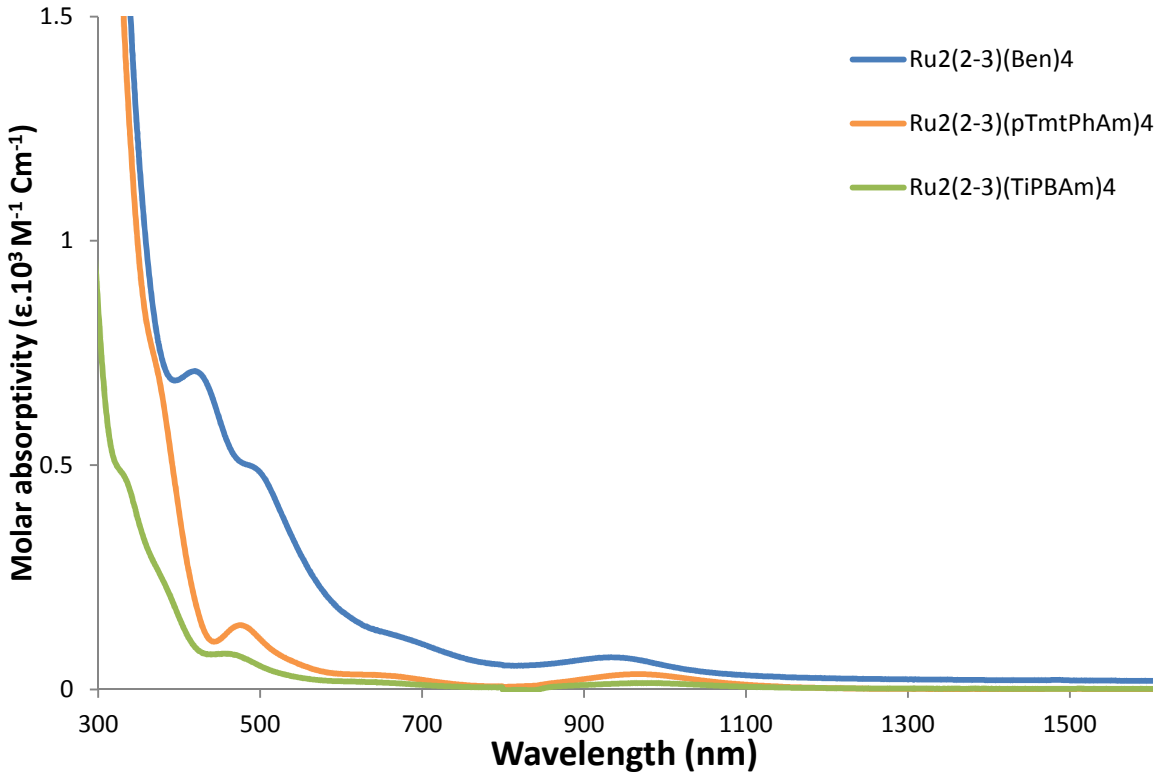

The $Ru_2(II,III)(amidate)_4$ complexes of ***$Ru_2^{II,III}(Ben)_4Cl$ (XVIII), $Ru_2^{II,III}(pTPhAm)_4Cl$ (XIX)*** and ***$Ru_2^{II,III}(TiPBAm)_4Cl$ (XX)*** show a few additional transitions to that observed for their direct $Ru_2(II,II)$ analogues, but are still very poor absorbing in the UV-Vis-NIR. This is reflected in the shades of brown in which the products are isolated. Peak data is provided in Table 4.3.2 below for reference.

Complex	Peak wavelength (λ)	molar absorptivity $\varepsilon \cdot 10^3 (M^{-1}\ cm^{-1})$
$Ru_2^{(II,III)}(Ben)_4Cl$	418	709
	494	493
	937	71
$Ru_2^{(II,III)}(4FPhFm)_4Cl$	479	143
	961	34
$Ru_2^{(II,III)}(TiPBAm)_4Cl$	457	80
	973	14

Figure 4.3.2 - Peak data for $Ru_2^{(II,III)}(amidate)_4$ complexes (3-5)

4.4 Conclusions

The synthesis of a range of bulk amidate complexes was conducted using a modified form of a previously reported Soxhlet scrubbed synthetic method.[129] The reaction conditions used to generate these of bulky amidates were optimised to afford them in good in yield but the products obtained were frequently intractable and highly polymeric, particularly the Ru_2(II,III).products which effectively form polymers in the solid state which greatly hindered their isolation and characterisation. The first two complexed generated, ***$Ru_2^{II,II}(Ben)_4$ (XVI)*** and ***$Ru_2^{II,III}(pTPhAm)_4$ (XVII)*** were Ru_2(II,II) whilst the remaining products ***$Ru_2^{II,III}(Ben)_4Cl$ (XVIII), $Ru_2^{II,III}(pTPhAm)_4Cl$ (XIX)*** and ***$Ru_2^{II,III}(TiPBAm)_4Cl$ (XX)*** formally Ru_2(II,III). These last three complexes represent the first examples of bulky Ru_2(II,III) amidates in the literature. Perhaps because this added bulk renders them incredibly difficult to work with once isolated in the solid state. A limited characterisation of these complexes, **(XVI-XX)** is presented however the intractable nature of the products severely limited what data could be readily obtained. It is also apparent from the UV-Vis-NIR spectra of these species that there are very few identifying features present in these compounds

4.5 Experimental

For details of physical measurement procedures please refer to section 2.5.1; for X-ray crystallographic details please refer to section 2.5.2; for general information on the sourcing and pre-treatment of reactants and reagents please refer to section 2.5.3 and the additional considerations outlined below:

$Ru_2(OAc)_4$[140] and $Ru_2(OAc)_4Cl$[135] were synthesised according to established literature procedures. Both diruthenium starting materials were analysed via MALDI-TOF-MS and IR (CO_2 vibrational mode frequency), and data obtained compared to reference data in accordance with previously a publish method.[140,141] H[Ben], N-phenylbenzamide, was purchased and purified by sublimation at 65 °C, 5 x 10^{-2} mbar prior to use.

4.5.1 Ligand Synthesis

H[pTmtPhCO$_2$] – [2,6-bis(p-tolyl)benzoic acid]

Modification of the general literature for the synthesis of *m*-terphenyls developed by Hart *et al.*[392–394] affords the 2,6-bis(p-tolyl)benzoic acid in good yield when coupled with a greatly simplified workup. An example procedure is provided below starting from the appropriate aryl bromide (A) or directly from the aryl Grignard if available (B).

A) Prep of RAr-MgBr – In a large, ca. 500 ml 3-necked RBF was placed 2.75 g, (0.113 mol) of magnesium turnings and a large oval stirrer bar, the vessel fitted with a b24 condenser in the middle of the three necks, which then had a 250ml pressure equalising dropping funnel affixed above it. This setup attached to a Schlenk line via two closable rotaflow™ type taps, one atop the dropping funnel and condenser assemble and the other installed into one of the remaining necks of the RBF containing the Mg turnings. The system was then evacuated and placed under inert atmosphere (3x) in accordance with standard Schlenk-line techniques and the large stirrer bar allowed to mechanically grind the magnesium turnings overnight prior to use.

To the ground magnesium turnings was added 2-4 small Iodine pellets and warmed to afford a purple iodine vapour after which it was then allowed to cool, coating the magnesium. To this ground, activated magnesium powder was added a solution of 17.96 g (0.105 Mol) of 4-bromo toluene in 100ml THF, dropwise over ca. 30 mins. On completion of the addition the resultant solution was heated to reflux for 1 hour to afford an opaque white solution of (*p*-tolyl)magnesium bromide. Continues as per B)

B) General procedure – To a solution of 0.105 mol (*p*-tolyl)magnesium bromide in 100ml THF, afforded from a commercial source, or via **A)**, that has been charged into the 500 ml RBF as described in the experimental setup of **A)**, was added, dropwise over 1 hr, a solution of 8.187 g (0.03 mol) 2,6-dichloro iodobenzene in 100 ml of THF. On completion of the addition the reaction mixture is heated to reflux for 4 hours before subsequently being allowed to cool to room temperature. Quenching via the bubbling of an excess of CO_2 from a separate, vented vessel overnight via large bore cannula affords the corresponding carboxylate as a heavy white precipitate.

Removal of the THF *in vacuo* followed extraction into toluene, acidification via by washing with 2x 150ml of 10M HCL and drying over $MgSO_4$ then affords a binary mixture of the carboxylates H[pTmtPhCO$_2$H] and (p-tolyl)benzoic acid. Recrystallisation from hot toluene followed by removal of any remaining (p-tolyl)benzoic acid sublimation 30 °C, 2x10^{-2} mbar overnight affords the target ligand H[pTmtPhCO$_2$] as a very pale cream coloured solid in excellent yield. Yield: 8.067 g, 89%. M_p: 181.2 °C. ^{1}H NMR (DMSO, 400 MHz): δ 2.36 (s, 6H C*H*$_3$), 7.24-7.40 (m, 10H Ar-*H*), 7.52 (t, 1H Ar-*H*), 12.78 (s, 1H O-*H*); ^{13}C NMR (DMSO, 400 MHz, DEPTQ/CPD): δ 20.74, 128.31, 128.61, 128.93, 133.98, 136.77, 137.46, 138.73, 170.24. HR-ESI-MS: calcd. monoisotopic MW for $C_{21}H_{18}O_2$ m/z: 302.1385, found m/z: 302.138 (M^+, 100%). IR (ATR, cm^{-1}): 3853.7 (s), 3748.4 (s), 1701.4 (s), 1653.1 (s) (consistent with literature.) Elemental analysis calcd. for $C_{21}H_{18}O_2$: C, 83.42%; H, 6.00%; O, 10.58%; found: C, 83.40%; H, 6.02%.

4.5.1.1 Amidation of bulky carboxylic acids to primary amides via HATU mediated peptide-type coupling

Conversion of the carboxylic acid to its corresponding primary amide was conducted via HATU mediated coupling of the respective acid with aqueous ammonia. This represents a hybridisation of the procedures demonstrated by Wang using the related coupling agent HOBt[391] and those of Bracker with respect effecatious workups when utilising HATU in DMF.[395] An example procedure for the synthesis of 2,6-bis(p-tolyl)benzamide as follows:

A 500 ml RBF is charged with 1 g, (3.3mmol) of 2,6-bis(p-tolyl)benzoic acid, 1.38 g, (3.6 mmol, 1.1 mol. equiv.) of HATU (1-[Bis(dimethylamino)methylene]-1H-1,2,3-triazolo[4,5-b]pyridinium 3-oxid hexafluorophosphate) and 50 ml dry, distilled DMF with the vessel under inert, argon atmosphere. To this solution is added 1.9 ml, (10.9 mmol, 3 mol. equiv.) of DIPEA/DIEA/Hünigs base, resulting in a yellow solution that was allowed to stir for 30 minutes. After this time 0.3 ml, (7.3 mmol, 2.2 equiv) of fresh 35% ammonium hydroxide solution was then injected and the reaction stirred for 16 hrs at room temperature. On completion the reaction was quenched via addition of ca. 350 ml of brine / saturated NaCl solution and cooled to 4 °C for 6 hrs. The bulky amide product precipitates preferentially on cooling and is isolated via filtration, washed with 2x 100ml deionised water and recrystallised from hot hexane yielding the desired product in near quantitative yield.

H[pTPhAm] – [2,6-bis(p-tolyl)benzamide]

Yield: 0.977 g, 98%. M_p: 213-216 °C. ^{1}H NMR ($CDCl_3$, 400 MHz): δ 2.41 (s, 6H C*H*$_3$), 5.30 (d, 2H N-*H*), 7.23-7.51 (m, 11H Ar-*H*); ^{13}C NMR ($CDCl_3$, 400 MHz, DEPTQ/CPD): δ 21.2, 128.62, 129.1, 129.1, 129.1, 134.9, 137.3, 137.6, 139.9, 171.2. HR-ESI-MS: calcd. monoisotopic MW for $C_{21}H_{19}NO$ m/z: 301.1467, found m/z: 301.147 (M^+, 100%). IR (ATR, cm^{-1}): Consistent with literature. Elemental analysis calcd. for $C_{21}H_{19}NO$: C, 83.69%; H, 6.35%; N, 4.65%; O, 5.31%; found: C, 83.34%; H, 6.28%; N, 4.44%.

H[TiPBAm] – [2,4,6-triisopropylbenzamide]

Conducted on 2x stated scale.

Yield: 1.58 g, 97%. M_p: 200 °C (sublimed). ^{1}H NMR (DMSO, 400 MHz): δ 1.15-1.27 (m, 18H iPr-C*H*$_3$); 2.87 (sep, 2H *p*-iPr-*H*), 3.00 (sep, 2H *o*-iPr-*H*), 7.02 (s, 2H Ar-*H*),7.56 (d, 2H N-*H*); ^{13}C NMR (DMSO, 400 MHz, DEPTQ/CPD): δ 24.5, 24.9, 30.8, 34.2, 120.6, 135.6, 144.1, 148.7, 172.1. HR-ESI-MS: calcd. monoisotopic MW for $C_{16}H_{25}NO$ m/z: 247.1936, found m/z: 247.194 (M^+, 100%). IR (ATR, cm^{-1}): Consistent with literature. Elemental analysis calcd. for $C_{16}H_{25}NO$: C, 77.68%; H, 10.19%; N, 5.66%; O, 6.47%; found: C, 77.63%; H, 9.98%; N, 5.57%.

4.5.2 Diruthenium (II/II) complexes

Complexes were synthesised via a optimised variations of the method reported by Ren[103,129] for which a general method is outlined below:

General synthetic procedure:

A Schlenk was charged with (0.2 mmol) of $Ru_2^{(II,II)}(OAc)_4$, (1.2 mmol, 10 mol. equiv.) of H[ligand] and fitted with a micro-Soxhlet adaptor and a high thermal efficiency condenser. A glass microfiber extraction thimble filled with an excess of K_2CO_3 and topped with sand was fitted into the Soxhlet and 40 ml of toluene added. The resultant mixture was allowed to reflux for 48 hours and then allowed to cool to room temperature.

On cooling any observed precipitate (chiefly ligand) was removed via filtration prior to concentration to minimal volume (ca. 2-5 ml). Product was then precipitated via addition of hexanes and recovered via filtration. Further purification via sublimation to remove excess ligands was typically required.

Alternate work-up: Where precipitation did not occur on addition of hexanes, solvent was removed *in vacuo* and excess ligand removed *in situ* via sublimation. Product was obtained via recrystallisation from hot toluene.

Synthesis of $Ru_2^{(II,II)}(Ben)_4$, (1)

Synthesised as per the general method and utilising the primary work-up conditions. Product obtained as light-ish brown solid. Yield: 0.122, 62%. MALDI-TOF-MS: calcd. monoisotopic MW for $Ru_2C_{52}H_{40}N_4O_4$ m/z: 988.1136, found m/z: 987.1(M-Cl, 100%). UV-VIS-NIR (DCM; 345-3300) [λ_{max}, nm (ε, M^{-1} cm^{-1})]: 410 (Sh. ca. 790), 682 (260), 918 (145).

Synthesis of $Ru_2^{(II,II)}(pTPhAm)_4$, (2)

Synthesised as per the general method with the following modifications: reaction solvent was changed to mesitylene and reaction time at reflux extended to 4 days. Product isolation proceeded via the primary work-up conditions. Product obtained as dark brown solid. Yield: 0.090, 32%. MALDI-TOF-MS: calcd. monoisotopic MW for $Ru_2C_{84}H_{72}N_4O_4$ m/z: 1404.3640,

found m/z: 1404.4(M-Cl, 100%). UV-VIS-NIR (DCM; 345-3300) [λ_{max}, nm (ε, M^{-1} cm^{-1})]: 640 (Sh. ca. 102), 957 (24).

4.5.3 Diruthenium (II/III) complexes

Synthesis of $Ru_2^{(II,III)}(Ben)_4Cl$, (3)

Synthesised via a variation of the procedure utilised for the corresponding Ru (II, II) analogues with the following modifications:

In addition to other reagents Schlenk was additionally charged with 0.135 g (20 mol. equiv.) of LiCl. Product isolated via primary workup as brown solid. Yield: 0.137 g, 73%. MALDI-TOF-MS: calcd. monoisotopic MW for $Ru_2C_{52}H_{40}N_4O_4Cl$ m/z: 1023.0825, found m/z: (M-Cl, 100%). UV-VIS-NIR (DCM; 345-3300) [λ_{max}, nm (ε, M^{-1} cm^{-1})]: 418 (709), 494 (493), 937 (71).

Synthesis of $Ru_2^{(II,III)}(pTPhAm)_4Cl$, (4)

Synthesised via variation of the method used for $Ru_2^{(II,III)}(Ben)_4Cl$ as described below:

Mesitylene utilised in place of toluene as reaction solvent and reflux extended to 5 days. Product isolated via primary work up, followed by removal of excess ligand via sublimation and recrystallisation from a hot 80:20 methanol:toluene mixture affording the product as a dark orange brown solid. Yield: 0.131 g, 45%, MALDI-TOF-MS: calcd. monoisotopic MW for $Ru_2C_{84}H_{72}N_4O_4Cl$ m/z: 1436.3329, found m/z: 1404.7 (M-Cl, 100%). UV-VIS-NIR (DCM; 345-3300) [λ_{max}, nm (ε, M^{-1} cm^{-1})]: 479 (143), 961 (34).

Synthesis of $Ru_2^{(II,III)}(TiPBAm)_4Cl$, (5)

Synthesised as per $Ru_2^{(II,III)}(pTPhAm)_4Cl$ with the modification of the use of 1,2-dichlorobenzene as the reaction solvent. Product as a dark brown solid. Yield: 0.103 g, 42%. MALDI-TOF-MS: calcd. monoisotopic MW for $Ru_2C_{64}H_{96}N_4O_4Cl$ m/z: 1223.52, found m/z: 1222.6 (M-Cl, 100%). UV-VIS-NIR (DCM; 345-3300) [λ_{max}, nm (ε, M^{-1} cm^{-1})]: 457 (80) 973 (14).

5 References

(1) Arockiam, P. B.; Bruneau, C.; Dixneuf, P. H. *Chem. Rev.* **2012**, *112* (11), 5879–5918.

(2) Vougioukalakis, G. C.; Grubbs, R. H. *Chem. Rev.* **2009**, *110* (3), 1746–1787.

(3) Arakawa, H.; Aresta, M.; Armor, J. N.; Barteau, M. A.; Beckman, E. J.; Bell, A. T.; Bercaw, J. E.; Creutz, C.; Dinjus, E.; Dixon, D. A.; Domen, K.; DuBois, D. L.; Eckert, J.; Fujita, E.; Gibson, D. H.; Goddard, W. A.; Goodman, D. W.; Keller, J.; Kubas, G. J.; Kung, H. H.; Lyons, J. E.; Manzer, L. E.; Marks, T. J.; Morokuma, K.; Nicholas, K. M.; Periana, R.; Que, L.; Rostrup-Nielson, J.; Sachtler, W. M. H.; Schmidt, L. D.; Sen, A.; Somorjai, G. A.; Stair, P. C.; Stults, B. R.; Tumas, W. *Chem. Rev.* **2001**, *101* (4), 953–996.

(4) Appl, M. In *Ullmann's Encyclopedia of Industrial Chemistry*; Wiley-VCH Verlag GmbH & Co. KGaA, 2000.

(5) Smil, V. *Enriching the Earth: Fritz Haber, Carl Bosch, and the Transformation of World Food Production*, illustrate.; MIT Press, 2004.

(6) Haber, F. In *Nobel lectures*; Royal Swedish Academy of Sciences, Stockholm, Sweden, 1920.

(7) Haber, F.; Rosssignol, R. . *Zeitschrift für Elektrochemie und Angew. Phys. Chemie* **1913**, *19* (2), 53–72.

(8) Bosch, C. In *Nobel lectures*; Royal Swedish Academy of Sciences, Stockholm, Sweden, 1932.

(9) Rittle, J.; Younker, J. M.; Green, M. T. *Inorg. Chem.* **2010**, *49* (8), 3610–3617.

(10) Matsui, T.; Iwasaki, M.; Sugiyama, R.; Unno, M.; Ikeda-Saito, M. *Inorg. Chem.* **2010**, *49* (8), 3602–3609.

(11) *Cytochrome p450 - Structure, Mechanism, and Biochemistry*, 3rd (2005) ed.; Montellano, P. O., Ed.; Springer: New York, 2005.

(12) Guallar, V.; Baik, M. H.; Lippard, S. J.; Friesner, R. A. *Proc. Natl Acad. Sci. USA* **2003**, *100* (12), 6998–7002.

(13) Loew, G. H.; Harris, D. L. *Chem. Rev.* **2000**, *100* (2), 407–420.

(14) Schlichting, I.; Berendzen, J.; Chu, K.; Stock, A. M.; Maves, S. A.; Benson, D. E.; Sweet, R. M.; Ringe, D.; Petsko, G. A.; Sligar, S. G. *Science (80-.).* **2000**, *287* (5458), 1615–1622.

(15) Schappacher, M.; Ricard, L.; Fischer, J.; Weiss, R.; Bill, E.; Montiel-montoya, R.; Winkler, H.; Trautwein, alfred x. *Eur. J. Biochem.* **1987**, *168* (2), 419–429.

(16) MacKay, D. J. C. *Sustainable energy : Without the hot air*; UIT: Cambridge, 2009.

(17) Olah, G. A.; Goeppert, A.; Prakash, G. K. S. *Beyond oil and gas : the methanol economy*; Wiley-VCH ; John Wiley: Weinheim; Chichester, 2006.

(18) Olah, G. A. *Angew. Chem., Int. Ed.* **2005**, *44* (18), 2636–2639.

(19) Demirbas, A. *Energy Convers. Manag.* **2008**, *49* (8), 2106–2116.

(20) Balat, M.; Balat, H. *Energy Convers. Manag.* **2008**, *49* (10), 2727–2741.

(21) Murray, E. P.; Tsai, T.; Barnett, S. A. *Nature* **1999**, *400* (6745), 649–651.

(22) Crabtree, G. W.; Dresselhaus, M. S.; Buchanan, M. V. *Phys. Today* **2004**, *57* (12), 39–44.

(23) Dunn, S. *Int. J. Hydrogen Energy* **2002**, *27* (3), 235–264.

(24) International Energy agency (IEA). - *Production costs of alternative transportation fuel & influence of crude oil price and technology maturity*; 2013.

(25) Higgins, I. J.; Best, D. J.; Hammond, R. C. *Nature* **1980**, *286* (5773), 561–564.

(26) Rosenzweig, A. C.; Frederick, C. A.; Lippard, S. J.; Nordlund, P. *Nature* **1993**, *366* (6455), 537–543.

(27) Couch, G. R.; IEA Coal Research; Clean Coal Centre. *Coal to Liquids*; International Energy Agency Coal Research, 2008.

(28) Reitmeier, R. E.; Atwood, K.; Bennett, H. A.; Baugh, H. M. *Ind. Eng. Chem.* **1948**, *40* (4), 620–626.

(29) Spalth, P. L.; Dayton, D. C.; (DOE), U. S. D. of E.; Energy, U. S. D. of. *Preliminary screening - technical and economic assessment of synthesis gas to fuels and chemicals with emphasis on the potential for biomass-derived syngas*; National Renewable energy lab., Golden, CO (US); Report no: NREL/TP-510-34929, 2003.

(30) Huber, G. W.; Iborra, S.; Corma, A. *Chem. Rev.* **2006**, *106* (9), 4044–4098.

(31) Avetisov, A. K.; Rostrup-Nielsen, J. R.; Kuchaev, V. L.; Hansen, J. H. B.; Zyskin, A. G.; Shapatina, E. N. *J. Mol. Cat. A-Chem* **2010**, *315* (2), 155–162.

(32) Aasberg-Petersen, K.; Hansen, J. H. B.; Christensen, T. S.; Dybkjaer, I.; Christensen, P. S.; Nielsen, C. S.; Madsen, S.; Rostrup Jr., N. *Appl. Catal., A* **2001**, *221* (1-2), 379–387.

(33) Rostrupnielsen, J. R.; Hansen, J. H. B. *J. Catal.* **1993**, *144* (1), 38–49.

(34) Chinchen, G. C.; Denny, P. J.; Jennings, J. R.; Spencer, M. S.; Waugh, K. C. *Appl. Catal.* **1988**, *36*, 1–65.

(35) Rabo, J. A.; Risch, A. P.; Poutsma, M. L. *J. Catal.* **1978**, *53* (3), 295–311.

(36) Poutsma, M. L.; Elek, L. F.; Ibarbia, P. A.; Risch, A. P.; Rabo, J. A. *J. Catal.* **1978**, *52* (1), 157–168.

(37) Farrauto, R. J.; Bartholomew, C. H. *Introduction to Industrial Catalytic Processes*; Chapman & Hall: London, UK, 1997.

(38) Rostrup-Nielsen, J. R. *Catal. Today* **2000**, *63* (2-4), 159–164.

(39) Klier, K.; Chatikavanij, V.; Herman, R. G.; Simmons, G. W. *J. Catal.* **1982**, *74* (2), 343–360.

(40) Stahl, S. S.; Labinger, J. A.; Bercaw, J. E. *Angew. Chem. Int. Ed. Engl.* **1998**, *37* (16), 2181–2192.

(41) Wang, Y.; Otsuka, K. *J. Chem. Soc. Farad. T.* **1995**, *91* (21), 3953–3961.

(42) Wang, Y.; Otsuka, K. *J. Chem. Soc. Chem. Comm.* **1994**, No. 19, 2209–2210.

(43) Wang, Y.; Otsuka, K. *J. Mol. Catal. A-Chem* **1996**, *111* (3), 341–356.

(44) Wang, Y.; Otsuka, K. *J. Catal.* **1995**, *155* (2), 256–267.

(45) Walker, G. S.; Lapszewicz, J. A.; Foulds, G. A. *Catal. Today* **1994**, *21* (2-3), 519–526.

(46) Baldwin, T. R.; Burch, R.; Squire, G. D.; Tsang, S. C. *Appl. Catal.* **1991**, *74* (1), 137–152.

(47) Burch, R.; Squire, G. D.; Tsang, S. C. *J. Chem. Soc. Farad. T.* **1989**, *85* (10), 3561–3568.

(48) Gesser, H. D.; Hunter, N. R.; Prakash, C. B. *Chem. Rev.* **1985**, *85* (4), 235–244.

(49) Pitchai, R.; Klier, K. *Catal. Rev.* **1986**, *28* (1), 13–88.

(50) Parkyns, N. D.; Warburton, C. I.; Wilson, J. D. *Catal. Today* **1993**, *18* (4), 385–442.

(51) Brown, M. J.; Parkyns, N. D. *Catal. Today* **1991**, *8* (3), 305–335.

(52) Krylov, O. V. *Catal. Today* **1993**, *18* (3), 209–302.

(53) Hall, T. J.; Hargreaves, J. S. J.; Hutchings, G. J.; Joyner, R. W.; Taylor, S. H. *Fuel Process. Technol.* **1995**, *42* (2-3), 151–178.

(54) Crabtree, R. H. *Chem. Rev.* **1995**, *95* (4), 987–1007.

(55) Periana, R. A.; Mironov, O.; Taube, D.; Bhalla, G.; Jones, C. J. *Science (80-.).* **2003**, *301* (5634), 814–818.

(56) Ahlquist, M.; Periana, R. A.; Goddard, W. A. *Chem. Commun.* **2009**, No. 17, 2373–2375.

(57) Periana, R. A.; Taube, D. J.; Gamble, S.; Taube, H.; Satoh, T.; Fujii, H. *Science (80-.).* **1998**, *280* (5363), 560–564.

(58) Sen, A.; Lin, M. R.; Kao, L. C.; Hutson, A. C. *J. Amer. Chem. Soc.* **1992**, *114* (16), 6385–6392.

(59) Kao, L. C.; Hutson, A. C.; Sen, A. *J. Amer. Chem. Soc.* **1991**, *113* (2), 700–701.

(60) Lin, M.; Sen, A. *Nature* **1994**, *368* (6472), 613–615.

(61) Periana, R. A.; Taube, D. J.; Evitt, E. R.; Loffler, D. G.; Wentrcek, P. R.; Voss, G.; Masuda, T. *Science (80-.).* **1993**, *259* (5093), 340–343.

(62) Jones, C. J.; Taube, D.; Ziatdinov, V. R.; Periana, R. A.; Nielsen, R. J.; Oxgaard, J.; Goddard, W. A. *Angew. Chem., Int. Ed.* **2004**, *43* (35), 4626–4629.

(63) Goldshle, N. F.; Tyabin, M. B.; Shilov, A. E.; A., S. A. *Russ. J. Phys. Chem.* **1969**, *43* (8), 1222.

(64) Muehlhofer, M.; Strassner, T.; Herrmann, W. A. *Angew. Chem., Int. Ed.* **2002**, *41* (10), 1745–1747.

(65) Strassner, T.; Muehlhofer, M.; Zeller, A.; Herdtweck, E.; Herrmann, W. A. *J. Organomet. Chem.* **2004**, *689* (8), 1418–1424.

(66) Roy, S. B.; Chaddah, P. *Phys. Rev. B* **1997**, *55* (17), 11100–11102.

(67) Pal, D.; Ramakrishnan, S.; Grover, A. K.; Yamamoto, E.; Haga, Y.; Hedo, M.; Inada, Y.; Onuki, Y. *J. Phys. Conf. Ser.* **2009**, *150* (5), 052206.

(68) Kittaka, S.; Sakakibara, T.; Hedo, M.; Ōnuki, Y.; Machida, K. *J. Phys. Soc. Japan* **2013**, *82* (12), 123706.

(69) Martín, V. S.; Palazón, J. M.; Rodríguez, C. M.; Nevill, C. R. In *Encyclopedia of Reagents for Organic Synthesis*; John Wiley & Sons, Ltd, 2001.

(70) Cotton, S. *Chemistry of Precious Metals*; Springer, 1997.

(71) Greenwood, N. N.; Earnshaw, A. *Chemistry of the Elements*, 2nd Ed.; Elsevier Science & Technology Books, 1997.

(72) Housecroft, C. E.; Sharpe, A. G. *Inorganic Chemistry*, 2nd Ed.; Pearson Prentice Hall, 2005.

(73) Kojima, T.; Hirai, Y.; Ishizuka, T.; Shiota, Y.; Yoshizawa, K.; Ikemura, K.; Ogura, T.; Fukuzumi, S. *Angew. Chemie Int. Ed.* **2010**, *49* (45), 8449–8453.

(74) Itoh, M.; Shikano, M.; Shimura, T. *Phys. Rev. B* **1995**, *51* (22), 16432–16435.

(75) Pandey, K. K.; Ahuja, S. R.; Poonia, N. S.; Bharti, S. *J. Chem. Soc. Chem. Commun.* **1982**, No. 21, 1268–1269.

(76) Juris, A.; Balzani, V.; Barigelletti, F.; Campagna, S.; Belser, P.; von Zelewsky, A. *Coord. Chem. Rev.* **1988**, *84* (0), 85–277.

(77) Balzani, V.; Juris, A.; Venturi, M.; Campagna, S.; Serroni, S. *Chem. Rev.* **1996**, *96* (2), 759–834.

(78) Collin, J.-P.; Gaviña, P.; Heitz, V.; Sauvage, J.-P. *Eur. J. Inorg. Chem.* **1998**, *1998* (1), 1–14.

(79) Lay, P. A.; Sargeson, A. M.; Taube, H.; Chou, M. H.; Creutz, C. In *Inorganic Syntheses*; John Wiley & Sons, Inc., 1986; pp 291–299.

(80) Baggaley, E.; Weinstein, J. A.; Williams, J. A. G. *Coord. Chem. Rev.* **2012**, *256* (15–16), 1762–1785.

(81) Gill, M. R.; Garcia-Lara, J.; Foster, S. J.; Smythe, C.; Battaglia, G.; Thomas, J. A. *Nat Chem* **2009**, *1* (8), 662–667.

(82) Foxon, S. P.; Alamiry, M. A. H.; Walker, M. G.; Meijer, A. J. H. M.; Sazanovich, I. V; Weinstein, J. A.; Thomas, J. A. *J. Phys. Chem. A* **2009**, *113* (46), 12754–12762.

(83) Lomoth, R.; Magnuson, A.; Sjödin, M.; Huang, P.; Styring, S.; Hammarström, L. *Photosynth. Res.* **2006**, *87* (1), 25–40.

(84) Hatzidimitriou, A.; Gourdon, A.; Devillers, J.; Launay, J.-P.; Mena, E.; Amouyal, E. *Inorg. Chem.* **1996**, *35* (8), 2212–2219.

(85) Waywell, P.; Gonzalez, V.; Gill, M. R.; Adams, H.; Meijer, A. J. H. M.; Williamson, M. P.; Thomas, J. A. *Chem. – A Eur. J.* **2010**, *16* (8), 2407–2417.

(86) Jones, H.; Newell, M.; Metcalfe, C.; Spey, S. E.; Adams, H.; Thomas, J. A. *Inorg. Chem. Commun.* **2001**, *4* (9), 475–477.

(87) Balzani, V. *Supramolecular Photochemistry*; NATO ASI Series: Mathematical and Physical Sciences; Springer, 1987.

(88) Sauvage, J. P.; Collin, J. P.; Chambron, J. C.; Guillerez, S.; Coudret, C.; Balzani, V.; Barigelletti, F.; De Cola, L.; Flamigni, L. *Chem. Rev.* **1994**, *94* (4), 993–1019.

(89) Teplý, F. *Collect. Czechoslov. Chem. Commun.* **2011**, *76* (7), 859–917.

(90) Nicewicz, D. A.; MacMillan, D. W. C. *Science (80-.).* **2008**, *322* (5898), 77–80.

(91) Ischay, M. A.; Anzovino, M. E.; Du, J.; Yoon, T. P. *J. Am. Chem. Soc.* **2008**, *130* (39), 12886–12887.

(92) Narayanam, J. M. R.; Tucker, J. W.; Stephenson, C. R. J. *J. Am. Chem. Soc.* **2009**, *131* (25), 8756–8757.

(93) Narayanam, J. M. R.; Stephenson, C. R. J. *Chem. Soc. Rev.* **2011**, *40* (1), 102–113.

(94) Yoon, T. P.; Ischay, M. A.; Du, J. *Nat Chem* **2010**, *2* (7), 527–532.

(95) Zeitler, K. *Angew. Chemie Int. Ed.* **2009**, *48* (52), 9785–9789.

(96) Sullivan, B. P.; Calvert, J. M.; Meyer, T. J. *Inorg. Chem.* **1980**, *19* (5), 1404–1407.

(97) Roche, S.; Adams, H.; Spey, S. E.; Thomas, J. A. *Inorg. Chem.* **2000**, *39* (11), 2385–2390.

(98) Adams, H.; Amado, A. M.; Félix, V.; Mann, B. E.; Antelo-Martinez, J.; Newell, M.; Ribeiro-Claro, P. J. A.; Spey, S. E.; Thomas, J. A. *Chem. – A Eur. J.* **2005**, *11* (7), 2031–2046.

(99) Nguyen, S. T.; Johnson, L. K.; Grubbs, R. H.; Ziller, J. W. *J. Amer. Chem. Soc.* **1992**, *114* (10), 3974–3975.

(100) Scholl, M.; Ding, S.; Lee, C. W.; Grubbs, R. H. *Org. Lett.* **1999**, *1* (6), 953–956.

(101) Kingsbury, J. S.; Harrity, J. P. A.; Bonitatebus, P. J.; Hoveyda, A. H. *J. Amer. Chem. Soc.* **1999**, *121* (4), 791–799.

(102) Garber, S. B.; Kingsbury, J. S.; Gray, B. L.; Hoveyda, A. H. *J. Amer. Chem. Soc.* **2000**, *122* (34), 8168–8179.

(103) Cotton, F. A.; Murillo, C. A.; Walton, R. A. *Multiple bonds between metal atoms*, 3rd ed.; Springer Science and Business Media: New York, NY, 2005.

(104) Bloomstrand, C. W. *J. Prakt. Chem.* **1857**, *71* (449).

(105) Bloomstrand, C. W. *J. Prakt. Chem.* **1859**, *77*, 88.

(106) Bloomstrand, C. W. *J. Prakt. Chem.* **1861**, *82*, 433.

(107) Brosset, C. *Ark. Kemi, Miner. Geol.* **1946**, *A20* (7).

(108) Brosset, C. *Ark. Kemi, Miner. Geol.* **1946**, *A22* (11).

(109) Vaughan, P. A.; Sturdivant, J. H.; Pauling, L. *J. Am. Chem. Soc.* **1950**, *72* (12), 5477–5486.

(110) Brosset, C. *Ark. Kemi, Miner. Geol.* **1935**, *128* (7).

(111) Brosset, C. *Nature* **1925**, *135*, 874.

(112) Dahl, L. F.; Ishishi, E.; Rundle, R. E. *J. Chem. Phys.* **1957**, *26* (6), 1750.

(113) Bertrand, J. A.; Cotton, F. A.; Dollase, W. A. *J. Am. Chem. Soc.* **1963**, *85* (9), 1349–1350.

(114) Bertrand, J. A.; Cotton, F. A.; Dollase, W. A. *Inorg. Chem.* **1963**, *2* (6), 1166–1171.

(115) Robinson, W. I.; Fergusson, J. E.; Penfold, B. R. *Proc. Chem. Soc.* **1963**, No. April, 116.

(116) Cotton, F. A. *Inorg. Chem.* **1964**, *3* (9), 1217–1220.

(117) Cotton, F. A.; Curtis, N. F.; Harris, C. B.; Johnson, B. F. G.; Lippard, S. J.; Mague, J. T.; Robinson, W. R.; Wood, J. S. *Science (80-.).* **1964**, *145* (3638), 1305–1307.

(118) Nguyen, T.; Sutton, A. D.; Brynda, M.; Fettinger, J. C.; Long, G. J.; Power, P. P. *Science (80-.).* **2005**, *310* (5749), 844–847.

(119) Stephenson, T. A. A.; Wilkinson, G. *J. Inorg. Nucl. Chem.* **1966**, *28* (10), 2285–2291.

(120) Mitchell, R. W.; Spencer, A.; Wilkinson, G. *J. Chem. Soc., Dalt. Trans.* **1973**, No. 8, 846–854.

(121) Bennett, M. J.; Caulton, K. G.; Cotton, F. A. *Inorg. Chem.* **1969**, *8* (1), 1–6.

(122) Cotton, F. A.; Ren, T. *Inorg. Chem.* **1995**, *34* (12), 3190–3193.

(123) Jiménez-Aparicio, R.; Urbanos, F. A.; Arrieta, J. M. *Inorg. Chem.* **2001**, *40* (4), 613–619.

(124) Bino, A.; Cotton, F. A.; Felthouse, T. R. *Inorg. Chem.* **1979**, *18* (9), 2599–2604.

(125) Malinski, T.; Chang, D.; Feldmann, F. N.; Bear, J. L.; Kadish, K. M. *Inorg. Chem.* **1983**, *22* (22), 3225–3233.

(126) Chakravarty, A. R.; Cotton, F. A. *Polyhedron* **1985**, *4* (11), 1957–1958.

(127) Chakravarty, A. R.; Cotton, F. A.; Tocher, D. A. *Polyhedron* **1985**, *4* (6), 1097–1102.

(128) Chakravarty, A. R.; Cotton, F. A.; Tocher, D. A. *Inorg. Chem.* **1985**, *24* (2), 172–177.

(129) Villalobos, L.; Cao, Z.; Fanwick, P. E.; Ren, T. *Dalton. Trans.* **2012**, *41* (2), 644–650.

(130) Chakravarty, A. R.; Cotton, F. A.; Schwotzer, W. *Polyhedron* **1986**, *5* (11), 1821–1827.

(131) Kadish, K. M.; Wang, L. L.; Thuriere, A.; Van Caemelbecke, E.; Bear, J. L. *Inorg. Chem.* **2003**, *42* (3), 834–843.

(132) Bear, J. L.; Li, Y. L.; Han, B. C.; VanCaemelbecke, E.; Kadish, K. M. *Inorg. Chem.* **1997**, *36* (24), 5449–5456.

(133) Legzdins, P.; Mitchell, R. W.; Rempel, G. L.; Ruddick, J. D.; Wilkinson, G. *J. Chem. Soc. A Inorganic, Phys. Theor.* **1970**, No. 0, 3322–3326.

(134) Rose, D.; Wilkinson, G. *J. Chem. Soc. (A), Inorg. Phys. Theor.* **1970**, 1791–1795.

(135) Mitchell, R. W.; Spencer, A.; Wilkinson, G. *J. Chem. Soc., Dalt. Trans.* **1973**, No. 8, 846.

(136) Kadish, K. M.; Han, B.; Shao, J.; Ou, Z.; Bear, J. L. *Inorg. Chem.* **2001**, *40* (26), 6848–6851.

(137) Kadish, K. M.; Phan, T. D.; Giribabu, L.; Shao, J. G.; Wang, L. L.; Thuriere, A.; Van Caemelbecke, E.; Bear, J. L. *Inorg. Chem.* **2004**, *43* (3), 1012–1020.

(138) Angaridis, P.; Cotton, F. A.; Murillo, C. A.; Villagran, D.; Wang, X. P. *Inorg. Chem.* **2004**, *43* (26), 8290–8300.

(139) Cotton, F. A.; Ren, T. *Inorg. Chem.* **1991**, *30* (19), 3675–3679.

(140) Lindsay, A. J.; Wilkinson, G.; Motevalli, M.; Hursthouse, M. B. *J. Chem. Soc., Dalt. Trans.* **1985**, No. 11, 2321.

(141) Lindsay, A. J.; Wilkinson, G.; Motevalli, M.; Hursthouse, M. B. *J. Chem. Soc., Dalt. Trans.* **1987**, No. 11, 2723–2736.

(142) Cotton, F. A.; Norman, J. G.; Spencer, A.; Wilkinson, G. *J. Chem. Soc. D Chem. Commun.* **1971**, No. 16, 967–968.

(143) Cotton, F. A.; Norman Jr., J. G. *Inorganica Chim. Acta* **1972**, *6* (0), 411–419.

(144) Lindsay, A. J.; Tooze, R. P.; Motevalli, M.; Hursthouse, M. B.; Wilkinson, G. *J. Chem. Soc. Chem. Commun.* **1984**, No. 20, 1383b – 1384.

(145) Cotton, F. A.; Miskowski, V. M.; Zhong, B. *J. Amer. Chem. Soc.* **1989**, *111* (16), 6177–6182.

(146) Cotton, F. A.; Labella, L.; Shang, M. Y. *Inorg. Chim. Acta.* **1992**, *197* (2), 149–158.

(147) Clark, D. L.; Green, J. C.; Redfern, C. M.; Quelch, G. E.; Hillier, I. H.; Guest, M. F. *Chem. Phys. Lett.* **1989**, *154* (4), 326–329.

(148) Quelch, G. E.; Hillier, I. H.; Guest, M. F. *J. Chem. Soc. Dalt. Trans.* **1990**, No. 10, 3075–3081.

(149) Slater, J. C. *Advances in Quantum Chemistry*, Volume 6.; Löwdin, P. O., Ed.; Elsevier Science: New York, 1973.

(150) Johnson, K. H. *Advances in Quantum Chemistry*, Volume 7.; Löwdin, P. O., Ed.; Elsevier Science: New York, 1973.

(151) Norman, J. G.; Renzoni, G. E.; Case, D. A. *J. Amer. Chem. Soc.* **1979**, *101* (18), 5256–5267.

(152) Estiú, G.; Cukiernik, F. D.; Maldivi, P.; Poizat, O. *Inorg. Chem.* **1999**, *38* (13), 3030–3039.

(153) Clark, D. L.; Green, J. C.; Redfern, C. M. *J. Chem. Soc. Dalt. Trans.* **1989**, No. 6, 1037–1044.

(154) Maldivi, P.; Giroud-Godquin, A.-M.; Marchon, J.-C.; Guillon, D.; Skoulios, A. *Chem. Phys. Lett.* **1989**, *157* (6), 552–555.

(155) Gracia, R.; Adams, H.; Patmore, N. J. *Dalton. Trans.* **2009**, No. 2, 259–261.

(156) Gracia, R.; Adams, H.; Patmore, N. J. *Inorg. Chim. Acta.* **2010**, *363* (14), 3856–3864.

(157) Gracia, R.; Patmore, N. J. *J. Clust. Sci.* **2010**, *21* (3), 339–350.

(158) Berry, M.; Garner, C. D.; Hillier, I. H.; MacDowell, A. A.; Clegg, W. *Inorganica Chim.*

Acta **1981**, *53* (0), L61–L63.

(159) Bear, J. L.; Li, Y. L.; Cui, J.; Han, B. C.; Van Caemelbecke, E.; Phan, T.; Kadish, K. M. *Inorg. Chem.* **2000**, *39* (4), 857 – +.

(160) Campos-Fernández, C. S.; Ouyang, X.; Dunbar, K. R. *Inorg. Chem.* **2000**, *39* (12), 2432–2433.

(161) Mizoguchi, T. J.; Kuzelka, J.; Spingler, B.; DuBois, J. L.; Davydov, R. M.; Hedman, B.; Hodgson, K. O.; Lippard, S. J. *Inorg. Chem.* **2001**, *40* (18), 4662–4673.

(162) Du Bois, J.; Mizoguchi, T. J.; Lippard, S. J. *Coord. Chem. Rev.* **2000**, *200*, 443–485.

(163) Bouwman, E.; Reedijk, J. *Coord. Chem. Rev.* **2005**, *249* (15-16), 1555–1581.

(164) Tolman, W. B.; Spencer, D. J. E. *Curr. Opin. Chem. Biol.* **2001**, *5* (2), 188–195.

(165) Que, J. L. *J. Chem. Soc., Dalt. Trans.* **1997**, No. 21, 3933–3940.

(166) Vincent, J. B.; Olivier-Lilley, G. L.; Averill, B. A. *Chem. Rev.* **1990**, *90* (8), 1447–1467.

(167) Kurtz, D. M. *Chem. Rev.* **1990**, *90* (4), 585–606.

(168) Zhao, M.; Helms, B.; Slonkina, E.; Friedle, S.; Lee, D.; DuBois, J.; Hedman, B.; Hodgson, K. O.; Frechet, J. M. J.; Lippard, S. J. *J. Amer. Chem. Soc.* **2008**, *130* (13), 4352–4363.

(169) Collman, J. P.; Fu, L.; Zingg, A.; Diederich, F. *Chem. Commun.* **1997**, No. 2, 193–194.

(170) Enomoto, M.; Kishimura, A.; Aida, T. *J. Amer. Chem. Soc.* **2001**, *123* (23), 5608–5609.

(171) Ogo, S.; Kabe, R.; Uehara, K.; Kure, B.; Nishimura, T.; Menon, S. C.; Harada, R.; Fukuzumi, S.; Higuchi, Y.; Ohhara, T.; Tamada, T.; Kuroki, R. *Science (80-.).* **2007**, *316* (5824), 585–587.

(172) Cammack, R. *Nature* **1995**, *373* (6515), 556–557.

(173) Volbeda, A.; Garcin, E.; Piras, C.; de Lacey, A. L.; Fernandez, V. M.; Hatchikian, E. C.; Frey, M.; Fontecilla-Camps, J. C. *J. Amer. Chem. Soc.* **1996**, *118* (51), 12989–12996.

(174) Canaguier, S.; Vaccaro, L.; Artero, V.; Ostermann, R.; Pécaut, J.; Field, M. J.; Fontecave, M. *Chem. – A Eur. J.* **2009**, *15* (37), 9350–9364.

(175) Vaccaro, L.; Artero, V.; Canaguier, S.; Fontecave, M.; Field, M. J. *Dalton. Trans.* **2010**, *39* (12), 3043–3049.

(176) Canaguier, S.; Fourmond, V.; Perotto, C. U.; Fize, J.; Pecaut, J.; Fontecave, M.; Field, M. J.; Artero, V. *Chem. Commun.* **2013**, *49* (44), 5004–5006.

(177) Canaguier, S.; Fontecave, M.; Artero, V. *Eur. J. Inorg. Chem.* **2011**, *2011* (7), 1094–1099.

(178) Tard, C.; Pickett, C. J. *Chem. Rev.* **2009**, *109* (6), 2245–2274.

(179) Simmons, T. R.; Artero, V. *Angew. Chemie Int. Ed.* **2013**, *52* (24), 6143–6145.

(180) Coufal, D. E.; Blazyk, J. L.; Whittington, D. A.; Wu, W. W.; Rosenzweig, A. C.; Lippard, S. J. *Eur. J. Biochem.* **2000**, *267* (8), 2174–2185.

(181) Lieberman, R. L.; Rosenzweig, A. C. *Crit. Rev. Biochem. Mol.* **2004**, *39* (3), 147–164.

(182) Lieberman, R. L.; Rosenzweig, A. C. *Nature* **2005**, *434* (7030), 177–182.

(183) Lieberman, R. L.; Shrestha, D. B.; Doan, P. E.; Hoffman, B. M.; Stemmler, T. L.; Rosenzweig, A. C. *Proc. Natl Acad. Sci. USA* **2003**, *100* (7), 3820–3825.

(184) Choi, D. W.; Kunz, R. C.; Boyd, E. S.; Semrau, J. D.; Antholine, W. E.; Han, J. I.; Zahn, J. A.; Boyd, J. M.; de la Mora, A. M.; DiSpirito, A. A. *J. Bacteriol.* **2003**, *185* (19), 5755–5764.

(185) Yu, S. S. F.; Chen, K. H. C.; Tseng, M. Y. H.; Wang, Y. S.; Tseng, C. F.; Chen, Y. J.; Huang, D. S.; Chan, S. I. *J. Bacteriol.* **2003**, *185* (20), 5915–5924.

(186) Chan, S. I.; Chen, K. H. C.; Yu, S. S. F.; Chen, C. L.; Kuo, S. S. J. *Biochemistry* **2004**, *43* (15), 4421–4430.

(187) Chan, S. I.; Yu, S. S. F. *Acc. Chem. Res.* **2008**, *41* (8), 969–979.

(188) Kim, H. J.; Graham, D. W.; DiSpirito, A. A.; Alterman, M. A.; Galeva, N.; Larive, C. K.; Asunskis, D.; Sherwood, P. M. A. *Science (80-.).* **2004**, *305* (5690), 1612–1615.

(189) Nguyen, H. H. T.; Elliott, S. J.; Yip, J. H. K.; Chan, S. I. *J. Biol. Chem.* **1998**, *273* (14), 7957–7966.

(190) Balasubramanian, R.; Smith, S. M.; Rawat, S.; Yatsunyk, L. A.; Stemmler, T. L.; Rosenzweig, A. C. *Nature* **2010**, *465* (7294), 115–U131.

(191) Rosenzweig, A. C. *Biochem. Soc. T.* **2008**, *36*, 1134–1137.

(192) Sazinsky, M. H.; Lippard, S. J. *Acc. Chem. Res.* **2006**, *39* (8), 558–566.

(193) Murray, L. J.; Garcia-Serres, R.; Naik, S.; Huynh, B. H.; Lippard, S. J. *J. Amer. Chem. Soc.* **2006**, *128* (23), 7458–7459.

(194) Murray, L. J.; Lippard, S. J. *Acc. Chem. Res.* **2007**, *40* (7), 466–474.

(195) Rudd, D. J.; Sazinsky, M. H.; Merkx, M.; Lippard, S. J.; Hedman, B.; Hodgson, K. O. *Inorg. Chem.* **2004**, *43* (15), 4579–4589.

(196) Merkx, M.; Kopp, D. A.; Sazinsky, M. H.; Blazyk, J. L.; Muller, J.; Lippard, S. J. *Angew. Chem., Int. Ed.* **2001**, *40* (15), 2782–2807.

(197) Liu, K. E.; Valentine, A. M.; Wang, D. L.; Huynh, B. H.; Edmondson, D. E.; Salifoglou, A.; Lippard, S. J. *J. Amer. Chem. Soc.* **1995**, *117* (41), 10174–10185.

(198) Blazyk, J. L.; Brandstetter, H.; Frederick, C. A.; Gassner, G. T.; Kopp, D. A.; Lippard, S. J.; Stahl, S. S.; Valentine, A. M.; Wagner, G.; Walters, K. J.; Whittington, D. A. *J. Inorg. Biochem.* **1999**, *74* (1-4), 37.

(199) Valentine, A. M.; Stahl, S. S.; Lippard, S. J. *J. Amer. Chem. Soc.* **1999**, *121* (16), 3876–3887.

(200) Beauvais, L. G.; Lippard, S. J. *Biochem. Biophys. Res. Co.* **2005**, *338* (1), 262–266.

(201) Beauvais, L. G.; Lippard, S. J. *J. Amer. Chem. Soc.* **2005**, *127* (20), 7370–7378.

(202) Baik, M. H.; Newcomb, M.; Friesner, R. A.; Lippard, S. J. *Chem. Rev.* **2003**, *103* (6), 2385–2419.

(203) Gherman, B. F.; Lippard, S. J.; Friesner, R. A. *J. Amer. Chem. Soc.* **2005**, *127* (3), 1025–1037.

(204) Gherman, B. F.; Baik, M. H.; Lippard, S. J.; Friesner, R. A. *J. Amer. Chem. Soc.* **2004**, *126* (9), 2978–2990.

(205) Chavez, F. A.; Ho, R. Y. N.; Pink, M.; Young, V. G.; Kryatov, S. V; Rybak-Akimova, E. V; Andres, H.; Munck, E.; Que, L.; Tolman, W. B.; Young, J. V. G.; Münck, E.; Que, J. L. *Angew. Chem., Int. Ed.* **2002**, *41* (1), 149–152.

(206) Holm, R. H.; Kennepohl, P.; Solomon, E. I. *Chem. Rev.* **1996**, *96* (7), 2239–2314.

(207) Yoon, S.; Lippard, S. J. *J. Amer. Chem. Soc.* **2005**, *127* (23), 8386–8397.

(208) Yoon, S. G.; Lippard, S. J. *J. Amer. Chem. Soc.* **2004**, *126* (51), 16692–16693.

(209) Yoon, S.; Kelly, A. E.; Lippard, S. J. *Polyhedron* **2004**, *23* (17), 2805–2812.

(210) Zhao, M.; Song, D. T.; Lippard, S. J. *Inorg. Chem.* **2006**, *45* (16), 6323–6330.

(211) Hecht, S.; Fréchet, J. M. J. *Angew. Chem., Int. Ed.* **2001**, *40* (1), 74–91.

(212) Jiang, D.-L.; Aida, T. *Chem. Commun.* **1996**, No. 13, 1523–1524.

(213) Lee, D.; Lippard, S. J. *J. Amer. Chem. Soc.* **2001**, *123* (19), 4611–4612.

(214) Carson, E. C.; Lippard, S. J. *J. Inorg. Biochem.* **2006**, *100* (5-6), 1109–1117.

(215) Carson, E. C.; Lippard, S. J. *Inorg. Chem.* **2006**, *45* (2), 828–836.

(216) Carson, E. C.; Lippard, S. J. *Inorg. Chem.* **2006**, *45* (2), 837–848.

(217) Moreira, R. F.; Tshuva, E. Y.; Lippard, S. J. *Inorg. Chem.* **2004**, *43* (14), 4427–4434.

(218) Kim, Y. J.; Feng, X. D.; Lippard, S. J. *Inorg. Chem.* **2007**, *46* (15), 6099–6107.

(219) Friedle, S.; Reisner, E.; Lippard, S. J. *Chem. Soc. Rev.* **2010**, *39* (8), 2768–2779.

(220) Tshuva, E. Y.; Lippard, S. J. *Chem. Rev.* **2004**, *104* (2), 987–1011.

(221) Xue, G.; Wang, D.; De Hont, R.; Fiedler, A. T.; Shan, X.; Münck, E.; Que, L. *Proc. Natl Acad. Sci. USA* **2007**, *104* (52), 20713–20718.

(222) Xue, G.; Fiedler, A. T.; Martinho, M.; Munck, E.; Que Jr., L. *Proc. Natl Acad. Sci. USA* **2008**, *105* (52), 20615–20620.

(223) Xue, G.; De Hont, R.; Münck, E.; Que, L. *Nat. Chem.* **2010**, *2* (5), 400–405.

(224) Gerhardt, C. *Annalen* **1858**, *108*, 219.

(225) Barker, J.; Kilner, M. *Coord. Chem. Rev.* **1994**, *133* (0), 219–300.

(226) Shriner, R. L.; Neumann, F. W. *Chem. Rev.* **1944**, *35* (3), 351–425.

(227) Taylor, E. C.; Ehrhart, W. A. *J. Org. Chem.* **1963**, *28* (4), 1108–1112.

(228) Ren, T. *Coord. Chem. Rev.* **1998**, *175* (1), 43–58.

(229) Cotton, F. A.; Haefner, S. C.; Matonic, J. H.; Wang, X.; Murillo, C. A. *Polyhedron* **1997**, *16* (3), 541–550.

(230) Ren, T.; DeSilva, V.; Zou, G.; Lin, C.; Daniels, L. M.; Campana, C. F.; C. Alvarez, J. *Inorg. Chem. Commun.* **1999**, *2* (7), 301–304.

(231) Angaridis, P.; Berry, J. F.; Cotton, F. A.; Lei, P.; Lin, C.; Murillo, C. A.; Villagrán, D. *Inorg. Chem. Comm.* **2004**, *7* (1), 9–13.

(232) Barral, M. C.; Herrero, S.; Jiménez-Aparicio, R.; Torres, M. R.; Urbanos, F. A. *Inorg. Chem. Comm.* **2004**, *7* (1), 42–46.

(233) Angaridis, P.; Berry, J. F.; Cotton, F. A.; Murillo, C. A.; Wang, X. *J. Am. Chem. Soc.* **2003**, *125* (34), 10327–10334.

(234) Wong, K.-T.; Lehn, J.-M.; Peng, S.-M.; Lee, G.-H. *Chem. Commun.* **2000**, No. 22, 2259–2260.

(235) Xu, G.; Ren, T. *Inorg. Chem.* **2001**, *40* (12), 2925–2927.

(236) Lin, C.; Ren, T.; Valente, E. J.; Zubkowski, J. D. *J. Chem. Soc., Dalt. Trans.* **1998**, No. 4, 571–576.

(237) Chen, W.-Z.; Ren, T. *Organometallics* **2005**, *24* (11), 2660–2669.

(238) Cao, Z.; Xi, B.; Jodoin, D. S.; Zhang, L.; Cummings, S. P.; Gao, Y.; Tyler, S. F.; Fanwick, P. E.; Crutchley, R. J.; Ren, T. *J. Am. Chem. Soc.* **2014**, *136* (34), 12174–12183.

(239) Añez, E.; Herrero, S.; Jiménez-Aparicio, R.; Priego, J. L.; Torres, M. R.; Urbanos, F. A. *Polyhedron* **2010**, *29* (1), 232–237.

(240) Wesemann, J. L.; Chisholm, M. H. *Inorg. Chem.* **1997**, *36* (15), 3258–3267.

(241) Cole, M. L.; Davies, A. J.; Jones, C.; Junk, P. C. *Z. Anorg. Allg. Chem.* **2011**, *637* (1), 50–55.

(242) Cole, M. L.; Junk, P. C.; Louis, L. M. *J. Chem. Soc., Dalt. Trans.* **2002**, No. 20, 3906–3914.

(243) Cole, M. L.; Davies, A. J.; Jones, C.; Junk, P. C. *J. Organomet. Chem.* **2004**, *689* (19), 3093–3107.

(244) Cole, M. L.; Davies, A. J.; Jones, C.; Junk, P. C. *New J. Chem.* **2005**, *29* (11), 1404–1408.

(245) Boer, R. T.; Cole, M. L.; Junk, P. C. *New J. Chem.* **2005**, *29* (1), 128.

(246) Cole, M. L.; Davies, A. J.; Jones, C.; Junk, P. C. *J. Organomet. Chem.* **2007**, *692* (12), 2508–2518.

(247) Drew, M. G. B.; Wilkins, J. D. *J. Chem. Soc. Dalt. Trans.* **1974**, No. 18, 1973–1977.

(248) Kondo, H.; Matsubara, K.; Nagashima, H. *J. Am. Chem. Soc.* **2002**, *124* (4), 534–535.

(249) Kondo, H.; Yamaguchi, Y.; Nagashima, H. *J. Amer. Chem. Soc.* **2001**, *123* (3), 500–501.

(250) Hayashida, T.; Yamaguchi, Y.; Kirchner, K.; Nagashima, H. *Chem. Lett.* **2001**, *30* (10), 954–955.

(251) Yamaguchi, Y.; Nagashima, H. *Organometallics* **2000**, *19* (5), 725–727.

(252) Cotton, F. A.; Daniels, L. M.; Murillo, C. A. *Inorg. Chem.* **1993**, *32* (13), 2881–2885.

(253) Cotton, F. A.; Daniels, L. M.; Murillo, C. A. *Angew. Chem. Int. Ed. Engl.* **1992**, *31* (6), 737–738.

(254) Cotton, F. A.; Wojtczak, W. A. *Polyhedron* **1994**, *13* (9), 1337–1341.

(255) Cotton, F. A.; Daniels, L. M.; Feng, X. J.; Maloney, D. J.; Matonic, J. H.; Murillo, C. A. *Inorg. Chim. Acta.* **1997**, *256* (2), 291–301.

(256) Cotton, F. A.; Ren, T. *J. Amer. Chem. Soc.* **1992**, *114* (6), 2237–2242.

(257) Cotton, F. A.; Feng, X. *Inorg. Chem.* **1989**, *28* (6), 1180–1183.

(258) Cotton, F. A.; Daniels, L. M.; Murillo, C. A. *Inorg. Chim. Acta.* **1994**, *224* (1-2), 5–9.

(259) Cotton, F. A.; Daniels, L. M.; Matonic, J. H.; Murillo, C. A. *Inorg. Chim. Acta.* **1997**, *256* (2), 277–282.

(260) Cotton, F. A.; Daniels, L. M.; Falvello, L. R.; Murillo, C. A. *Inorg. Chim. Acta.* **1994**, *219* (1-2), 7–10.

(261) Cotton, F. A.; Daniels, L. M.; Maloney, D. J.; Murillo, C. A. *Inorg. Chim. Acta.* **1996**, *242* (1-2), 31–42.

(262) Cotton, F. A.; Daniels, L. M.; Maloney, D. J.; Murillo, C. A. *Inorg. Chim. Acta.* **1996**, *252* (1-2), 293–298.

(263) Cotton, F. A.; Daniels, L. M.; Falvello, L. R.; Matonic, J. H.; Murillo, C. A.; Wang, X.; Zhou, H. *Inorg. Chim. Acta.* **1997**, *266* (1), 91–102.

(264) Cotton, F. A.; Luck, R. L.; Son, K.-A. *Inorg. Chim. Acta.* **1991**, *184* (2), 177–183.

(265) Siegbahn, P. E. M. *Inorg. Chem.* **1999**, *38* (12), 2880–2889.

(266) Britovsek, G. J. P.; England, J.; White, A. J. P. *Inorg. Chem.* **2005**, *44* (22), 8125–8134.

(267) Britovsek, G. J. P.; England, J.; Spitzmesser, S. K.; White, A. J. P.; Williams, D. J. *Dalton. Trans.* **2005**, No. 5, 945–955.

(268) England, J.; Britovsek, G. J. P.; Rabadia, N.; White, A. J. P. *Inorg. Chem.* **2007**, *46* (9), 3752–3767.

(269) England, J.; Davies, C. R.; Banaru, M.; White, A. J. P.; Britovsek, G. J. P. *Adv. Synth. Catal.* **2008**, *350* (6), 883–897.

(270) England, J.; Gondhia, R.; Bigorra-Lopez, L.; Petersen, A. R.; White, A. J. P.; Britovsek, G. J. P. *Dalton. Trans.* **2009**, No. 27, 5319–5334.

(271) Timmer, G. H.; Berry, J. F. *Comptes Rendus Chim.* **2012**, *15* (2–3), 192–201.

(272) Vendemiati, B.; Prini, G.; Meetsma, A.; Hessen, B.; Teuben, J. H.; Traverso, O. *Eur. J. Inorg. Chem.* **2001**, *2001* (3), 707–711.

(273) Lim, B. S.; Rahtu, A.; Park, J.-S.; Gordon, R. G. *Inorg. Chem.* **2003**, *42* (24), 7951–7958.

(274) Nijhuis, C. A.; Jellema, E.; Sciarone, T. J. J.; Meetsma, A.; Budzelaar, P. H. M.; Hessen, B. *Eur. J. Inorg. Chem.* **2005**, No. 11, 2089–2099.

(275) Sciarone, T. J. J.; Nijhuis, C. A.; Meetsma, A.; Hessen, B. *Dalton. Trans.* **2006**, No. 41, 4896–4904.

(276) Sciarone, T. J. J.; Nijhuis, C. A.; Meetsma, A.; Hessen, B. *Organometallics* **2008**, *27* (9), 2058–2065.

(277) Jellema, E.; Sciarone, T. J. J.; Navarrete, N. M.; Hettinga, M. J.; Meetsma, A.; Hessen, B. *Eur. J. Inorg. Chem.* **2011**, *2011* (1), 91–100.

(278) Schmidt, J. A. R.; Arnold, J. *J. Chem. Soc., Dalt. Trans.* **2002**, No. 18, 3454–3461.

(279) Clark, J. A.; Kilner, M.; Pietrzykowski, A. *Inorganica Chim. Acta* **1984**, *82* (1), 85–92.

(280) Cotton, F. A.; Daniels, L. M.; Falvello, L. R.; Matonic, J. H.; Murillo, C. A. *Inorganica Chim. Acta* **1997**, *256* (2), 269–275.

(281) Zall, C. M.; Zherebetskyy, D.; Dzubak, A. L.; Bill, E.; Gagliardi, L.; Lu, C. C. *Inorg. Chem.* **2012**, *51* (1), 728–736.

(282) Bragg, W. H. *Nature* **1923**, *111* (2790), 532–532.

(283) Cotton, F. A.; Daniels, L. M.; Murillo, C. A.; Schooler, P. *J. Chem. Soc. Dalt. Trans.* **2000**, No. 13, 2001–2005.

(284) Hagen, K. S. *Inorg. Chem.* **2000**, *39* (25), 5867–5869.

(285) Payne, S. C.; Hagen, K. S. *J. Amer. Chem. Soc.* **2000**, *122* (27), 6399–6410.

(286) Abdou, H. E.; Mohamed, A. A.; López-de-Luzuriaga, J. M.; Fackler Jr., J. P. *J. Clust. Sci.* **2004**, *15* (4), 397–411.

(287) Abdou, H. E.; Mohamed, A. A.; López-de-Luzuriaga, J. M.; Monge, M.; Fackler Jr., J. P. *Inorg. Chem.* **2012**, *51* (4), 2010–2015.

(288) Roberts, R. M. *J. Amer. Chem. Soc.* **1949**, *71* (11), 3848–3849.

(289) Roberts, R. M. *J. Am. Chem. Soc.* **1950**, *72* (8), 3603–3608.

(290) Roberts, R. M.; DeWolfe, R. H.; Ross, J. H. *J. Amer. Chem. Soc.* **1951**, *73* (5), 2277–2281.

(291) Roberts, R. M.; DeWolfe, R. H. *J. Am. Chem. Soc.* **1954**, *76* (9), 2411–2414.

(292) Archibald, S. J.; Alcock, N. W.; Busch, D. H.; Whitcomb, D. R. *J. Clust. Sci.* **2000**, *11* (1), 261–283.

(293) Abdou, H. E.; Mohamed, A. A.; Fackler Jr., J. P. *J. Clust. Sci.* **2007**, *18* (3), 630–641.

(294) Abdou, H. E.; Mohamed, A. A.; Fackler Jr., J. P. *J. Chinese Chem. Soc.* **2007**, *54* (5), 1107–1113.

(295) Lin, C.; Protasiewicz, J. D.; Smith, E. T.; Ren, T. *Inorg. Chem.* **1996**, *35* (22), 6422–6428.

(296) Ren, T.; Lin, C.; Valente, E. J.; Zubkowski, J. D. *Inorganica Chim. Acta* **2000**, *297* (1–2), 283–290.

(297) Lin, C.; Protasiewicz, J. D.; Ren, T. *Inorg. Chem.* **1996**, *35* (25), 7455–7458.

(298) Carlson-Day, K. M.; Eglin, J. L.; Lin, C.; Smith, L. T.; Staples, R. J.; Wipf, D. O. *Polyhedron* **1999**, *18* (6), 817–824.

(299) Harada, Y.; Ikeue, T.; Ide, Y.; Kimura, Y.; Hiromitsu, I.; Yoshioka, D.; Mikuriya, M.;

Kataoka, Y.; Handa, M. *Inorganica Chim. Acta* **2015**, *424*, 186–193.

(300) Anulewicz, R.; Marek Krygowski, T.; Pniewska, B. *J. Crystallogr. Spectrosc. Res.* **1987**, *17* (5), 661–670.

(301) Anulewicz, R.; Krygowski, T. M.; Pniewska, B. *Acta Crystallogr. Sect. C* **1990**, *46* (11), 2121–2123.

(302) Anulewicz, R.; Wawer, I.; Krygowski, T. M.; Männle, F.; Limbach, H.-H. *J. Am. Chem. Soc.* **1997**, *119* (50), 12223–12230.

(303) Ren, T.; Radak, S.; Ni, Y.; Xu, G.; Lin, C.; Shaffer, K.; DeSilva, V. *J. Chem. Crystallogr.* **2002**, *32* (7), 197–203.

(304) Arnold, D. I.; Cotton, F. A.; Maloney, D. J.; Matonic, J. H.; Murillo, C. A. *Polyhedron* **1997**, *16* (1), 133–141.

(305) Cotton, F. A.; Daniels, L. M.; Maloney, D. J.; Matonic, J. H.; Murillo, C. A. *Polyhedron* **1994**, *13* (5), 815–823.

(306) Senko, M. .

(307) Cotton, F. A.; Luck, R. L.; Son, K.-A. *Inorg. Chim. Acta.* **1991**, *179* (1), 11–15.

(308) Hardt, H.-D.; Möller, W. *Z. Anorg. Allg. Chem.* **1961**, *313* (1-2), 57–69.

(309) Weber, B.; Betz, R.; Bauer, W.; Schlamp, S. *Z. Anorg. Allg. Chem.* **2011**, *637* (1), 102–107.

(310) Herold, S.; Lippard, S. J. *J. Amer. Chem. Soc.* **1997**, *119* (1), 145–156.

(311) Tulinsky, A.; Worthington, C. R.; Pignataro, F. *Acta Crystallogr.* **1959**, *12* (9), 623–626.

(312) Tulinsky, A.; Worthington, C. R. *Acta Crystallogr.* **1959**, *12* (9), 626–634.

(313) Tulinsky, A. *Acta Crystallogr.* **1959**, *12* (9), 634–637.

(314) Sheldrick, G. M. University of Gottingen, Germany 1996.

(315) Sheldrick, G. M. *Acta Cryst.* **2008**, *A46*, 112–122.

(316) Bruker. Bruker Analytical X-Ray Instruments Inc., Madison, WI 2008.

(317) Spek, A. *Acta Crystallogr. Sect. D* **2009**, *65* (2), 148–155.

(318) van der Sluis, P.; Spek, A. L. *Acta Crystallogr. Sect. A* **1990**, *46* (3), 194–201.

(319) Chai, C.; Armarego, W. L. F. *Purification of Laboratory Chemicals*, 6th ed.; Butterworth-Heinemann, 2009.

(320) Tanaka, S.; Mashima, K. *Inorg. Chem.* **2011**, *50* (22), 11384–11393.

(321) Mohamed, A. A.; Abdou, H. E.; Irwin, M. D.; López-de-Luzuriaga, J. M.; Fackler Jr., J. P. *J. Clust. Sci.* **2003**, *14* (3), 253–266.

(322) Long, A. K. M.; Yu, R. P.; Timmer, G. H.; Berry, J. F. *J. Amer. Chem. Soc.* **2010**, *132* (35), 12228–12230.

(323) Long, A. K. M.; Timmer, G. H.; Pap, J. S.; Snyder, J. L.; Yu, R. P.; Berry, J. F. *J. Amer. Chem. Soc.* **2011**, *133* (33), 13138–13150.

(324) Corcos, A. R.; Long, A. K. M.; Guzei, I. A.; Berry, J. F. *Eur. J. Inorg. Chem.* **2013**, *2013* (22-23), 3808–3811.

(325) Harvey, M. E.; Musaev, D. G.; Du Bois, J. *J. Am. Chem. Soc.* **2011**, *133* (43), 17207–17216.

(326) Villalobos, L.; Barker Paredes, J. E.; Cao, Z.; Ren, T. *Inorg. Chem.* **2013**, *52* (21), 12545–12552.

(327) Khokhar, M. D.; Shukla, R. S.; Jasra, R. V. *J. Mol. Catal. A Chem.* **2009**, *299* (1–2), 108–116.

(328) Komiya, N.; Nakae, T.; Sato, H.; Naota, T. *Chem. Commun.* **2006**, No. 46, 4829–4831.

(329) Liu, Y.; Nocera, D. G. *J. Phys. Chem. C* **2014**, *118* (30), 17060–17066.

(330) Huynh, M.; Bediako, D. K.; Nocera, D. G. *J. Am. Chem. Soc.* **2014**, *136* (16), 6002–6010.

(331) Esswein, A. J.; Surendranath, Y.; Reece, S. Y.; Nocera, D. G. *Energy Environ. Sci.* **2011**, *4* (2), 499–504.

(332) Kanan, M. W.; Surendranath, Y.; Nocera, D. G. *Chem. Soc. Rev.* **2009**, *38* (1), 109–114.

(333) Teets, T. S.; Nocera, D. G. *Inorg. Chem.* **2012**, *51* (13), 7192–7201.

(334) Surendranath, Y.; Kanan, M. W.; Nocera, D. G. *J. Am. Chem. Soc.* **2010**, *132* (46), 16501–16509.

(335) Nocera, D. G. *Acc. Chem. Res.* **2012**, *45* (5), 767–776.

(336) Bediako, D. K.; Lassalle-Kaiser, B.; Surendranath, Y.; Yano, J.; Yachandra, V. K.; Nocera, D. G. *J. Am. Chem. Soc.* **2012**, *134* (15), 6801–6809.

(337) Bediako, D. K.; Costentin, C.; Jones, E. C.; Nocera, D. G.; Savéant, J.-M. *J. Am. Chem. Soc.* **2013**, *135* (28), 10492–10502.

(338) Farrow, C. L.; Bediako, D. K.; Surendranath, Y.; Nocera, D. G.; Billinge, S. J. L. *J. Am. Chem. Soc.* **2013**, *135* (17), 6403–6406.

(339) Kataoka, Y.; Miyazaki, Y.; Sato, K.; Saito, T.; Nakanishi, Y.; Kiatagwa, Y.; Kawakami, T.; Okumura, M.; Yamaguchi, K.; Mori, W. *Supramol. Chem.* **2011**, *23* (3-4), 287–296.

(340) Barral, M. C.; Jiménez-Aparicio, R.; Priego, J. L.; Royer, E. C.; Urbanos, F. A.; Amador, U. *Inorganica Chim. Acta* **1998**, *279* (1), 30–36.

(341) Cotton, F. A.; Matusz, M. *J. Amer. Chem. Soc.* **1988**, *110* (17), 5761–5764.

(342) Hillard, E. *Curr. Inorg. Chem.* **2013**, *3* (2), 112–143.

(343) Chisholm, M. H.; D'Acchioli, J. S.; Hadad, C. M. *J. Clust. Sci.* **2006**, *18* (1), 27–49.

(344) Norman, J. G.; Kolari, H. J.; Gray, H. B.; Trogler, W. C. *Inorg. Chem.* **1977**, *16* (5), 987–993.

(345) Klotzbuecher, W.; Ozin, G. A.; Norman, J. G.; Kolari, H. J. *Inorg. Chem.* **1977**, *16* (11), 2871–2877.

(346) Norman, J. G.; Kolari, H. J. *J. Chem. Soc. Chem. Commun.* **1975**, No. 15, 649–651.

(347) Rizzi, G. A.; Casarin, M.; Tondello, E.; Piraino, P.; Granozzi, G. *Inorg. Chem.* **1987**, *26* (20), 3406–3409.

(348) Cotton, F. A.; Feng, X.; Matusz, M. *Inorg. Chem.* **1989**, *28* (3), 594–601.

(349) Becke, A. D. *J. Chem. Phys.* **1993**, *98* (2), 1372.

(350) Becke, A. D. *J. Chem. Phys.* **1993**, *98* (7), 5648.

(351) Becke, A. D. *Phys. Rev. A* **1988**, *38* (6), 3098–3100.

(352) Lee, C.; Yang, W.; Parr, R. G. *Phys. Rev. B* **1988**, *37* (2), 785–789.

(353) Perdew, J. P.; Ernzerhof, M.; Burke, K. *J. Chem. Phys.* **1996**, *105* (22), 9982.

(354) Stephens, P. J.; Devlin, F. J.; Chabalowski, C. F.; Frisch, M. J. *J. Phys. Chem.* **1994**, *98* (45), 11623–11627.

(355) Kim, K.; Jordan, K. D. *J. Phys. Chem.* **1994**, *98* (40), 10089–10094.

(356) Paier, J.; Marsman, M.; Kresse, G. *J. Chem. Phys.* **2007**, *127* (2), 024103.

(357) Becke, A. D. *J. Chem. Phys.* **1996**, *104* (3), 1040.

(358) Davidson, E. R.; Hagstrom, S. A.; Chakravorty, S. J.; Umar, V. M.; Fischer, C. F. *Phys. Rev. A* **1991**, *44* (11), 7071–7083.

(359) Tao, J.; Gori-Giorgi, P.; Perdew, J. P.; McWeeny, R. *Phys. Rev. A* **2001**, *63* (3), 32513.

(360) Bursten, B. E.; Chisholm, M. H.; D'Acchioli, J. S. *Inorg. Chem.* **2005**, *44* (16), 5571–5579.

(361) Castro, M. A.; Roitberg, A. E.; Cukiernik, F. D. *Inorg. Chem.* **2008**, *47* (11), 4682–4690.

(362) Sizova, O. V; Skripnikov, L. V; Sokolov, A. Y.; Lyubimova, O. O. *J. Struct. Chem.* **2007**, *48* (1), 28–36.

(363) Castro, M. A.; Roitberg, A. E.; Cukiernik, F. D. *J. Chem. Theory Comput.* **2013**, *9* (6), 2609–2616.

(364) Su, J.; Shi, L.; Sun, X.; Guan, W.; Wu, Z. *Dalton. Trans.* **2011**, *40* (42), 11131–11137.

(365) Gracia, R.; Patmore, N. J. *Dalton. Trans.* **2013**, *42* (36), 13118–13125.

(366) Perdew, J. P.; Burke, K.; Ernzerhof, M. *Phys. Rev. Lett.* **1996**, *77* (18), 3865–3868.

(367) Perdew, J. P.; Burke, K.; Ernzerhof, M. *Phys. Rev. Lett.* **1997**, *78* (7), 1396.

(368) Cotton, F. A.; Feng, X. J. *J. Amer. Chem. Soc.* **1997**, *119* (32), 7514–7520.

(369) Reiher, M.; Salomon, O.; Artur Hess, B. *Theor. Chem. Acc.* **2001**, *107* (1), 48–55.

(370) Andrae, D.; Hauessermann, U.; Dolg, M.; Preuss, H. *Theor. Chim. Acta.* **1990**, *77* (2), 123.

(371) Hehre, W. J.; Radom, L.; Schleyer, P. V. R.; Pople, J. A. *Ab Initio Molecular Orbital Theory*; John Wiley & Sons, New York, 1986.

(372) Stratmann, R. E.; Scuseria, G. E.; Frisch, M. J. *J. Chem. Phys.* **1998**, *109* (19), 8218.

(373) Casida, M. E.; Jamorski, C.; Casida, K. C.; Salahub, D. R. *J. Chem. Phys.* **1998**, *108* (11),

4439.

(374) Bauernschmitt, R.; Ahlrichs, R. *Chem. Phys. Lett.* **1996**, *256* (4–5), 454–464.

(375) Szabo, A.; Ostlund, N. *Modern Quantum Chemistry: Introduction to Advanced Electronic Structure Theory*, 3rd ed.; Dover Publications, Inc.: Mineola, NY, 1996.

(376) Ring, S.; Meijer, A. J. H. M.; Patmore, N. J. *Polyhedron* **2016**, *103*, 87–93.

(377) Drysdale, K. D.; Beck, E. J.; Stanley Cameron, T.; Robertson, K. N.; A.S. Aquino, M. *Inorg. Chim. Acta.* **1997**, *256* (2), 243–252.

(378) Bear, J. L.; Han, B. C.; Huang, S. R.; Kadish, K. M. *Inorg. Chem.* **1996**, *35* (10), 3012–3021.

(379) Chen, W. Z.; Ren, T. *Inorg. Chem.* **2003**, *42* (26), 8847–8852.

(380) Bear, J. L.; Li, Y.; Han, B.; Van Caemelbecke, E.; Kadish, K. M. *Inorg. Chem.* **1996**, *35* (10), 3053–3055.

(381) Pap, J. S.; DeBeer George, S.; Berry, J. F. *Angew. Chemie Int. Ed.* **2008**, *47* (52), 10102–10105.

(382) Evans, D. F. *J. Chem. Soc.* **1959**, No. 0, 2003–2005.

(383) Schubert, E. M. *J. Chem. Educ.* **1992**, *69* (1), 62.

(384) Ostfeld, D.; Cohen, I. A. *J. Chem. Educ.* **1972**, *49* (12), 829.

(385) Evans, D. F.; James, T. A. *J. Chem. Soc. Dalt. Trans.* **1979**, No. 4, 723–726.

(386) Ruzzi, M.; Sartori, E.; Moscatelli, A.; Khudyakov, I. V; Turro, N. J. *J. Phys. Chem. A* **2013**, *117* (25), 5232–5240.

(387) Ryde, K.; Tocher, D. A. *Inorg. Chim. Acta.* **1986**, *118* (2), L49–L51.

(388) Barral, M. C.; Jiménez-Aparicio, R.; Priego, J. L.; Royer, E. C.; Urbanos, F. A.; Monge, A.; Ruíz-Valero, C. *Polyhedron* **1993**, *12* (24), 2947–2953.

(389) Chakravarty, A. R.; Cotton, F. A.; Tocher, D. A. *J. Am. Chem. Soc.* **1984**, *106* (21), 6409–6413.

(390) Delgado, P.; Gonzalez-Prieto, R.; Jimenez-Aparicio, R.; Perles, J.; Priego, J. L. J. L.; Torres, R. M.; González-Prieto, R.; Jiménez-Aparicio, R.; Perles, J.; Priego, J. L. J. L.; Torres, R. M. *Dalton. Trans.* **2012**, *41* (38), 11866–11874.

(391) Chen, S.-T.; Wu, S.-H.; Wang, K.-T. *Synthesis (Stuttg).* **1989**, *1989* (01), 37–39.

(392) Saednya, A.; Hart, H. *Synthesis (Stuttg).* **1996**, No. 12, 1455–1458.

(393) Du, C. J. F.; Hart, H.; Ng, K. K. D. *J. Org. Chem.* **1986**, *51* (16), 3162–3165.

(394) Hart, H.; Rajakumar, P. *Tetrahedron* **1995**, *51* (5), 1313–1336.

(395) Krishnamurthy, V. M.; Semetey, V.; Bracher, P. J.; Shen, N.; Whitesides, G. M. *J. Am. Chem. Soc.* **2007**, *129* (5), 1312–1320.

Appendix A – MALDI-TOF-MS Spectra

A-1 $FeCl_2(H[amidinate])_2$ intermediates

A-1-1 $FeCl_2(H[TMOPhFm])_2$ (III)

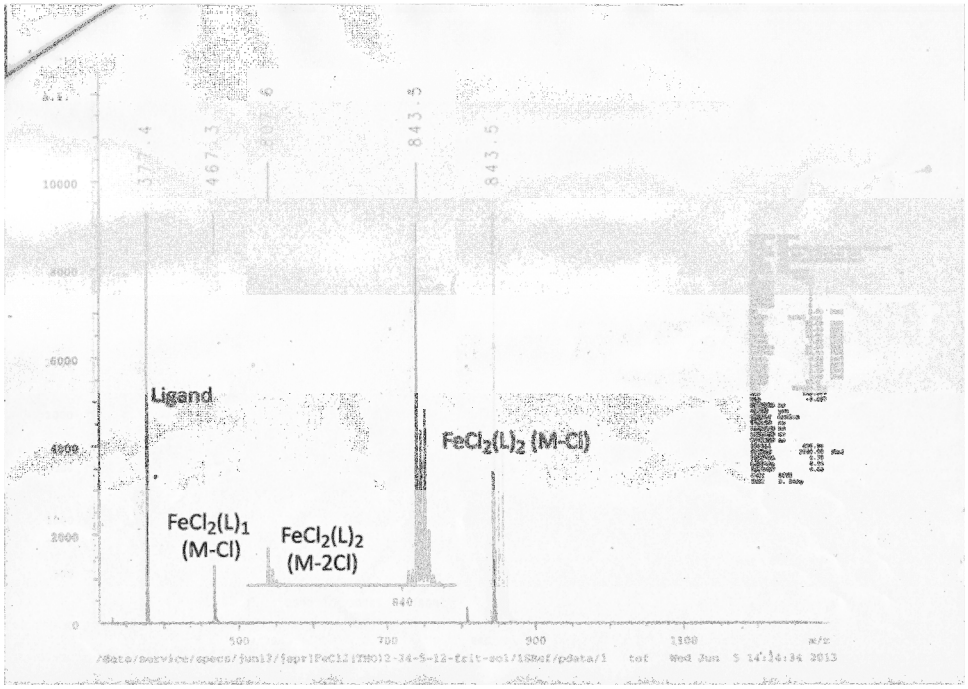

A-2 Attempted synthesis of $Fe_2(DMOPhFm])_4$

A-2-1 Formation of $Fe_2^{II,I}(DMOPhFm)_3$ on addition of ^{n}BuLi at 0 °C

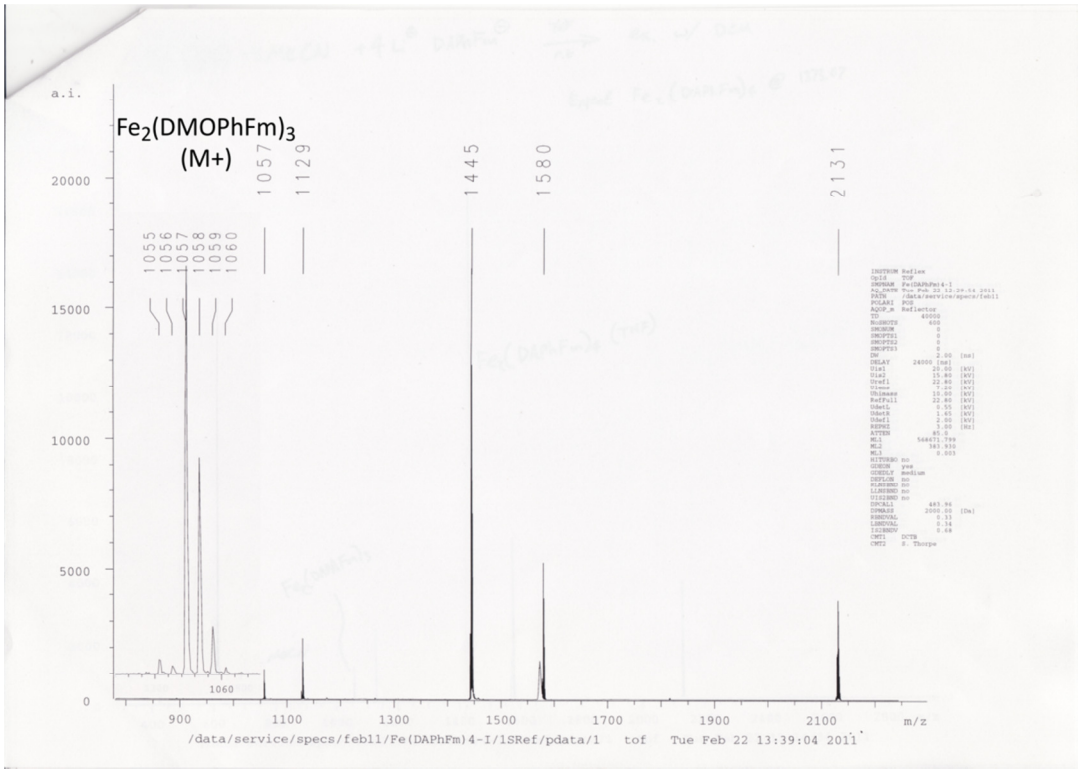

A-2-2 Product mixtures favouring $Fe_3^{II,II,I}(O)(amidinate)_3$ (VII)

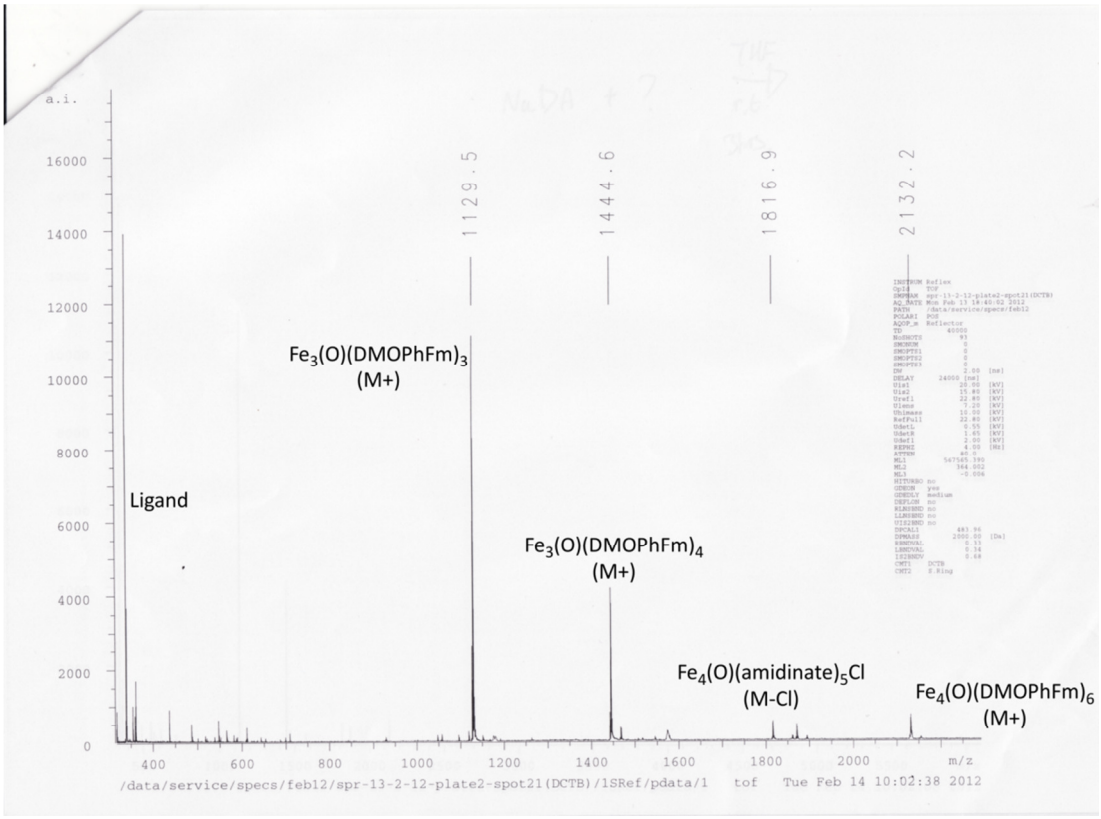

A-2-3 Mixtures of (VII) & (VIII) as isolated in DCM

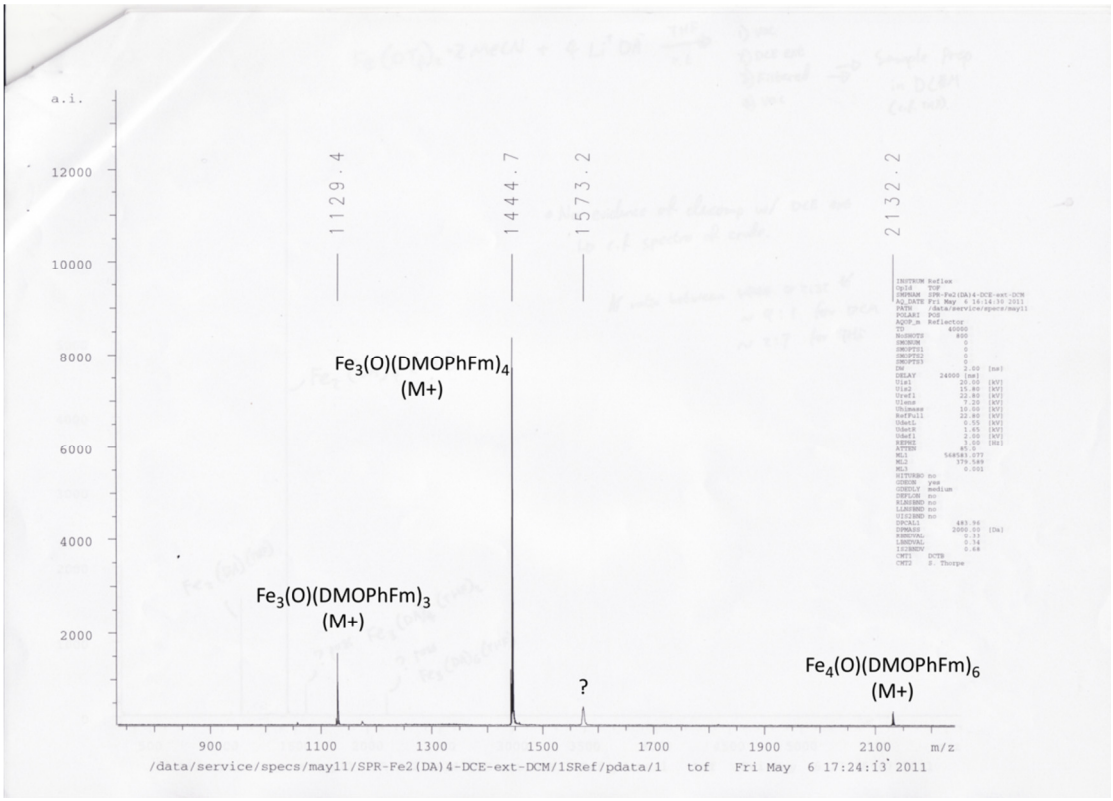

A-2-4 Mixtures of (VII) & (VIII) on prolonged exposure to THF

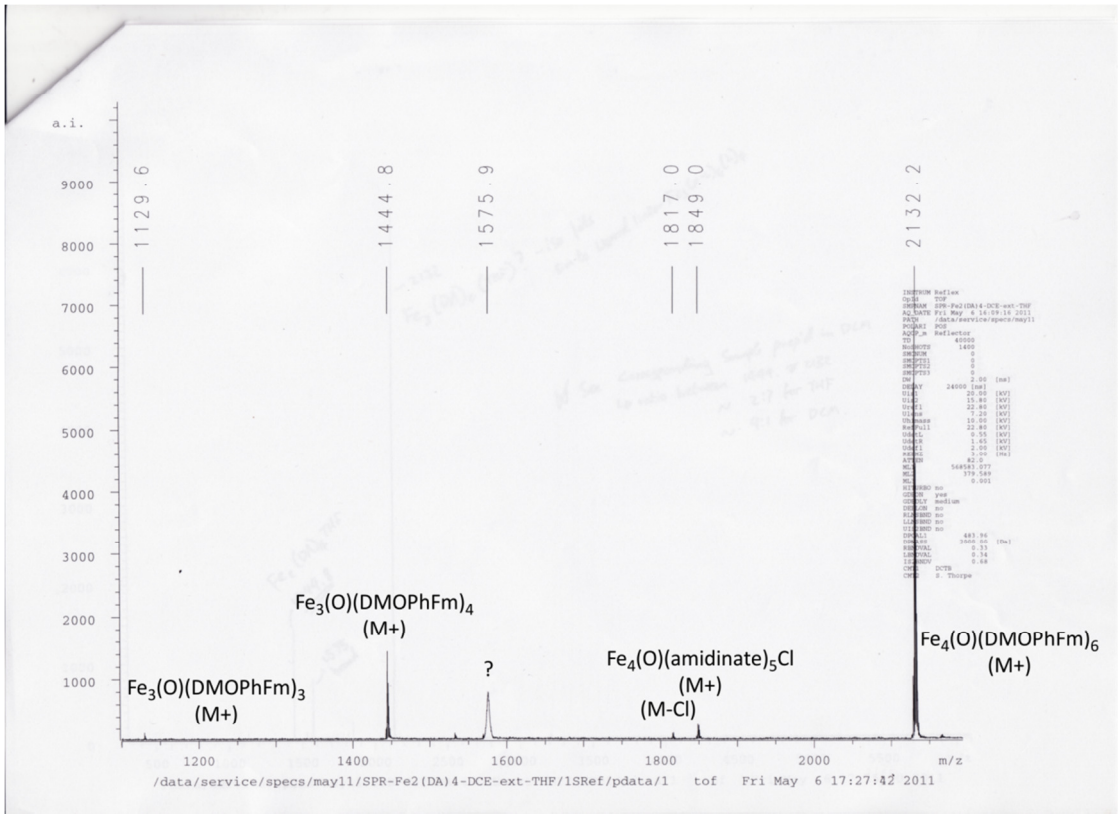

A-2-5 Mixtures of (VII) & (VIII) on exposure to trace H_2O on storage

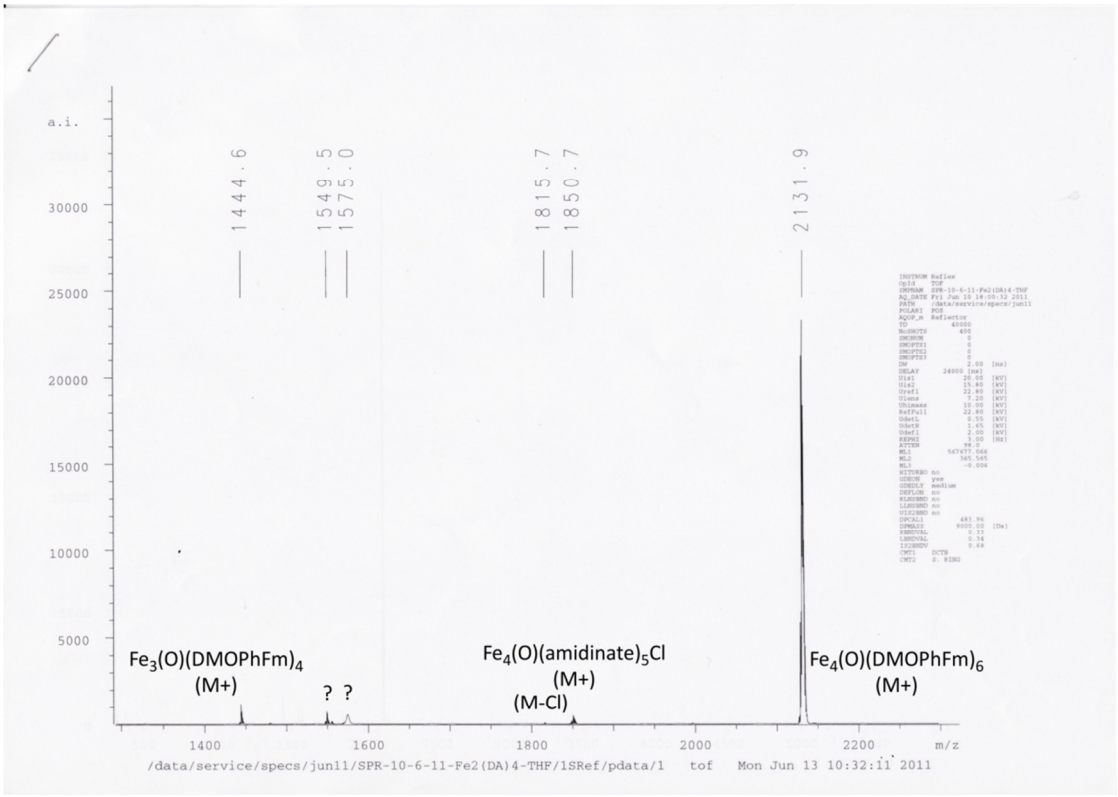
a.i.
30000
25000
20000
15000
10000
5000
1444.6
1549.5
1575.0
1815.7
1850.7
2131.9
Fe3(O)(DMOPhFm)4
(M+)
? ?
Fe4(O)(amidinate)5Cl
(M+)
(M-Cl)
Fe4(O)(DMOPhFm)6
(M+)
1400
1600
1800
2000
2200
m/z
/data/service/specs/jun11/SPR-10-6-11-Fe2(DA)4-THF/1SRef/pdata/1 tof Mon Jun 13 10:32:11 2011

Appendix B – Crystal and structure refinement tables

B-1 H[DMOPhFm]

Identification code	H[DMOPhFm]
Empirical formula	$C_{17}H_{20}N_2O_4$
Formula weight	316.35
Temperature/K	100
Crystal system	triclinic
Space group	P-1
a/Å	6.2333(3)
b/Å	10.7462(6)
c/Å	12.5093(7)
α/°	79.972(3)
β/°	88.296(3)
γ/°	75.924(3)
Volume/Å^3	800.28(7)
Z	2
ρ_{calc}g/cm^3	1.313
μ/mm^{-1}	0.094
F(000)	336.0
Crystal size/mm^3	0.4 × 0.2 × 0.1
Radiation	MoKα (λ = 0.71073)
2Θ range for data collection/°	3.3 to 55.2
Index ranges	-8 ≤ h ≤ 8, -13 ≤ k ≤ 13, -16 ≤ l ≤ 16
Reflections collected	13717
Independent reflections	3675 [Rint = 0.0598, Rsigma = 0.0487]
Data/restraints/parameters	3675/0/212
Goodness-of-fit on F^2	1.048
Final R indexes [I>=2σ (I)]	R1 = 0.0448, wR2 = 0.1142
Final R indexes [all data]	R1 = 0.0584, wR2 = 0.1228
Largest diff. peak/hole / e Å^{-3}	0.23/-0.23

B-2 $Fe_4(O)(DMOPhFm)_6$ (IX)

Identification code	(IX) / NJP246-P-1
Empirical formula	$C_{102}H_{114}N_{12}O_{25}Fe_4$
Formula weight	2131.45
Temperature/K	100
Crystal system	Triclinic
Space group	P-1
a/Å	13.3180(7)
b/Å	14.2526(6)
c/Å	14.8626(7)
α/°	106.728(2)
β/°	113.190(2)
γ/°	90.521(2)
Volume/$Å^3$	2459.3(2)
Z	1
$\rho_{calc}g/cm^3$	1.439
μ/mm^{-1}	0.661
F(000)	1114.0
Crystal size/mm^3	0.25 x 0.2 x0.15
Radiation	MoKα (λ = 0.71073)
2Θ range for data collection/°	3.02 to 55.1
Index ranges	-16 ≤ h ≤ 17, -18 ≤ k ≤ 18, -19 ≤ l ≤ 19
Reflections collected	25875
Independent reflections	11151 [R_{int} = 0.0540, R_{sigma} = 0.0657]
Data/restraints/parameters	11151/0/711
Goodness-of-fit on F^2	1.272
Final R indexes [I>=2σ (I)]	R_1 = 0.0789, wR_2 = 0.1828
Final R indexes [all data]	R_1 = 0.1029, wR_2 = 0.1925
Largest diff. peak/hole / e $Å^{-3}$	0.37/-0.50

B-3 $Ru_2(DMOPhFm)_4$ (X)

Identification code	(X) / njp243_p4(1)
Empirical formula	$C_{73}H_{88}N_8O_{16}Ru_2$
Formula weight	1535.65
Temperature/K	100(2)
Crystal system	Tetragonal
Space group	$P4_12_12$
a/Å	11.3950(3)
b/Å	11.3950(3)
c/Å	52.4067(15)
α/°	90
β/°	90
γ/°	90
Volume/$Å^3$	6804.8(3)
Z	4
$\rho_{calc}g/cm^3$	1.499 Mg/m3
μ/mm^{-1}	0.520
F(000)	3192
Crystal size/mm^3	
Radiation	MoKα (λ = 0.71073)
2Θ range for data collection/°	2.13 to 27.50
Index ranges	-14≤h≤14, -14≤k≤14, -67≤l≤68
Reflections collected	127548
Independent reflections	7813 [R(int) = 0.0395]
Data/restraints/parameters	7813 / 45 / 439
Goodness-of-fit on F^2	1.318
Final R indexes [I>=2σ (I)]	R1 = 0.0593, wR2 = 0.1387
Final R indexes [all data]	R1 = 0.0594, wR2 = 0.1387
Largest diff. peak/hole / e $Å^{-3}$	2.163 and -1.347 eA-3

B-4 $Ru_2(DMOPhFm)_4$ (X)

Identification code	(X) / njp243_P4(1) -sqz
Empirical formula	$C_{68}H_{76}N_8O_{16}Ru_2$
Formula weight	1463.51
Temperature/K	100.0
Crystal system	tetragonal
Space group	$P4_12_12$
a/Å	11.3950(3)
b/Å	11.3950(3)
c/Å	52.4067(15)
α/°	90.00
β/°	90.00
γ/°	90.00
Volume/$Å^3$	6804.8(3)
Z	4
$\rho_{calc}g/cm^3$	1.429
μ/mm^{-1}	0.516
F(000)	3024.0
Crystal size/mm^3	0.61 × 0.52 × 0.1
Radiation	MoKα (λ = 0.71073)
2Θ range for data collection/°	3.1 to 55
Index ranges	-14 ≤ h ≤ 14, -14 ≤ k ≤ 14, -67 ≤ l ≤ 68
Reflections collected	127819
Independent reflections	7816 [Rint = 0.0395, Rsigma = 0.0156]
Data/restraints/parameters	7816/0/384
Goodness-of-fit on F^2	1.287
Final R indexes [I>=2σ (I)]	R1 = 0.0472, wR2 = 0.1129
Final R indexes [all data]	R1 = 0.0477, wR2 = 0.1131
Largest diff. peak/hole / e $Å^{-3}$	0.56/-1.08

B-5 $Ru_2(3,5\text{-}(CF_3)_2PhFm)_3(OAc)_2$ (XIII-b)

Identification code	XIII-b / mo_SamNP_1_0m
Empirical formula	C72H35F48N8O4Ru2
Formula weight	2190.22
Temperature/K	150
Crystal system	triclinic
Space group	P-1
a/Å	14.0156(6)
b/Å	14.5012(6)
c/Å	23.7576(10)
α/°	85.4172(12)
β/°	78.3431(12)
γ/°	64.1648(11)
Volume/Å^3	4256.1(3)
Z	2
ρ_{calc}g/cm^3	1.709
μ/mm^{-1}	0.512
F(000)	2150
Crystal size/mm^3	0.2 × 0.1 × 0.1
Radiation	MoKα (λ = 0.71073)
2Θ range for data collection/°	4 to 61.2
Index ranges	-20 ≤ h ≤ 20, -20 ≤ k ≤ 20, -34 ≤ l ≤ 34
Reflections collected	135371
Independent reflections	26148 [Rint = 0.0444, Rsigma = 0.0439]
Data/restraints/parameters	26148/0/1113
Goodness-of-fit on F^2	1.099
Final R indexes [I>=2σ (I)]	R1 = 0.0545, wR2 = 0.1383
Final R indexes [all data]	R1 = 0.0815, wR2 = 0.1483
Largest diff. peak/hole / e Å^{-3}	1.54/-1.46

B-6 $Ru_2(OAc)_4(H[DMOPhFm])_2$ (XV)

Identification code	njp255_0m
Empirical formula	C21H26N2O8Ru
Formula weight	535.51
Temperature/K	100
Crystal system	triclinic
Space group	P-1
a/Å	8.262(5)
b/Å	12.492(5)
c/Å	14.200(5)
α/°	69.413(5)
β/°	76.462(5)
γ/°	74.484(5)
Volume/$Å^3$	1305.9(11)
Z	2
$\rho_{calc}g/cm^3$	1.362
μ/mm^{-1}	0.643
F(000)	548.0
Crystal size/mm^3	0.2 × 0.15 × 0.1
Radiation	MoKα (λ = 0.71073)
2Θ range for data collection/°	3.1 to 55.32
Index ranges	-10 ≤ h ≤ 10, -15 ≤ k ≤ 16, -17 ≤ l ≤ 18
Reflections collected	11299
Independent reflections	5627 [Rint = 0.1230, Rsigma = 0.2237]
Data/restraints/parameters	5627/0/271
Goodness-of-fit on F^2	0.850
Final R indexes [I>=2σ (I)]	R1 = 0.0890, wR2 = 0.1877
Final R indexes [all data]	R1 = 0.1749, wR2 = 0.2154
Largest diff. peak/hole / e $Å^{-3}$	2.92/-1.44